Chiral Dynamics and Final State Interactions in Semileptonic B Meson Decay and Antinucleon-Nucleon Scattering

Dissertation

zur

Erlangung des Doktorgrades (Dr. rer. nat.)

der

Mathematisch-Naturwissenschaftlichen Fakultät

der

Rheinischen Friedrich-Wilhelms-Universität Bonn

vorgelegt von
Xian-Wei Kang

aus
Henan, China

Bonn, May 2014

Angefertigt mit Genehmigung
der
Mathematisch-Naturwissenschaftlichen Fakultät
der
Rheinischen Friedrich-Wilhelms-Universität Bonn

1. Gutachter: Prof. Dr. Ulf-G. Meißner

2. Gutachter: PD Dr. Johann Haidenbauer

Tag der Promotion: 08.08.2014

Erscheinungsjahr: 2014

Summary

Chiral effective field theory (EFT) is a powerful tool to study the low energy hadron physics. Combining the heavy quark symmetry and chiral symmetry, the heavy hadron (moson and baryon) chiral perturbation theory is constructed. Among them, the heavy meson chiral perturbation theory describes the interaction between pseudoscalar and (heavy) B (or D) mesons, and the heavy baryon chiral perturbation theory deals with the pseudoscalar-baryon interaction, where the baryon (including the nucleon) is treated nonrelativistically. In this thesis, we apply these chiral Lagrangians to the semileptonic decay of B meson as well as the antinucleon-nucleon interaction. The final state interactions between the hadrons are taken into account model-independently. We summarize the pertinent points contained in this thesis as below:

- for the decay $B \to \pi\pi l\bar{\nu}_l$

  The Cabibbo–Kobayashi–Maskawa (CKM) matrix element $|V_{ub}|$ has been determined by both inclusive decay modes $B \to X_u l\bar{\nu}_l$ and exclusive ones $B \to \pi(\rho) l\bar{\nu}_l$, but they do not match within uncertainties, which is the well-known "$|V_{ub}|$ puzzle". Our emphasis is put on the reexamination of the theoretical uncertainties in the exclusive mode $B \to \rho l\bar{\nu}_l$. In fact we note that this transition suffers from sizable uncertainties due to the large width of ρ meson, and instead, one should rely on the analysis of a full four-body semileptonic channel $B \to \pi\pi l\bar{\nu}_l$, which also serves as a cross check for the extraction of $|V_{ub}|$. The form factors of hadronic matrix elements of B to $\pi\pi$ transitions are analyzed by dispersion theory, which is a model-independent approach to take into account the $\pi\pi$ final state interactions. The heavy meson chiral perturbation theory is used as an input to fix the subtraction constants appearing in the dispersion relations. Our formalism allows, for the first time, to use the full information for $\pi\pi$ invariant mass below 1 GeV to extract $|V_{ub}|$ without the need to refer to a particular resonance such as ρ or $f_0(980)$. The partial decay rate $d\Gamma/(|V_{ub}| ds\, ds_l)$ below $s = 1\ \text{GeV}^2$ at fixed $s_l = (m_B - 1\,\text{GeV})^2$ is presented for illustration, where s and s_l denote the invariant mass squared for pion pairs and lepton pairs, respectively. Our such proposal can be examined in Belle and LHCb and thus the experimental data is highly desirable.

- for antinucleon-nucleon interaction

  We observe that there is still no satisfactory description of antinucleon-nucleon scattering in view of chiral EFT. The tools available are the various phenomenological

models, which played a very important role in the history of studying the nuclear force. However, they do not have the obvious connections with the underlying theory: quantum chromodynamics (QCD). Chiral EFT is related to QCD through the chiral symmetry, and a systematic improvement can be done due to the power counting rule.

The recent partial-wave analysis of the antiproton-proton ($\bar{p}p$) scattering data provides an opportunity to examine how the chiral EFT works for the antinucleon-nucleon interactions. We then calculate the antinucleon-nucleon potential up to next-to-next-to-leading order using the chiral EFT based on a modified Weinberg power counting, in close analogy to pertinent studies of the nucleon-nucleon interaction. Solving the Lippmann-Schwinger equation one obtains the scattering amplitude and futher observables. Our results show that the overall quality of the achieved description of the $\bar{N}N$ amplitudes is comparable to the one found in case of the nucleon-nucleon interaction at the same order. A good agreement is achieved for the phase shifts and inelasticities in most of the S-wave channels and several P-wave channels. We also calculate the scattering length, and the level shifts and widths of antiprotonic hydrogen atom, by our potential utilizing effective theory. They are all in line with the experimental information, as well as the Jülich model D (as an example of a phenomenological model). We also find there are bound states by the strong interaction in isospin-0 $^3P_0$ and isospin-0 $^3S_1 - {}^3D_1$ partial waves, and their positions and widths are provided.

- for reactions $e^+e^- \leftrightarrow \bar{p}p$

  A significant enhancement in the cross section near the $\bar{p}p$ threshold is observed in various reactions, e.g., $J/\psi \to \gamma\bar{p}p$, $J/\psi \to \omega\bar{p}p$, $\psi' \to \gamma\bar{p}p$ as well as the one $e^+e^- \to \bar{p}p$ we are considering. This enhancement phenomenon in the decays $J/\psi \to \gamma\bar{p}p$ is the most prominent one. Several theoretical explanations have been proposed, e.g., it is induced by the $\bar{N}N$ bound states, or the unobserved resonance so far, or even an exotic state like a glueball. However, in all these processes that contain a $\bar{p}p$ pair, the $\bar{p}p$ interaction is an important ingredient and can have large influence on the energy dependence of an observable. In the reactions $e^+e^- \leftrightarrow \bar{p}p$, only $^3S_1$ and $^3D_1$ partial waves are allowed assuming the one-photon exchange approximation. Then we rigorously take into account the $\bar{p}p$ interactions in the initial or final states. It is shown that the existing experimental data including integrated and differential cross sections are well described in our approach. We also present spin-dependent observables as predictions for the future measurements.

Contents

Introduction

In the Standard Model of particle physics, the strong interactions are described by Quantum Chromodynamics (QCD), which is based on a local non-Abelian gauge symmetry, namely, $\mathrm{SU}(3)_{\mathrm{color}}$. In QCD, the fundamental degrees of freedom are the quarks and gluons, where the former are the matter fields and the latter serve as the media that propagate the strong force. They both are never directly observed, instead, one observes the hadrons, which can be regarded as bound states that are made from the quarks and gluons. This phenomenon is known as the confinement. The six quark flavors are commonly divided into two groups by their masses: the light ones u, d, s and the heavy ones c, b, t. While the light quarks are almost massless and need to be treated relativistically, the heavy quarks can be treated nonrelativistically, which is the basis for the heavy hadron (meson and baryon) chiral perturbation theory discussed in Chap. 1. In the limit of vanishing quark masses, QCD exhibits chiral symmetry. More specifically speaking, the left-handed and right-handed components of massless quarks do not mix in the QCD Lagrangian $\mathcal{L}^0_{\mathrm{QCD}}$ (the superscript 0 means the quark mass matrix vanishes). And thus one can find that $\mathcal{L}^0_{\mathrm{QCD}}$ is invariant under the global unitary transformation $SU(2)_L \times SU(2)_R$ (for the case of two flavors), where "L (R)" means the transformation acts on the left- (right-) handed quark field. This $SU(2)_L \times SU(2)_R$ symmetry is known as chiral symmetry.

At high energies, the strong coupling constant α_S is much smaller than one, thus the physical quantities can be expanded in powers of α_S. This is the so-called perturbative QCD approach which has achieved great success. However, at the low energy region, α_S becomes larger and the nonperturbative effect is apparent. The dynamics of the strong interactions in the low energy region is still poorly known in terms of the underlying theory, QCD. Hadron physics, or more explicitly, the study of hadron-hadron interactions plays an important role towards a better understanding of the low-energy QCD. The effective field theory (EFT) approach is a powerful tool to study the hadron interaction. In EFT, the basic freedom is hadron due to the "confinement". The Weinberg "folk theorem" is the basis for EFT approach and here we quote the original statement by Weinberg [1]:

"If one writes down the most general possible Lagrangian, including all terms consistent with assumed symmetry principles, and then calculates matrix elements with this Lagrangian to any given order of perturbation theory, the result will simply be the most general possible S-matrix consistent with analyticity, perturbative unitarity, cluster decomposition, and the assumed symmetry principles."

From the above statement, we know that to construct the Lagrangian, one should

examine the symmetry properties and how these symmetries are broken. Besides, one should design a power counting scheme, which is used to distinguish the more and the less important contributions.

At the low energy region, the chiral symmetry allows one to construct the chiral effective Lagrangian. When it refers to the interaction between the Goldstone bosons, we normally use the terminology "chiral perturbation theory", while in the topic of nuclear force, the term "chiral EFT" is used, because in the former case, the amplitude is expanded and for the latter one, the calculated quantity is the potential and not the conventional amplitude. The fundamental difference between the chiral EFT and a phenomenological model is that the chiral EFT has a firm link with the underlying theory QCD, i.e. it obeys the chiral symmetry of QCD. In this thesis we apply the chiral EFT to various aspects, specifically, the semileptonic decay of B mesons and the antinucleon-nucleon scattering. On the other hand, we note that the final state interaction plays a very important role in the hadronic reactions. In our work we take into account the final state interaction between pion pairs in the decay of $B \to \pi\pi l\bar{\nu}_l$, and the final state interaction between $\bar{p}p$ in the reactions $e^+e^- \leftrightarrow \bar{p}p$ rigorously.

The current thesis is structured as follows. In Chap. 1, we briefly discuss the theoretical tools that we use, i.e. the chiral EFT and some methods to treat the final state interaction. In Chap. 2, we investigate the decay channel $B \to \pi\pi l\bar{\nu}_l$ aiming at providing a novel way to extract the Cabibbo–Kobayashi–Maskawa (CKM) matrix element V_{ub}. The form factors for the hadronic part of B to $\pi\pi$ transitions are analyzed in dispersion theory, where the final state interaction between $\pi\pi$ pairs are incorporated model-independently, and πB interactions are approximated by the B^* pole. The free parameters resulting from the dispersion theory are fixed by the predictions of the heavy meson chiral perturbation theory at threshold. And finally the partial decay rate at a selected region is predicted. Once the experimental data is available, one could extract the value of $|V_{ub}|$ by our proposal.

We have also examined the interaction between baryons from the viewpoint of chiral EFT. In Chap. 3, we calculate the antinucleon-nucleon potentials up to the next-to-next-to-leading order adopting the modified Weinberg power-counting rule by using the chiral EFT, and then solve the Lippmann-Schwinger equation to get the scattering amplitudes. The scattering lengths (volumes) for S-wave (P-wave), and the level shifts and widths for antiproton-proton atom are calculated. They are all in line with the existing experimental information. Note that the Lippmann-Schwinger equation takes the rescattering effects into account to infinite orders, i.e. an infinite summation. The antinucleon-nucleon potential has some common pieces with the nucleon-nucleon potential, thus we first present a brief review for the nucleon-nucleon case in Sec. 3.2 in Chap. 3. In Chap. 4, we apply the chiral antinucleon-nucleon potential constructed by us to the reactions $e^+e^- \leftrightarrow \bar{p}p$. There we fully takes into account the antiproton-proton interactions and find the measured cross sections and differential cross sections can be quite well described solely by final-state-interaction effects. Then the spin observables are also presented as predictions.

Chapter 1

Theoretical background

1.1 Chiral effective field theory

1.1.1 Chiral perturbation theory for light meson sector

The standard chiral perturbation theory (ChPT) for light pseudoscalar mesons has been constructed by Gasser and Leutwyler in the 1980s [2, 3]. In this part, we give a basic introduction following the discussions in Ref. [4].

As mentioned in the Introduction, QCD exhibits an exact chiral symmetry in the limit of vanishing quark masses. We introduce the basic concept of chiral symmetry breaking by considering the QCD with two-flavor massless u and d quarks and then we generalize to three-flavor case, since SU(2) ChPT (for two flavors) converges more rapidly than SU(3) ChPT (for three flavors). For the vanishing masses of u and d quarks, i.e., $m_u, m_d \to 0$, the QCD Lagrangian exhibits the $SU(2)_L \times SU(2)_R$ symmetry. Then Noether theorem dictates that there are six conserved currents: three left-handed and three right-handed ones. They can be combined into three conserved vector (V) and three axial-vector (A) currents. The empirical facts about the hadron spectrum suggest that $SU(2)_V$ symmetry is preserved [1], and the symmetry broken mode is $SU(2)_L \times SU(2)_R \to SU(2)_V$. For such a symmetry breaking, one expects three massless bosons, which are known as Goldstone bosons. Pions with the small masses are candidates of Goldstone bosons, where the (small) finite masses are due to the nonzero quark masses m_u and m_d. The pion fields can be organized into a two-dimensional matrix

$$\Pi(x) = \sum_{i=1}^{3} \tau_i \phi_i(x) = \begin{pmatrix} \phi_3 & \phi_1 - i\phi_2 \\ \phi_1 + i\phi_2 & -\phi_3 \end{pmatrix} \equiv \begin{pmatrix} \pi^0 & \sqrt{2}\pi^+ \\ \sqrt{2}\pi^- & -\pi^0 \end{pmatrix}, \tag{1.1}$$

where τ_i, $i = 1, 2, 3$ are the ususal Pauli matrices which are the generators of $SU(2)_{\text{flavor}}$. For the case of three flavors (u, d, s quarks), they are octet pseudoscalars and can be

[1] Vafa and Witten has proved that the vector-like global symmetry is not spontaneously broken in QCD [5].

organized into a 3×3 matrix through

$$\begin{aligned}\phi(x) = \sum_{a=1}^{8} \lambda_a \phi_a(x) &= \begin{pmatrix} \phi_3 + \sqrt{\frac{1}{3}}\phi_8 & \phi_1 - i\phi_2 & \phi_4 - i\phi_5 \\ \phi_1 + i\phi_2 & -\phi_3 + \frac{1}{\sqrt{3}}\phi_8 & \phi_6 - i\phi_7 \\ \phi_4 + i\phi_5 & \phi_6 + i\phi_7 & -\frac{2}{\sqrt{3}}\phi_8 \end{pmatrix} \\ &= \begin{pmatrix} \pi^0 + \sqrt{\frac{1}{3}}\eta & \sqrt{2}\pi^+ & \sqrt{2}K^+ \\ \sqrt{2}\pi^- & -\pi^0 + \sqrt{\frac{1}{3}}\eta & \sqrt{2}K^0 \\ \sqrt{2}K^- & \sqrt{2}\bar{K}^0 & -\sqrt{\frac{2}{3}}\eta \end{pmatrix} \end{aligned} \tag{1.2}$$

In the Lagrangian, these Goldstone Bosons appear in the matrix-valued field $U \in SU(3)$, which transforms under the chiral transformation $SU(3)_L \times SU(3)_R$ as

$$U \longrightarrow U'(X) = RU(x)L^\dagger = RU(x)L^{-1} \tag{1.3}$$

with $R/L \in SU(3)_{R/L}$. A popular choice for U is the exponential parametrization

$$U(x) = \exp\left(i\frac{\phi(x)}{F_0}\right), \tag{1.4}$$

where F_0 is the pion decay constant in the chiral limit (in the following chapters, we will use the physical value of the pion decay constant, which is denoted by f_π and takes $f_\pi \approx 92.4$ MeV). Goldstone bosons interact only when they carry momentum, thus only terms in powers of $\partial_\mu U$ appear in Lagrangian. Moreover, only even powers of $\partial_\mu U$ are allowed due to Lorentz invariance, i.e. the Lorentz indices should be contracted with the metric tensor $g^{\mu\nu}$ or Levi-Civita tensor $\epsilon^{\mu\nu\alpha\beta}$ to get scalars. If one denotes the small momentum carried by the Goldstone boson by p generically, a derivative on the Goldstone boson field generates a term p. The pion mass is also accounted as order of p. More precisely speaking, p denotes the soft scale and typically 0.1 GeV. The chiral symmetry breaking scale $\Lambda_\chi = 4\pi F_0 \approx 1$ GeV is referred to as a hard scale comparing to the small quantity p. The Lagrangian can be expanded as a power series of p/Λ_χ, and this expansion is known as the chiral expansion. Then the most general Lagrangian describing the interaction between Goldstone bosons can be written as

$$\mathcal{L}_{\pi\pi} = \mathcal{L}_{\pi\pi}^{(2)} + \mathcal{L}_{\pi\pi}^{(4)} + \mathcal{L}_{\pi\pi}^{(6)} + \cdots, \tag{1.5}$$

where the superscript indicates the chiral order, and we have used π to denotes Goldstone boson symbolically in the subscript. The lowest order effective Lagrangian (order of $(p/\Lambda_\chi)^2$) reads

$$\mathcal{L}_{\pi\pi}^{(2)} = \frac{F_0^2}{4}\,\mathrm{Tr}\left(\partial_\mu U \partial^\mu U^\dagger\right) + \underbrace{\frac{F_0^2 B_0}{2}\,\mathrm{Tr}\left(\mathcal{M}U^\dagger + U\mathcal{M}^\dagger\right)}_{\mathcal{L}_{\chi\mathrm{SB}}}, \tag{1.6}$$

with the quark mass matrix

$$\mathcal{M} = \begin{pmatrix} m_u & 0 & 0 \\ 0 & m_d & 0 \\ 0 & 0 & m_s \end{pmatrix}, \tag{1.7}$$

and B_0 is a constant. Three remarks will be done for Eq. (1.6): first, quark mass is counted as order of p^2, and this point together with the physical interpretation of B_0 can be seen from Eq. (1.10) below; secondly, the term $\mathcal{L}_{\chi\text{SB}}$ signifies the explicit chiral symmetry breaking due to the finite quark masses; last, the Lagrangian density written as Eq. (1.6) is chiral invariant assuming $\mathcal{M}$ transforms like

$$\mathcal{M} \longrightarrow R\mathcal{M}L^\dagger. \tag{1.8}$$

Expanding the term $\mathcal{L}_2$, one gets

$$\begin{aligned} \mathcal{L}_{\chi\text{SB}} &= -\frac{B_0}{2}\,\text{Tr}\,(\phi^2\mathcal{M}) + \text{ higher orders of } \phi \\ &= -\frac{B_0}{2}\Big\{2(m_u+m_d)\pi^+\pi^- + 2(m_u+m_s)K^+K^- + 2(m_d+m_s)K^0\bar{K}^0 \\ &\quad +(m_u+m_d)\pi^0\pi^0 + \frac{2}{\sqrt{3}}(m_u-m_d)\pi^0\eta + \frac{m_u+m_d+4m_s}{3}\eta^2\Big\}. \end{aligned} \tag{1.9}$$

In the isospin limit $m_u = m_d = m$, $\pi-\eta$ mixing term will vanish in Eq. (1.9). The following mass relations can also be found,

$$\begin{aligned} M_\pi^2 &= 2B_0 m, \\ M_K^2 &= B_0(m+m_s), \\ M_\eta^2 &= \frac{2}{3}B_0(m+2m_s), \end{aligned} \tag{1.10}$$

from which one finds that the quark masses are on the level of meson mass squared and thus will be counted as $\mathcal{O}(p^2)$ as mentioned earlier. Comparing with the Gell-Mann-Oakes-Renner relation [6] [2]

$$M_\pi^2 = (m_u+m_d) \times |\langle 0|\bar{u}u|0\rangle| \times \frac{1}{F_0^2}, \tag{1.11}$$

one finds that B_0 is a constant related to the chiral quark consendate as

$$\begin{aligned} B_0 &= \frac{1}{F_0^2} \times |\,\langle 0|\,\bar{u}u\,|0\rangle\,| \\ &= \frac{1}{2F_0^2} \times |\,\langle 0|\,\bar{q}q\,|0\rangle\,|, \end{aligned} \tag{1.12}$$

[2] Here the physical interpretation of B_0 is obtained by matching Eq. (1.10) to the Gell-Mann-Oakes-Renner relation. In fact the physical meaning of B_0 can also be identified from the comparision of ChPT and QCD, see e.g. Ref. [4]. Then the Gell-Mann-Oakes-Renner relation could be viewed as a result of chiral Lagrangian.

with $\langle 0|\,\bar{q}q\,|0\rangle$ representing the isospin average of up- and down-quark condensates. It is also interesting that the Gell-Mann-Okubo relation $4M_K^2 = 3M_\eta^2 + M_\pi^2$ and also the following quark mass ratios are obtained,

$$\begin{aligned}\frac{M_K^2}{M_\pi^2} &= \frac{m+m_s}{2m} \Longrightarrow \frac{m_s}{m} = 25.9,\\ \frac{M_\eta^2}{M_\pi^2} &= \frac{2m_s+m}{3m} \Longrightarrow \frac{m_s}{m} = 24.3.\end{aligned} \tag{1.13}$$

To conclude, the leading-order ChPT is equivalent to the current algebra.

For higher order Lagrangians and their various applications, one may refer to the reviews, e.g. [7–10].

1.1.2 Heavy meson chiral perturbation theory

In the heavy quark limit $m_Q \to \infty$, the dynamics of the strong interactions exhibits the heavy quark flavor and spin symmetry, where the former means that the interaction is unchanged under the exchange of heavy quark flavors (charm and beauty quark) and the latter means that the interaction does not change under an arbitrary transformation on the spin of the heavy quark. In the real physics, there are corrections that scale as powers of $\Lambda_{\rm QCD}/m_Q$, with $\Lambda_{\rm QCD}$ being the nonperturbative scale generated by QCD, and experimentally, $\Lambda_{\rm QCD} \sim 200$ MeV. The heavy meson chiral perturbation theory (HMChPT) [11, 12] is constructed for describing the interactions between the heavy mesons (B, D) and the light pseudoscalar bosons (π, K, η) by union of heavy quark symmetry and chiral symmetry (as outlined in Sec. 1.1.1). We will present a brief review following Ref. [13].

In heavy quark system, the four-velocity v of the heavy quark is fixed in the interactions with the external field. The multiplets of the states implied by heavy quark spin symmetry can be organized into a single field [14],

$$H_a = \frac{1+\not{v}}{2}(P^*_{a\mu}\gamma^\mu - P_a\gamma_5), \tag{1.14}$$

where $P^*_{a\mu}$ is the field operator that destroys P^*_a meson with velocity v satisfying $v^\mu P^*_{a\mu} = 0$, and P_a destroys a P_a meson of velocity v. For the b quark, we have

$$\begin{aligned}(P_1,\, P_2,\, P_3) &= (B^-,\, \overline{B}^0,\, \overline{B}_s^0),\\ (P_1^*,\, P_2^*,\, P_3^*) &= (B^{*-},\, \overline{B}^{*0},\, \overline{B}_s^{*0}),\end{aligned} \tag{1.15}$$

and for the c quark

$$\begin{aligned}(P_1,\, P_2,\, P_3) &= (D^0,\, D^+,\, D_s^+),\\ (P_1^*,\, P_2^*,\, P_3^*) &= (D^{*0},\, D^{*+},\, D_s^{*+}).\end{aligned} \tag{1.16}$$

The factors of $\sqrt{m_P}$ and $\sqrt{m_{P^*}}$ have been absorbed into the P and P^* fields, and these consequently have dimension $[\text{mass}]^{3/2}$. The conjugate of H is defined as

$$\bar{H}_a = \gamma^0 H_a^\dagger \gamma^0 = (P^{*\dagger}_{a\mu}\gamma^\mu + P_a^\dagger \gamma_5)\frac{1+\not{v}}{2} \tag{1.17}$$

The field H contains the heavy quark and one light antiquark, and thus it transforms under the Lorentz transformation as a bispinor,

$$H_a \to D(\Lambda) H_a D(\Lambda)^{-1}, \tag{1.18}$$

where $D(\Lambda)$ is a matrix representation of Lorentz group. Under the heavy-quark spin symmetry $SU(2)_v$,

$$H_a \to S H_a. \tag{1.19}$$

Besides the transformation rules under the Lorentz and $SU(2)_v$ transformations, one also needs to know the transformation behavior of H_a under the chiral $SU(3)_L \times SU(3)_R$ transformation for combining the heavy quark symmetry and the chiral symmetry. For that purpose, we define the square root of $U(x)$ by $u^2(x) = U(x)$. Recalling the transformation property of $U(x)$, Eq. (1.3), and the nonlinear realization of group $SU(3)_L \times SU(3)_R$, we define the function K (satisfying the unitarity $K^\dagger = K^{-1}$) by

$$u(x) \longrightarrow u'(x) = \sqrt{RUL^\dagger} \equiv Ru(x)K^{-1}. \tag{1.20}$$

From Eq. (1.20), one can solve for K,

$$K = u'^{-1}RU = \sqrt{RUL^\dagger}^{-1} R\sqrt{U} \equiv K(L,R,U), \tag{1.21}$$

where the function $K(L,R,U)$ depends not only on L, R but also $U(x)$. Furthermore, one can verify

$$RuK^\dagger = KuL^\dagger \tag{1.22}$$

and observe

$$U(x) = u^2(x) \to Ru(x)K^\dagger K u(x) L^\dagger = RUL^\dagger. \tag{1.23}$$

In Ref. [13], it is shown that, for the heavy meson field H, one can choose the transformation rule under the chiral $SU(3)_L \times SU(3)_R$ as

$$H \longrightarrow HK^\dagger \tag{1.24}$$

to construct the chiral invariant Lagrangian. In component form it is $H_a \to H_b K^\dagger_{ba}$. And then $\bar{H}$ transforms as $\bar{H} \to K\bar{H}$. For an operator $\widehat{O}$ transforming as $K\widehat{O}K^\dagger$, the operator blocks $H\widehat{O}\bar{H}$ is therefore chiral invariant. In order to describe the interactions between heavy and light mesons, we need to construct such operators from the field u. Two combinations of u field involving one derivative are

$$\Gamma_\mu = \frac{1}{2}(u^\dagger \partial_\mu u + u\partial_\mu u^\dagger), \quad u_\mu = i(u^\dagger \partial_\mu u - u\partial_\mu u^\dagger), \tag{1.25}$$

which transform under chiral $SU(3)_L \times SU(3)_R$ as

$$u_\mu \longrightarrow K u_\mu K^\dagger, \quad \Gamma_\mu \longrightarrow K\Gamma_\mu K^\dagger + K\partial_\mu K^\dagger. \tag{1.26}$$

The Γ_μ field can be used to define a chiral covariant derivative

$$D_\mu = \partial_\mu + \Gamma_\mu. \tag{1.27}$$

This covariant derivative acts on $\bar{H}$ as

$$D_\mu \bar{H} = (\partial_\mu + \Gamma_\mu)\bar{H}, \tag{1.28}$$

and acts on H as

$$D_\mu H = H(\overleftarrow{\partial_\mu} - \Gamma_\mu) = \partial_\mu H - H\Gamma_\mu. \tag{1.29}$$

Under the chiral $SU(3)_L \times SU(3)_R$ transformation, we have

$$(D_\mu \bar{H}) \longrightarrow K(D_\mu \bar{H}), \quad (D_\mu H) \longrightarrow (D_\mu H)K^\dagger. \tag{1.30}$$

In the Lagrangian, the term without derivative is the H-field mass term $M_H \mathrm{Tr}\, \bar{H}_a H_a$, which can be removed by rescaling the field by $\exp(-iM_H v \cdot x)$. The only allowed terms with one derivative are

$$\mathcal{L}_{\pi B} = -i\mathrm{Tr}\, \bar{H}_a v_\mu \left(\partial^\mu \delta_{ab} - \Gamma^\mu_{ab}\right) H_b + g_\pi \mathrm{Tr}\, \bar{H}_a H_b \gamma_\nu \gamma_5 u^\nu_{ba}. \tag{1.31}$$

Here the trace "Tr" is performed over the 4×4 Dirac γ-matrices. The $SU(3)$ flavor indices a, b are explicitly displayed and the repeated indices are summed over 1, 2, 3 (cf. Eqs. (1.15) (1.16)). The coupling g_π satisfies $g_\pi = g_{B^*B\pi} = g_{B^*B^*\pi}$ under the heavy quark spin symmetry. From the transformation rule $\bar{H}_a \to \bar{H}_a S^{-1}$, $\bar{H}_a \to D(\Lambda)\bar{H}_a D(\Lambda)^{-1}$, one can easily verify that Eq. (1.31) satisfies chiral symmetry, heavy quark spin symmetry, Lorentz symmetry and parity.

We provide here some simplifications for Eq. (1.31). After calculating the traces, we obtain

$$\begin{aligned} \mathrm{Tr}\left[\bar{H}_a H_b \gamma^\alpha \gamma^5\right] &= 2P^{*\dagger\alpha}_a P_b - 2iP^{*\dagger}_{a\mu} P^*_{b\nu} v_\sigma \epsilon^{\mu\sigma\nu\alpha}, \\ \mathrm{Tr}\left[\bar{H}_a H_b\right] &= 2P^{*\dagger}_{a\mu} P^{*\mu}_b - 2P^\dagger_a P_b, \end{aligned} \tag{1.32}$$

where the superscript "†" denotes the conjugation. u_μ gives the terms with odd numbers of Goldstone bosons,

$$\begin{aligned} \Big(u_\mu\Big)_{1\pi} &= -\frac{\partial_\mu \phi}{F_0} \\ \Big(u_\mu\Big)_{3\pi} &= -\frac{1}{24F_0^3}\left(2\phi\partial_\mu\phi\cdot\phi - \phi^2\partial_\mu\phi - \partial_\mu\phi\cdot\phi^2\right), \end{aligned} \tag{1.33}$$

while Γ_μ contains terms with even numbers of Goldstone bosons

$$\Big(\Gamma_\mu\Big)_{2\pi} = \frac{1}{4F_0^2}(\phi\partial_\mu\phi - \partial_\mu\phi\cdot\phi)$$

$$\Big(\Gamma_\mu\Big)_{4\pi} = \frac{1}{192F_0^4}\left(-\phi^3\partial_\mu\phi + 3\phi^2\partial_\mu\phi\cdot\phi - 3\phi\partial_\mu\phi^2 + \partial_\mu\phi\cdot\phi^3\right) \tag{1.34}$$

It is possible to include the effects of heavy quark symmetry violation and chiral symmetry violation. At order $\Lambda_{\rm QCD}/m_Q$, heavy quark spin symmetry is violated by the magnetic moment operator. At leading order in the derivative expansion, this effect can be taken into account by adding

$$\delta\mathcal{L}_1 = \frac{\lambda_1}{m_Q}\mathrm{Tr}\ \bar{H}_a\sigma_{\mu\nu}H_a\sigma^{\mu\nu} \tag{1.35}$$

to the Langrangian density. The only effect of Eq. (1.35) is to give rise to the mass splitting between the degenerate doublet,

$$\Delta_Q = m_{P^*} - m_P = -8\frac{\lambda_1}{m_Q}. \tag{1.36}$$

To include the effect of chiral symmetry breaking induced by the quark mass $\mathcal{M}$ (see Eq. (1.7)), we can add the terms

$$\begin{aligned}\delta\mathcal{L}_2 &= \lambda_1'\mathrm{Tr}\ \bar{H}_aH_b\left(u\mathcal{M}^\dagger u + u^\dagger\mathcal{M}u^\dagger\right)_{ba}\\ &\quad +\lambda_2'\mathrm{Tr}\ \bar{H}_aH_a\left(u\mathcal{M}^\dagger u + u^\dagger\mathcal{M}u^\dagger\right)_{bb}\end{aligned} \tag{1.37}$$

into the Lagrangian. The first term in Eq. (1.37) contributes to the mass differences between the heavy mesons with $\bar{s}$ quark and $\bar{u}$ or $\bar{d}$ quark, while the second term contributes an equal amount to the heavy meson masses.

As a commonly used scheme, we neglect the effects of $\delta\mathcal{L}_2$, but do include the contribution of $\delta\mathcal{L}_1$ which describes the deviation from $m_Q\to\infty$ limit and induces in the propagator the mass splittings between the vector and scalar mesons. One can decompose the four-momentum of a heavy meson (with mass m) as

$$p^\mu = mv^\mu + k^\mu, \tag{1.38}$$

where k^μ is the small residual momentum representing the off-shell amount, $v\cdot k \ll m$. Defining

$$\begin{aligned}\Delta_b &= m_{B^*} - m_B,\\ \mu_b &= m_{B_s} - m_B,\\ m_{B_s^*} - m_B &\approx \Delta_b + \mu_b,\end{aligned} \tag{1.39}$$

we have the propergators

$$\begin{aligned}B:&\quad \frac{i}{2v\cdot k}\\ B^*:&\quad \frac{-i(g_{\mu\nu}-v_\mu v_\nu)}{2(v\cdot k-\Delta)},\end{aligned}$$

$$B_s: \quad \frac{i}{2v\cdot k-\mu}$$
$$B_s^*: \quad \frac{-i(g_{\mu\nu}-v_\mu v_\nu)}{2(v\cdot k-\Delta-\mu)}, \tag{1.40}$$

where we have made use of the rescaling $H \longrightarrow e^{3i\Delta_Q v\cdot x/4}H$. And for charm quark sector, one just needs to replace Δ_b and μ_b by $\Delta_c = m_{D^*} - m_D$ and $\mu_c = m_{D_s} - m_D$, respectively.

For the semileptonic decays of the heavy mesons, one needs the left-hand current $L_{\nu a} = \bar{q}^a\gamma_\nu(1-\gamma_5)Q$ with $\bar{q}_a = \bar{u}, \bar{d}, \bar{s}$. At zero order in the derivative expansion, it has the form

$$L_{\nu a} = \frac{i\beta}{2}\mathrm{Tr}[\gamma^\nu(1-\gamma_5)H_b u^\dagger_{ba}]. \tag{1.41}$$

Equation (1.41) transforms as $(\bar{\mathbf{3}}_L, \mathbf{1}_R)$ under $SU(3)_L \times SU(3)_R$, that is the same as the left-hand current. Explicitly, Eq. (1.41) is

$$L_{\nu a} = i\beta(P^*_{b\nu} - v^\nu P_b)u^\dagger_{ba}. \tag{1.42}$$

Taking the transition from B meson to vacuum, one has the definition of the decay constant

$$\langle 0|\,\bar{u}\gamma_\mu\gamma_5 b\,\big|B^-(v)\big\rangle = if_B p_B^\mu, \tag{1.43}$$

which gives

$$\beta = f_B\sqrt{m_B}. \tag{1.44}$$

1.1.3 Heavy baryon chiral perturbation theory

Let us first say a few words on the relativistic formulation of nucleons in chiral perturbation theory. As mentioned in the HMChPT, it involves the chiral invariant structure $\bar{\Psi}\widehat{O}\Psi$, which transform under the chiral $SU(3)_L \times SU(3)_R$ transformations as $\Psi \longrightarrow K\Psi$, $\bar{\Psi} \longrightarrow \bar{\Psi}K^\dagger, \widehat{O} \longrightarrow K\widehat{O}K^\dagger$. Ψ is the relativistic four-component Dirac spinor. The lowest order Lagrangian (with only one derivative) is [15]

$$\mathcal{L}^{(1)}_{\pi N} = \bar{\Psi}\left(i\gamma^\mu D_\mu - \mathring{m}_N + \frac{\mathring{g}_A}{2}\gamma^\mu\gamma_5 u_\mu\right)\Psi, \tag{1.45}$$

where $\mathring{m}_N$ and $\mathring{g}_A$ are the nucleon mass and pion nucleon coupling constant in the chiral limit (Still, m_N and g_A will denote the corresponding physical values); the covariant derivative is defined as

$$D_\mu = \partial_\mu + \Gamma_\mu, \tag{1.46}$$

and see Eq. (1.25) for the definition of Γ_μ and u_μ. The Lagrangian is chosen such that in the case of no external fields and no pion fields it describes a free nucleon of mass $\mathring{m}_N$.

More explicitly, the leading order relativistic πN Lagrangian, Eq. (1.45), for $SU(2)$ sector, reads

$$\mathcal{L}_{\pi N}^{(1)} = \bar{\Psi}\left(i\gamma^\mu\partial_\mu - \mathring{m}_N - \frac{1}{4F_0^2}\gamma^\mu\boldsymbol{\tau}\cdot(\boldsymbol{\pi}\times\partial_\mu\boldsymbol{\pi}) - \frac{\mathring{g}_A}{2F_0}\gamma^\mu\gamma_5\boldsymbol{\tau}\cdot\partial_\mu\boldsymbol{\pi} + \cdots\right)\Psi, \tag{1.47}$$

where $\boldsymbol{\pi} = (\pi_1, \pi_2, \pi_3)$, see Eq. (1.1). There is an important feature in Eq. (1.47): the term proportional to $\mathring{g}_A/(2F_0)$ is the familiar axial-vector πNN coupling, while the term proportional to $1/(4F_0^2)$ is the Weinberg-Tomozawa term [16].

However, treatment of nucleons as relativistic particles in chiral perturbation theory leads to problems. One can observe this from the derivative term, whose time component will generate a factor $E \approx m_N$ which is a not small quantity compared to the chiral symmetry scale $\Lambda_\chi \approx 1$ GeV. The solution to this problem is the so-called heavy baryon formalism [17, 18], based on the technique of heavy quark effective field theory (HQET). In that way, nucleons (or baryons) are treated as extreme nonrelativistic static fields. As in the HQET, the relativistic four-component Dirac spinor field Ψ can be decomposed into

$$\Psi = e^{-imv\cdot x}\left[N_v + h_v\right]. \tag{1.48}$$

with

$$N_v \equiv e^{imv\cdot x}\frac{1+\not{v}}{2}\Psi, \quad h_v \equiv e^{imv\cdot x}\frac{1-\not{v}}{2}\Psi, \tag{1.49}$$

Choosing a special case, $v^\mu = (1, 0, 0, 0)$, one will find for a positive-energy solution of the Dirac equation, N_v is the large/upper component of the Dirac wave function, whereas h_v is the small/lower component associated with the $1/m$ factor. Inserting Eq. (1.48) into Eq. (1.45), one has the form

$$\mathcal{L}_{\pi N} = \bar{N}_v\left(i\gamma^\mu D_\mu + \frac{\mathring{g}_A}{2}\gamma^\mu\gamma_5 u_\mu\right)N_v + \cdots, \tag{1.50}$$

where the ellipis contains the field of h_v which will finally appear in $1/m_N$-suppressed terms. Since N_v only contains the upper components, Eq. (1.50) is simplified to

$$\mathcal{L}_{\pi N}^{\rm HB} = \bar{N}_v\left(iD_0 - \frac{\mathring{g}_A}{2}\vec{\sigma}\cdot\vec{u}\right)N_v, \tag{1.51}$$

which is the leading order pion-nucleon Lagrangian in the heavy baryon (HB) formalism. The above descriptions are very sketchy, and for a careful derivation, refer to e.g., Ref. [4]. The higher order terms are explored in Refs. [19–21]. Nucleon contact Lagrangians will be also needed to calculate nucleon-nucleon scattering. Since their effects are incorporated in the contact terms discussed in Chap. 3, we will not mention them here.

1.2 The theory of final state interaction

1.2.1 The (generalized) Omnès problem

Let us first review some basics for the dispersion theory used in particle physics. Consider a function of one complex variable z, $f(z)$, which is analytic in the whole complex plane except for the cut $[s_0, \infty)$ along the real axis. For a given point z that is not in $[s_0, \infty)$ ($z \notin [s_0, \infty)$), from the Schwartz reflection principle, we have

$$f(z^*) = [f(z)]^*. \tag{1.52}$$

Applying the Cauchy integral formula, we have

$$f(z) = \frac{1}{2\pi i} \int_\gamma \frac{f(z')}{z' - z} dz', \tag{1.53}$$

where we choose the contour γ as a counter-clockwise infinite circle but circumventing the branch cut $[s_0, \infty)$. Then ($\epsilon = 0^+$)

$$\begin{aligned} f(z) &= \lim_{\epsilon \to 0^+} \frac{1}{2\pi i} \int_{s_0}^\infty \frac{f(s + i\epsilon) - f(s - i\epsilon)}{s - z} ds \\ &= \frac{1}{\pi} \lim_{\epsilon \to 0^+} \int_{s_0}^\infty \frac{\text{Im } f(s + i\epsilon)}{s - z} ds. \end{aligned} \tag{1.54}$$

In the following, we will suppress the symbol $\lim_{\epsilon \to 0^+}$ and just write the above equation as

$$f(s) = \frac{1}{\pi} \int_{s_0}^\infty \frac{\text{Im } f(s')}{s' - s - i\epsilon} ds', \tag{1.55}$$

which appears usually in the literature. We should note that the function $f(s')$ is understood as the continuation to real axis from above the cut. Equation (1.55) is a form of an unsubtracted dispersion relation, which is based on the assumption that $f(z)$ falls off quickly for $|z| \to \infty$ so that there is no contribution for the integral along the circle. If this does not hold, or we want to reduce the dependence on Im $f(s')$ at large s', we may write a subtracted form. Defining

$$g(s) = \frac{f(s) - f(\bar{s})}{s - \bar{s}}, \tag{1.56}$$

where $\bar{s} < s_0$ is called the subtraction point, $g(s)$ will have the same analytic properties as above. Similarly, we will get

$$g(s) = \frac{1}{\pi} \int_{s_0}^\infty \frac{\text{Im } g(s')}{s' - s - i\epsilon} ds',$$

$$\begin{aligned}\frac{f(s)-f(\bar{s})}{s-\bar{s}} &= \frac{1}{\pi}\int_{s_0}^{\infty} ds' \frac{1}{s'-s-i\epsilon}\mathrm{Im}\,\left(\frac{f(s')-f(\bar{s})}{s'-\bar{s}}\right), \\ f(s) &= f(\bar{s}) + \frac{s-\bar{s}}{\pi}\int_{s_0}^{\infty} ds' \frac{\mathrm{Im}\ f(s')}{(s'-\bar{s})(s'-s-i\epsilon)}, \end{aligned} \tag{1.57}$$

where we have used Im $f(\bar{s}) = 0$.

One can apply the above method to a physical problem, say, a scattering process $a + b \to c + d$. Denoting the scattering amplitude by $\mathcal{T}$, we can perform a partial wave expansion (assuming they are all spin-0 particles for simplicity):

$$\mathcal{T}_{ab\to cd}(s, \cos\theta) = \sum_{l=0}^{\infty}(2l+1) f_l(s) P_l(\cos\theta), \tag{1.58}$$

where $\mathcal{T}$ has an explicit dependence on $s = (E_a + E_b)^2$ and the scattering angle θ in the CMS, $P_l(\cos\theta)$ is the standard Legendre polynomial, and $f_l(s)$ is the so-called partial-wave amplitude. From the dispersion theory discussed above, one can write $f_l(s)$ as

$$f_l(s) = \int_{s_0}^{\infty} \frac{\mathrm{Im}\ f_l(s')}{s'-s-i\epsilon} ds'. \tag{1.59}$$

To simplify the discussion, we confine ourselves to the unsubtracted form. In the region of the elastic scattering of the final particles $c + d \to c + d$ (final state interaction), one has the partial-wave expansion

$$\mathcal{T}_{cd\to cd}(s, \cos\theta) = \sum_{m=0}^{\infty}(2m+1) t_m(s) P_m(\cos\theta). \tag{1.60}$$

The partial-wave amplitude $f_l(s)$ is connected with $t_l(s)$ by

$$\mathrm{Im}\ f_l(s) = \sigma_{ab}\, t_l^*(s)\, f_l(s), \tag{1.61}$$

where $\sigma_{ab} = 2q_{\mathrm{cm}}/\sqrt{s}$ is the phase factor and q_{cm} is the modulus of the three-momentum in the CMS. Equation (1.61) is obtained from the optical theorem, see e.g., the derivation in Ref. [25]. For elastic scattering itself ($|cd\rangle = |ab\rangle$), one has

$$t_l(s) = \frac{1}{\sigma_{ab}}\ \sin\delta_l^{\mathrm{el}}\, e^{i\delta_l^{\mathrm{el}}}, \tag{1.62}$$

where δ_l^{el} denotes the (elastic) scattering phase shift. From Eq. (1.61) and Eq. (1.62), one finds a conclusion: for an elastic scattering, the phase of its partial-wave amplitude $f_l(s)$ (denoted by δ_l, $f_l = |f_l| e^{i\delta_l(s)}$) is equal to the (elastic) scattering phase shift δ_l^{el}. This is known as the Watson's final state interaction theorem [22], and more explicitly, it is written as

$$\mathrm{Im}\ f_l(s) = f_l(s) e^{-i\delta_l(s)} \sin\delta_l(s). \tag{1.63}$$

Here we will understand $\delta_l(s)$ as the elastic scattering phase shift of final states, and mostly, it is known and used as input for a pratical question.

With Eq. (1.63), Eq. (1.55) becomes

$$f_l(s) = \frac{1}{\pi}\int_{s_0}^{\infty} ds' \frac{f_l(s')e^{-i\delta_l(s')}\sin\delta_l(s')}{s'-s-i\epsilon}. \tag{1.64}$$

The solution to this integral equation is given by the Omnès function $\Omega(s)$ [23], up to a factor of a polynomial $P(s)$. Let us write it as $f(s) = P(s)\Omega(s)$, where we assume $\Omega(s)$ has no zeros on the cut, and the zeros of $f(s)$ can be absorbed into $P(s)$. In the following, we supress the partial wave l in the subscript, and concentrate at the derivation of the solution. The Schwartz reflection principle implies

$$e^{-2i\delta(s)}\Omega(s+i\epsilon) = \Omega(s-i\epsilon). \tag{1.65}$$

Taking the logarithm of Eq. (1.65), we get

$$D(s+i\epsilon) - D(s-i\epsilon) = 2i\delta(s), \tag{1.66}$$

with $D(s) \equiv \ln\Omega(s)$. Constructing a dispersion relation for $D(s)$, subtracted at $s=0$, we have

$$D(s) = \frac{s}{\pi}\int_{s_0}^{\infty} \frac{\delta(s')}{s'(s'-s-i\epsilon)} ds'. \tag{1.67}$$

Here once subtraction is appropriate for the case that $\delta(s)$ asymptotically goes to a constant for large s. Thus the expression for the Omnès function reads

$$\Omega(s) = \exp\left\{\frac{s}{\pi}\int_{s_0}^{\infty} \frac{\delta(s')}{s'(s'-s-i\epsilon)} ds'\right\}. \tag{1.68}$$

The above procedure can be generalized to the inhomogeneous condition [24] (for this reason we call it generalized Omnès problem)

$$\text{Im } f(s) = \left(f(s) + \hat{f}(s)\right) e^{-i\delta(s)}\sin\delta(s) \tag{1.69}$$

for s lying in the cut along the real axis, where $\hat{f}(s)$ is a real function. The solution to this case has been given in Ref. [24]. We provide a simple derivation, see Ref. [25]. For that purpose, let us define a function $g(s) = f(s)/\Omega(s)$. Since $\Omega(s)$ is analytic and non-zero on the complex plane with cut $[s_0,\infty)$ (called cut plane for short), $g(s)$ is also analytic on the cut plane. Then the imaginary part of $g(s)$ reads

$$\begin{aligned}
\text{Im } g(s) &= \frac{\text{Im}\left(f(s)\right)\text{Re}\left(\Omega(s)\right) - \text{Re}\left(f(s)\right)\text{Im}\left(\Omega(s)\right)}{|\Omega(s)|^2} \\
&= \frac{\text{Im}\left(f(s)\right)\Omega(s) - f(s)\text{Im}\left(\Omega(s)\right)}{|\Omega(s)|^2}
\end{aligned}$$

$$
\begin{aligned}
&= \frac{\Big(f(s)+\hat{f}(s)\Big)e^{-i\delta(s)}\sin\delta(s)\Omega(s) - f(s)\Omega(s)e^{-i\delta(s)}\sin\delta(s)}{|\Omega(s)|^2} \\
&= \frac{\hat{f}(s)e^{-i\delta(s)}\sin\delta(s)\Omega(s)}{|\Omega(s)|^2} = \frac{\hat{f}(s)\sin\delta(s)}{|\Omega(s)|}. \qquad (1.70)
\end{aligned}
$$

Thus we can write a n-times subtracted dispersion relation for $g(s)$ as

$$
g(s) = P_{n-1}(s) + \frac{(s-\bar{s})^n}{\pi}\int_{s_0}^{\infty} ds' \frac{\hat{f}(s')\sin\delta(s')}{|\Omega(s')|(s'-s)^n(s'-s-i\epsilon)}, \qquad (1.71)
$$

where $P_{n-1}(s)$ is a polynomial of order $n-1$. For the solution for $f(s)$, any solution for the homogeneous case can be added. And finally we have

$$
f(s) = \Omega(s)\left\{P(s) + \frac{(s-\bar{s})^n}{\pi}\int_{s_0}^{\infty} ds' \frac{\hat{f}(s')\sin\delta(s')}{|\Omega(s')|(s'-\bar{s})^n(s'-s-i\epsilon)}\right\}, \qquad (1.72)
$$

where $P(s)$ is a polynomial.

1.2.2 Treatments of final state interaction

A very simple treatment of final state interaction (FSI) effects was proposed by Watson and Migdal [27,28], which relates the total reaction amplitude A to the T-matrix elements of the two interacting final states by a constant. Explicitly,

$$
A = N_0 A_0 T, \qquad (1.73)
$$

where A_0 is the production amplitude without FSI effects and N_0 is a normalization constant. The treatment of Eq. (1.73) is a very crude approximation and only applicable for large scattering length. Close to the threshold, the invariant amplitude is dominated by the S-wave, and the the effective range expansion holds,

$$
\begin{aligned}
T &= \frac{1}{k\cot\delta - ik}, \\
k\cot\delta &= -\frac{1}{a} + \frac{1}{2}rk^2 + \mathcal{O}(k^4), \qquad (1.74)
\end{aligned}
$$

where a and r are the scattering length and effective range, respectively, and k is the momentum between the two interacting particles. Equation (1.73) then becomes

$$
A = N_0 A_0 \left[-\frac{1}{a} + \frac{rk^2}{2} - ik\right]^{-1}. \qquad (1.75)
$$

A better method for inclusion of FSI is the Jost function approach, where the enhancement factor at the level of amplitude is given by $1/\mathcal{J}(-k)$ [29]. As discussed above, one has the form of dispersion relation for $\mathcal{J}(k)$,

$$
\mathcal{J}(k) = 1 - \frac{1}{\pi}\int_{-\infty}^{\infty} dk' \frac{\mathcal{J}(k')e^{-i\delta(k')}\sin\delta(k')}{k'-k+i\epsilon}, \qquad (1.76)
$$

where the minus appears because the integration contour is chosen as the lower half plane including the real axis from $+\infty$ to ∞ and the infinite semicircle. There is the solution to Eq. (1.76) (see the Omnès function Eq. (1.68)),

$$\mathcal{J}(k) = \exp\left[-\frac{1}{\pi}\int_{-\infty}^{\infty} dk' \frac{\delta(k')}{k' - k + i\epsilon}\right], \tag{1.77}$$

From Eq. (1.74), we know the expression of δ,

$$\begin{aligned} \delta(k) &= \tan^{-1}\left[\frac{k}{-1/a + (r/2)k^2}\right] \\ &= \frac{i}{2}\ln\left[\frac{-1/a + (r/2)k^2 - ik}{-1/a + (r/2)k^2 + ik}\right] = \frac{i}{2}\ln\left[\frac{(k - i\beta_1)(k + i\beta_2)}{(k + i\beta_1)(k - i\beta_2)}\right], \end{aligned} \tag{1.78}$$

where β_1, β_2 are related to to a, r by

$$\begin{aligned} \frac{1}{2}r(\beta_1 - \beta_2) &= 1\,, \\ \frac{1}{2}r\beta_1\beta_2 &= -\frac{1}{a}\,. \end{aligned} \tag{1.79}$$

Then the Jost function, Eq. (1.77), can be calculated analytically, which reads

$$\mathcal{J}(k) = \frac{k - i\beta_2}{k - i\beta_1}. \tag{1.80}$$

Thus

$$\mathcal{J}(-k) = \frac{k + i\beta_2}{k + i\beta_1}, \tag{1.81}$$

and the enhancement factor is given by [29]

$$1/\mathcal{J}(-k) = \frac{(k^2 + \beta_1^2)r/2}{-1/a + (r/2)k^2 - ik}. \tag{1.82}$$

Equation (1.82) has the correct normalization, since in the limit $q \to \infty$ it tends to unity (as it should). This approach is improved through its numerator compared to Eq. (1.75), and concide with Eq. (1.75) for $q \ll \beta_1$. Equation (1.82) has been exploited, e.g., in Refs. [30–32] for extracting the ΛN scattering length. We stress that Eq. (1.74) has been used in the evaluation of the integral in Eq. (1.77). Thus, this approach is applicable under the assumption that the effective range expansion holds over the whole energy region.

Some more sophisticated forms are also available. From the viewpoint of field theory, we can write the amplitude as

$$A = A_0^{\rm on} + A_0^{\rm off} G_0 T, \tag{1.83}$$

where A_0 is the production amplitude of the whole process, and the superscripts "on" and "off" denote the on-shell and off-shell quantities, respectively, G_0 is the free Green function,

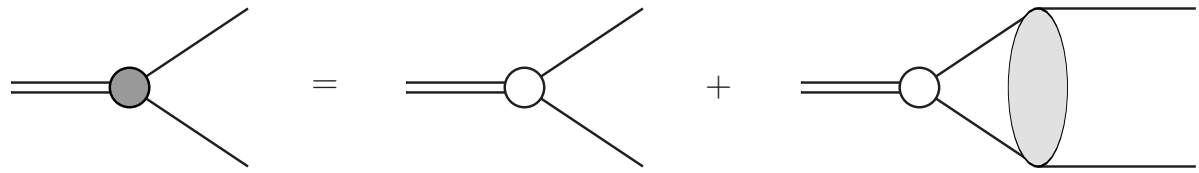

Figure 1.1: Inclusion of final state interaction (FSI) effects for a decay process $A \to B + C$. In the second figure, the white circle denotes a bare vertex for the production amplitude, corresponding to $A_0^{\rm on}$. In the third one the shaded area means the rescattering between the final states B and C, which corresponds to the part $A_0^{\rm off}G_0T$. Their sum is the total amplitude, denoted by a shaded circle in the first graph.

T is the scattering T-matrix element of the final states. Summing over the production part and the rescattering part, one will obtain the full amplitude A. Its diagrammatic interpretation is given by Fig. 1.1. For a reaction, once the amplitude A is known, the observables such as the differential cross section and/or cross section can be calculated. Up to present, Eq. (1.83) is exactly fulfilled since we have not imposed any assumptions. However, in an actual application, one needs to know the production mechanism A_0 well, and this is not the usual case. Assuming the production amplitude has only weak momentum dependence at near-threshold region, we will get

$$A = A_0(1 + G_0T), \tag{1.84}$$

where A_0 now is assumed as a constant and this overall normalization factor can be fixed by experiment. And normally one is only interested in the dynamical energy dependence and thus it has no much physical significance. The T-matrix elements in Eq. (1.84) is not limited to the effective range expansion, and can be calculated in a more realistic way. Thus it is improved compared Eq. (1.82). Besides, it can be applied to the inelastic channel, e.g., antiproton-proton ($\bar{p}p$) scattering which includes the annihilation dynamics (as discussed in Chap.4), in which case Eq. (1.82) fails.

From the discussions above, an important ingredient for inclusion of the FSI is the T-matrix elements of the final states. In Fig. 1.2, we show the differences between the various treatments of effective range expansion, the Jost function calculated from effective range expansion, Watson-Migdal approach, and the true Jost function. We normalize them to the value at origin. The $NN\,T$-matrix elements are calculated with the Bonn OBEPT model [33].

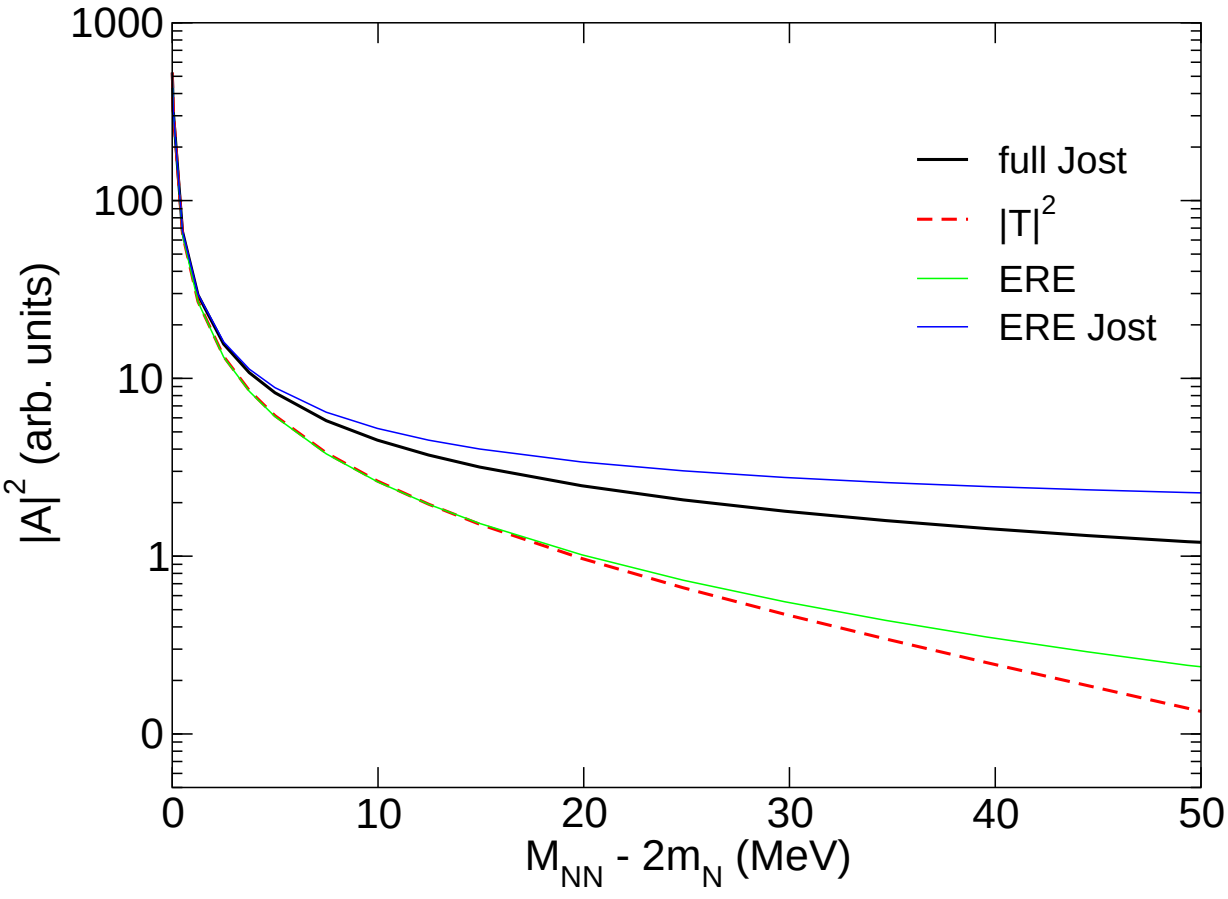

Figure 1.2: Illustration of final state interaction effects in NN system. ERE, ERE Jost, T^2 and full Jost correspond to Eqs. (1.75), (1.82), (1.73), (1.84), respectively. They are normalized to the value at the origin.

Part I

Semileptonic B meson decay

Chapter 2

B_{l4} decay and the extraction of $|V_{ub}|$ *

2.1 Introduction

Precisely determining the elements of the Cabibbo–Kobayashi–Maskawa (CKM) matrix [34] plays a very important role in testing the Standard Model. Any deviations from the unitarity of the CKM matrix would be viewed as a sign of new physics. The element $|V_{ub}|$ has been measured from inclusive charmless semileptonic B decay as well as from the exclusive decays $B \to \pi(\rho) l \bar{\nu}_l$. For a review on the determination of $|V_{ub}|$, see Ref. [35]. The value of $|V_{ub}|$ preferred by the current global analysis of CKM data is about 15% smaller than the one from inclusive charmless semileptonic B decays [36–38], a problem unresolved to date. Furthermore, the inclusive determinations of $|V_{ub}|$ are about two standard deviations larger than those obtained from $B \to \pi l \bar{\nu}$, with presently a smaller uncertainty. The value of $|V_{ub}|$ predicted from the measured CKM angle $\sin 2\beta$, however, is closer to the exclusive result [39], and it should be stressed that various theoretical extractions based on exclusive decays are remarkably consistent among each other [36, 40–43]. These discrepancies prompted a reexamination of the sources of theoretical uncertainty in the inclusive determination [44, 45].

In the present chapter, we investigate the four-body semileptonic decay mode $B^- \to \pi^+\pi^- l^- \bar{\nu}_l$ (which we will abbreviate as B_{l4} for short), and propose a method that allows one to extract $|V_{ub}|$ in a model-independent way. As a major step forward to a reliable treatment of the hadron-physics aspects of this decay, we use an approach based on dispersion theory without the need to explicitly match on specific resonance contributions or to separate these from non-resonant background. In fact, the cut range applied to the invariant mass of the pion pairs for selecting the ρ meson signal in the experimental analysis needs to be sufficiently large, and also, the S-wave contributions can not be be neglected [46]. Thus our approach presents a significant improvement compared to previous studies of $B \to \rho l \bar{\nu}_l$ [47], and should serve as a valuable cross-check for the inclusive determination. In the future the distributions derived below could be used directly in the Monte-Carlo generators of the experiments.

*The pertinent contents of this chapter has been published in Phys. Rev. D 89, 053015 (2014).

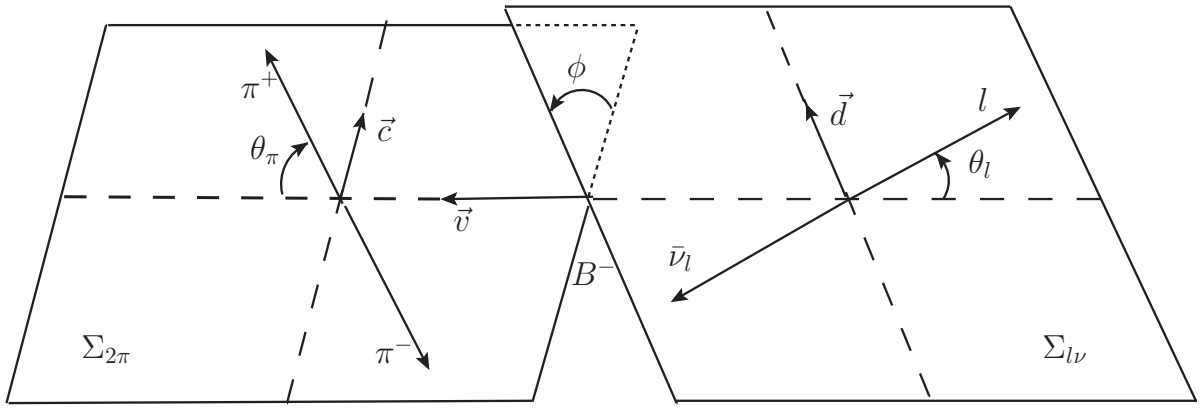

Figure 2.1: Illustration of the kinematical variables for B_{l4}.

We include the kinematic range for invariant masses of the $\pi\pi$ pair below the $K\bar{K}$ threshold in our analysis, and expand the form factors for the full B_{l4} transition matrix element in $\pi\pi$ partial waves up to P-waves; D- and higher partial waves have been checked to be negligible at these energies. While this model-independent description of the form factor dependence on the $\pi\pi$ invariant mass is in principle general and holds for arbitrary dilepton invariant masses, in practice we make use of matching to heavy-meson chiral perturbation theory to fix the normalization of the matrix element—a prerequisite for the extraction of $|V_{ub}|$. This scheme applies in the kinematics where heavy-quark effective field theory is valid, i.e. for very large dilepton invariant masses. We point to Ref. [48] for a lucid illustration of the different effective theories applicable in different kinematic regimes for this decay.

This chapter is organized as follows. In Sec. 2.2 the kinematics for the process of the four-body semileptonic B decay is reviewed, and the form factors for the hadronic transition of $B \to \pi\pi l\bar{\nu}_l$ are defined. In Sec. 2.3, we show in detail how to treat these form factors within dispersion theory: the analytic properties are summarized in Sec. 2.3.1, the required pole terms calculated in heavy-meson chiral perturbation theory in Sec. 2.3.2, before we provide the expressions for the various form factors in the Omnès representation in Sec. 2.3.3. We discuss the required matching to leading order heavy-meson chiral perturbation theory in Sec. 2.3.4. Numerical results are discussed in Sec. 3.5; we summarize our findings in Sec. 2.5. Some technical details are relegated to the appendices.

2.2 Kinematics, form factors, partial waves, decay rates

The kinematics of the process $B^-(p_B) \to \pi^+(p_+)\pi^-(p_-)l^-(p_l)\bar{\nu}_l(p_\nu)$ is described in terms of the five variables displayed in Fig. 2.1 [49–51]:

- the effective mass squared of the pion pair $s = (p_+ + p_-)^2 = M_{\pi\pi}^2$;
- the effective mass squared of the dilepton pair $s_l = (p_l + p_\nu)^2$;

- the angle θ_π of the π^+ in the $\pi^+\pi^-$ center-of-mass frame $\Sigma_{2\pi}$ with respect to the dipion line-of-flight in the B^- rest frame Σ_B;
- the angle θ_l of the charged lepton l in the lepton center-of-mass system $\Sigma_{l\nu}$ with respect to the dilepton line-of-flight in Σ_B;
- the angle ϕ between the dipion and dilepton planes.

Two additional Mandelstam variables are defined as

$$\begin{aligned} t &= (p_B - p_+)^2\,, \quad u = (p_B - p_-)^2\,, \\ \Sigma_0 &\equiv s + t + u = 2M_\pi^2 + m_B^2 + s_l\,. \end{aligned} \tag{2.1}$$

We define the combinations of four vectors $P = p_+ + p_-$, $Q = p_+ - p_-$, $L = p_l + p_\nu$, and make use of the kinematical relations

$$(PL) \equiv P \cdot L = \frac{m_B^2 - s - s_l}{2}\,, \quad t - u = -2\sigma_\pi X \cos\theta_\pi\,, \tag{2.2}$$

where

$$\sigma_\pi = \sqrt{1 - \frac{4M_\pi^2}{s}}\,, \quad X = \frac{1}{2}\lambda^{1/2}(m_B^2, s, s_l)\,, \tag{2.3}$$

and the Källén triangle function is given by $\lambda(a,b,c) = a^2 + b^2 + c^2 - 2(ab + ac + bc)$. The mathematical derivation for the kinematical relations is arranged into Sec. A.3. Some detailed calculation for the differential decay rates, especially for the four-body phase space can be found in Ref. [52]. A recent K_{e4} analysis has been done in Ref. [26].

We decompose the matrix element in terms of form factors according to

$$\begin{aligned} T &= \frac{G_F}{\sqrt{2}} V_{ub}^* \bar{v}(p_\nu)\gamma^\mu(1-\gamma_5)u(p_l) I_\mu\,, \\ I_\mu &= \langle \pi^+(p_+)\pi^-(p_-)|\bar{u}\gamma_\mu(1-\gamma_5)b|B^-(p_B)\rangle \\ &= -\frac{i}{m_B}(P_\mu F + Q_\mu G + L_\mu R) - \frac{H}{m_B^3}\epsilon_{\mu\nu\rho\sigma}L^\nu P^\rho Q^\sigma\,, \end{aligned} \tag{2.4}$$

where $G_F = 1.166365 \times 10^{-5}\,\mathrm{GeV}^{-2}$ is the Fermi constant, and we use the convention $\epsilon_{0123} = 1$. The first three terms correspond to the axial current part, whereas the last term corresponds to the vector current. The dimensionless form factors F, G, H, and R are analytic functions of three independent variables, e.g. s, s_l, and $t - u$. Their partial-wave expansions for fixed s_l read [49, 51]

$$\begin{aligned} F &= \sum_{l\geq 0} P_l(\cos\theta_\pi) f_l - \frac{\sigma_\pi (PL)}{X}\cos\theta_\pi G\,, \\ G &= \sum_{l\geq 1} P_l'(\cos\theta_\pi) g_l\,, \quad H = \sum_{l\geq 1} P_l'(\cos\theta_\pi) h_l\,, \end{aligned}$$

$$R = \sum_{l\geq 0} P_l(\cos\theta_\pi) r_l + \frac{\sigma_\pi s}{X}\cos\theta_\pi G\,, \tag{2.5}$$

where $P_l(z)$ are the standard Legendre polynomials and $P_l'(z) = dP_l(z)/dz$. An alternative set of form factors is given by

$$\begin{aligned} &F_1 = X\cdot F + \sigma_\pi (PL)\cos\theta_\pi G\,, \quad F_2 = G\,, \quad F_3 = H\,,\\ &F_4 = -(PL)F - s_l R - \sigma_\pi X\cos\theta_\pi G\,, \end{aligned} \tag{2.6}$$

whose partial-wave expansions

$$\begin{aligned} &F_1 = X\sum_{l\geq 0} P_l(\cos\theta_\pi) f_l\,, \qquad F_2 = \sum_{l\geq 1} P_l'(\cos\theta_\pi) g_l\,,\\ &F_3 = \sum_{l\geq 1} P_l'(\cos\theta_\pi) h_l\,, \qquad F_4 = \sum_{l\geq 0} P_l(\cos\theta_\pi)\tilde{r}_l\,, \quad \tilde{r}_l = -\big((PL) f_l + s_l r_l\big)\,, \end{aligned} \tag{2.7}$$

directly follow from Eqs. (2.5) and (2.6). Note that all partial waves f_l, g_l, h_l, r_l ($\tilde{r}_l$) are functions of s and s_l. The lowest angular-momentum $\pi\pi$ state contributing to the form factors F_2 and F_3 is the P-wave state, whereas the form factors F_1 and F_4 start with S-waves. For the partial-wave decomposition up to P-waves, we can therefore write

$$\begin{aligned} &F_1 = X\big[f_0(s,s_l) + f_1(s,s_l)\cos\theta_\pi + \ldots\big]\,,\\ &F_2 = g_1(s,s_l) + \ldots\,, \qquad F_3 = h_1(s,s_l) + \ldots\,,\\ &F_4 = \tilde{r}_0(s,s_l) + \tilde{r}_1(s,s_l)\cos\theta_\pi + \ldots\,, \end{aligned} \tag{2.8}$$

where the ellipses denote higher partial waves. In the following, we sometimes suppress the dependence on s_l in order to ease notation.

With the definition of Eq. (2.6), the partial decay rate can be written as [49]

$$\begin{aligned} d\Gamma_5 \;&=\; G_F^2 |V_{ub}|^2 (1-z_l)\sigma_\pi X/(2^{13}\pi^6 m_B^5) J_5(s, s_l, \theta_\pi, \theta_l, \phi)\\ &\quad\times ds\, ds_l\, d(\cos\theta_\pi)\, d(\cos\theta_l)\, d\phi, \end{aligned} \tag{2.9}$$

where

$$z_l \;=\; m_l^2/s_l, \tag{2.10}$$

$$\begin{aligned} J_5 \;=\;& 2(1-z_l)[I_1 + I_2\cos\theta 2\theta_l + I_3\sin^2\theta_l\cos 2\phi + I_4\sin 2\theta_l\cos\phi\\ &+I_5\sin\theta_l\cos\phi + I_6\cos\theta_l + I_7\sin\theta_l\sin\phi + I_8\sin 2\theta_l\sin\phi\\ &+I_9\sin^2\theta_l\sin 2\phi] \end{aligned} \tag{2.11}$$

and

$$\begin{aligned} I_1 \;&=\; \frac{1}{4}\{(1+z_l)|F_1|^2 + \frac{1}{2}(3+z_l)(|F_2|^2+|F_3|^2)\sin^2\theta_\pi + 2z_l|F_4|^2\},\\ I_2 \;&=\; -\frac{1}{4}(1-z_l)\{|F_1|^2 - \frac{1}{2}(|F_2|^2+|F_3|^2)\sin^2\theta_\pi\}, \end{aligned}$$

$$
\begin{aligned}
I_3 &= -\frac{1}{4}(1-z_l)\{|F_2|^2-|F_3|^2\}\sin^2\theta_\pi,\\
I_4 &= \frac{1}{2}(1-z_l)\mathrm{Re}(F_1^*F_2)\sin\theta_\pi,\\
I_5 &= -\{\mathrm{Re}(F_1^*F_3)+z_l\mathrm{Re}(F_4^*F_2)\}\sin\theta_\pi,\\
I_6 &= -\mathrm{Re}(F_2^*F_3)\sin^2\theta_\pi+z_l\mathrm{Re}(F_1^*F_4),\\
I_7 &= -\{\mathrm{Im}(F_1^*F_2)+z_l\mathrm{Im}(F_4^*F_3)\}\sin\theta_\pi,\\
I_8 &= \frac{1}{2}(1-z_l)\mathrm{Im}(F_1^*F_3)\sin\theta_\pi,\\
I_9 &= -\frac{1}{2}(1-z_l)\mathrm{Im}(F_2^*F_3)\sin^2\theta_\pi. \qquad (2.12)
\end{aligned}
$$

The form factors are independent on ϕ and θ_l, after integration over these two angles, it has the form

$$
\begin{aligned}
d\Gamma &= G_F^2|V_{ub}|^2N(s,s_l)J_3(s,s_l,\theta_\pi)ds\,ds_l\,d\cos\theta_\pi\,,\\
J_3(s,&s_l,\theta_\pi) = \frac{2+z_l}{3}|F_1|^2+z_l|F_4|^2\\
&+\frac{(2+z_l)\sigma_\pi^2 s\,s_l}{3}\left(|F_2|^2+\frac{X^2}{m_B^4}|F_3|^2\right)\sin^2\theta_\pi\,, \qquad (2.13)
\end{aligned}
$$

with

$$
N(s,s_l)=\frac{(1-z_l)^2\sigma_\pi X}{2(4\pi)^5m_B^5}\,. \qquad (2.14)
$$

In most of the available phase space (including the kinematic regime where chiral perturbation theory can be applied), the mass of the lepton can be neglected (i.e. $z_l \ll 1$), and the contribution of F_4 to the decay rate is therefore invisible in particular for B_{e4} decays, since it is always associated with a factor of z_l. We will not analyze the form factor F_4 and its partial waves $\tilde{r}_i$ in the following. Integrating Eq. (2.13) over $\cos\theta_\pi$ yields the partial decay rate $d\Gamma/(ds\,ds_l)$; neglecting terms of order z_l and inserting the partial-wave expansions Eq. (2.7), we find

$$
\begin{aligned}
\frac{d\Gamma}{ds\,ds_l} &= G_F^2|V_{ub}|^2N(s,s_l)J_2(s,s_l)\,,\\
J_2(s,s_l) &= \int_{-1}^{1}d\cos\theta_\pi J_3(s,s_l,\cos\theta_\pi)\\
&= \frac{4X^2}{3}\left(|f_0(s)|^2+\frac{1}{3}|f_1(s)|^2\right)\\
&+\frac{8}{9}\sigma_\pi^2 s\,s_l\left(|g_1(s)|^2+\frac{X^2}{m_B^4}|h_1(s)|^2\right)+\dots\,, \qquad (2.15)
\end{aligned}
$$

where the ellipsis denotes the neglected D- and higher waves. Interference terms between different partial waves vanish upon angular integration, such that the partial-wave contributions to the decay rate can be easily read off.

2.3 Form factors in dispersion theory

2.3.1 Analytic properties

The principle of maximal analyticity, which states that amplitudes possess no other singularities than those stemming from unitarity and crossing [53], tells us that the partial-wave amplitudes f_l, g_l, and h_l have the following analytic properties.

- At fixed s_l, they are analytic in the complex s plane, cut along the real axis for $s \geq 4M_\pi^2$ and $s \leq 0$. The presence of left-hand cuts $s \leq 0$ follows from the relations

$$t = \frac{\Sigma_0 - s}{2} - \sigma_\pi X \cos\theta_\pi \,,$$
$$t(\cos\theta_\pi = -1, s < 0) \geq (m_B + M_\pi)^2 \tag{2.16}$$

  (and equivalent expressions for u), since the form factors F, G, and H have cuts for t, $u \geq (m_B + M_\pi)^2$.

- In the interval $0 \leq s \leq 4M_\pi^2$, they are real.

- In the interval $4M_\pi^2 \leq s \leq 16M_\pi^2$, Watson's theorem [22] is satisfied and therefore the phases of the partial-wave amplitudes (f_l, g_l, h_l) coincide with the corresponding pion–pion scattering phases.

- For the crossed (t- and u-) channels, due to the lack of experimental information on πB phase shifts, we will approximate the πB interaction by B^* pole terms.

In practice, the range of validity of Watson's theorem can be extended to a larger domain, e.g. for the S-wave to $s \leq s_K = 4M_K^2 \approx 1\,\text{GeV}^2$, since inelasticities due to four or more pions are strongly suppressed both by phase space and by chiral symmetry. As pointed out e.g. in Refs. [54, 55], chiral perturbation theory predicts the inelasticity parameter of the $\pi\pi$ S- and P-waves to be of order p^8 below the $K\bar{K}$ threshold, while the corresponding scattering phase shifts are of order p^2. Phenomenological analyses of the $\pi\pi$ interactions show that final states containing more than two particles start playing a significant role only well above the $K\bar{K}$ threshold s_K [56]. Here we refrain from performing a coupled-channel study, which limits the applicability of our approach to the region below s_K. The subtleties associated with the strong onset of inelasticities in the S-wave in the vicinity of s_K (very close to the $f_0(980)$ resonance) for scalar form factors of the pion will be briefly discussed in Sec. 2.4.1.

We stress again the existence of B^* pole due to $m_{B^*} < m_B + m_\pi$, whereas the lowest excited $D^*(2007)^0$ state can decay to $D^0\pi^0$. Furthermore, from the fact that $M_\rho - M_\pi =$

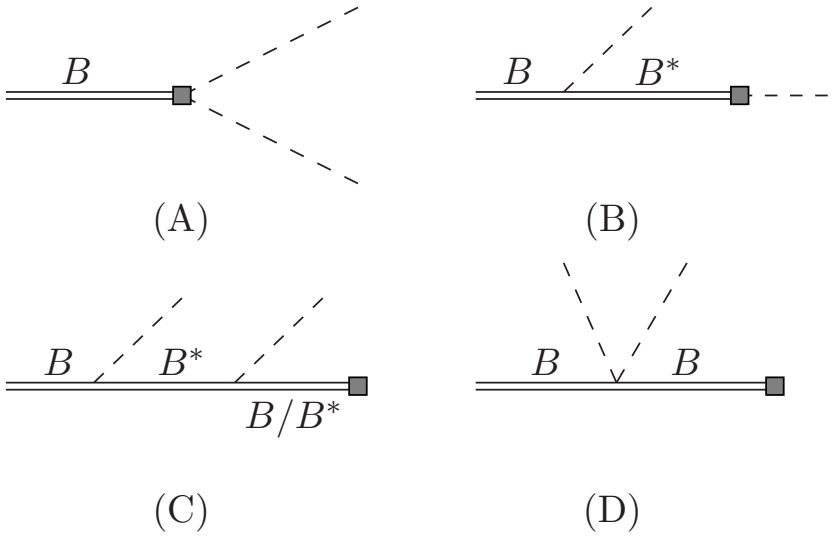

Figure 2.2: Leading-order diagrams for $B \to \pi\pi$ matrix elements of the hadronic current. Diagrams (B) and (C) contain u-channel pole terms. Solid double lines and dashed lines represent heavy mesons and pseudo-Goldstone bosons, respectively. The shaded square denotes an insertion of the left-handed leptonic current. Diagram (C) involves both $BB^*\pi$ and $B^*B^*\pi$ vertices.

635.92 MeV, $M_{K^*} - M_K = 397.983$ MeV, $m_{D^*} - m_D = 137.36$ MeV, $\Delta = m_{B^*} - m_B = 45.78$ MeV, we find the mass splitting between the spin-flip meson pairs decrease for the heavy quark systems. The mass splitting is attributed to the spin dependence of the interaction between quarks [57]. In Ref. [58], the authors calculated light and heavy pseudoscalar and vector mesons, based on the quark model with a spin-dependent potential motivated by QCD, and the good qualitative agreement with experiment is obtained.

2.3.2 Leading-order Feynman diagrams

In the process $B^- \to \pi^+\pi^- l^- \bar{\nu}_l$, u-channel contributions contain pole terms, while t-channel contributions do not. We obtain the pole terms by computing the leading-order diagrams (B) and (C) of Fig. 2.2 in the framework of heavy-meson chiral perturbation theory [11, 59, 60]. $f_\pi \simeq 92.2\,\text{MeV}$ is the pion decay constant [61]. The leading-order Lagrangian describing the interactions of the B family and the Goldstone bosons reads [11]

$$\begin{aligned}\mathcal{L} = &-i\,\mathrm{Tr}\bar{H}_a v_\mu \partial^\mu H_a + \frac{1}{2}\mathrm{Tr}\bar{H}_a H_b v^\mu \left(u^\dagger \partial_\mu u + u\partial_\mu u^\dagger\right)_{ba} \\ &+ \frac{ig}{2}\mathrm{Tr}\bar{H}_a H_b \gamma_\nu \gamma_5 \left(u^\dagger \partial^\nu u - u\partial^\nu u^\dagger\right)_{ba}. \end{aligned} \tag{2.17}$$

Determining the coupling $g = g_{B^*B\pi} = g_{B^*B^*\pi}$, using heavy-quark symmetry, from the partial decay width for $D^{*+} \to D^0\pi^+$ leads to $g = g_{D^*D\pi} = 0.58 \pm 0.07$, with the error

given by the uncertainty in the width of the D^{*+}. This is in surprisingly good agreement with the most recent lattice simulations, which find $g_{B^*B\pi} = 0.516 \pm 0.052$ [62] and $g_{B^*B\pi} = 0.569 \pm 0.076$ [63] (we have added different error sources in quadrature for simplicity in both cases). In the present analysis, we stick to the experimental number extracted from D^{*+} decays for illustration. The dominant parts of the B_{l4} amplitude will depend on g in a very simple manner (being directly proportional either to g or to g^2), thus suggesting a straightforward strategy towards an extraction of $|V_{ub}|$ via lattice calculations of $g_{B^*B\pi}$.

As stated in Chap. 1, we will include the $B^* - B$ mass splitting (which is in the order of $1/m_Q$) into the propagators (cf. Eq. (1.40)). We do not otherwise include heavy-quark-symmetry-breaking effects, and stick to Eq. (2.17) for the determination of the interaction vertices.

For the weak process here, it involves the left-handed current $L_{\nu a} = \bar{u}\gamma_\nu(1-\gamma_5)b$. At the zero order in the derivative expansion, it has the following form in chiral perturbation theory (cf. Sec. 1.1.2)

$$L_{\nu a} = i\sqrt{m_B} f_B (P^*_{b\nu} - v_\nu P_b) u^\dagger_{ba} \,, \tag{2.18}$$

where f_B is the B meson decay constant; averaging the most recent lattice calculations with 2+1 dynamical quark flavors leads to the very precise value $f_B = 190.5 \pm 4.2\,\mathrm{MeV}$ [64]. The whole B_{l4} decay amplitude is proportional to f_B, such that any uncertainty on this parameter directly translates into a contribution to the error in the extraction of $|V_{ub}|$.

We briefly discuss the chiral power counting of the B_{l4} amplitudes and form factors. If we denote soft pion momenta, or derivatives acting on the pion field, by p generically, the current of Eq. (2.18) is $\mathcal{O}(p^0)$, and so we expect to be the leading-order amplitude resulting from the diagrams in Fig. 2.2. Eq. (2.4) then suggests the leading contributions to the form factors F, G, H, and R to be of chiral orders p^{-1}, p^{-1}, p^{-2}, and p^0, respectively (remember that the dilepton momentum L_μ is large, of order m_B); the alternative form factors F_1 and F_4 both are $\mathcal{O}(p^0)$.

The results for the individual diagrams of Fig. 2.2 are given in Appendix A.1. In order to ensure that we do not miss any effects of the nontrivial analytic structure of triangle graphs, resulting from the B^* pole terms once rescattering between the two outgoing pions is taken into account, we keep the full relativistic form of the denominator part of the propagator. The latter is connected with the form of heavy-meson approximation by [12]

$$\begin{aligned} \frac{i}{2v\cdot k} &\longrightarrow \frac{-im_B}{(p_B-k)^2 - m_B^2} \,, \\ \frac{i}{2(v\cdot k + \Delta)} &\longrightarrow \frac{-im_{B^*}}{(p_B-k)^2 - m_{B^*}^2} \,, \end{aligned} \tag{2.19}$$

where $p_B = m_B v$ is the on-shell B meson momentum. Written in terms of s and s_l, the pole terms can then be easily identified as

$$\begin{aligned} F^{\mathrm{pole}} &= R^{\mathrm{pole}} - G^{\mathrm{pole}} \,, \quad R^{\mathrm{pole}} = \frac{\tilde{\alpha}}{u - m_{B^*}^2} \,, \\ F_2^{\mathrm{pole}} &= G^{\mathrm{pole}} = \frac{\tilde{\beta}}{u - m_{B^*}^2} \,, \; F_3^{\mathrm{pole}} = H^{\mathrm{pole}} = \frac{\tilde{\gamma}}{u - m_{B^*}^2} \,, \end{aligned}$$

$$\begin{aligned} F_1^{\text{pole}} &= X \cdot F_{\text{pole}} + \sigma_\pi (PL) \cos\theta_\pi G_{\text{pole}} \\ &= \frac{X(\tilde{\alpha} - \tilde{\beta}) + \sigma_\pi (PL) \cos\theta_\pi \tilde{\beta}}{u - m_{B^*}^2} , \end{aligned} \tag{2.20}$$

using the abbreviations

$$\begin{aligned} \tilde{\alpha} &\equiv -\frac{g^2 f_B m_B^2 m_{B^*}}{f_\pi^2 (m_B^2 - s_l)} \left(s - 2M_\pi^2\right) , \\ \tilde{\beta} &\equiv -\frac{g f_B m_B^2 m_{B^*}}{2 f_\pi^2} , \quad \tilde{\gamma} \equiv -\frac{g^2 f_B m_B^3 m_{B^*}^2}{f_\pi^2 (m_{B^*}^2 - s_l)} . \end{aligned} \tag{2.21}$$

All pole contributions start to contribute at the expected leading chiral orders. We note, though, that $\tilde{\alpha} = \mathcal{O}(p)$ is subleading to $\tilde{\beta} = \mathcal{O}(p^0)$ in F^{pole} and F_1^{pole}, and can be neglected; they are indeed partially an artifact of the translation of the heavy-meson formalism back into relativistic kinematics in the calculation of Ref. [59]. We will use the contributions $\propto \tilde{\alpha}$ in the partial waves f_i later on to illustrate potential higher-order effects, although these are neither complete nor necessarily dominant amongst the subleading contributions (cf. the discussion of the scaling behavior of higher-order terms in the current in Ref. [65]). For the purpose of the (s-channel) partial-wave projections to be performed later, the u-channel pole can be written in terms of s and $\cos\theta_\pi$

$$\begin{aligned} u(s, \cos\theta_\pi) - m_{B^*}^2 &= \sigma_\pi X (\cos\theta_\pi + y) , \\ y &= \frac{\Sigma_0 - s - 2m_{B^*}^2}{2\sigma_\pi X} . \end{aligned} \tag{2.22}$$

Finally, also the remaining, non-pole, parts of the amplitude can be extracted from the expressions in Appendix A.1. There are non-vanishing contributions to the form factor F_1 only, which in view of the required partial-wave expansion we write as

$$\begin{aligned} \frac{F_1(s)^{\chi\text{PT}} - F_1^{\text{pole}}}{X} &= M_0(s)^{\chi\text{PT}} + \frac{2\sigma_\pi \cos\theta_\pi}{X} M_1(s)^{\chi\text{PT}} , \\ M_0(s)^{\chi\text{PT}} &= -\frac{(1-g)^2 f_B m_B}{4 f_\pi^2} , \\ M_1(s)^{\chi\text{PT}} &= \frac{(1-g^2) f_B m_B}{4 f_\pi^2 (m_B^2 - s_l)} X^2 . \end{aligned} \tag{2.23}$$

$M_0(s)^{\chi\text{PT}}$ and $M_1(s)^{\chi\text{PT}}$ are found to be of chiral orders p^0 and p, respectively, and therefore suppressed by one order compared to the pole terms [65], as explained in Appendix A.1. We will use these expressions in Sec. 2.3.4 to match the polynomial parts of the dispersive representations of the corresponding amplitudes, but again rather in order to illustrate potential uncertainties due to subleading effects: these contributions are not complete even at the chiral order at which they occur.

To conclude this section, we point out that in order for the chiral counting scheme to work consistently, we have to assume the lepton invariant mass squared s_l to be large, of

the order of m_B^2. This limits the kinematic range of applicability of our approach to match the dispersive representation derived in the following to heavy-meson chiral perturbation theory.

2.3.3 Omnès representation

Having fixed the tree-level decay amplitude and in particular the pole terms, we proceed to analyze the effects of pion–pion rescattering using dispersion relations. This will give access to the s-dependence of the decay form factors (roughly up to 1 GeV, as detailed in Sec. 2.3.1) in a model-independent way. We will resort to the formalism based on Omnès representations as introduced in Ref. [24]. For its application to the closely related process of K_{l4} decays, see Refs. [25, 66]. Note, however, that everything discussed in the following is to be understood at fixed s_l: dispersion theory as applied here does not allow us to improve on the form factor dependence on the dilepton invariant mass, beyond what the chiral representation in the previous section includes. We emphasize once more that the dispersive aspect of our analysis is in principle independent of the matching to heavy-meson chiral perturbation theory: the validity of any theoretical description of the different form factors in the soft-pion limit ($s \approx 0$) can be extended at least to the whole kinematic region of elastic $\pi\pi$ scattering with this method.

We may write an alternative form of the partial-wave expansion Eq. (2.8) for the pole-term-subtracted amplitudes, neglecting terms beyond P-waves,

$$\begin{aligned}
\frac{F_1(s,t,u)}{X} &= \frac{F_1^{\text{pole}}}{X} + M_0(s) - \frac{(t-u)}{X^2} M_1(s)\,, \\
F_2(s,t,u) &= F_2^{\text{pole}} + U_1(s)\,, \\
F_3(s,t,u) &= F_3^{\text{pole}} + V_1(s)\,.
\end{aligned} \tag{2.24}$$

Here and in the following we suppress the dependence on s_l, which is kept fixed. The additional factor of X^2 in the definition of M_1 avoids the introduction of kinematic singularities at the zeros of X (in particular at the limit of the physical decay region $s = (m_B - \sqrt{s_l})^2$). The functions M_0, M_1, U_1, and V_1 defined this way possess right-hand unitarity branch cuts as their only non-trivial analytic structure, and no poles. Since the pole terms F_1^{pole}/X, F_2^{pole}, F_3^{pole} are real, one immediately finds

$$\begin{aligned}
&\operatorname{Im} f_0(s) = \operatorname{Im} M_0(s)\,, \quad \operatorname{Im}\Big(\frac{X}{2\sigma_\pi} f_1\Big) = \operatorname{Im} M_1(s)\,, \\
&\operatorname{Im} g_1(s) = \operatorname{Im} U_1(s)\,, \quad \operatorname{Im} h_1(s) = \operatorname{Im} V_1(s)\,,
\end{aligned} \tag{2.25}$$

which allows us to write

$$\begin{aligned}
&f_0(s) = M_0(s) + \hat{M}_0(s)\,, \;\; f_1(s) = \frac{2\sigma_\pi}{X}\big(M_1(s) + \hat{M}_1(s)\big)\,, \\
&g_1(s) = U_1(s) + \hat{U}_1(s)\,, \quad h_1(s) = V_1(s) + \hat{V}_1(s)\,.
\end{aligned} \tag{2.26}$$

The real "hat functions" $\hat{M}_0(s)$, $\hat{M}_1(s)$, $\hat{U}_1(s)$, and $\hat{V}_1(s)$ are the partial-wave projections of the pole terms given in Eqs. (2.20)–(2.21), which explicitly read

$$\begin{aligned}
\hat{M}_0(s) &= \frac{\xi\, Q_0(y) + (PL)\tilde{\beta}}{X^2}\,, \quad \hat{M}_1(s) = -\frac{3\xi}{2\sigma_\pi X} Q_1(y)\,, \\
\xi &= \frac{X}{\sigma_\pi}(\tilde{\alpha} - \tilde{\beta}) - (PL) y \tilde{\beta}\,, \\
\hat{U}_1(s) &= \frac{\tilde{\beta}}{\sigma_\pi X}\Big(Q_0(y) - Q_2(y)\Big)\,, \\
\hat{V}_1(s) &= \frac{\tilde{\gamma}}{\sigma_\pi X}\Big(Q_0(y) - Q_2(y)\Big)\,,
\end{aligned} \tag{2.27}$$

where the $Q_l(y)$ are Legendre functions of the second kind,

$$\begin{aligned}
Q_l(y) &= \frac{1}{2}\int_{-1}^{1} \frac{dz}{y-z} P_l(z)\,, \\
(-1)^l Q_l(z') &= \frac{1}{2}\int_{-1}^{1} \frac{dz}{z'+z} P_l(z)\,.
\end{aligned} \tag{2.28}$$

Explicitly, the first three of these read

$$\begin{aligned}
Q_0(y) &= \frac{1}{2}\log\frac{y+1}{y-1}\,, \quad Q_1(y) = y Q_0(y) - 1\,, \\
Q_2(y) &= \frac{3y^2-1}{2} Q_0(y) - \frac{3}{2} y\,.
\end{aligned} \tag{2.29}$$

We have projected onto the partial waves of F_2 and F_3 (whose partial-wave expansions proceed in *derivatives* of Legendre polynomials, see Eq. (2.7)) using

$$\int_{-1}^{1} P_i'(z)\big[P_{j-1}(z) - P_{j+1}(z)\big]dz = 2\delta_{ij}\,. \tag{2.30}$$

From Eq. (2.30) one gets

$$\begin{aligned}
g_1(s, s_l) &= \frac{1}{2}\int_{-1}^{1} F_2(s, \cos\theta_\pi)[1 - P_2(\cos\theta_\pi)] d(\cos\theta_\pi)\,, \\
g_2(s, s_l) &= \frac{1}{2}\int_{-1}^{1} F_2(s, \cos\theta_\pi)[\cos\theta_\pi - P_3(\cos\theta_\pi)] d(\cos\theta_\pi)\,.
\end{aligned} \tag{2.31}$$

An alternative orthogonality relation is also available,

$$\int_{-1}^{1} P_k'(x) P_l'(x) dx = \begin{cases} 0, & \text{for } k+l = \text{odd numbers} \\ l(l+1), & \text{for } k+l = \text{even numbers and } k \geq l \end{cases}\,,$$

from which we have

$$\begin{aligned} g_1(s,s_l) &= \frac{3}{5}\int_{-1}^{1} F_2(s,\cos\theta_\pi)P_1'(\cos\theta_\pi)d(\cos\theta_\pi) \\ &\quad -\frac{1}{10}\int_{-1}^{1} F_2(s,\cos\theta_\pi)P_3'(\cos\theta_\pi)d(\cos\theta_\pi)\,, \\ g_2(s,s_l) &= \frac{5}{21}\int_{-1}^{1} F_2(s,\cos\theta_\pi)P_2'(\cos\theta_\pi)d(\cos\theta_\pi) \\ &\quad -\frac{1}{14}\int_{-1}^{1} F_2(s,\cos\theta_\pi)P_4'(\cos\theta_\pi)d(\cos\theta_\pi)\,. \end{aligned} \tag{2.32}$$

An easy bookkeeping can show Eq. (2.31) and Eq. (2.32) are equivalent. Note that, in order to show that the partial-wave-projected pole terms above indeed are real everywhere along the right-hand cut, i.e. for all $s \geq 4M_\pi^2$, care has to be taken about the correct analytic continuation. For example, X, only defined unambiguously in the physical decay region in Eq. (2.3), is continued according to [67, 68]

$$X = \begin{cases} |X|\,, & s \in \left[4M_\pi^2, (m_B - \sqrt{s_l})^2\right], \\ i|X|\,, & s \in \left[(m_B - \sqrt{s_l})^2, (m_B + \sqrt{s_l})^2\right], \\ -|X|\,, & s \in \left[(m_B + \sqrt{s_l})^2, \infty\right) \end{cases} \tag{2.33}$$

(where the last range is of no practical relevance for our dispersive integrals). Furthermore, in the range of $(m_B - \sqrt{s_l})^2 < s < (m_B + \sqrt{s_l})^2$, the argument y of the Legendre functions of the second kind becomes purely imaginary; the lowest one can be expressed as $Q_0(y) = i(\pi/2 - \arctan|y|)$. In particular, no singularities arise at the zeros of X, $s = (m_B \pm \sqrt{s_l})^2$. Physically, the reality of the pole terms is based on the fact that the B^* cannot go on its mass shell in any kinematic configuration.

In the elastic regime, the right-hand cut of the partial waves f_i ($i = 0, 1$), g_1, h_1 for $s > 4M_\pi^2$ is given by discontinuity equations relating them to the elastic $\pi\pi$ partial-wave amplitudes $t_i^i(s)$, $i = 0, 1$,[1] according to

$$\begin{aligned} \mathrm{disc}\, f_i(s) &= f_i(s+i\epsilon) - f_i(s-i\epsilon) = 2i\,\mathrm{Im}\, f_i(s) \\ &= 2i\sigma_\pi f_i(s)\left[t_i^i(s)\right]^* = f_i(s)e^{-i\delta_i^i(s)}\sin\delta_i^i(s)\,, \end{aligned} \tag{2.34}$$

where we have expressed $t_i^i(s)$ in terms of the corresponding phase shift $\delta_i^i(s)$ in the usual way. Analogous equations hold for g_1 and h_1. Eq. (2.34) implies Watson's theorem: the

[1] We use this somewhat unusual notation owing to the fact that we only consider S- and P-waves, and isospin $I = 2$ is not allowed. From the viewpoint of the strong interaction, any pion pairs can be regarded as identical bosons, and Bose symmetry can be applied, which requires $l + S + I$ is a even number. Thus the S-wave is associated with $I = 0$ while the P-wave corresponds to $I = 1$. The absence of isospin $I = 2$ is caused by that the isospin of both the current and B meson is $1/2$, and therefore, they can only couple to $I = 0$ or $I = 1$. Do not be confused with $\Delta I = 1/2$ rule, which concerns for the non-leptonic decays.

phase of the partial wave equals the elastic phase shift. From Eqs. (2.25) and (2.26), one finds

$$\mathrm{Im}\, M_i(s) = \Big(M_i(s) + \hat{M}_i(s)\Big)\, e^{-i\delta_i^i(s)} \sin\delta_i^i(s)\,, \tag{2.35}$$

and similarly for $U_1(s)$, $V_1(s)$.

Eq. (2.35) demonstrates that the hat functions constitute inhomogeneities in the discontinuity equations. The solution is given by [24]

$$M_i(s) = \Omega_i^i(s)\left\{P_{n-1}(s) + \frac{s^n}{\pi}\int_{4M_\pi^2}^\infty \frac{\hat{M}_i(s')\sin\delta_i^i(s')ds'}{|\Omega_i^i(s')|(s'-s-i\epsilon)s'^n}\right\}, \tag{2.36}$$

where $P_{n-1}(s)$ is a subtraction polynomial of degree $n-1$, and the Omnès function is defined as [23]

$$\Omega_l^I(s) = \exp\left\{\frac{s}{\pi}\int_{4M_\pi^2}^\infty \frac{\delta_l^I(s')ds'}{s'(s'-s-i\epsilon)}\right\}. \tag{2.37}$$

The standard Omnès solution $P_{n-1}(s)\Omega_i^i(s)$ of the *homogeneous* discontinuity equation ($\hat{M}_i = 0$), valid for form factors without any left-hand pole or cut structures, is modified by a dispersion integral over the inhomogeneities $\hat{M}_i$, which in the present case are given by the partial-wave projected pole terms.

The minimal order of the subtraction polynomial is dictated by the requirement of the dispersive integral to converge. First we note that, if the phase $\delta_l^I(s)$ asymptotically approaches a constant value $c\pi$, then the corresponding Omnès function falls off asymptotically $\sim s^{-c}$. We will assume both $\pi\pi$ input phases to approach π for large energies,

$$\delta_0^0(s) \longrightarrow \pi\,, \quad \delta_1^1(s) \longrightarrow \pi\,, \tag{2.38}$$

such that $\Omega_0^0(s)$, $\Omega_1^1(s) \sim 1/s$ for large s.

A more problematic question concerns the behavior of the hat functions for large s. In principle, this is entirely determined by the partial-wave-projected B^* pole terms as given in Eq. (2.27). However, as we have decided to include the *relativistic* pole graphs, these explicitly contain the scale m_B, and the asymptotic behavior is only reached for $\sqrt{s} \gg m_B$ — far too high a scale, given that we realistically know the pion–pion phase shifts only up to well below 2 GeV, and that we presently neglect all inelastic contributions, which set in above 1 GeV. We can formally remedy this problem by just considering the large-s behavior of the heavy-meson approximation of the pole terms,[2] in which m_B only features parametrically as a prefactor; being aware that corrections to the heavy-meson approximation scale like $\sqrt{s}/m_B$, which is not a very small quantity in the region of $1\,\mathrm{GeV} \lesssim \sqrt{s} \lesssim 2\,\mathrm{GeV}$, say. In the heavy-meson approximation, i.e., at leading order in an expansion of $1/m_B$, the inhomogeneities of Eq. (2.27) behave according to

$$\hat{M}_0(s) \sim s^{-1/2}\,, \qquad\qquad \hat{M}_1(s) \sim s^0\,,$$

[2]Remember that we made use of the relativistic pole terms mainly to ensure the correct analytic properties at *low* energies, i.e. in the near-threshold region.

$$\hat{U}_1(s) \sim s^{-1/2}\,, \qquad\qquad \hat{V}_1(s) \sim s^{-1/2}\,. \tag{2.39}$$

Together with the large-s behavior of the Omnès functions, we conclude that the representation for $M_1(s)$ requires at least two subtractions, while for $M_0(s)$, $U_1(s)$, and $V_1(s)$, one subtraction each seem to be sufficient. However, looking at the behavior of the various hat functions in the low-energy region in Fig. 2.3 (for a special value of $s_l = (m_B - 1\,\text{GeV})^2$), we note that the falling of $\hat{M}_0(s)$, $\hat{U}_1(s)$, and $\hat{V}_1(s)$ barely seems to set in in the kinematical region $s \lesssim 1\,\text{GeV}^2$ where we have to assume the spectral function to be saturated, while $\hat{M}_1(s)$ even grows at those energies instead of approaching a constant value. It seems therefore advisable to oversubtract all the dispersive representations once, such as to allow for two subtraction constants each for $M_0(s)$, $U_1(s)$, and $V_1(s)$, and three for $M_1(s)$. This way, inelastic contributions at higher energies that we do not take into account explicitly should also be more effectively suppressed. The complete set of dispersion relations of the Omnès type therefore reads

$$\begin{aligned}
M_0(s) &= \Omega_0^0(s)\left\{a_0 + a_1 s + \frac{s^2}{\pi}\int_{4M_\pi^2}^\infty \frac{\hat{M}_0(s')\sin\delta_0^0(s')ds'}{|\Omega_0^0(s')|(s'-s-i\epsilon)s'^2}\right\},\\
M_1(s) &= \Omega_1^1(s)\left\{a_0' + a_1' s + a_2' s^2 + \frac{s^3}{\pi}\int_{4M_\pi^2}^\infty \frac{\hat{M}_1(s')\sin\delta_1^1(s')ds'}{|\Omega_1^1(s')|(s'-s-i\epsilon)s'^3}\right\},\\
U_1(s) &= \Omega_1^1(s)\left\{b_0 + b_1 s + \frac{s^2}{\pi}\int_{4M_\pi^2}^\infty \frac{\hat{U}_1(s')\sin\delta_1^1(s')ds'}{|\Omega_1^1(s')|(s'-s-i\epsilon)s'^2}\right\},\\
V_1(s) &= \Omega_1^1(s)\left\{c_0 + c_1 s + \frac{s^2}{\pi}\int_{4M_\pi^2}^\infty \frac{\hat{V}_1(s')\sin\delta_1^1(s')ds'}{|\Omega_1^1(s')|(s'-s-i\epsilon)s'^2}\right\}.
\end{aligned} \tag{2.40}$$

The subtraction constants are *a priori* unknown, and need to be determined either by further theoretical input, or by fitting to experimental data. It is easy to check that the functions $M_0(s)$, …, $V_1(s)$ themselves do not satisfy Watson's theorem; however, taking into account Eq. (2.26), the partial-wave amplitudes f_0 (f_1, g_1, h_1) do, i.e., their phases equal the elastic scattering phases δ_0^0 (δ_1^1).

We add a few further remarks concerning Fig. 2.3. All of the partial-wave-projected pole terms display singular behavior of square-root type at $s = 0$ (suppressed as $s^{3/2}$ in the case of $\hat{M}_1(s)$; note that also $\hat{M}_0(s)$ has a square-root singularity, which is hard to discern in Fig. 2.3 due to the axis scaling). These left-hand singularities obviously carry over to the partial waves: close to the $\pi\pi$ threshold, the partial-wave amplitudes cannot be represented by simple scalar or vector form factors.

The uncertainty bands for $\hat{M}_i(s)$, $i = 0, 1$, in Fig. 2.3 indicate the effect of the (incomplete) higher-order contribution $\propto \tilde{\alpha}$ in Eq. (2.27), suppressed by $1/m_B$ and found to be surprisingly small. We do *not* include the uncertainty due to the overall scaling with the coupling constant g, which translates directly into an uncertainty of a projected

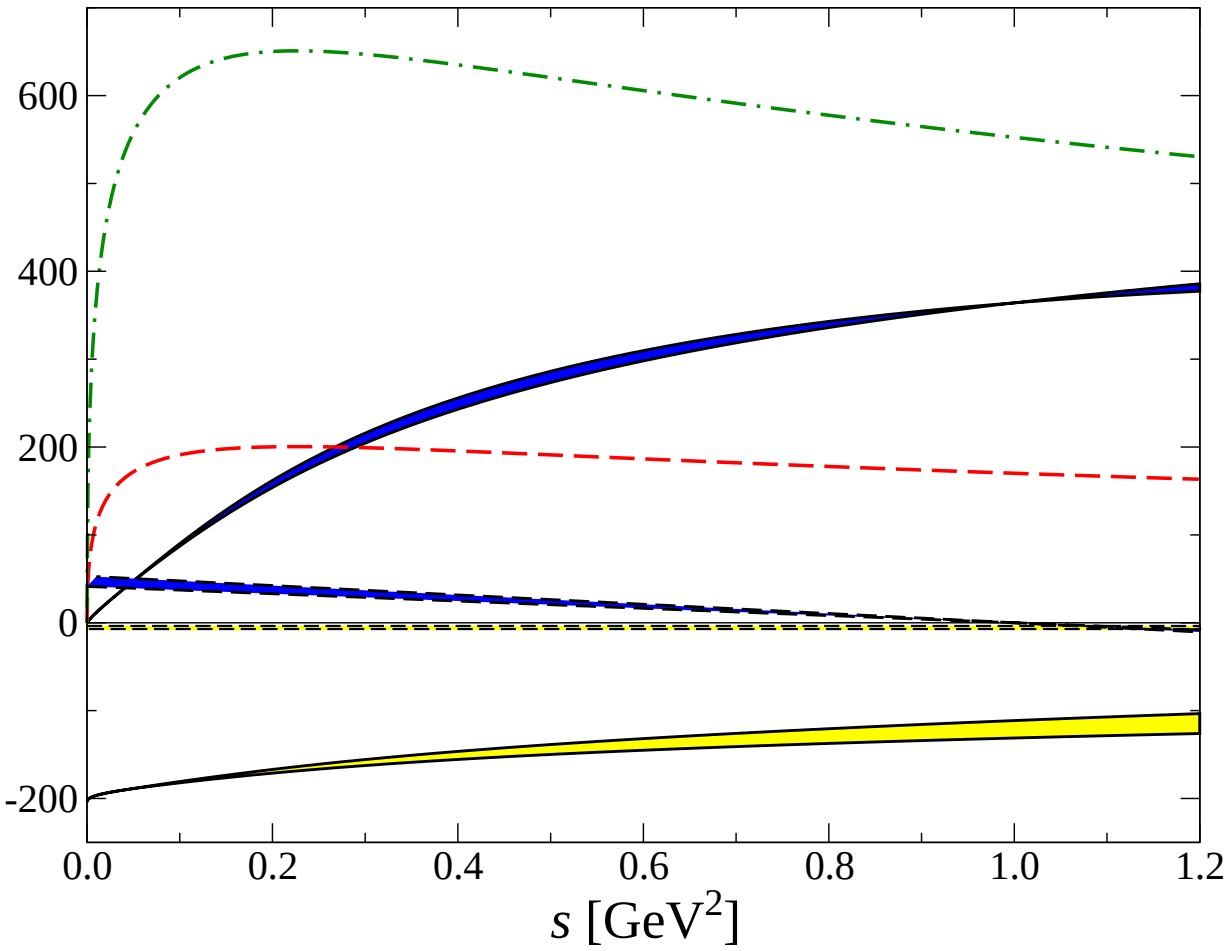

Figure 2.3: Hat functions $\hat{M}_0(s)$ (yellow band with full lines), $\hat{M}_1(s)$ (blue band with full lines), $\hat{U}_1(s)$ (red dashed line), and $\hat{V}_1(s)$ (green dot-dashed line), for $s_l = (m_B - 1\,\text{GeV})^2$. We also show the polynomial contributions to the form factor F_1/X, for S- (yellow band with dashed lines) and P-wave (blue band with dashed lines), which are seen to be strongly suppressed. $\hat{M}_1(s)$ as well as the P-wave polynomial $M_1(s)^{\chi\text{PT}}$ are given in units of GeV^{-2}, all other functions are dimensionless.

extraction of $|V_{ub}|$, but does not (at this order) affect the *shape* of the distributions. The inhomogeneities scale with g according to $\hat{M}_i(s)$, $\hat{U}_1(s) \propto g$, $\hat{V}_1(s) \propto g^2$.

The dispersive method using inhomogeneities as described above has by now been used for a variety of low-energy processes, such as $\eta \to 3\pi$ [24, 69], $\omega/\phi \to 3\pi$ [70], $K \to \pi\pi$ [71], K_{l4} [25, 66], $\gamma\gamma \to \pi\pi$ [72, 73], or $\gamma\pi \to \pi\pi$ [74, 75]. In several of those cases, the inhomogeneities (given in terms of hat functions), which incorporate left-hand-cut structures, and the amplitudes given in terms of Omnès-type solutions with a right-hand cut only are calculated iteratively from each other, until convergence is reached. In our present analysis, the ansatz is comparably simpler, as the left-hand cut is approximated by pole terms, whose partial-wave projections then determine the inhomogeneities. This is closely related to the method of Ref. [72] for $\gamma\gamma \to \pi\pi$, where the left-hand structures are approximated by Born terms and resonance contributions to $\gamma\pi \to \gamma\pi$.

2.3.4 Matching the subtraction constants

We need to consider two essentially different contributions to the subtraction constants in the representation Eq. (2.40), writing them formally as

$$a_i = \bar{a}_i + \hat{a}_i \,, \tag{2.41}$$

and similar decompositions for the a_i', b_i, and c_i. We discuss the contributions $\hat{a}_i$ etc. first. We argue in Appendix A.2 that for inhomogeneities of essentially constant ($\hat{M}_0$, $\hat{U}_1$, $\hat{V}_1$) or approximately linear ($\hat{M}_1$) behavior over a large part of the kinematical region of interest, the coefficients of the highest power in the subtraction polynomials (a_1, a_2', b_1, and c_1) need to be adjusted in order to provide a reasonable high-energy behavior.[3] These coefficients are given by the derivative of the corresponding Omnès function at $s = 0$, multiplied with the constant/the derivative of the inhomogeneity in question. Obviously, the hat functions are not exactly constant/linear: to the contrary, they include square-root singularities at $s = 0$ due to the left-hand cut. There is, therefore, necessarily an uncertainty due to the choice of a "matching point" s_m at which to evaluate these "constants",

$$\begin{aligned} \hat{a}_1 &= \hat{M}_0(s_m) \times \dot{\Omega}_0^0(0) \,, & \hat{a}_2' &= \frac{\hat{M}_1(s_m)}{s_m} \times \dot{\Omega}_1^1(0) \,, \\ \hat{b}_1 &= \hat{U}_1(s_m) \times \dot{\Omega}_1^1(0) \,, & \hat{c}_1 &= \hat{V}_1(s_m) \times \dot{\Omega}_1^1(0) \,. \end{aligned} \tag{2.42}$$

We choose $s_m = M_\rho^2$, due to the expected strong enhancement of the distribution at the ρ resonance peak. Here, $\dot{\Omega}_l^I(0) = d\Omega_l^I(s)/ds|_{s=0}$. All other subtraction constants do not receive "hat" contributions.

[3] This can be corroborated to some extent by arguments from Brodsky–Lepage quark counting rules [76] and soft-collinear effective theory [77], albeit in kinematic regions with completely different scaling of s_l with respect to m_B^2 (taken as fixed and not particularly large here). Assuming the large-s behavior of the different form factors and partial waves is independent thereof, we indeed need to require the leading powers in s to cancel between the dispersion integrals over the inhomogeneities and the subtraction polynomial.

The second contribution to the subtraction constants, dominantly to those of *low* polynomial order in s, stems from matching to the non-pole part of the chiral amplitude Eq. (2.23), which yields (for fixed s_l) a polynomial contribution in s. In this exploratory study we use the leading-order expressions only. We expect the chiral expansion to converge best at the sub-threshold point $s = 0$, as opposed to, e.g., the $\pi\pi$ threshold [78].

As we match the dispersive representation Eq. (2.40) to the leading chiral *tree-level* amplitude, which does not contain any rescattering/loop corrections, we identify the subtraction constants $\bar{a}_{0-1}$, $\bar{a}'_{0-2}$ by setting the scattering phases to zero, i.e., $\Omega_i^i(s) \equiv 1$, and the dispersive integrals over the inhomogeneities vanish. At $s = 0$, we find from Eq. (2.23)

$$\begin{aligned}
\bar{a}_0 &= -\frac{(1-g)^2 f_B m_B}{4f_\pi^2}\,, & \bar{a}_1 &= 0\,,\\
\bar{a}'_0 &= \frac{(1-g^2) f_B m_B}{16 f_\pi^2}\big(m_B^2 - s_l\big)\,, & &\\
\bar{a}'_1 &= -\frac{(1-g^2) f_B m_B}{8 f_\pi^2}\frac{m_B^2 + s_l}{m_B^2 - s_l}\,, & \bar{a}'_2 &= \frac{(1-g^2) f_B m_B}{16 f_\pi^2 (m_B^2 - s_l)}\,.
\end{aligned} \tag{2.43}$$

The term $\propto \bar{a}'_2 s^2$, stemming from the expansion of X^2, is chirally suppressed and could as well be neglected. F_2 and F_3 at leading order coincide with their pole terms, thus the matching implies the parameters $\bar{b}_i$ and $\bar{c}_i$ to vanish.

In order to illustrate the relative importance of the (partial-wave projected) pole terms relative to the subtraction polynomial—that is, the decompositions $M_i(s) + \hat{M}_i(s)$ on tree level, for $i = 0,\, 1$ — we also show these, for $s_l = (m_B - 1\,\mathrm{GeV})^2$, in Fig. 2.3. We verify the expected dominance of the pole terms/the hat functions in $f_0(s)$ and $f_1(s)$, as suggested by power counting arguments. For the uncertainty bands of the polynomial corrections with mixed dependence on g, we have varied this coupling within its assumed uncertainty, $g = 0.58 \pm 0.07$.

Remember that $g_1(s)$ and $h_1(s)$ consist of B^* pole terms only at leading order: this pole dominance should have very favorable consequences for the reliability of the form factor prediction, as the pole contributions are essentially fixed by the coupling constant g (as well as f_B) beyond the chiral expansion; the latter affects only the precision of the polynomial contribution. Next-to-leading-order corrections to the residues of the pole terms seem to have surprisingly little effect.

2.4 Results

2.4.1 Scattering phase input

The $\pi\pi$ phase shifts are known to sufficient accuracy in the region $s \lesssim s_0 \equiv (1.4\ \mathrm{GeV})^2$ (cf. Refs. [79, 80]). In order to ensure the assumed asymptotic behavior $\delta_0^0(s)$, $\delta_1^1(s) \to \pi$ for $s \to \infty$, we continue the phases beyond s_0 according to the prescription [81]

$$\delta_i^i(s \geq s_0) = \pi + \big(\delta_i^i(s_0) - \pi\big) f\Big(\frac{s}{s_0}\Big)\,,\ f(x) = \frac{2}{1 + x^{3/2}}\,. \tag{2.44}$$

There is a further subtlety concerning the S-wave phase shift: as we have discussed in Sec. 2.3.1, the elastic approximation breaks down at the $K\bar{K}$ threshold s_K with the occurrence of the $f_0(980)$ resonance. Both the phase of the partial wave $\arg t_0^0(s)$ and, e.g., the phase of the non-strange scalar form factor of the pion $\arg F_\pi^S(s)$ differ significantly from $\delta_0^0(s)$ in this region: they quickly drop and then roughly follow the energy dependence of $\delta_0^0(s)$ again, with $\delta_0^0(s) - \arg t_0^0(s) \approx \delta_0^0(s) - \arg F_\pi^S(s) \approx \pi$ [82]. Therefore a single-channel approximation to the pion scalar form factor only works for $s < s_K$ if a phase of the form of either $\arg t_0^0(s)$ or $\arg F_\pi^S(s)$ are used as input to the Omnès function instead of $\delta_0^0(s)$. We use such a form factor phase taken from Ref. [83]. Obviously, we cannot provide a reliable description of pion–pion rescattering effects where the inherent two-channel nature of the problem becomes important, hence our dispersive description is confined to below s_K.

With the phase shift input thus continued formally up to infinity, the Omnès integrals can be fully performed. We have checked that different continuation prescriptions from the one given in Eq. (2.44) above s_0 have very little impact on the physics at low energies, i.e., below 1 GeV.

The phase input allows us to evaluate the derivatives of the Omnès functions required in Eq. (2.42) via the sum rules

$$\dot{\Omega}_l^I(0) = \frac{1}{\pi}\int_{4M_\pi^2}^\infty ds' \frac{\delta_l^I(s')}{s'^2}\,, \tag{2.45}$$

leading to $\dot{\Omega}_0^0(0) = 2.5\,\mathrm{GeV}^{-2}$, $\dot{\Omega}_1^1(0) = 1.8\,\mathrm{GeV}^{-2}$ (cf. Sec. A.4). This corresponds to squared radii of the pion scalar and vector form factors $\langle r_S^2\rangle = 0.58\,\mathrm{fm}^2$, $\langle r_V^2\rangle = 0.42\,\mathrm{fm}^2$, both only around 5% below the central values of more sophisticated evaluations [84–86].

In order to ensure numerically stable results, we perform the dispersion integrals over the inhomogeneities Eq. (2.40) up to $\sqrt{s} = 3\,\mathrm{GeV}$. This upper limit of the integration does not have any real physical significance: it merely represents an attempt to sum up the high-energy remainder of the integral to reasonable approximation, and does not mean we pretend to understand $\pi\pi$ interactions at such scales.

2.4.2 Subtraction constants, spectrum

We illustrate the results of our discussion for a sample value of $s_l = (m_B - 1\,\mathrm{GeV})^2$, which means the kinematically allowed range in the invariant mass of the pion pair extends to $\sqrt{s} = 1\,\mathrm{GeV}$. Evaluating the (nonvanishing) subtraction constants obtained from matching to the non-pole, polynomial parts of the chiral tree-level amplitude, Eq. (2.43), we find

$$\begin{aligned} \bar{a}_0 &= -5.3 \pm 1.8\,, & \bar{a}_0' &= (48 \pm 6)\,\mathrm{GeV}^2\,,\\ \bar{a}_1' &= -48 \pm 6\,, & \bar{a}_2' &= (0.5 \pm 0.1)\,\mathrm{GeV}^{-2}\,, \end{aligned} \tag{2.46}$$

where the errors refer to the uncertainty in g only. The "hat" contributions to the subtractions of Eq. (2.42), at $s_l = (m_B - 1\,\mathrm{GeV})^2$, are found to be

$$\hat{a}_1 = (-363\ldots-330)\Big(\frac{g}{0.58}\Big)\,\mathrm{GeV}^{-2}\,,$$

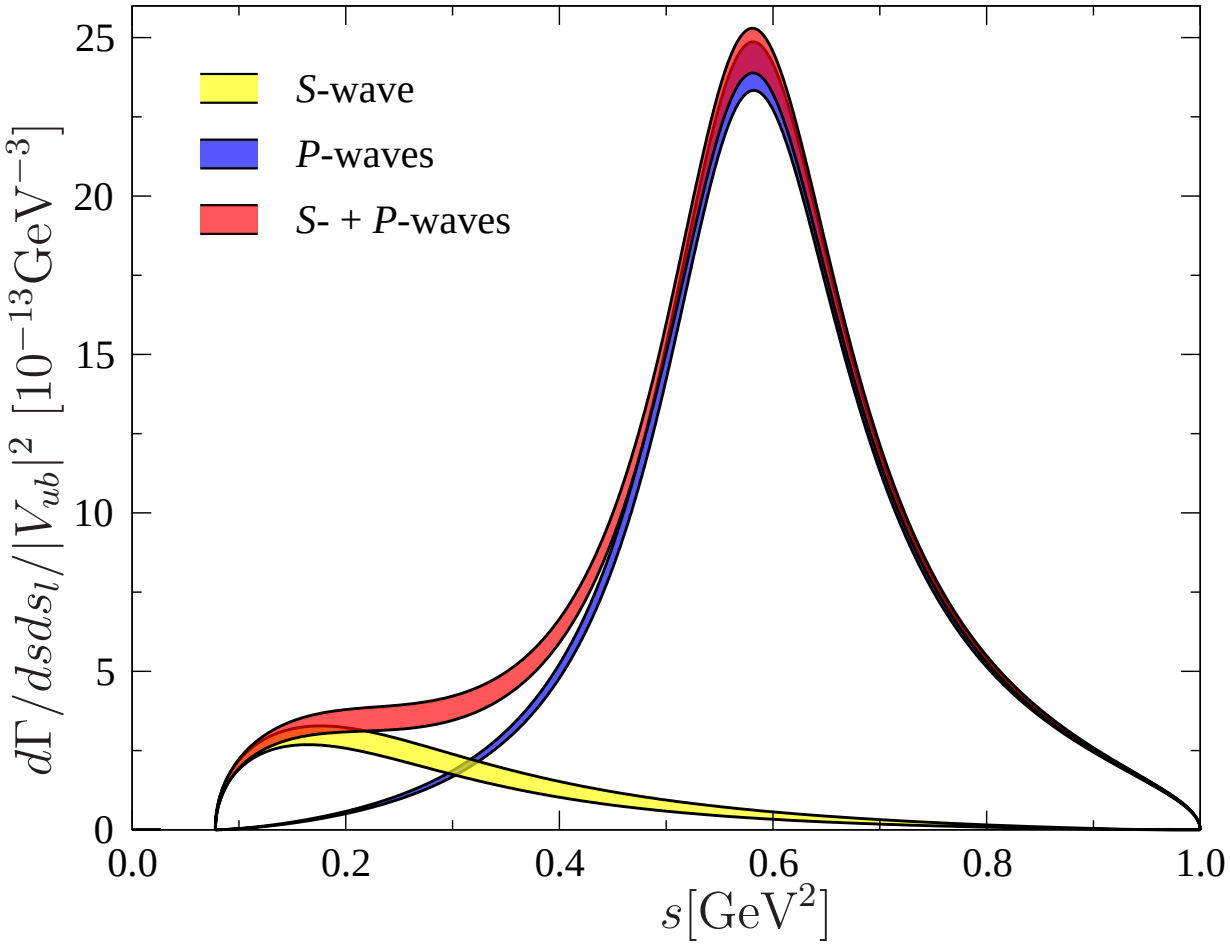

Figure 2.4: Differential decay width $d\Gamma/dsds_l$ divided by $|V_{ub}|^2$ for the example value of $s_l = (m_B - 1\,\mathrm{GeV})^2$, decomposed into S- and P-wave contributions. For details, see discussion in main text.

$$\hat{a}_2' = (888\ldots924)\Big(\frac{g}{0.58}\Big)\,\mathrm{GeV}^{-2}\,,$$
$$\hat{b}_1 = 332\Big(\frac{g}{0.58}\Big)\,\mathrm{GeV}^{-2}\,,\quad \hat{c}_1 = 1078\Big(\frac{g}{0.58}\Big)^2\,\mathrm{GeV}^{-2}\,, \tag{2.47}$$

where we have displayed the scaling with g explicitly, and shown the range of parameters in the F_1 partial waves due to the higher-order corrections discussed above.

For demonstration, we plot the partial decay rate in Fig. 2.4 for the dilepton invariant mass squared $s_l = (m_B - 1\,\mathrm{GeV})^2$. We find that the S-wave contribution leads to a significant enhancement of the spectrum at low $\pi\pi$ invariant masses, beyond what might be considered ρ dominance. The near-threshold dominance of the S-wave was already pointed out in Ref. [65] in the context of heavy-meson chiral perturbation theory. Concerning the different P-waves, we find that the kinematical prefactor X^2/m_B^4 strongly suppresses the partial wave h_1 or the form factor F_3 for the values of s_l considered here. Of the other two,

g_1 yields a contribution to the differential rate roughly twice as large as f_1.

2.5 Discussion and summary

We wish to emphasize that matching to chiral perturbation theory at leading order can only be considered an estimate, and mainly serves for illustration purposes here. Higher-order corrections are expected to be significant. Ultimately, the subtraction constants that influence the shape ought to be determined by fits to experimental data; they can be thought of as parametrizing a " background polynomial ," beyond the dominant pole terms, albeit with completely correct rescattering corrections, obeying Watson's theorem. The necessary theoretical normalization of the form factors is essentially provided at $s = M_\rho^2$, via Eq. (2.42); its stability under higher-order corrections still merits further investigation in order to provide a theoretical uncertainty for $|V_{ub}|$ extracted from B_{l4} decays.

To summarize, we have provided a description of the form factors for the decay $B^- \to \pi^+\pi^- l^- \bar{\nu}_l$ using dispersion theory, which should lead to an improved method to measure $|V_{ub}|$. Pion–pion final-state interactions have been included non-perturbatively in the elastic approximation, while left-hand-cut structures in the πB interaction are approximated by B^* pole terms. We stress that our formalism allows, for the first time, to use the full information for $\pi\pi$ invariant masses below 1 GeV, without the need to refer to particular parametrization for selected resonances such as the $\rho(770)$ (or the $f_0(980)$); it allows for a full exhaustion of the corresponding spectra. Improved experimental data to allow for such an analysis to be performed in practice is therefore highly desirable.

As an outlook concerning theoretical improvement, we have hinted at the possibility to extend the present analysis to lower values of the dilepton invariant mass squared s_l, beyond the range of applicability of heavy-meson chiral perturbation theory, but still making use of dispersion relation for the dependence on the dipion invariant mass squared s. One promising constraint could be obtained from soft-pion theorems [87], which relate linear combinations of B_{l4} form factors at $s = M_\pi^2$, but arbitrary s_l, to $B \to \pi l\nu$ (B_{l3}) form factors at same s_l. Given reliable phenomenological information on the form factors for B_{l3}, this may provide precisely (part of) the matching information needed to extend the dispersive method of this article to lower values of s_l.

Part II

Antinucleon-Nucleon Scattering

Chapter 3

Antinucleon-nucleon interaction in chiral effective field theory *

3.1 Introduction

The antinucleon-nucleon ($\bar{N}N$) interaction has been studied quite extensively in the past [88–96], not least because of the wealth of data collected at the LEAR facility at CERN, cf. the reviews [97–99]. The majority of those investigations has been performed in the traditional meson-exchange framework where the G-parity transformation is exploited to connect the elastic part of the $\bar{N}N$ interaction with the dynamics in the nucleon-nucleon (NN) system. Annihilation processes are described either by a simple optical potential (which is often assumed to be spin- as well as energy-independent) [88,89,92,94] or in terms of a coupling to a small number of effective two-body annihilation channels [90, 91, 96].

In the last two decades chiral effective field theory (EFT) has become a standard tool in the studies of the NN interaction at low energies. This development was initiated by two seminal papers by Weinberg [100, 101] in which he proposed that EFT and the power-counting rules associated with it should be applied to the NN potential rather than to the reaction amplitude. The reaction amplitude is then obtained from solving a regularized Lippmann-Schwinger equation for the derived interaction potential. His suggestion is based on the observation that diagrams with purely nucleonic intermediate states are strongly enhanced and, therefore, not amenable to a perturbative treatment. However, they can be taken into account and they are actually summed up to infinite order when solving the Lippmann-Schwinger equation. The chiral NN potential contains pion exchanges and a series of contact interactions with an increasing number of derivatives. The latter represent the short-range part of the NN force and are parametrized by low-energy constants (LECs), that need to be fixed by a fit to data. For reviews we refer the reader to the Refs. [102–104]. Presently the most refined calculations extend up to next-to-next-to-next-to-leading order ($\mathrm{N^3LO}$) [105, 106] and they yield a rather accurate description of the NN phase shifts up

*Most parts of this chapter except for Section 3.2 (a review of nucleon-nucleon potential) have been published in JHEP 1402, 113 (2014).

to laboratory energies of 250-300 MeV.

Naturally, the success of chiral EFT in the NN sector provides a strong motivation to apply the same approach also to the $\bar{N}N$ interaction. First and most important for the practical implementation, recently an update of the Nijmegen partial-wave analysis (PWA) of antiproton-proton ($\bar{p}p$) scattering data [107] has been published. For the new PWA [108] the resulting phase shifts and inelasticities are explicitly given and can be readily used for applying the chiral EFT approach to the $\bar{N}N$ interaction in the very same way as it has been done for the NN system.

A further incentive for exploring the feasibility of investigating the $\bar{N}N$ system within chiral EFT comes from the expected increase in interest in the $\bar{N}N$ interaction in the future due to the Facility for Antiproton and Ion Research (FAIR) in Darmstadt whose construction is finally on its way. Among the various project planned at this site is the PANDA experiment [109] which aims to study the interactions between antiprotons and fixed target protons and nuclei in the momentum range of 1.5-15 GeV/c using the high energy storage ring HESR.

Finally, chiral EFT could be a very powerful tool to analyze data from recent measurements of the $\bar{p}p$ invariant mass in the decays of J/ψ, B mesons, etc., and of the reaction $e^+e^- \to \bar{p}p$. In several of those reactions a near-threshold enhancement in the mass spectrum was found [110–113] and this enhancement could allow one to extract information on the $\bar{p}p$ interaction at very low energies [114–122].

In the present chapter we report on results of an exploratory study of the antinucleon-nucleon interaction within chiral EFT. In our application of chiral EFT to the $\bar{N}N$ interaction we follow exactly the approach used by Epelbaum et al. [106, 123, 124] in the NN case. It is consistent with the scheme originally proposed by Weinberg except that one aims for an energy-independent representation of the chiral potential [125]. For the time being we restrict ourselves to an evaluation of the potential up to next–to–next–to–leading order (NNLO). At leading order (LO) the potential is given by one–pion exchange (OPE) and two contact terms without derivatives. At next–to–leading order (NLO) contributions from the leading two–pion exchange (TPE) diagrams as well as seven more contact operators arise. Finally, at NNLO one gets contributions from the subleading TPE with one insertion of dimension two pion–nucleon vertices. Once the potential is established it has to be inserted into a regularized scattering equation in order to obtain the reaction amplitude. For the regularization we follow again closely the procedure adopted by Epelbaum et al. [106, 124] and others [105], in their study of the NN interaction and introduce a momentum-dependent exponential regulator function.

For investigations of the $\bar{N}N$ interaction within EFT based on other schemes see Refs. [126, 127], where the Kaplan-Savage-Wise resummation scheme [128] is employed. These authors considered the $\bar{N}N$ interaction up to NLO. There have been also attempts to compute specific $\bar{p}p$ annihilation channels in chiral EFT [129].

The $\bar{N}N$ interacting potentials are composed of elastic part and annihilation. The latter is a new ingredient compared to the NN scattering, while the former can be obtained by performing a G-parity transformation of NN potentials, i.e., transforming the $NN\pi$ vertex

to the $\bar{N}\bar{N}\pi$ vertex via charge conjugation and a rotation in the isospin space. Due to such close connection, we will first review some general formalism of NN potentials in Sec. 3.2, where the expressions for contact terms are discussed, and the pion-exchange potentials in both dimensional and spectral-function regularization schemes are provided. The potential with spectral-function regularization will be used in the study of $\bar{N}N$ scattering.

The other contents of the present chapter is structured as follows: The effective $\bar{N}N$ potential up to NNLO is described in Sec. 3.3. We start with a brief review of the underlying power counting and then provide explicit expressions for the contributions from pion exchange and for the contact terms. We also discuss how we treat the annihilation processes. In Sec. 3.4, we introduce the Lippmann-Schwinger equation that we solve and the parameterization of the S-matrix that we use. In Sec. 3.5 we indicate our fitting procedure and then we present the results achieved at NLO and at NNLO. Phase shifts and inelasticities for S-, P-, and D- waves, obtained from our EFT interaction, are displayed and compared with those of the $\bar{N}N$ phase-shift analysis. Furthermore, predictions for S-wave scattering lengths are given. A summary of our work and an outlook on future investigations is given in Sec. 3.6.

3.2 Nucleon-nucleon scattering and the general formalism

In this chapter, we briefly review some general formalism on the field of nucleon-nucleon (NN) scattering below the pion production threshold, i.e., the laboratory kinetic energy is confined to $T_{\rm lab} = 280$ MeV [2]. Beyond the energy region $T_{\rm lab} > 280$ MeV, on one hand, it is not relevant to the conventional nuclear structure calculations; on the other hand, meson production will happen, and the present descriptions are inadequate. There are lots of studies in this direction, for a review see Ref. [130].

Furthermore, we will only focus on the application of chiral effective field theory (EFT). As we know, the phenomenological meson-exchange models have very successfully described NN scattering, such as Bonn potential [33, 131], Paris potential [132], Nijmegen potential [133] and Argonne potential [134]. For a review, one may refer to Refs. [135, 136] and especially, some details concerning the formalism can be found in Ref. [136]. The essential difference between EFT and phenomenological models is that, EFT satisfies all relevant symmetry properties of the underlying theory, QCD.

[2] This value can be obtained as follows. With k representing the modulus of the three-momentum in the center-of-mass system (CMS), m_N (M_π) the mass of the nucleon (pion), we have

$$\begin{aligned} T_{\rm lab} &= \frac{2k^2}{m_N} \Longrightarrow E_{CM} = 2\sqrt{k^2+m_N^2} = \sqrt{4m_N^2+2m_N T_{\rm lab}}\ , \\ 4m_N^2+2m_N T_{\rm lab} &\leq (2m_N+M_\pi)^2 \Longrightarrow T_{\rm lab} \leq 2M_\pi + \frac{M_\pi^2}{2m_N} \sim 280\ \text{MeV}. \end{aligned}$$

3.2.1 Hierarchy of nuclear force

As mentioned earlier, a modern tool for calculating nuclear forces is the effective field theory (EFT) approach. However, in principle, the effective Lagrangian can have infinitely many terms, as long as they obey the corresponding symmetries. This will generate infinitely many Feynman diagrams contributing to a given reaction. Taking $\pi\pi$ scattering as an example, multi-derivative/multi-pion terms can be involved in Lagrangian, as a result, these multi-pions (two pions, four pions ...) can appear as intermediate states in the loops. Such number of diagrams can be infinite. One should find a scheme to manage and organize them, i.e. to distinguish which are the important contributions, and which are the less important, such that at a definite order, only a finite number of diagrams occurs. Only in this way could the theory be calculable. This is also the case we have known for QED (except that QED is renormalizable), where we collect the graphs into different orders by $(\alpha/(4\pi))^n$ with $\alpha \approx 1/137.036$ being the fine structure constant.

In chiral EFT, the potential V between nucleons receives contributions of the different orders of Q/Λ, i.e.,

$$V \sim (Q/\Lambda)^\nu, \tag{3.1}$$

where $Q \sim M_\pi$ refers to the soft scale, typically the small external momentum, and Λ to the hard scale (either the chiral symmetry breaking scale $\Lambda_\chi \approx 1\,\mathrm{GeV}$, or the ultraviolet cutoff to render the scattering equation finite [137]). Determining the power ν in Eq. (3.1) is just known as the power counting. For a given connected irreducible diagram [3] with A nucleons, the power ν reads [102]

$$\begin{aligned} \nu &= -4 + 2A + 2L + \sum_i \Delta_i, \\ \Delta_i &= d_i + \frac{n_i}{2} - 2, \end{aligned} \tag{3.2}$$

where L denotes the number of loops, Δ_i signifies the structure of vertices and involves d_i which is the number of derivatives or pion mass insertions in vertex i, and the number of nucleon legs n_i. The sum runs over all vertices.

For an irreducible two-body NN diagram that is our main theme, the power counting ν is

$$\nu = 2L + \sum_i \Delta_i. \tag{3.3}$$

Note that $\Delta_i \geq 0$ for all kinds of interaction in the framework of chiral effective theory: for purely pionic interaction, it involves at least two derivatives, see the lowest order Lagrangian $\mathcal{L}^{(2)}_{\pi\pi}$ in Eq. (1.6), one has $d_i \geq 2$, $n_i = 0$; for interactions of pions with nucleons, there is at least one derivative, see lowest order πN Lagrangian $\mathcal{L}^{(1)}_{\pi N}$, one has $d_i \geq 1$, $n_i = 2$; for lowest order NN contact terms, one has $n_i = 4$, $d_i \geq 0$. The condition $\nu \geq 0$ implies the convergence, i.e. the expansion $(Q/\Lambda)^\nu$ indeed works, and in principle, the next order

[3] An irreducible diagram is defined as the diagram that cannot be devided into separate physical sub-diagrams by cutting only nucleon lines.

is smaller than the current one. All the low energy constants (see e.g., Tables 3.1, 3.2 in this thesis) are of the order 1.

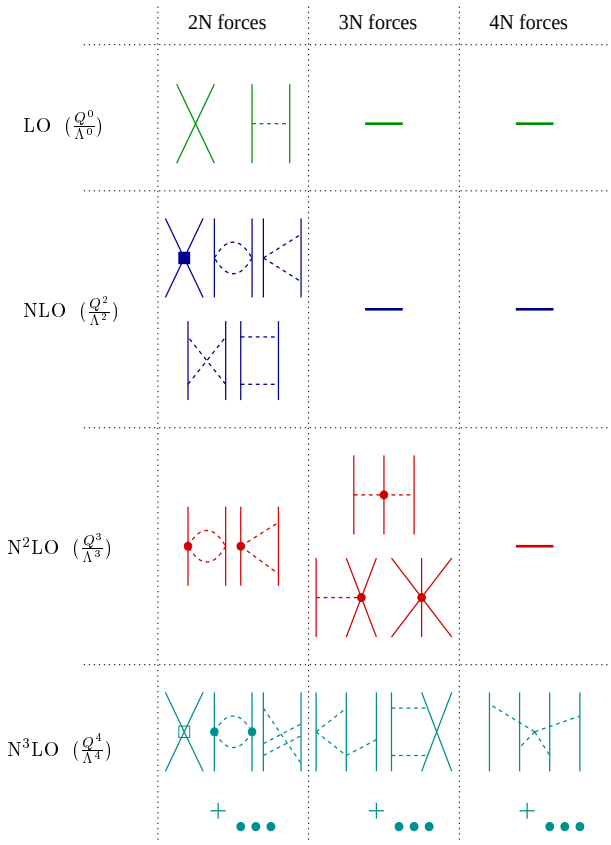

Figure 3.1: Hierarchy of nuclear forces in ChEFT. Solid lines represent nucleons and dashed lines pions. Small dots, large solid dots, solid squares,and solid diamonds depict vertices of index $\Delta = 0$, 1, 2, and 4, respectively. For the explanations see text. This figure is taken from Ref. [103].

According to the power counting rule, the graphs contributing to the two-nucleon force are classified in the first column of Fig. 3.1, and the three-nucleon force (3NF) and four-nucleon force (4NF) are organized in column 2 and 3, respectively.

Let us explain a bit more on the 2NF (further details can be found in the reviews [102, 103]), while the 3NF and 4NF will be simply mentioned. At leading order (LO), $\nu = 0$, and the NN amplitude is composed of the leading contact interactions and the leading static one pion exchange (without any loops). The former contributes constant terms of the order of $(Q/\Lambda)^0$, cf. Sec. 3.2.4 below. For the vertices in both contact graph and one-pion-exchange graph one has $\Delta_i = 0$. Combining with loop number $L = 0$, one easily sees $\nu = 0$. The LO contribution only provides a crude approximation for the 2NF, but already accounts for some important aspects — the generated tensor force is necessary

to describe the deuteron, and explains the peripheral partial waves with high angular momentum, e.g., $L \geq 4$.

For the diagrams with $\nu = 1$, all contributions vanish due to the parity and time-reversal invariance.

Consequently, $\nu = 2$ is known as the next-to-leading order (NLO), where the two-pion exchange (TPE) starts to contribute. Together with loop number $L = 1$ we already have $\nu = 2$, thus all the vertices have $\Delta_i = 0$, i.e., only the lowest order πNN and $\pi\pi NN$ vertices are allowed. The contact interaction, shown by the four-nucleon-leg graph with one solid square ($\Delta = 2$), generates seven contact terms contributing to $S-$ and $P-$waves. The main problem for this order is the insufficient intermediate-range attraction, which will be accounted for at NNLO.

At NNLO, the $\pi\pi NN$ vertices with one derivative appear. With the loop numer $L = 1$, one has $\nu = 2\times 1+1 = 3$. In the conventional meson-exchange models, the correlated TPE contributions and $\Delta(1232)$-isobar contributions are essential parts, and the calculation at NNLO can pick up these pieces. Thus NNLO is required to get a quantitative and realistic TPE contribution. There are no new contact terms at this order.

At NNNLO ($\mathrm{N^3LO}$), one has $\nu = 4$. In the second graph, there are one loop and two vertices with one derivative for each, thus $\nu = 2 \times 1 + 1 + 1 = 4$. In the third graph, three-pion-exchange involves two loops, where the number of loops can be easily identified as the number of integration variables, then one has $L = 2, \sum_i \Delta_i = 0$. In our work of the $\bar{N}N$ scattering below, all the three-pion exchange contributions are neglected since we only work up to NNLO ($\nu = 3$). The first graph depicts the four-nucleon contact interaction with dimension $(Q/\Lambda)^4$ represented by open square, which produces 15 new contact terms contributing up to $D-$wave. With these increasing numbers of parameters, a good description for NN scattering up to the kinetic laboratory energy of 300 MeV can be obtained. The precision at $\mathrm{N^3LO}$ is as good as the conventional phenomenological studies, whereas both the NLO and NNLO are not sufficient to get such a precision. $\mathrm{N^3LO}$ is the state of the art.

For a $n-$nucleon irreducibly connected diagram, the leading order starts from $\nu = 2n-4$, where we have put $L = 0$ and $\sum_i \Delta_i = 0$. Thus the three-nucleon force (3NF) will start at $\nu = 2$, and four-nucleon force (4NF) starts at $\nu = 4$. However, the contributions for 3NF at $\nu = 2$ happen to cancel [138–141], thus it is only seen starting from $\nu = 3$. These arguments from power counting provide a straightforward explanation for the empirically known fact $\mathrm{2NF} \gg \mathrm{3NF} \gg \mathrm{4NF} \cdots$.

In summary, the irreducible NN diagrams are classified according to the power counting rule given in Eq. (3.1). At a definite order ν, the number of diagrams are finite, and the (small) contribution left out will be estimated of the order of $(Q/\Lambda)^{\nu+1}$. In principle, one can get any desired accuracy, but this requires more complicated calculations and some more free parameters in contact terms.

3.2.2 Regulator function

In Lippmann-Schwinger equation, the potential V is iterated infinite times. In order to avoid the divergence in LS equation, the potentials should be cut off for high momentum. This is implemented by a monopole or dipole form factor

$$F_\alpha(q^2) = \left(\frac{\Lambda_\alpha^2 - m_\alpha^2}{\Lambda_\alpha^2 + q^2}\right)^{n_\alpha} \tag{3.4}$$

in Bonn model [33], where m_α is the mass of the exchanged meson, Λ_α is the value of chosen cutoff, $\vec{q}$ is the three-momentum transfer, $n_\alpha = 1$ defines the monopole form and $n_\alpha = 2$ the dipole. Each vertex is multiplied with the form factor $F_\alpha(q^2)$ for the one-boson-exchange (OBE) potentials. In chiral effective field theory, we choose a regulator function $f^\Lambda(p', p)$ multiplied by the total potential defined as above,

$$V(\vec{p}\,', \vec{p}\,) \longrightarrow V(\vec{p}\,', \vec{p}\,)\, f^\Lambda(\vec{p}\,', \vec{p}\,), \quad p' = |\vec{p}\,'|,\ p = |\vec{p}\,|, \tag{3.5}$$

and the regulator function is usually chosen as exponential form

$$f^\Lambda(\vec{p}\,', \vec{p}\,) = \exp\left[-\left(p'/\Lambda\right)^{2n} - \left(p/\Lambda\right)^{2n}\right]. \tag{3.6}$$

In Eq. (3.6), Λ should be smaller or of order of 1 GeV, and the typical choice is $\Lambda \approx 500$ MeV, the power n is chosen such that the accuracy that one is working with at a given order is not affected, e.g., at the next-to-leading order (NLO), $\nu = 2$, one chooses at least $n = 2$.

In the following, we will elaborate the pion-exchange contributions and contact terms in order.

3.2.3 Pion-exchange contributions

In principal, infinite number of pions can be exchanged in the process of NN scattering. According to the number of the exchanged pions, one could organize their contributions as

$$V_\pi = V_{1\pi} + V_{2\pi} + \cdots, \tag{3.7}$$

where the ellipsis stands for the 3π and more-pion exchange. Each term in Eq. (3.7) can expanded in the power of $(Q/\Lambda)^\nu$ as,

$$\begin{aligned} V_{1\pi} &= V_{1\pi}^{(0)} + V_{1\pi}^{(2)} + V_{1\pi}^{(3)} + \cdots, \\ V_{2\pi} &= V_{2\pi}^{(2)} + V_{2\pi}^{(3)} + \cdots, \end{aligned} \tag{3.8}$$

where the power ν is indicated in the superscript and ellipsis stands for the fourth and higher order contributions. For a n-pion exchange, $n-1$ loops will be generated, and the leading order (no derivatives, $\sum_i \Delta_i = 0$) contribution for NN scattering starts at the

order of $\nu = 2n-2$. Thus $V_{1\pi}$ starts from zeroth order, and $V_{2\pi}$ second order, and so forth. The first order one-pion exchange $V_{1\pi}^{(1)}$ vanishes because of the parity and time-reversal invariance, as mentioned earlier.

According to the power counting given in Eq. (3.3.2), the pion exchange diagrams up to NNLO are summarized in Fig. 3.2. Now we write out the pion exchange potential up to NNLO for NN scattering, where the pion loops have been treated with two methods: dimensional regularization scheme (in Sec. 3.2.3) and spectral-function regularization scheme (in Sec. 3.2.3). The detailed calculation for pion loop diagrams in dimensional regularization, such as triangle, football, box and crossed-box diagrams, are elegantly organized in Appendix B, C in Ref. [103]. Some details for calculating the results in spectral-function regularization are presented in appendix. In all expressions given below, we will state only the nonpolynomial contributions, whereas the polynomial contributions will be absorbed by the contact terms.

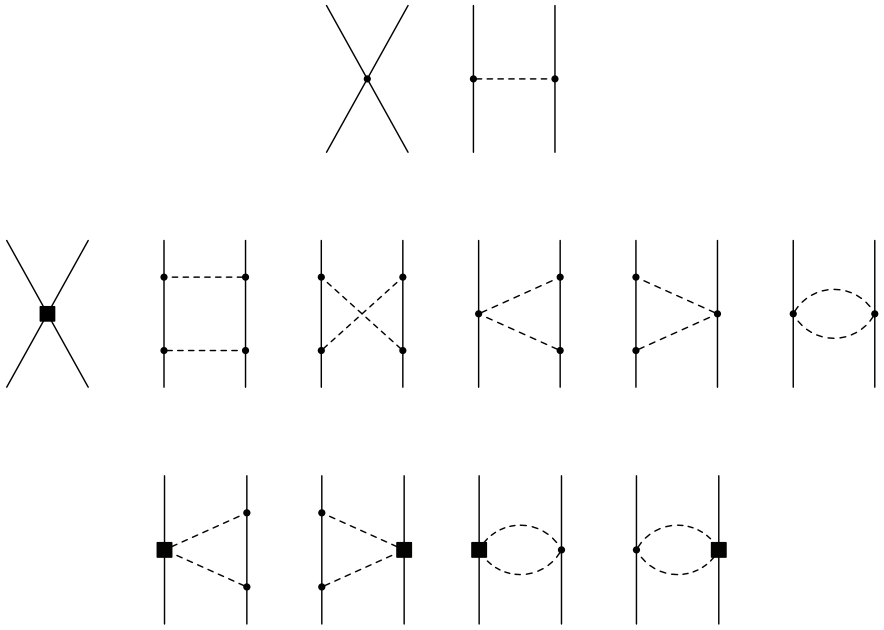

Figure 3.2: Relevant diagrams up-to-and-including NNLO. Solid and dashed lines denote the antinucleon/nucleon and the pion, respectively. The square symbolizes a contact vertex with two derivatives or a subleading πN vertex. The contributions at LO, NLO, and NNLO are displayed from top to bottom.

The NN potential calculated from chiral EFT can be expressed in terms of momenta in the center-of-mass system (CMS) as [103]

$$\begin{aligned} V(\vec{p}\,',\vec{p}) &= V_C(q) + \boldsymbol{\tau}_1\cdot\boldsymbol{\tau}_2\, W_C(q) + [V_S(q) + \boldsymbol{\tau}_1\cdot\boldsymbol{\tau}_2\, W_S(q)]\,\vec{\sigma}_1\cdot\vec{\sigma}_2 \\ &\quad + [V_{LS}(q) + \boldsymbol{\tau}_1\cdot\boldsymbol{\tau}_2\, W_{LS}(q)]\left(-i\vec{S}\cdot(\vec{q}\times\vec{k})\right) \end{aligned}$$

$$
\begin{aligned}
&+ [V_T(q) + \boldsymbol{\tau}_1 \cdot \boldsymbol{\tau}_2 \, W_T(q)] \, \vec{\sigma}_1 \cdot \vec{q} \; \vec{\sigma}_2 \cdot \vec{q} \\
&+ [V_{\sigma L}(q) + \boldsymbol{\tau}_1 \cdot \boldsymbol{\tau}_2 \, W_{\sigma L}(q)] \, \vec{\sigma}_1 \cdot (\vec{q} \times \vec{k}) \; \vec{\sigma}_2 \cdot (\vec{q} \times \vec{k}),
\end{aligned} \tag{3.9}
$$

where $\vec{p}\,'$ ($\vec{p}$) is the momentum of the final (initial) states in the CMS, and

$$
\begin{aligned}
\vec{q} &\equiv \vec{p}\,' - \vec{p} \quad \text{is the momentum transfer,} \\
\vec{k} &\equiv \frac{1}{2}(\vec{p}\,' + \vec{p}) \quad \text{the average momentum,} \\
\vec{S} &\equiv \frac{1}{2}(\vec{\sigma}_1 + \vec{\sigma}_2) \quad \text{the total spin,}
\end{aligned}
$$

$\vec{\sigma}_{1,2}$ and $\boldsymbol{\tau}_{1,2}$ are the spin and isospin operators, respectively. The pieces with C, S, LS, $T, \sigma L$ are associated with the terminologies: central, spin-spin, spin-orbit, tensor and quadratic spin-orbit, respectively, in tje nuclear physics community. The isospin dependent part is isolated by W (isovector part), whereas isospin independent part is denoted as V (isoscalar part). The above notations and conventions are similar to the ones used by Kaiser et. al [142–144] except for two differences: the spin-orbit potentials V_{LS} and W_{LS} differ by a factor of $(+2)$ and all other potentials differ by a factor of (-1). In Epelbaum's notations (see Eq. (G.1) in P.192 of Ref. [145]), the isospin factors $\boldsymbol{\tau}_1 \cdot \boldsymbol{\tau}_2$ is not explicitly shown, and the contact potential $V_{\sigma k}$ is also listed there.

Pion exchanges with dimensional regularization

We have the familiar one-pion-exchange (OPE) potential

$$
V_{1\pi}(\vec{p}\,', \vec{p}) = -\frac{g_A^2}{4 f_\pi^2} \, \boldsymbol{\tau}_1 \cdot \boldsymbol{\tau}_2 \, \frac{\vec{\sigma}_1 \cdot \vec{q} \; \vec{\sigma}_2 \cdot \vec{q}}{q^2 + M_\pi^2}, \tag{3.10}
$$

where $f_\pi = 92.4$ MeV is the pion decay constant, g_A is the axial-vector coupling constant. In the study of nucleon-nucleon interactions, one often takes a larger value of $g_A = 1.29$ (instead of 1.26) to account for the Goldberger-Treiman discrepancy, see Refs. [106, 124]. This choice of g_A, together with the used f_π, implies the pion-nucleon coupling constant $g_{NN\pi} = 13.1$ which is consistent with the empirical value obtained from πN and NN data [146, 147] and also with modern determinations utilizing the GMO sum rule [148]. Equation (3.10) is derived from the leading-order tree-level diagram, but appropriate to the third order ($\mathrm{N^2LO}$). At the orders of NLO and NNLO, appart from the renormalization of various low-energy constants in the contact terms below, no new momentum dependence is produced [102].

Specifically, we will write the (irreducible) TPE potential up to NNLO as

$$
\begin{aligned}
V_{2\pi}^{(2)} &= W_C^{(2)}(q) \, \boldsymbol{\tau}_1 \cdot \boldsymbol{\tau}_2 + V_S^{(2)}(q) \, \vec{\sigma}_1 \cdot \vec{\sigma}_2 + V_T^{(2)}(q) \, \vec{\sigma}_1 \cdot \vec{q} \; \vec{\sigma}_2 \cdot \vec{q} \, , \\
V_{2\pi}^{(3)} &= V_C^{(3)}(q) + W_S^{(3)}(q) \, \boldsymbol{\tau}_1 \cdot \boldsymbol{\tau}_2 \; \vec{\sigma}_1 \cdot \vec{\sigma}_2 + W_T^{(3)}(q) \, \boldsymbol{\tau}_1 \cdot \boldsymbol{\tau}_2 \; \vec{\sigma}_1 \cdot \vec{q} \; \vec{\sigma}_2 \cdot \vec{q} \, .
\end{aligned} \tag{3.11}
$$

- at the next-to-leading order (NLO) [142]

$$\begin{aligned} W_C^{(2)}(q) &= -\frac{L(q)}{384\pi^2 f_\pi^4}\left[4M_\pi^2(5g_A^4-4g_A^2-1)+q^2(23g_A^4-10g_A^2-1)+\frac{48g_A^4M_\pi^4}{\omega^2}\right], \\ V_T^{(2)}(q) &= -\frac{1}{q^2}V_S^{(2)}(q) = -\frac{3g_A^4L(q)}{64\pi^2 f_\pi^4}, \end{aligned} \tag{3.12}$$

with

$$L(q) \equiv \frac{\omega}{q}\ln\frac{\omega+q}{2M_\pi}, \quad \omega \equiv \sqrt{4M_\pi^2+q^2}. \tag{3.13}$$

- at the next-to-next-to-leading order (NNLO)

$$\begin{aligned} V_C^{(3)}(q) &= -\frac{3g_A^2}{16\pi f_\pi^4}\left[2M_\pi^2(2c_1-c_3)-c_3q^2\right](2M_\pi^2+q^2)A(q), \\ W_T^{(3)}(q) &= -\frac{1}{q^2}W_S^{(3)}(q) = -\frac{g_A^2}{32\pi f_\pi^4}c_4(4M_\pi^2+q^2)A(q). \end{aligned} \tag{3.14}$$

with

$$A(q) \equiv \frac{1}{2q}\arctan\frac{q}{2M_\pi}, \tag{3.15}$$

and $c_i, i = 1, 3, 4$ are the parameters in πN Lagrangians, see e.g., the review [149]. Note that as Weinberg argued in the powering counting, the nucleon mass m_N should be counted as $Q/m_N \sim Q^2/\Lambda^2$ to take into account the precense of the shallow-lying bound states [100, 101]. In Ref. [104], there is a simple example to see that. In the present thesis, we adopt this counting rule and in this way, the $1/m_N$ terms originally appearing at NNLO will be shifted to N^{3}LO [150].

Pion exchanges with spectral-function regularization

As stated in Ref. [123,124], by applying the spectral-function regularization (SFR) scheme, it allows for a consistent implementation of containts from pion-nucleon scattering data. As a side effect, it provides an improved convergence in peripheral partial waves with angular momentum $l \geq 2$, compared to the calculation using dimensional regularization (DR). For a review, refer to Ref. [102, 104]. Let's briefly review the results with SFR below. Some detailed derivations for the expressions are provided in Appendix B.3.

With the momentum cutoff $\Lambda \sim 1$ GeV in the regulator function (see Eq. (3.6)), the isoscalar central part of TPE potential at NNLO becomes so strongly attractive that the unphysically deep bound states appear. In fact, the (unphysical) part of the strongly attractive contribution comes from the short-distance portion of loop integrals in DR, which can not be treated appropriately by EFT. This idea is investigated in the analysis of the octet baryon masses and and $SU(3)$ baryon chiral perturbation theory [151–153].

In Ref. [151], the authors compared an exemplary loop integral with DR and a Gaussian cutoff $\exp(-\vec{k}^2/\Lambda^2)$ in Fig. 1 therein. It clearly shows that the curve with DR gets extraordinarily large contribution in short range, whereas the one calculated by cutoff scheme is reasonable. The cutoff with dipole form

$$\left(\frac{\Lambda^2}{\Lambda^2 - k^2}\right)^2 \tag{3.16}$$

had also been checked and results in the same phenomenology [151]. For a critical discussion on the issue of cutoff schemes in ChPT, refer to Ref. [154].

In the following, we will discuss the TPE potential at NNLO in spectral-function representation. Clearly, OPE potential does not alter. The potentials $V_i(q)$, $W_i(q)$ can be expressed as continuous superposition of Yukawa-type potentials [142],

$$\begin{aligned} V_i(q) &= \frac{1}{\pi}\int_{2M_\pi}^{\infty} d(\mu^2)\frac{\rho_i(\mu)}{\mu^2+q^2}, \\ W_i(q) &= \frac{1}{\pi}\int_{2M_\pi}^{\infty} d(\mu^2)\frac{\eta_i(\mu)}{\mu^2+q^2}, \end{aligned} \tag{3.17}$$

where $\rho_i(\mu)$, $\eta_i(\mu)$ are the corresponding spectral functions. Subtracted dispersion integral may be used if necessary, such that the dispersion integrals are convergent. These spectral functions can be obtained via

$$\begin{aligned} \rho_i(\mu) &= \mathrm{Im}\Big[V_i(0^+ - i\mu)\Big], \\ \eta_i(\mu) &= \mathrm{Im}\Big[W_i(0^+ - i\mu)\Big]. \end{aligned} \tag{3.18}$$

The whole dynamical information is contained in these spectral functions. And of course, the lowest μ should be larger or equal to $2M_\pi$ (π meson as a Goldstone boson is the lightest meson). Once the functions $\rho_i(\mu)$, $\eta_i(\mu)$ are known, substituting them into Eq. (3.17), the potentials will be obtained.

How to understand the cutoff applied into the spectral function? In fact, it is fully equivalent to the cutoff directly applied to the loop integral. As an example, consider the isoscalar central part of the TPE potential at order $\nu = 3$, which results from the triangle diagrams and is given by [104]

$$V_C(q) = \frac{3g_A^2}{16f_\pi^4}\int\frac{d^3l}{(2\pi)^3}\frac{l^2-q^2}{\omega_-^2\omega_+^2}\big(8c_1M_\pi^2 + c_3(l^2-q^2)\big), \tag{3.19}$$

where $q \equiv |\vec{q}|$, $l \equiv |\vec{l}|$ and

$$\omega_\pm = \sqrt{(q\pm l)^2 + 4M_\pi^2}. \tag{3.20}$$

This integral is cubically divergent and needs to be regularized. Applying dimensional regularization, it is just the results written in Eq. (3.14). Let us now calculate the spectral

function $\rho_C^{\tilde{\Lambda}}(\mu)$ resulting from the integral, Eq. (3.19), regularized with a cutoff $\tilde{\Lambda}$. We use the symbol $\tilde{\Lambda}$ to denote the cutoff applied to the pion-loop integrals or spectral functions, whereas Λ denotes the cutoff in Eq. (3.6) . For convenience, one may choose a regulator function $f^{\tilde{\Lambda}}(l)$

$$\begin{aligned} f^{\tilde{\Lambda}}(l) &= \theta(\tilde{\Lambda}-l), \\ \theta(\tilde{\Lambda}-l) &= \begin{cases} 0, & \tilde{\Lambda} > l \\ 1, & \tilde{\Lambda} < l \end{cases}. \end{aligned} \tag{3.21}$$

Performing the integration over angles, one obtains

$$\begin{aligned} V_C^{\tilde{\Lambda}}(q) &= \frac{3g_A^2}{128\pi^2 f_\pi^4}\int_0^{\tilde{\Lambda}} dl \frac{l(l^2-q^2)}{q(l^2+q^2+4M_\pi^2)}\big(8c_1M_\pi^2+c_3(l^2-q^2)\big) \\ &\quad\times\Big[\ln\big((l+q)^2+4M_\pi^2\big)-\ln\big((l-q)^2+4M_\pi^2\big)\Big]. \end{aligned} \tag{3.22}$$

Then the spectral function can be obtained,

$$\begin{aligned} \rho_C^{\tilde{\Lambda}}(\mu) &= \mathrm{Im}\Big[V_C^{\tilde{\Lambda}}(0^+-i\mu)\Big] \\ &= \frac{3g_A^2}{64f_\pi^4}\frac{1}{\mu}\Big(2M_\pi^2(2c_1-c_3)+c_3\mu^2\Big)(\mu^2-2M_\pi^2), \\ &\quad\times\theta(\mu-2M_\pi)\theta(\sqrt{\tilde{\Lambda}^2+4M_\pi^2}-\mu). \end{aligned} \tag{3.23}$$

The entire $\tilde{\Lambda}$ dependence is reflected in the θ–function $\theta(\sqrt{\tilde{\Lambda}^2+4M_\pi^2}-\mu)$, We stress that this is different from the DR method which does not contain any cutoff dependence. From Eq. (3.23), one could see that, cutting off the momentum l in the integral at $l=\tilde{\Lambda}$ leads to a cutoff in the TPE spectral functions at $\sqrt{\tilde{\Lambda}^2+4M_\pi^2}$. Here we take the sharp cutoff for the purpose of obtaining some analytical expression. Similar relations can be also obtained for other parts of TPE potentials.

Therefore, one may use a cutoff in spectral function to get the potentials. To be specific, the CR spectral functions $\rho_i^{\tilde{\Lambda}}(\mu)$, $\eta_i^{\tilde{\Lambda}}(\mu)$ will be defined according to

$$\begin{aligned} \rho_i^{\tilde{\Lambda}}(\mu) &= \rho_i(\mu)\theta(\tilde{\Lambda}-\mu), \\ \eta_i^{\tilde{\Lambda}}(\mu) &= \eta_i(\mu)\theta(\tilde{\Lambda}-\mu), \end{aligned} \tag{3.24}$$

in the current work, where $\rho_i(\mu)$, $\eta_i(\mu)$ are the corresponding spectral functions obtained from DR representation. With this definition, combining the DR expressions Eqs. (3.12) and (3.14), one could obtain the cufoff spectral function at NLO

$$\eta_C^{\tilde{\Lambda}(2)}(\mu) = \frac{1}{768\pi f_\pi^4}\left[4M_\pi^2(5g_A^4-4g_A^2-1)-\mu^2(23g_A^4-10g_A^2-1)-\frac{48g_A^4M_\pi^4}{\mu^2-4M_\pi^2}\right]$$

$$\times \frac{\sqrt{\mu^2-4M_\pi^2}}{\mu}\theta(\mu-2M_\pi)\theta(\tilde{\Lambda}-\mu),$$

$$\rho_T^{\tilde{\Lambda}(2)}(\mu) = \frac{1}{\mu^2}\rho_S^{\tilde{\Lambda}}(\mu) = \frac{3g_A^4}{128\pi f_\pi^4}\frac{\sqrt{\mu^2-4M_\pi^2}}{\mu}\theta(\mu-2M_\pi)\theta(\tilde{\Lambda}-\mu), \tag{3.25}$$

and at NNLO,

$$\begin{aligned}
\rho_C^{\tilde{\Lambda}(3)}(\mu) &= -\frac{3g_A^2}{64f_\pi^4}\Big(2M_\pi^2(2c_1-c_3)+c_3\mu^2\Big)\frac{2M_\pi^2-\mu^2}{\mu}\theta(\mu-2M_\pi)\theta(\tilde{\Lambda}-\mu),\\
\eta_T^{\tilde{\Lambda}(3)}(\mu) &= -\frac{1}{\mu^2}\eta_S^{\tilde{\Lambda}}(\mu) = \frac{g_A^2}{128f_\pi^4}\frac{\mu^2-4M_\pi^2}{\mu}\theta(\mu-2M_\pi)\theta(\tilde{\Lambda}-\mu).
\end{aligned} \tag{3.26}$$

Substituting these spectral functions into Eq. (3.17), one gets the potential form at NLO and NNLO with the same structure as DR, but replacing the functions $L(q)$ and $A(q)$ by

$$\begin{aligned}
L^{\tilde{\Lambda}}(q) &= \frac{\omega}{2q}\ln\frac{(\tilde{\Lambda}\omega+q\bar{s})^2}{4M_\pi^2(\tilde{\Lambda}^2+q^2)}\,, \quad \bar{s}=\sqrt{\tilde{\Lambda}^2-4M_\pi^2}\,,\\
A^{\tilde{\Lambda}}(q) &= \frac{1}{2q}\arctan\frac{q(\tilde{\Lambda}-2M_\pi)}{q^2+2\tilde{\Lambda}M_\pi}\,.
\end{aligned} \tag{3.27}$$

We notice that $\tilde{\Lambda}$ is a large quantity comparing to both the pion mass and the momentum q, thus $L(q)$ and $A(q)$ can be expanded in powers of $q/\tilde{\Lambda}$ or $M_\pi/\tilde{\Lambda}$. Keeping the leading term, we have

$$\begin{aligned}
L^{\tilde{\Lambda}}(q) &\longrightarrow \frac{\omega}{2q}\ln\frac{\omega^2\tilde{\Lambda}^2+q^2\tilde{\Lambda}^2+2q\omega\tilde{\Lambda}^2}{4M_\pi^2\tilde{\Lambda}^2}\\
&= \frac{\omega}{q}\ln\frac{\omega+q}{2M_\pi},\\
A^{\tilde{\Lambda}}(q) &\longrightarrow \frac{1}{2q}\arctan\frac{q\tilde{\Lambda}}{2\tilde{\Lambda}M_\pi}\\
&= \frac{1}{2q}\arctan\frac{q}{2M_\pi}.
\end{aligned} \tag{3.28}$$

Thus one finds that the CR and DR expressions differ by higher orders of $1/\tilde{\Lambda}$. The amputated contribution is a portion of short-range interactions, and will be taken care of by contact terms. In fact, it is simple to observe the relation between CR and DR expressions, i.e., Eq. (3.28), since the leading term is obtained by taking the limit $\tilde{\Lambda}\to\infty$, which is, of course, equivalent to no cutoff, and CR will recover the case of DR. In Ref. [104], the potentials $V_C^{(3)}$ with the DR and SFR are compared to the corresponding phenomenological Bonn potential. Again, one clearly sees that at large distance, they agree with each other, and at short distance, the SFR result agrees with the Bonn potential while the DR not. In the present thesis, we will adopt the potentials corresponding to SFR.

We stress again that the cutoffs Λ and $\tilde{\Lambda}$ are two independent ones and have obviously different physical meanings. The cutoff $\tilde{\Lambda}$ removes the short-distance portion of (irreducible) TPE nuclear force. The cutoff Λ guarantees the nucleon states with large momentum do not contribute. In principal, some more elegant cutoff schemes exist, e.g. lattice regularization scheme, which can treat the two cutoffs in a consistent way, i.e. no need to introduce two independent cutoffs. For the choice of Λ and $\tilde{\Lambda}$, values below 1 GeV (chiral symmetry breaking scale) are appropriate. It has been checked that the dependence on $\tilde{\Lambda}$ is very weak [155], and we also find this point independently in our work of $\bar{N}N$ scattering in Chap. 3. To find a reasonable region of Λ, the fitting χ^2 for reproduction of np scattering data in various energy regions at both NLO and NNLO are shown in Figs. 2–5 in Ref. [155]. There one can see that at the region $450\,\mathrm{MeV} \leq \Lambda \leq 850\,\mathrm{MeV}$, χ^2 is insensitive to the variation of Λ.

3.2.4 Contact terms

As is known, in a field theory infinities produced from the loop integrals will be encountered anyway, when going beyond the tree-level diagrams. One commonly used regularization scheme is the dimensional regularization, which will unavoidably introduce an infinite part as well as the scale dependence. The contact terms are needed to cancel them, such that the physical quantity is finite and has no scale dependence.

On the other hand, the contact terms will take care of the short-range interaction (also annihilations for $\bar{N}N$ channel). Although pion-exchange contributions alone may describe the peripheral partial waves ($L \geq 3$) [103, 142], the low partial waves, $L \leq 2$ (S–, P–, D–waves) dominate physical observables – cross section, analysing power, etc.. These low partial waves mainly involve short-range interactions.

We recall that in the conventional meson theory, the short-distance part of nuclear force is described by exchange of heavy mesons, where the notable one would be ω meson. The point that a short range corresponds to exchange of a heavy meson can be seen from

$$\int d^3q \frac{e^{i\vec{q}\cdot\vec{r}}}{\vec{q}^2 + m^2} \sim \frac{e^{-mr}}{r}, \tag{3.29}$$

where the scale $r_0 \sim 1/m$ represents the range of the interaction. One can clearly see that a short range is equivalent to the exchange of a heavy meson.

In Chiral EFT, the exchanged meson can be only pions with small momenta. We also know that the ρ, ω exchanges play important roles to get a reliable intermediate-range NN interaction in the phenomenological potentials. Thus it is suggestive of thinking other freedoms to mimic the effect of heavy meson ρ, ω exchanges. As mentioned above, the contact terms will take on that. This point can be more clearly seen by expanding the propagator of a heavy meson,

$$\frac{1}{Q^2 + m^2} = \frac{1}{m^2}\Big(1 - \frac{Q^2}{m^2} + \frac{Q^4}{m^4} - + \cdots\Big), \tag{3.30}$$

where m is typically the ρ (or ω) mass, and approximate to the hard scale Λ. From Eq. (3.30) one finds that the short-range interaction is represented by a series with powers of $(Q^2/\Lambda^2)^\nu$, It hints that one can construct the contact terms as

$$V_{\rm ct} = V_{\rm ct}^{(0)} + V_{\rm ct}^{(2)} + V_{\rm ct}^{(4)} + \cdots , \tag{3.31}$$

where the superscript denotes the chiral order ν. This conjecture is supported by Ref. [156], there the authors showed that the low-energy coefficients (LECs) can be uderstood as resonance saturations. Note that the expansion of the contact terms as given in Eq. (3.31) is consistent with the perturbative scheme for pions.

- at the leading order (LO)

  The well-known lowest order Lagrangian constructed by Weinberg reads [100, 101]

  $$\mathcal{L}_{NN}^{(0)} = -\frac{1}{2}C_S \bar{N}N\bar{N}N - \frac{1}{2}(\bar{N}\vec{\sigma}N)(\bar{N}\vec{\sigma}N), \tag{3.32}$$

  where C_S and C_T are free parameters and can be determined by fitting to experiment. And in practice, the following LECs $\tilde{C}_{^1S_0}, \tilde{C}_{^3S_1}$ are fitted. Equation (3.32) leads to the following NN contact potentials

  $$V_{\rm ct}^{(0)}(\vec{p}\,', \vec{p}) = C_S + C_T \vec{\sigma}_1 \cdot \vec{\sigma}_2. \tag{3.33}$$

  Projecting into the terms of partial waves, one has

  $$\begin{aligned} V_{\rm ct}^{(0)}({}^1S_0) &= \tilde{C}_{^1S_0} = 4\pi(C_S - 3C_T), \\ V_{\rm ct}^{(0)}({}^3S_1) &= \tilde{C}_{^3S_1} = 4\pi(C_S + C_T). \end{aligned} \tag{3.34}$$

- at the next-to-leading order (NLO)

  Following the NLO contact Lagrangian [157], the NN contact potentials can be given by:

  $$\begin{aligned} V_{\rm ct}^{(2)}(\vec{p}\,', \vec{p}) &= C_1 q^2 + C_2 k^2 + (C_3 q^2 + C_4 k^2)\vec{\sigma}_1 \cdot \vec{\sigma}_2 + C_5\Big(- i\vec{S} \cdot (\vec{q} \times \vec{k})\Big) \\ &\quad + C_6(\vec{\sigma}_1 \cdot \vec{q})(\vec{\sigma}_2 \cdot \vec{q}) + C_7(\vec{\sigma}_1 \cdot \vec{k})(\vec{\sigma}_2 \cdot \vec{k}). \end{aligned} \tag{3.35}$$

  Projecting into partial waves, one gets

  $$\begin{aligned} V_{\rm ct}^{(2)}({}^1S_0) &= C_{^1S_0}(p^2 + p'^2), \\ V_{\rm ct}^{(2)}({}^3P_0) &= C_{^3P_0}\, p\, p', \\ V_{\rm ct}^{(2)}({}^1P_1) &= C_{^1P_1}\, p\, p', \\ V_{\rm ct}^{(2)}({}^3P_1) &= C_{^3P_1}\, p\, p', \\ V_{\rm ct}^{(2)}({}^3S_1) &= C_{^3S_1}(p^2 + p'^2), \end{aligned}$$

$$\begin{aligned} V_{\rm ct}^{(2)}({}^3S_1 - {}^3D_1) &= C_{{}^3S_1-{}^3D_1}\, p^2, \\ V_{\rm ct}^{(2)}({}^3D_1 - {}^3S_1) &= C_{{}^3S_1-{}^3D_1}\, p'^2, \\ V_{\rm ct}^{(2)}({}^3P_2) &= C_{{}^3P_2}\, p\, p'. \end{aligned} \tag{3.36}$$

These parameters will be determined by fitting to the scattering data. The relations between $C_{{}^1S_0} \cdots C_{{}^3P_2}$ and C_i are irrelevant for our purpose and not listed here.

- At NNLO, there are no extra contact terms.

We can see at the zeroth order (LO) contact terms contribute to only S-wave, and the second order (NLO) contributes up to $P-$wave.

3.2.5 A short summary

The one-pion exchange potential is given by Eq. (3.10) and the irreducible two-pion exchange contribution, according to the order of low momentum expansion, is written as

$$V_{2\pi} = V_{2\pi}^{(2)} + V_{2\pi}^{(3)} + \cdots . \tag{3.37}$$

$V_{2\pi}^{(2)}$ and $V_{2\pi}^{(3)}$ are given in Eqs. (3.12) and (3.14), respectively, in dimensional regularization scheme; Replacing the functions $L(q)$, $A(q)$ by $L^{\tilde{\Lambda}}(q)$, $A^{\tilde{\Lambda}}(q)$ (cf. Eq. (3.27)), one will get the potentials in spectral-function regularization scheme. The contact terms are presented in Sec. (3.2.4). In summary, the NN potential up to NNLO will be given by

$$\begin{aligned} V_{\rm LO} &= V_{1\pi} + V_{\rm ct}^{(0)}, \\ V_{\rm NLO} &= V_{\rm LO} + V_{2\pi}^{(2)} + V_{\rm ct}^{(2)}, \\ V_{\rm NNLO} &= V_{\rm NLO} + V_{2\pi}^{(3)}, \end{aligned} \tag{3.38}$$

where there are no additional contact terms at NNLO.

3.3 Antinucleon-nucleon potential up to NNLO

The contributions to the NN interaction up to NNLO are described in detail in Refs. [106, 123, 124]. The structure of the $\bar{N}N$ interaction is practically identical and, therefore, the potential given in Refs. [106, 124] can be adapted straightforwardly for the $\bar{N}N$ case. For the ease of the reader and also for defining our potential uniquely we provide the explicit expressions below.

3.3.1 Elastic part

In line with [106] we adopt the following expression for the one-pion exchange potential

$$V_{1\pi}(q) = \left(\frac{g_A}{2f_\pi}\right)^2 \left(1 - \frac{p^2+p'^2}{2m_N^2}\right) \boldsymbol{\tau}_1 \cdot \boldsymbol{\tau}_2 \, \frac{\vec{\sigma}_1 \cdot \vec{q}\, \vec{\sigma}_2 \cdot \vec{q}}{q^2 + M_\pi^2} \ . \tag{3.39}$$

Obviously here relativistic $1/m_N^2$ corrections to the static one-pion exchange potential (cf. Eq. (3.10)) have been taken into account. For the nucleon (antinucleon) and pion mass we use the isospin-averaged values $m_N = 938.918$ MeV and $M_\pi = 138.039$ MeV, respectively. Note that the contribution of one-pion exchange to the $\bar{N}N$ interaction is of opposite sign as that in the NN case. This sign difference arises from transforming the $NN\pi$ vertex to the $\bar{N}\bar{N}\pi$ vertex via charge conjugation and a rotation in the isospin space and is commonly referred to as G-parity transformation.

In the current work of $\bar{N}N$ interaction, for the two-pion exchange contributions, we adopt the potentials obtained by using the spectral function regularization [106]. At NLO it is given by

$$V_{2\pi}^{(2)}(q) = W_C^{(2)}(q)\,\boldsymbol{\tau}_1\cdot\boldsymbol{\tau}_2 + V_T^{(2)}(q)\,\vec{\sigma}_1\cdot\vec{q}\,\vec{\sigma}_2\cdot\vec{q} + V_S^{(2)}(q)\,\vec{\sigma}_1\cdot\,\vec{\sigma}_2\ , \tag{3.40}$$

where

$$\begin{aligned} W_C^{(2)}(q) &= -\frac{1}{384\pi^2 f_\pi^4}\,L^{\tilde{\Lambda}}(q)\left\{4M_\pi^2(5g_A^4-4g_A^2-1)+q^2(23g_A^4-10g_A^2-1)+\frac{48g_A^4M_\pi^4}{4M_\pi^2+q^2}\right\}, \\ V_T^{(2)}(q) &= -\frac{1}{q^2}V_S^{(2)}(q) = -\frac{3g_A^4}{64\pi^2F_\pi^4}\,L^{\tilde{\Lambda}}(q)\ , \end{aligned}$$

and at NNLO by

$$V_{2\pi}^{(3)}(q) = V_C^{(3)}(q) + W_S^{(3)}(q)\,\boldsymbol{\tau}_1\cdot\boldsymbol{\tau}_2\,\vec{\sigma}_1\cdot\,\vec{\sigma}_2 + W_T^{(3)}(q)\,\boldsymbol{\tau}_1\cdot\boldsymbol{\tau}_2\,\vec{\sigma}_1\cdot\vec{q}\,\vec{\sigma}_2\cdot\vec{q}\,, \tag{3.41}$$

with

$$\begin{aligned} V_C^{(3)}(q) &= -\frac{3g_A^2}{16\pi f_\pi^4}\left\{2M_\pi^2(2c_1-c_3)-c_3q^2\right\}(2M_\pi^2+q^2)A^{\tilde{\Lambda}}(q)\ , \\ W_T^{(3)}(q) &= -\frac{1}{q^2}W_S^{(3)}(q) = -\frac{g_A^2}{32\pi F_\pi^4}\,c_4(4M_\pi^2+q^2)A^{\tilde{\Lambda}}(q)\,. \end{aligned}$$

The NLO and NNLO loop functions $L^{\tilde{\Lambda}}(q)$ and $A^{\tilde{\Lambda}}(q)$ are given by

$$\begin{aligned} L^{\tilde{\Lambda}}(q) &= \theta(\tilde{\Lambda}-2M_\pi)\,\frac{\omega}{2q}\,\ln\frac{(\tilde{\Lambda}\omega+q\bar{s})^2}{4M_\pi^2(\tilde{\Lambda}^2+q^2)}\ , \\ \omega &= \sqrt{q^2+4M_\pi^2}\ , \quad \bar{s}=\sqrt{\tilde{\Lambda}^2-4M_\pi^2}\,, \end{aligned} \tag{3.42}$$

and

$$A^{\tilde{\Lambda}}(q) = \theta(\tilde{\Lambda}-2M_\pi)\,\frac{1}{2q}\,\arctan\frac{q(\tilde{\Lambda}-2M_\pi)}{q^2+2\tilde{\Lambda}M_\pi}\,. \tag{3.43}$$

Note that the two-pion-exchange potential for the $\bar{N}N$ scattering is the same as NN because of the G-parity.

For the LECs c_1 and c_4 we adopt the central values from the Q^3–analysis of the πN system [158]: $c_1 = -0.81$ GeV^{-1}, $c_4 = 3.40$ GeV^{-1}. For the constant c_3 the value $c_3 = -3.40$ GeV^{-1} is used, which is on the lower side but still consistent with the results from Ref. [158]. Note that slightly different values are employed in the $\bar{N}N$ partial-wave analysis [108], namely $c_1 = -0.76$ GeV^{-1}, $c_3 = -5.8$ GeV^{-1} and $c_4 = 4.0$ GeV^{-1}. These values are also consistent with the recent determination in [159].

3.3.2 Annihilation

For $\bar{N}N$ scattering, there is spin dependent contact potential at LO, while at NLO it is spin- and momentum- dependent. This feature is the same as NN case, see Sec. 3.2.4. There are no additional contact terms at NNLO. Note that the Pauli principle is absent in case of the $\bar{N}N$ interaction. Accordingly, each partial wave that is allowed by angular momentum conservation occurs in the isospin $I = 0$ and in the $I = 1$ channel. Therefore, there are now twice as many contact terms as in NN.

The main new feature in the $\bar{N}N$ interaction is the presence of annihilation processes. The $\bar{N}N$ system annihilates into a multitude of $n\,\pi$ channels, where the decay to 4 to 6 pions is dominant in the low-energy region of $\bar{N}N$ scattering [97]. The threshold energy of those channels is in the order of 700 MeV while the $\bar{N}N$ threshold is at 1878 MeV. Therefore, one does not expect that annihilation introduces a new scale into the problem. Accordingly, there should be no need to modify the power counting when going from NN to $\bar{N}N$ because the momenta associated with the annihilation channels should be, in average, much larger than those in the $\bar{N}N$ system itself. This conjecture is supported by the fact that phenomenological models of the $\bar{N}N$ interaction can describe the bulk properties of annihilation very well by simple energy-independent optical potentials of Woods-Saxon or Gaussian type [88,89,92,94]. The ranges associated with those interactions are of the order of 1 fm or less. The above considerations suggest that annihilation processes are primarily tied to short-distance physics and, therefore, can be and should be simply incorporated into the contact terms which anyway are meant to parameterize effectively the short-range part of (elastic) NN and/or $\bar{N}N$ scattering.

Nonetheless we want to emphasize that the above arguments are of pragmatical nature and not fundamental ones. There are definitely annihilation channels that open near the $\bar{N}N$ threshold. Specifically, there are indications that a sizeable part of the annihilation into multipion channels proceeds via two-meson doorway modes like $\bar{N}N \to \rho\rho \to 4\pi$ or $\bar{N}N \to f_2(1270)\omega \to 5\pi$, and some of those have nominal thresholds close to that of $\bar{N}N$ scattering. On the other hand, according to empirical information the actual branching ratios into individual two-body channels are typically of the order of 1% [94] only and, therefore, they do not have any noticeable impact on the description of the bulk properties of $\bar{N}N$ annihilation. In fact, all the two-body annihilation channels together – as far as they have been measured – yield only about 30% of the total annihilation cross section at the $\bar{N}N$ threshold which is a strong evidence for the dominance of annihilation into 3 or more (uncorrelated) pions.

The study of $\bar{N}N$ scattering in EFT in Refs. [126, 127] followed the above arguments and took into account annihilation by simply using complex LECs in Eq. (3.36). However, this prescription has an unpleasant drawback – it does not allow one to impose sensible unitarity requirements on the resulting scattering amplitude. With unitarity requirements we mean a condition that guarantees that for each partial wave its contribution to the total cross section is larger than its contribution to the integrated elastic cross section. In case of strict two-body unitary like for NN scattering below the pion production threshold these two quantities are, of course, identical.

Since we want an approach that manifestly fulfils unitarity constraints we treat annihilation in a different way. We start out from the observation that unitarity requires the $\bar{N}N$ annihilation potential to be of the form

$$V_{\rm ann} = \sum_{X=2\pi,3\pi,\ldots} V_{\bar{N}N\to X} G_X V_{X\to\bar{N}N} \tag{3.44}$$

where X is the sum over all open annihilation channels, and G_X is the propagator of the intermediate state X. Note that Eq. (3.44) is exact under the assumption that there is no interaction in and no transition between the various annihilation channels. Performing an expansion of $V_{\bar{N}N\to X}$ up to NNLO analogous to the $\bar{N}N$ interaction and evaluating formally the sum and integral in Eq. (3.44) yields a contribution from the unitarity cut that can be written as

$$V_{\rm ann}^{L=0} = -i\,(\tilde{C}^a_{^1S_0} + C^a_{^1S_0} p^2)(\tilde{C}^a_{^1S_0} + C^a_{^1S_0} p'^2), \qquad V_{\rm ann}^{L=1} = -i\,(C^a_\xi)^2 pp', \tag{3.45}$$

where ξ stands for the $^3P_0$, $^1P_1$, $^3P_1$, and $^3P_2$ partial waves. For the coupled $^3S_1 - {}^3D_1$ partial wave we get

$$\begin{aligned} V_{\rm ann}^{S\to S} &= -i\,(\tilde{C}^a_{^3S_1} + C^a_{^3S_1} p^2)(\tilde{C}^a_{^3S_1} + C^a_{^3S_1} p'^2), \qquad V_{\rm ann}^{S\to D} = -i\,(\tilde{C}^a_{^3S_1} + C^a_{^3S_1} p^2)\, C^a_{\epsilon_1} p'^2, \\ V_{\rm ann}^{D\to S} &= -i\, C^a_{\epsilon_1} p^2\,(\tilde{C}^a_{^3S_1} + C^a_{^3S_1} p'^2), \qquad V_{\rm ann}^{D\to D} = -i\,(C^a_{\epsilon_1})^2 p^2 p'^2\ . \end{aligned} \tag{3.46}$$

In those expressions the parameters $\tilde{C}^a$ and C^a are real. Thus, for each partial wave we essentially recover the structure of the potential that follows from the contact terms considered above, with the same number of free parameters. However, in Eqs. (3.45)–(3.46) the sign of V_{ann} as required by unitarity is already explicitly fixed and does not depend on the sign of the parameters $\tilde{C}^a$ and C^a anymore. Moreover, and most importantly, we see that a term proportional to $p^2 p'^2$ arises in the S-waves at NLO and NNLO from unitarity constraints and it has to be included in order to make sure that unitarity is fulfilled at any energy. Some further explanations are presented in Sec. B.5.

Note that, in principle, there is also a contribution from the principal-value part of the integral in Eq. (3.44). However, it is real and, therefore, its structure is already accounted for by the standard LECs in Eq. (3.36).

Finally we would like to add that in practice the treatment of annihilation via Eqs. (3.45)–(3.46) corresponds to the introduction of an effective two-body annihilation channel with a threshold significantly below the one of $\bar{N}N$ so that the center-of-mass momentum in the annihilation channel is already fairly large and its variation in the low-energy region of $\bar{N}N$ scattering considered by us is negligible.

3.4 Parametrization of the S–matrix elements

In the actual calculation a partial-wave projection of the interaction potentials is performed, as described in Ref. [106] and also shown in Appendix B.4. The reaction amplitudes

for transitions of partial wave L' to L'' are obtained from the solution of a relativistic Lippmann-Schwinger (LS) equation:

$$T_{L''L'}(p'', p'; E_k) = V_{L''L'}(p'', p') + \sum_L \int_0^\infty \frac{dp\, p^2}{(2\pi)^3} V_{L''L}(p'', p) \frac{1}{2E_k - 2E_p + i0^+} T_{LL'}(p, p'; E_k). \quad (3.47)$$

Here, $E_q = \sqrt{m^2 + k^2}$, where k is the on-shell momentum. We adopt here a relativistic scattering equation so that our amplitudes fulfil the relativistic unitarity condition at any order, as done also in the NN sector [103,106]. On the other hand, relativistic corrections to the potential are calculated order by order, but appear first at next-to-next-to-next-to-leading order ($\mathrm{N^3LO}$) in the Weinberg scheme, see Ref. [106].

Like in the NN case we have either uncoupled spin-singlet and triplet waves (where $L'' = L' = L = J$) or coupled partial waves (where each of L'', L', L can take $J-1$ or $J+1$). We solve the LS equation in the isospin basis, i.e. for $I = 0$ and $I = 1$ separately, and we compare the resulting phase shifts with those in Ref. [108] that are likewise given in the isospin basis. It should be said, however, that for a comparison directly with data a more refined treatment is required. Then one should solve the LS equation in particle basis and consider the coupling between the $\bar{p}p$ and $\bar{n}n$ channels explicitly. In this case one can take into account the mass difference between p ($\bar{p}$) and n ($\bar{n}$) and, thereby, implement the fact that the physical thresholds of the $\bar{p}p$ and $\bar{n}n$ channels are separated by about 2.5 MeV, and also one can add the Coulomb interaction in the $\bar{p}p$ channel. The potential in the LS equation is cut off with a regulator function,

$$f^\Lambda(p', p) = \exp\left[-\left(p'^6 + p^6\right)/\Lambda^6\right], \quad (3.48)$$

in order to remove high-energy components [106]. The cutoff values are chosen in the range $\Lambda = 450$ – $600\,\mathrm{MeV}$ at NLO and $\Lambda = 450$ – $650\,\mathrm{MeV}$ at NNLO, similar to what was used for chiral NN potentials [106,124].

The relation between the S- and on-the-energy-shell T–matrix is given by

$$S_{LL'}(k) = \delta_{LL'} - \frac{i}{8\pi^2}\, k\, E_k\, T_{LL'}(k)\ . \quad (3.49)$$

The phase shifts in the uncoupled cases can be obtained from the S–matrix via

$$S_{LL} \equiv S_L = \eta_L\, e^{2i\delta_L}\ . \quad (3.50)$$

For the coupled channels ($J > 0$) in case of elastic scattering, the phase parameters in the so–called Stapp parametrization [160] are real quantities while in the presence of inelasticities they become complex (as the current situation). Because of that, in the past several generalizations of these formulae have been proposed that still allow one to write the S-matrix in terms of real parameters [108,161]. We follow here Ref. [162] and calculate

and present simply the real and imaginary parts of the phase shifts and the mixing parameters obtained via the aforementioned parameterization. More clearly, we can include the inelasticity parameter and write it as

$$\begin{pmatrix} S_{LL} & S_{LL'} \\ S_{L'L} & S_{L'L'} \end{pmatrix} = \begin{pmatrix} \eta_L \cos 2\epsilon_J \, e^{2i\delta_L} & -i\sqrt{\eta_L \eta_{L'}} \sin 2\epsilon_J \, e^{i(\delta_L+\delta_{L'})} \\ -i\sqrt{\eta_L \eta_{L'}} \sin 2\epsilon_J \, e^{i(\delta_L+\delta_{L'})} & \eta_{L'} \cos 2\epsilon_J \, e^{2i\delta_{L'}} \end{pmatrix} , \quad (3.51)$$

where $L = J - 1$ and $L' = J + 1$. The real part of the phase shift is identical to δ_L, $\delta_{L'}$, while the imaginary part is written in terms of an inelasticity parameter η_L as

$$\mathrm{Im}\, \delta_L = -(\log \eta_L)/2. \quad (3.52)$$

For uncoupled partial waves, Eq. (3.52) implies that $\mathrm{Im}\, \delta_L \geq 0$ since $\eta \leq 1$ because of unitarity, but these relation do not hold for the coupled case, where the products $\eta_L \cos \epsilon_J$ and $\eta_{L'} \cos \epsilon_J$ are both smaller or equal than one and η_L, $\eta_{L'}$ themselves can be larger than one. Since our calculation implements unitarity, the optical theorem

$$\mathrm{Im}\, a_{LL}(k) \geq k \sum_{L'} |a_{LL'}(k)|^2 \, , \quad (3.53)$$

is fulfilled for each partial wave, where $a_{LL'}(k) = (S_{LL'} - \delta_{LL'})/(2ik) = -1/(4\pi)^2 \cdot E_k \, T_{LL'}(k)$.

For the fitting procedure and for the comparison of our results with those by Zhou and Timmermans, we reconstructed the S-matrix based on the phase shifts listed in Tables VIII–X in Ref. [108] (cf. Eq. (B.57) in Appendix B.4) and then converted them to our convention specified in Eqs. (3.50) and (3.51).

3.5 Results

3.5.1 Phase shifts and inelasticities

In the fitting procedure we follow very closely the strategy of Epelbaum et al. in their study of the NN interaction [106, 124]. In particular, we consider the same ranges for the cutoffs, namely for the cutoff in the LS equation values of $\Lambda = 450$–600 MeV at NLO and $\Lambda = 450$–650 MeV at NNLO while for the spectral function regularization variations we consider values in the range $\tilde{\Lambda} = 500$–700 MeV. For any combination of the cutoffs Λ and $\tilde{\Lambda}$, the LECs $C_{S,T}$ and $C_{1\ldots7}$ are fixed from a fit to the $\bar{N}N$ S- and P-waves and the mixing parameter ϵ_1 of Ref. [108] for laboratory energies below 125 MeV ($p_{\rm lab} \leq 500$ MeV/c). The numerical values of the LECs are compiled in Tables 3.1 (NLO) and 3.2 (NNLO) for a selected combination of the cutoffs. The values for $\tilde{C}_{^1S_0}$ in the isospin $I = 1$ case found in the fitting procedure turned out to be very small and, therefore, we set them to zero.

Our results are displayed and compared with the $\bar{N}N$ PWA [108] in Figs. 3.3-3.7. The bands represent the variation of the obtained phase shifts and mixing parameters with

the cutoff. Those variations can be viewed as an estimate for the theoretical uncertainty. Thus, in principle for the same variation of the cutoff those bands should become narrower and narrower when one goes to higher order. However, as argued in Ref. [124], in practice one has to be careful in the interpretation of the bands, specifically for the transition from NLO to NNLO. Since the same number of contact terms are present in the interactions at NLO and NNLO one rather should expect variations of similar magnitude. In particular, for reasons discussed in [124] the cutoff variation underestimates the uncertainty for the NLO results. In any case one has to keep in mind that, following Ref. [124], we use a larger cutoff region at NNLO than for the NLO case.

Let us now discuss the individual partial waves. Results for the $^1S_0$ channel can be found in the upper part of Fig. 3.3. Obviously, the phase shift for isospin $I = 0$ (we use here the spectral notation $^{(2I+1)(2S+1)}L_J$) is very well described up to fairly high energies – even at NLO – and likewise the inelasticity, presented in terms of the imaginary part of the phase shift. Moreover, the dependence on the cutoff is very small. In the $I = 1$ channel the situation is rather different. Here we observe a sizeable cutoff dependence of the results for energy above 150 MeV. This has to do with the fact that the PWA suggests a resonance-like behavior of the phase in this region. Since this resonance lies in an energy region where we expect our results to show increasing uncertainties, based on the experience from the NN case [124], it is not surprising that it is difficult to reproduce this structure quantitatively. Nevertheless, there is a visible improvement when going from NLO to NNLO and at the latter order the empirical phase shifts already lie within the error bands of theory.

We want to emphasize that this improvement is entirely due to inclusion of the subleading two-pion exchange potential, since as already stressed above no new contact terms arise at NNLO and thus the number of adjustable parameters is the same at NLO and NNLO. Also, it should be said that the NLO result, shown here up to $T_{\rm lab} = 200$ MeV, exhibits a similar trend like the one for NNLO at higher energies, i.e. the phases reach a maximum and then become more negative again.

The situation for the $^3P_0$ partial wave is similar, see Fig. 3.3 (lower part). Also here the $I = 0$ phase shifts are well reproduced while in the $I = 1$ case there is an even larger cutoff dependence than in the $^{31}S_0$. Obviously also the $^{33}P_0$ amplitude of the PWA [108] exhibits a resonance-like behavior. Its reproduction requires a potential that is repulsive at large separations of the antinucleon and nucleon but becomes attractive for short distances. Since there is only a single LEC up to NNLO for P waves, the magnitude and range of such an attraction cannot be adequately accounted for. For improvements one has to wait for a N^{3}LO calculation.

Results for the $^1P_1$ and $^3P_1$ partial waves are shown in Fig. 3.4. In general, the description improves when going from NLO to NNLO. Specifically for the two $^1P_1$ channels and the $^{33}P_1$ the results at NNLO agree with those of the PWA within the uncertainty bands for energies up to 150 MeV and often even up to 250 MeV. An exception is the $^{13}P_1$ partial wave where the phase shift can only be described up to 50 MeV or so. Similar to the $^{33}P_0$, the PWA yields a negative phase at low energies which tends towards positive values at larger energies [108] and one encouters the same difficulty as discussed above.

LEC		{450, 500}	{600, 500}	{450, 700}	{600, 700}
$I=0$	$\tilde{C}_{^1S_0}$	−0.151	−0.267	−0.151	−0.273
	$C_{^1S_0}$	0.455	0.436	0.454	0.426
	$\tilde{C}^a_{^1S_0}$	0.270	0.232	0.232	0.177
	$C^a_{^1S_0}$	−0.915	−0.277	−0.905	−0.206
	$C_{^3P_0}$	1.150	1.453	1.398	1.724
	$C^a_{^3P_0}$	0.769	0.478	0.754	0.455
$I=1$	$\tilde{C}_{^1S_0}$	0	0	0	0
	$C_{^1S_0}$	0.446	0.692	0.449	0.675
	$\tilde{C}^a_{^1S_0}$	1.329	2.108	1.460	2.202
	$C^a_{^1S_0}$	−1.118	−0.369	−1.214	−0.498
	$C_{^3P_0}$	−0.357	−0.074	−0.321	0.041
	$C^a_{^3P_0}$	0.501	0.232	0.498	0.222
$I=0$	$C_{^1P_1}$	0.384	−0.015	0.394	0.020
	$C^a_{^1P_1}$	0.711	0.714	0.709	0.705
	$C_{^3P_1}$	−0.374	−0.235	−0.296	−0.146
	$C^a_{^3P_1}$	0.381	0.190	0.378	0.194
	$\tilde{C}_{^3S_1}$	−0.132	−0.083	−0.122	−0.075
	$C_{^3S_1}$	−0.497	−0.623	−0.731	−0.853
	$\tilde{C}^a_{^3S_1}$	0.334	0.325	0.319	0.301
	$C^a_{^3S_1}$	0.221	−0.573	0.325	−0.438
	C_{ϵ_1}	0.496	0.520	0.557	0.585
	$C^a_{\epsilon_1}$	−0.599	−0.218	−0.653	−0.290
$I=1$	$C_{^1P_1}$	−0.623	−0.735	−0.659	−0.858
	$C^a_{^1P_1}$	0.682	0.544	0.688	0.573
	$C_{^3P_1}$	−0.180	−0.373	−0.201	−0.443
	$C^a_{^3P_1}$	0.716	0.628	0.719	0.645
	$\tilde{C}_{^3S_1}$	−0.089	−0.120	−0.087	−0.122
	$C_{^3S_1}$	0.698	0.148	0.707	0.188
	$\tilde{C}^a_{^3S_1}$	0.399	0.210	0.398	0.224
	$C^a_{^3S_1}$	0.164	0.665	0.124	0.602
	C_{ϵ_1}	0.245	0.182	0.279	0.237
	$C^a_{\epsilon_1}$	0.015	0.111	−0.019	−0.046
$I=0$	$C_{^3P_2}$	0.225	0.466	0.363	0.630
	$C^a_{^3P_2}$	0.674	0.428	0.661	0.410
$I=1$	$C_{^3P_2}$	−0.362	−0.268	−0.361	−0.266
	$C^a_{^3P_2}$	0.528	0.350	0.529	0.351

Table 3.1: The LECs at NLO for the different cutoff combinations $\{\Lambda\,[\text{MeV}],\ \tilde{\Lambda}\,[\text{MeV}]\}$. The values of the $\tilde{C}_i$ are in unit of 10^4 GeV^{-2} and the C_i in 10^4 GeV^{-4}. The parameters related to annihilation, $\tilde{C}_i^a$ and C_i^a (see Eqs. (3.45)–(3.46)), are in units of 10^2 GeV^{-1} and 10^2 GeV^{-3}, respectively.

LEC		{450, 500}	{650, 500}	{450, 700}	{650, 700}
$I=0$	$\tilde{C}_{^1S_0}$	−0.140	−0.278	−0.141	−0.299
	$C_{^1S_0}$	0.456	0.459	0.456	0.463
	$\tilde{C}^a_{^1S_0}$	0.208	0.247	0.155	0.219
	$C^a_{^1S_0}$	−1.063	−0.337	−1.045	−0.233
	$C_{^3P_0}$	0.031	0.310	−0.444	−0.217
	$C^a_{^3P_0}$	0.796	0.492	0.828	0.556
$I=1$	$\tilde{C}_{^1S_0}$	0.025	0.095	0.052	−0.011
	$C_{^1S_0}$	0.453	0.213	0.450	0.189
	$\tilde{C}^a_{^1S_0}$	1.884	2.483	2.129	3.847
	$C^a_{^1S_0}$	−1.733	−2.778	−2.566	−4.474
	$C_{^3P_0}$	−0.535	−0.117	−0.531	−0.116
	$C^a_{^3P_0}$	0.514	0.182	0.517	0.182
$I=0$	$C_{^1P_1}$	0.400	−0.113	0.438	−0.069
	$C^a_{^1P_1}$	0.722	0.637	0.721	0.634
	$C_{^3P_1}$	−0.521	−0.339	−0.596	−0.432
	$C^a_{^3P_1}$	0.417	0.168	0.421	0.175
	$\tilde{C}_{^3S_1}$	−0.162	−0.100	−0.183	−0.103
	$C_{^3S_1}$	0.353	0.204	0.728	0.526
	$\tilde{C}^a_{^3S_1}$	0.364	0.371	0.397	0.415
	$C^a_{^3S_1}$	0.087	−0.841	−0.117	−1.125
	C_{ϵ_1}	0.205	0.236	0.062	0.106
	$C^a_{\epsilon_1}$	−0.485	−0.002	−0.362	0.167
$I=1$	$C_{^1P_1}$	−1.013	−1.294	−1.349	−1.869
	$C^a_{^1P_1}$	0.711	0.535	0.775	0.668
	$C_{^3P_1}$	−0.530	−0.902	−0.794	−1.356
	$C^a_{^3P_1}$	0.742	0.630	0.788	0.735
	$\tilde{C}_{^3S_1}$	−0.067	−0.143	−0.044	−0.125
	$C_{^3S_1}$	1.150	0.764	1.325	1.235
	$\tilde{C}^a_{^3S_1}$	0.413	0.282	0.411	0.402
	$C^a_{^3S_1}$	−0.336	0.211	−0.896	−0.441
	C_{ϵ_1}	0.320	0.287	0.376	0.383
	$C^a_{\epsilon_1}$	−0.065	0.021	−0.182	−0.162
$I=0$	$C_{^3P_2}$	−0.300	−0.120	−0.518	−0.399
	$C^a_{^3P_2}$	0.707	0.402	0.731	0.443
$I=1$	$C_{^3P_2}$	−0.648	−0.558	−0.821	−0.782
	$C^a_{^3P_2}$	0.544	0.329	0.565	0.377

Table 3.2: The LECs at NNLO for the different cutoff combinations $\{\Lambda\,[\mathrm{MeV}],\ \tilde{\Lambda}\,[\mathrm{MeV}]\}$. The values of the $\tilde{C}_i$ are in unit of 10^4 GeV^{-2} and the C_i in 10^4 GeV^{-4}. The parameters related to annihilation, $\tilde{C}^a_i$ and C^a_i (see Eqs. (3.45)–(3.46)), are in units of 10^2 GeV^{-1} and 10^2 GeV^{-3}, respectively.

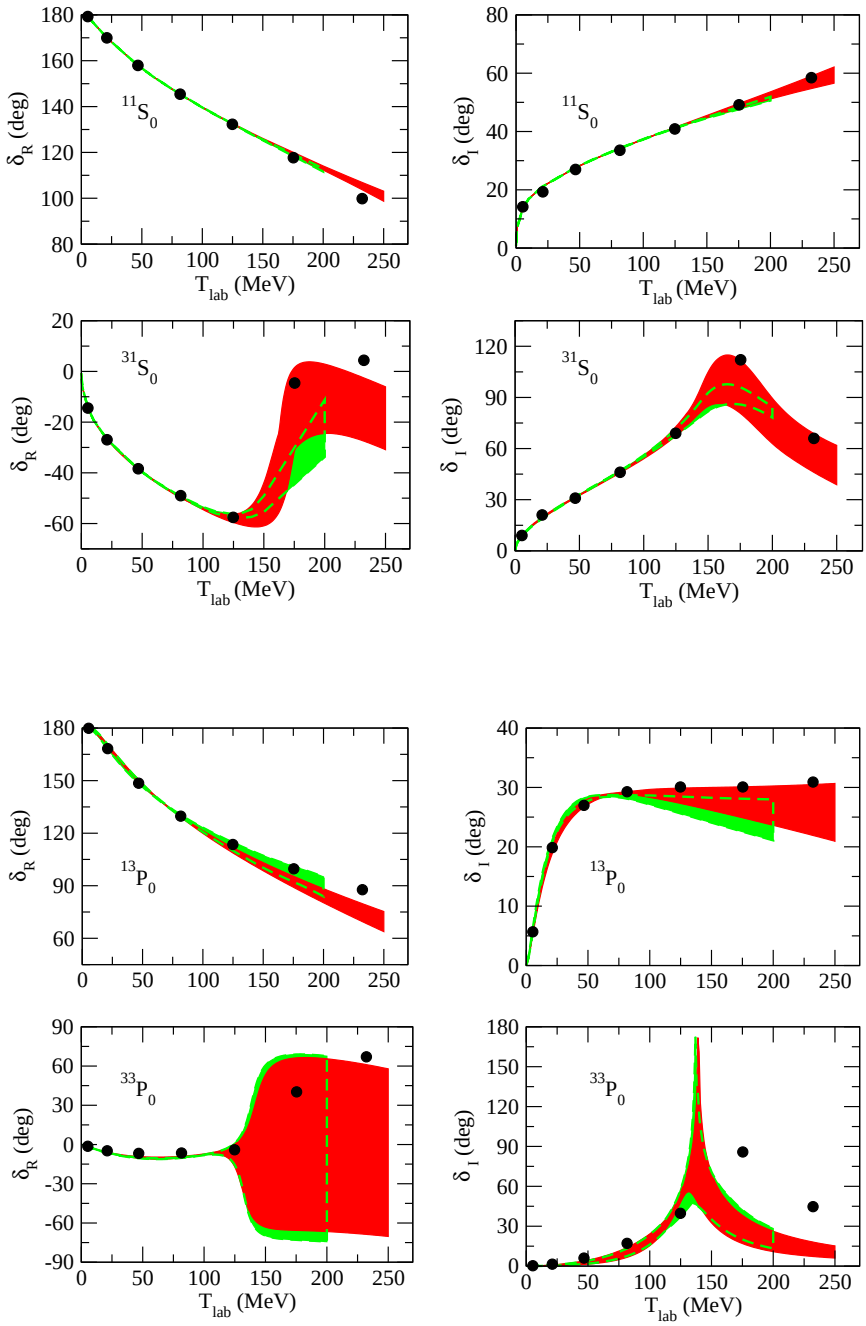

Figure 3.3: Real and imaginary parts of the phase shift in the $^1S_0$ and $^3P_0$ partial waves. The red/dark band shows the chiral EFT results up to NNLO for variations of the cutoff in the range $\Lambda = 450$–650 MeV in the Lippmann-Schwinger equation, while the green/light band are results to NLO for $\Lambda = 450$–600 MeV. The cutoff in the pion loops is varied independently in the range $\tilde{\Lambda} = 500$–700 MeV. The solid circles represent the solution of the PWA of Ref. [108].

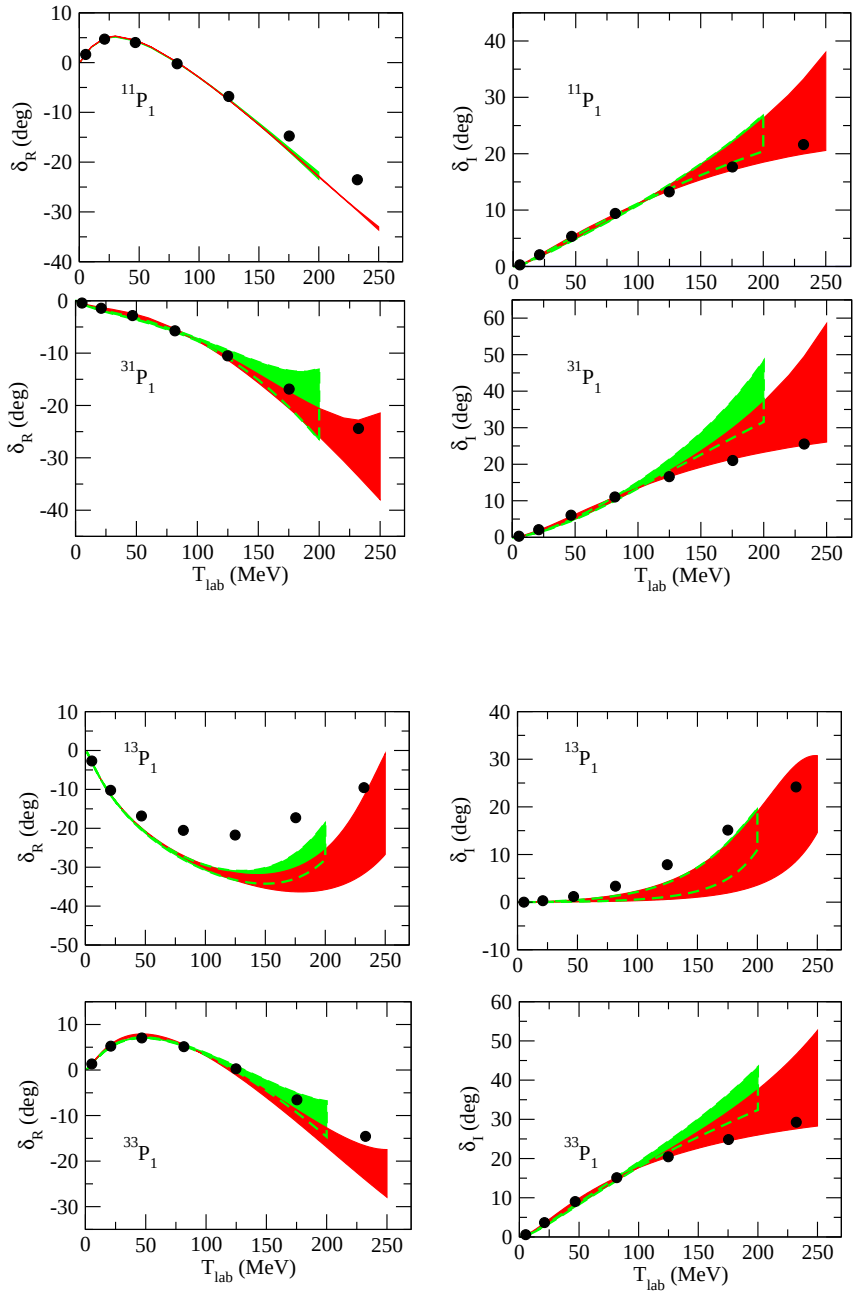

Figure 3.4: Real and imaginary parts of the phase shift in the $^1P_1$ and $^3P_1$ partial waves. The red/dark band shows the chiral EFT results up to NNLO for variations of the cutoff in the range $\Lambda = 450$–650 MeV in the Lippmann-Schwinger equation, while the green/light band are results to NLO for $\Lambda = 450$–600 MeV. The cutoff in the pion loops is varied independently in the range $\tilde{\Lambda} = 500$–700 MeV. The solid circles represent the solution of the PWA of Ref. [108].

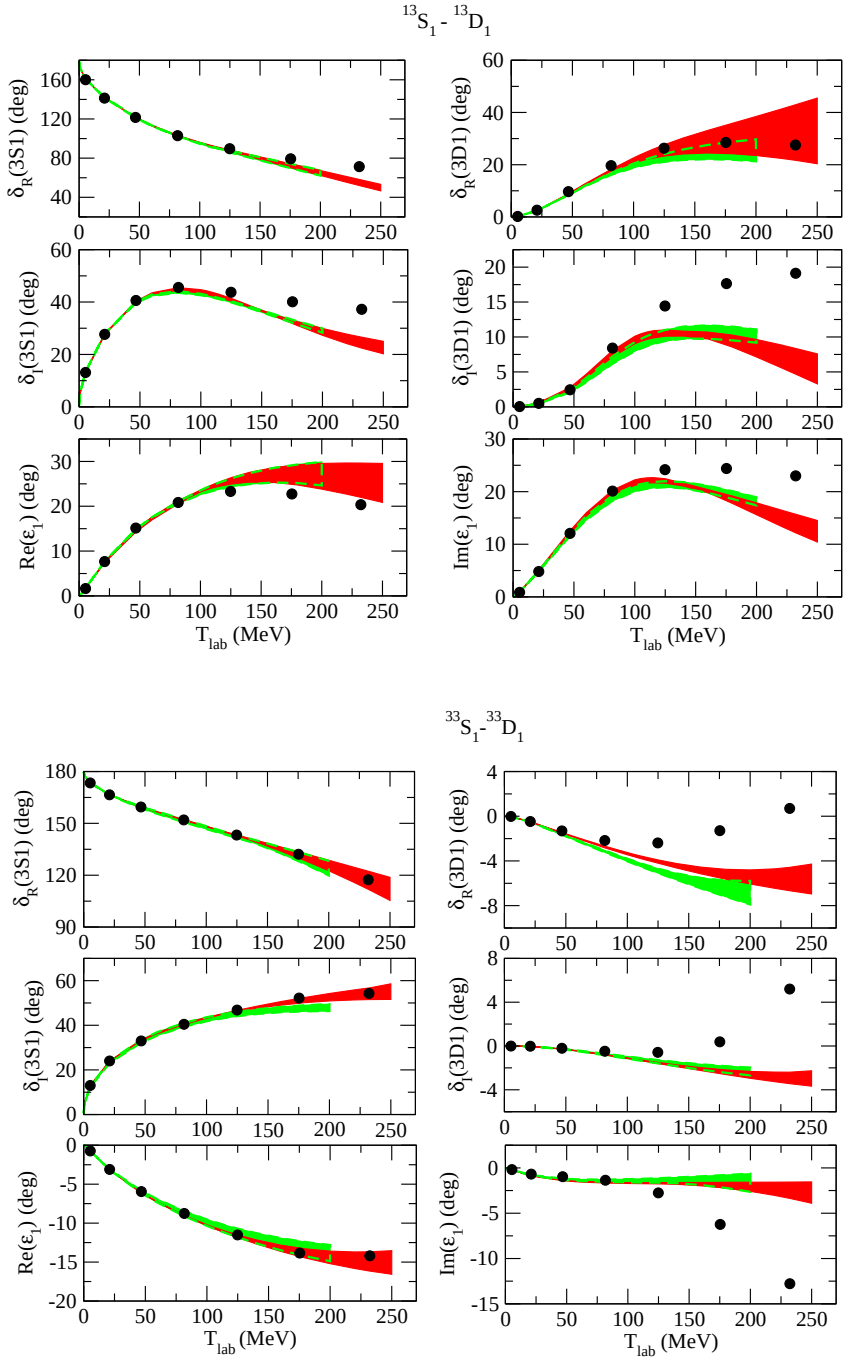

Figure 3.5: Real and imaginary parts of the phase shift in the ${}^3S_1 - {}^3D_1$ partial wave. The red/dark band shows the chiral EFT results up to NNLO for variations of the cutoff in the range $\Lambda = 450$–650 MeV in the Lippmann-Schwinger equation, while the green/light band are results to NLO for $\Lambda = 450$–600 MeV. The cutoff in the pion loops is varied independently in the range $\tilde{\Lambda} = 500$–700 MeV. The solid circles represent the solution of the PWA of Ref. [108].

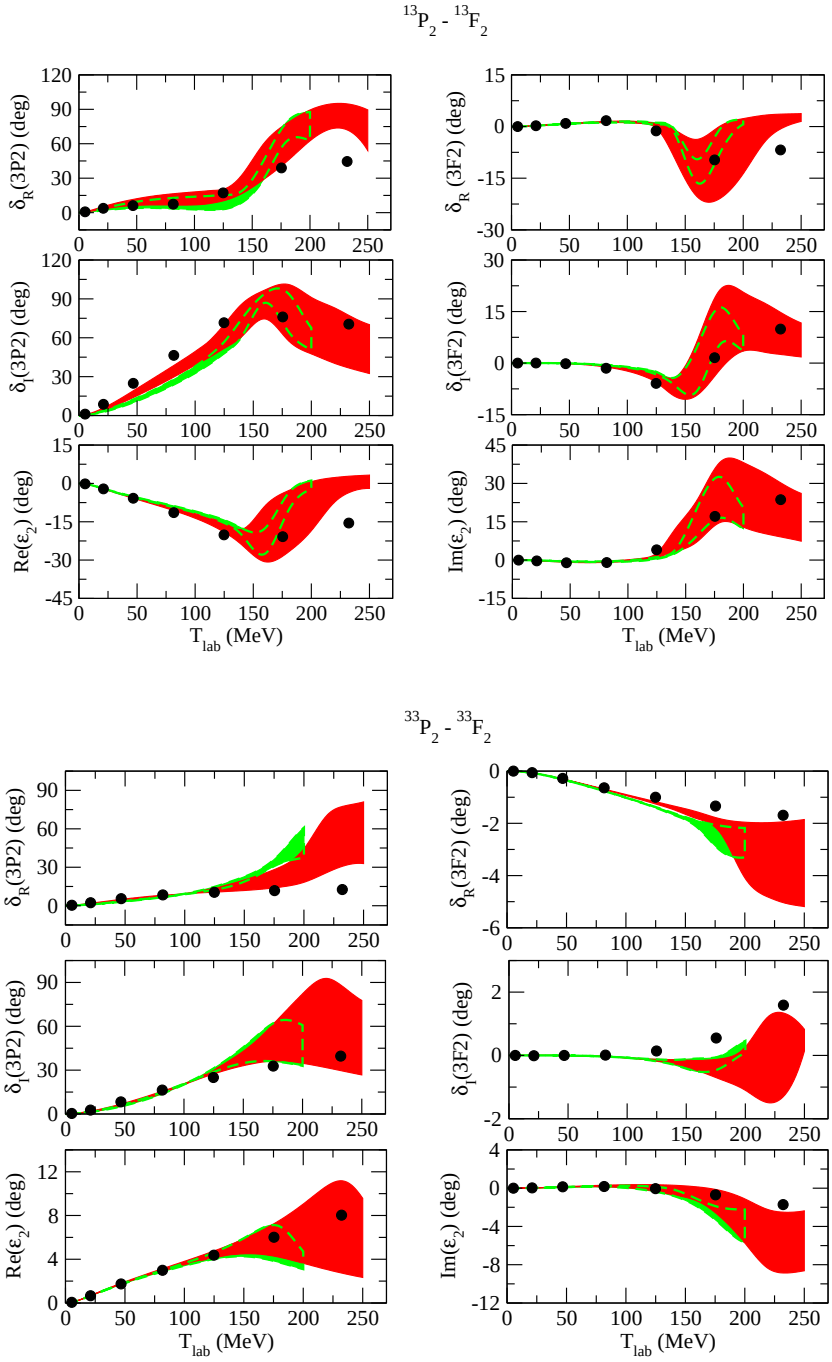

Figure 3.6: Real and imaginary parts of the phase shift in the $^3P_2 - {}^3F_2$ partial wave. The red/dark band shows the chiral EFT results up to NNLO for variations of the cutoff in the range $\Lambda = 450$–650 MeV in the Lippmann-Schwinger equation, while the green/light band are results to NLO for $\Lambda = 450$–600 MeV. The cutoff in the pion loops is varied independently in the range $\tilde{\Lambda} = 500$–700 MeV. The solid circles represent the solution of the PWA of Ref. [108].

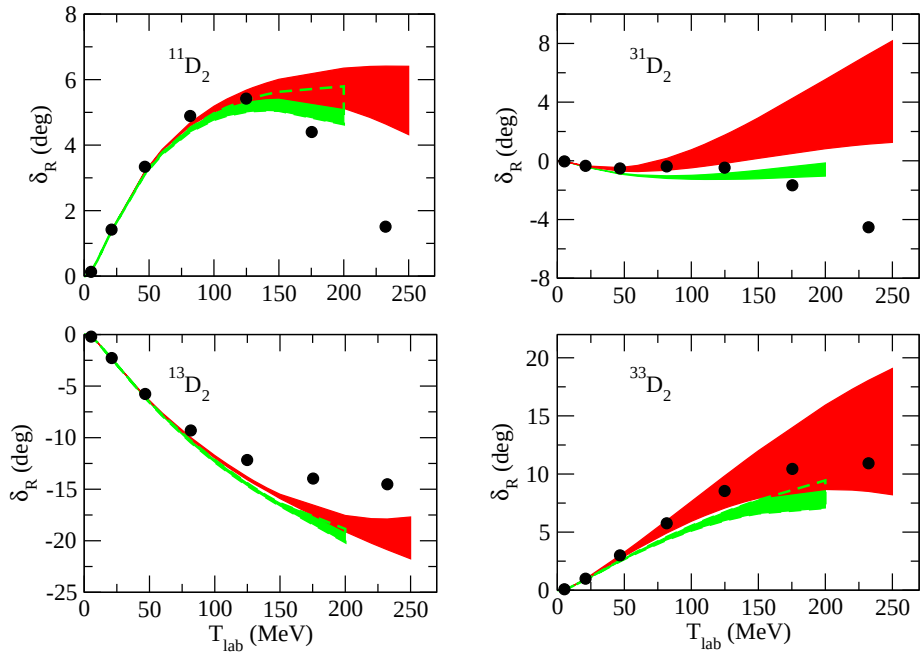

Figure 3.7: Real part of the phase shift in the ${}^1D_2$ and ${}^3D_2$ partial waves. The red/dark band shows the chiral EFT results up to NNLO for variations of the cutoff in the range $\Lambda = 450$–650 MeV in the Lippmann-Schwinger equation, while the green/light band are results to NLO for $\Lambda = 450$–600 MeV. The cutoff in the pion loops is varied independently in the range $\tilde{\Lambda} = 500$–700 MeV. The solid circles represent the solution of the PWA of Ref. [108].

In Fig. 4.2 one can find our results for the coupled ${}^3S_1 - {}^3D_1$ partial wave. Here the S-wave phase shifts (and also the inelasticities) are satisfactorily described over the whole energy range considered with uncertainties comparable to those observed for the NN interaction [124]. There is a larger cutoff dependence in the D waves and the mixing parameter ϵ_1, specifically for $I = 0$. However, one has to keep in mind that there is no LEC up to NNLO for the D waves. The ${}^{33}D_1$ exhibits the trend of turning from negative to positive values at higher energies which cannot be described in an NNLO calculation, as discussed above.

The situation in the ${}^3P_2 - {}^3F_2$ channel is displayed in Fig. 3.6. In general our results agree with those of the PWA up to about 200 MeV within the uncertainty. Stronger deviations are visible again for those phases which show a resonance-like behavior like, e.g., the ${}^{13}P_2$.

At last, in Fig. 3.7 the ${}^1D_2$ and ${}^3D_2$ phase shifts are presented. There are no LECs in those partial waves up to NNLO and, thus, our results are genuine predictions. The potential consists only of one- and two-pion exchange and, consequently, there is no contribution to annihilation. Thus, $\delta_I \equiv 0$ and we do not show this quantity.

3.5.2 Scattering lengths and volumes

One can calculate scattering lengths (for S-waves) or volumes (for P-waves) from the phase shifts. The effective range expansion for arbitrary angular momentum L is defined as

$$k^{2L+1} \cot\left(\delta_L\left(k\right)\right) = -\frac{1}{a} + \frac{1}{2}\, r_0\, k^2 + \sum_{n=2}^{\infty} v_n\, k^{2n}, \tag{3.54}$$

and for $S-$wave, we get the familiar expression

$$k\, \cot \delta_S = -\frac{1}{a} + \frac{1}{2}\, r_0\, k^2 + \mathcal{O}(k^4), \tag{3.55}$$

where a is the scattering length, r_0 is the effective range parameter, and v_i are the shape parameters. Then the scattering lengths/volumes are calculated by

$$a_S = -\lim_{k\to 0} \frac{\tan \delta_S}{k}, \tag{3.56}$$

and

$$a_P = -\lim_{k\to 0} \frac{\tan \delta_P}{k^3}. \tag{3.57}$$

The results are summarized in Table 3.3. They are complex numbers because of the presence of annihilation. Note also that the phase shifts are complex values. The corresponding information implied directly by the PWA of [108] are not provided in that reference. Thus, the lowest energy that enters our fitting procedure concerns the phase shifts at $p_{\rm lab} = 100$ MeV/c which corresponds to $T_{\rm lab} = 5.3$ MeV. In view of that one can consider our values as predictions of chiral EFT. As one can see in Table 3.3 we get

		I=0	I=1
$^1S_0$	NLO	$-0.21 - \mathrm{i}\,(1.20 \cdots 1.21)$	$(1.03 \cdots 1.04) - \mathrm{i}\,(0.56 \cdots 0.58)$
	NNLO	$-0.21 - \mathrm{i}\,(1.21 \cdots 1.22)$	$(1.02 \cdots 1.04) - \mathrm{i}\,(0.57 \cdots 0.61)$
	model D	$-0.23 - \mathrm{i}\,1.01$	$0.99 - \mathrm{i}\ 0.58$
$^3S_1$	NLO	$(1.34 \cdots 1.37) - \mathrm{i}\,(0.88 \cdots 0.90)$	$(0.43 \cdots 0.44) - \mathrm{i}\,(0.87 \cdots 0.90)$
	NNLO	$(1.37 \cdots 1.38) - \mathrm{i}\,(0.86 \cdots 0.88)$	$(0.43 \cdots 0.44) - \mathrm{i}\,(0.91 \cdots 0.92)$
	model D	$1.55 - \mathrm{i}\,1.45$	$0.33 - \mathrm{i}\,0.96$
$^3P_0$	NLO	$-(3.55 \cdots 4.32) - \mathrm{i}\,(7.35 \cdots 8.45)$	$(2.42 \cdots 2.47) - \mathrm{i}\,(0.03 \cdots 0.10)$
	NNLO	$-(3.08 \cdots 3.78) - \mathrm{i}\,(6.93 \cdots 7.55)$	$(2.35 \cdots 2.42) - \mathrm{i}\,(0.03 \cdots 0.12)$
	model D	$-7.40 - \mathrm{i}\,3.21$	$2.50 - \mathrm{i}\ 1.23$
$^1P_1$	NLO	$-(2.84 \cdots 2.86) - \mathrm{i}\,(0.24 \cdots 0.29)$	$(0.89 \cdots 0.92) - \mathrm{i}\,(0.19 \cdots 0.20)$
	NNLO	$-(2.87 \cdots 2.89) - \mathrm{i}\,(0.25 \cdots 0.31)$	$(0.78 \cdots 0.86) - \mathrm{i}\,(0.20 \cdots 0.29)$
	model D	$-3.26 - \mathrm{i}\,0.50$	$0.45 - \mathrm{i}\ 0.55$
$^3P_1$	NLO	$(4.80 \cdots 4.82) - \mathrm{i}\,(0.00 \cdots 0.02)$	$-(1.95 \cdots 1.97) - \mathrm{i}\,(0.37 \cdots 0.40)$
	NNLO	$(4.76 \cdots 4.77) - \mathrm{i}\,(0.00 \cdots 0.02)$	$-(2.02 \cdots 2.09) - \mathrm{i}\,(0.39 \cdots 0.52)$
	model D	$4.87 - \mathrm{i}\,0.06$	$-2.05 - \mathrm{i}\ 1.37$
$^3P_2$	NLO	$-(0.31 \cdots 0.42) - \mathrm{i}\,(0.27 \cdots 0.51)$	$-(0.20 \cdots 0.21) - \mathrm{i}\,(0.16 \cdots 0.21)$
	NNLO	$-(0.45 \cdots 0.78) - \mathrm{i}\,(0.47 \cdots 0.65)$	$-(0.28 \cdots 0.37) - \mathrm{i}\,(0.18 \cdots 0.25)$
	model D	$-0.14 - \mathrm{i}\,1.27$	$-0.37 - \mathrm{i}\ 0.50$

Table 3.3: Scattering lengths (in fm) for the $S-$waves and scattering volumes (in fm^3) for the $P-$waves in the isospin $I = 0$ and $I = 1$ channels. Results based on the NLO and NNLO potentials are given and compared with the predictions of the Jülich $\bar{N}N$ model D [94].

practically the same results at NLO and at NNLO and, moreover, there is very little cutoff dependence. Actually, in case of $\mathrm{Re}\, a_{^1S_0}$ in the $I = 0$ channel there is no variation in the first two digits and, therefore, only a single number is given.

Table 3.3 contains also scattering lengths and volumes predicted by the most refined meson-exchange potential developed by the Jülich group, namely model D published in [94]. It is interesting to see that at least for the S waves the results are very similar not only on a qualitative level but in most cases even on a quantitative level. One has to keep in mind that there are no data that would allow one to fix the relative magnitude of the singlet- and triplet- contributions near threshold. Moreover, the Jülich $\bar{N}N$ potential was only fitted to integrated cross sections. Differential cross sections or polarization data were not considered.

There is some experimental information that puts constraints on these scattering lengths. Measurements of the level shifts and widths of antiproton-proton allow one to deduce values for the spin-averaged $\bar{p}p$ scattering lengths via the Deser-Trueman formula [163] (cf. Eqs. (3.58) and (3.59)). Corresponding results taken from Ref. [164] are listed in Table 3.4. In that reference one can also find values for the imaginary part of the scattering lengths that are inferred from measurements of the ($\bar{n}p$ and $\bar{p}p$) annihilation cross section. A comparison directly with the measured level shifts and widths [165–168] is provided in Table 3.5 where now the Deser-Trueman formula was applied to the theory results.

A simple form for the Deser-Trueman formula is obatianed by taking the leading order contribution of the expansion of the parameter a/r_B, where a is the complex scattering length and r_B is the Bohr radius of the atom. For S-wave, it reads (see Ref. [164]),

$$\begin{aligned} \Delta E_{nS} + i\Gamma_{nS}/2 &= -\frac{2\pi}{m_{\rm red}} \left|\Psi_{nS}(0)\right|^2 a_S \\ &= -\frac{2}{m_{\rm red} r_B^3} \frac{1}{n^3}\, a_S \end{aligned} \tag{3.58}$$

and for P-wave,

$$\begin{aligned} \Delta E_{nP} + i\Gamma_{nP}/2 &= -\frac{6\pi}{m_{\rm red}} \left|\Delta\Psi_{nP}(0)\right|^2 a_P \\ &= -\frac{3}{16 m_{\rm red} r_B^5} \frac{32(n^2-1)}{3n^5}\, a_P, \end{aligned} \tag{3.59}$$

where $m_{\rm red}$ is the reduced mass and takes $m_N/2$ for the case of $\bar{N}N$, and

$$\begin{aligned} r_B &= \frac{1}{m_{\rm red}\alpha Z_1 Z_2} \ (Z_1,\, Z_2 = 1 \ \text{ are the atom numbers/nuclear charges}) \\ &= \frac{1}{\frac{M_p}{2} \times \frac{1}{137.036}} [\mathrm{MeV}^{-1}] \xrightarrow{\hbar c = 197.33\,\mathrm{MeV\cdot fm}} 57.6\,\mathrm{fm}. \end{aligned} \tag{3.60}$$

As far as we know, this experimental evidence was not taken into account in the PWA [108]. Nonetheless, for completeness we provide the predictions based on our EFT

	chiral EFT		model D	Experiment
$\bar{a}_{S,\bar{p}p}$	NLO	$(0.77 \cdots 0.79)$	$0.80 - \mathrm{i}\,1.10$	(0.95 ± 0.02)
		$-\,\mathrm{i}\,(0.88 \cdots 0.90)$		$-\,\mathrm{i}\,(0.73 \pm 0.03)$
	NNLO	$(0.78 \cdots 0.79)$		
		$-\,\mathrm{i}\,(0.89 \cdots 0.91)$		
Im $\bar{a}_{S,I=1}$	NLO	$(-0.82 \cdots -0.79)$	-0.86	(-0.83 ± 0.07)
	NNLO	$(-0.84 \cdots -0.83)$		
Im $\bar{a}_{S,I=0}$	NLO	$(-0.98 \cdots -0.96)$	-1.34	(-0.63 ± 0.08)
	NNLO	$(-0.97 \cdots -0.95)$		
$\bar{a}_{P,\bar{p}p}$	NLO	$-(0.06 \cdots 0.07)$	$-0.31 - \mathrm{i}\,0.87$	-0.61 ± 0.81
		$-\,\mathrm{i}\,(0.55 \cdots 0.56)$		$-\,\mathrm{i}\,(0.77 \pm 0.06)$
	NNLO	$-(0.12 \cdots 0.20)$		
		$-\,\mathrm{i}\,(0.57 \cdots 0.61)$		

Table 3.4: Spin-averaged scattering lengths for $S-$wave ($\bar{a}_S$; in fm) and scattering volumes for $P-$wave ($\bar{a}_P$; in fm^3). Results based on the NLO and NNLO potentials are given and compared with the predictions of the Jülich $\bar{N}N$ model D [94]. The experimental information is taken from Ref. [164].

		ΔE (eV)	Γ (eV)
$^1S_0$	NLO	$-(306 \cdots 361)$	$(1528 \cdots 1553)$
	NNLO	$-(302 \cdots 361)$	$(1545 \cdots 1589)$
	model D	-330	1380
	Experiment [165]	-740 ± 150	1600 ± 400
	[166]	-440 ± 75	1200 ± 250
$^3S_1$	NLO	$-(768 \cdots 786)$	$(1519 \cdots 1562)$
	NNLO	$-(781 \cdots 790)$	$(1537 \cdots 1563)$
	model D	-816	2092
	Experiment [166]	-785 ± 35	940 ± 80
	[167]	-850 ± 42	770 ± 150
		ΔE (meV)	Γ (meV)
$^3P_0$	NLO	$+(13 \cdots 23)$	$(159 \cdots 232)$
	NNLO	$+(8 \cdots 17)$	$(173 \cdots 186)$
	model D	$+60$	109
	Experiment [168]	$+139 \pm 28$	120 ± 25
		ΔE_{1S} (eV)	Γ_{1S} (eV)
	NLO	$-(668 \cdots 686)$	$(1528 \cdots 1562)$
	NNLO	$-(677 \cdots 686)$	$(1546 \cdots 1580)$
	model D	-694	1910
	Experiment [166]	-721 ± 14	1097 ± 42
		ΔE_{2P} (meV)	Γ_{2P} (meV)
	NLO	$+(1 \cdots 2)$	$+27$
	NNLO	$+(3 \cdots 5)$	$+(28 \cdots 30)$
	model D	$+8$	21
	Experiment [168]	$+15 \pm 20$	38.0 ± 2.8

Table 3.5: Hadronic shifts and broadenings in hyperfine states of $\bar{p}$H. Results based on the NLO and NNLO potentials are given and compared with the predictions of the Jülich $\bar{N}N$ model D [94]. The experimental information is taken from Refs. [165–168].

interaction. One should be cautious, however, in comparing our results with the experimental numbers. As said above, our calculations are performed in the isospin basis so that $a_{\bar{p}p}$ is simply given by $(a_{I=0} + a_{I=1})/2$. It is known that the presence of the Coulomb force in $\bar{p}p$ and the p-n mass difference lead to changes of the S-wave scattering lengths in the order of 0.1 fm [169] and, therefore, one should not take quantitative differences too serious. Note also that additional assumptions have to be made in order to deduce the splitting of the ${}^1S_0$ and ${}^3S_1$ level shifts from the experiment [164, 170].

More relevant details on Table 3.4 are arranged into Table 3.6, where we show the scattering volumes for P-waves in particle basis corresponding to the four cutoff combinations. The range (upper and lower limits) for a quantity is determined by singling out the maximum and minimum of the four values. The spin-averaged P-wave scattering length $a_{P,\bar{p}p}$ is obtained by

$$a_{P,\bar{p}p} = \frac{5}{12}\, a_{\,^3P_2,\bar{p}p} + \frac{3}{12}\, a_{\,^3P_1,\bar{p}p} + \frac{3}{12}\, a_{\,^1P_1,\bar{p}p} + \frac{1}{12}\, a_{\,^3P_0,\bar{p}p}, \tag{3.61}$$

and

$$a_{L,\bar{p}p} = \frac{1}{2}\left(a_L^{I=0} + a_L^{I=1}\right). \tag{3.62}$$

3.5.3 Bound states

Now let us discuss $\bar{N}N$ bound states. Several of the phase shifts tabulated in Ref. [108] start at 180° at $T_{\rm lab} = 0$ MeV, namely ${}^{11}S_0$, ${}^{13}P_0$, ${}^{13}S_1$, and ${}^{33}S_1$, which according to the standard convention based on the Levinson theorem signals the presence of a bound state. Therefore, we performed a search for possible bound states generated by our EFT interaction where we restricted ourselves to energies not too far from the $\bar{N}N$ threshold. We did not find any near-threshold poles in the ${}^{11}S_0$ and ${}^{33}S_1$ – ${}^{33}D_1$ partial waves. In case of the ${}^{13}S_1$ – ${}^{13}D_1$ interaction there is a pole which corresponds to a "binding" energy of $Q_0 = +(5.6 \cdots 7.7) - \mathrm{i}\,(49.2 \cdots 60.5)$ MeV, depending on the cutoffs $\{\Lambda, \tilde{\Lambda}\}$, at NLO and $Q_0 = +(4.8 \cdots 21.3) - \mathrm{i}\,(60.6 \cdots 74.9)$ MeV at NNLO. The positive sign of the real part of Q_0 indicates that the poles we found are actually located above the $\bar{N}N$ threshold. But they move below the threshold when we switch off the imaginary part of the potential and that is the reason why we refer to them as bound states. To be precise these are unstable bound states in the terminology of Ref. [171]. Note that those poles lie on the physical sheet and, therefore, do not correspond to resonances. Evidently, the width of the state, $\Gamma = -2\,\mathrm{Im}\,Q_0$, is rather large. There is also a pole in the ${}^{13}P_0$ partial wave. It corresponds to a binding energy of $Q_0 = (-1.1 \cdots +1.9) - \mathrm{i}\,(17.8 \cdots 22.4)$ MeV at NLO and $Q_0 = -(3.7 \cdots 0.2) - \mathrm{i}\,(22.0 \cdots 26.4)$ MeV at NNLO. In this context we want to mention that bound states and also resonances have been likewise found in other studies of the $\bar{N}N$ interaction, see Refs. [95, 96] for recent examples.

Further information on the pole positions mentioned above can be found in Table 3.7.

	NLO	NNLO
$^{13}P_0$	$1.29 - \mathrm{i}\,22.44$	$-0.20 - \mathrm{i}\,24.23$
	$-1.06 - \mathrm{i}\,19.29$	$-2.80 - \mathrm{i}\,22.04$
	$1.88 - \mathrm{i}\,21.49$	$-1.49 - \mathrm{i}\,26.40$
	$-0.33 - \mathrm{i}\,17.82$	$-3.73 - \mathrm{i}\,25.41$
$^{13}S_1 - {}^{13}D_1$	$5.92 - \mathrm{i}\,60.50$	$4.77 - \mathrm{i}\,68.22$
	$7.69 - \mathrm{i}\,52.15$	$12.05 - \mathrm{i}\,60.55$
	$5.64 - \mathrm{i}\,58.07$	$6.78 - \mathrm{i}\,74.92$
	$6.07 - \mathrm{i}\,49.24$	$21.34 - \mathrm{i}\,66.99$

Table 3.7: Binding energies (in MeV) of bound states in partial waves $^{13}P_0$ and $^{13}S_1 - {}^{13}D_1$. For each partial wave, the four numbers from top to bottom for NLO correspond to cutoffs $\{\Lambda,\, \tilde{\Lambda}\}$ =$\{450,\ 500\}$ MeV, $\{600,\ 500\}$ MeV, $\{450,\ 700\}$ MeV, $\{600,\ 700\}$ MeV, respectively, whereas for NNLO they are $\{\Lambda,\, \tilde{\Lambda}\}$ =$\{450,\ 500\}$ MeV, $\{650,\ 500\}$ MeV, $\{450,\ 700\}$ MeV, $\{650,\ 700\}$ MeV.

Meantime, for $^{13}S_1 - {}^{13}D_1$ partial wave at NNLO, we also examined the cases for another two cutoff combinations $\{\Lambda,\, \tilde{\Lambda}\}$=$\{600, 500\}$ MeV, $\{600, 500\}$ MeV, and the results are

$$\begin{aligned} &\{\Lambda,\, \tilde{\Lambda}\} = \{600,\, 500\}\,\mathrm{MeV}, \qquad Q_0 = 9.46 - \,i\,60.55, \\ &\quad \tilde{C}_{^3S_1} = -0.108, \quad C_{^3S_1} = 0.207, \quad \tilde{C}^a_{^3S_1} = 0.360, \\ &\quad C^a_{^3S_1} = -0.706, \quad C_{\epsilon_1} = 0.234, \quad C^a_{\epsilon_1} = -0.077; \end{aligned} \tag{3.63}$$

$$\begin{aligned} &\{\Lambda,\, \tilde{\Lambda}\} = \{600,\, 700\}\,\mathrm{MeV}, \qquad Q_0 = 15.55 - \,i\,66.89, \\ &\quad \tilde{C}_{^3S_1} = -0.117, \quad C_{^3S_1} = 0.547, \quad \tilde{C}^a_{^3S_1} = 0.404, \\ &\quad C^a_{^3S_1} = -0.973, \quad C_{\epsilon_1} = 0.095, \quad C^a_{\epsilon_1} = 0.082. \end{aligned} \tag{3.64}$$

3.6 Summary and outlook

In this chapter we presented an exploratory study of the $\bar{N}N$ interaction in a chiral effective field theory approach based on a modified Weinberg power counting, analogous to the NN case in [106, 124]. The $\bar{N}N$ potential has been evaluated up to NNLO in the perturbative expansion and the arising low-energy constants have been fixed by a fit to the phase shifts and inelasticities provided by a recently published phase-shift analysis of $\bar{p}p$ scattering data [108]. It turned out that the overall quality of the description of the $\bar{N}N$ amplitudes that can be achieved at NNLO is comparable to the one found in case of the NN interaction at the same order [124]. Specifically, for the S-waves ($^{11}S_0$, $^{13}S_1$, $^{33}S_1$) nice agreement with

the phase shifts and inelasticities of [108] has been obtained up to laboratory energies of about 200 MeV, i.e. over almost the whole energy region considered. The same is also the case for many of the P-waves. Thus, we conclude that the chiral EFT approach, applied successfully in Refs. [105, 106] to the NN interaction and in Refs. [172, 173] to the hyperon-nucleon interaction, is very well suited for studies of the $\bar{N}N$ interaction too.

Of course, there are also some visible deficiencies in our results. They occur primarily in those partial waves where the partial-wave analysis of [108] suggests the presence of (presumably strongly inelastic) resonances at energies around $T_{\rm lab} \approx 200 - 250$ MeV. It is not surprising that structures in this energy region cannot be reproduced reliably within our NNLO calculation. Clearly, here an extension of our investigation to N^{3}LO is necessary for improving the description of the $\bar{N}N$ interaction. Therefore, we plan to extend our study to N^{3}LO in the future. At this stage it will become sensible to perform the calculation in particle basis so that the Coulomb interaction in the $\bar{p}p$ system can be taken into account rigorously, and to compute observables and compare them directly with scattering data for $\bar{p}p$ elastic scattering and for the charge-exchange reaction $\bar{p}p \to \bar{n}n$. Annihilation processes that occur predominantly at short distances reduce the magnitude of the S-wave amplitudes so that higher partial waves start to become import at much lower energies as compared to what one knows from the NN interaction. Thus, without a realistic description of higher partial waves, and particularly of the D-waves, it is not meaningful to confront the amplitudes resulting from our NNLO interaction directly with $\bar{N}N$ data and, therefore, we have refrained from doing so in the present work.

	NLO	NNLO
$^1S_0$	$0.412 - \mathrm{i}\,0.887$	$0.410 - \mathrm{i}\,0.895$
	$0.413 - \mathrm{i}\,0.884$	$0.405 - \mathrm{i}\,0.893$
	$0.412 - \mathrm{i}\,0.889$	$0.411 - \mathrm{i}\,0.903$
	$0.414 - \mathrm{i}\,0.888$	$0.410 - \mathrm{i}\,0.911$
$^3S_1$	$0.894 - \mathrm{i}\,0.889$	$0.903 - \mathrm{i}\,0.897$
	$0.896 - \mathrm{i}\,0.895$	$0.903 - \mathrm{i}\,0.897$
	$0.890 - \mathrm{i}\,0.889$	$0.910 - \mathrm{i}\,0.899$
	$0.897 - \mathrm{i}\,0.883$	$0.904 - \mathrm{i}\,0.893$
$^3P_0$	$-\ 0.859 - \mathrm{i}\,3.725$	$-0.710 - \mathrm{i}\,3.657$
	$-0.550 - \mathrm{i}\,4.060$	$-0.373 - \mathrm{i}\,3.789$
	$-0.952 - \mathrm{i}\,3.787$	$-0.589 - \mathrm{i}\ 3.521$
	$-0.654 - \mathrm{i}\,4.239$	$-0.334 - \mathrm{i}\ 3.518$
$^1P_1$	$-0.963 - \mathrm{i}\,0.221$	$-1.008 - \mathrm{i}\,0.227$
	$-0.980 - \mathrm{i}\,0.239$	$-1.033 - \mathrm{i}\,0.270$
	$-0.965 - \mathrm{i}\,0.217$	$-1.044 - \mathrm{i}\,0.242$
	$-0.986 - \mathrm{i}\,0.243$	$-1.055 - \mathrm{i}\,0.299$
$^3P_1$	$1.428 - \mathrm{i}\,0.198$	$1.377 - \mathrm{i}\,0.204$
	$1.422 - \mathrm{i}\,0.198$	$1.369 - \mathrm{i}\,0.227$
	$1.434 - \mathrm{i}\,0.191$	$1.333 - \mathrm{i}\,0.225$
	$1.423 - \mathrm{i}\,0.204$	$1.344 - \mathrm{i}\,0.260$
$^3P_2$	$-0.274 - \mathrm{i}\,0.359$	$-0.364 - \mathrm{i}\,0.394$
	$-0.314 - \mathrm{i}\,0.241$	$-0.482 - \mathrm{i}\,0.322$
	$-0.254 - \mathrm{i}\,0.343$	$-0.432 - \mathrm{i}\,0.440$
	$-0.281 - \mathrm{i}\,0.217$	$-0.575 - \mathrm{i}\,0.436$

Table 3.6: scattering lenghs (in fm) for S-wave and scattering volumes (in fm^3) for $P-$waves in the particle channel $\bar{p}p \to \bar{p}p$. For each partial wave, the four numbers from top to bottom for NLO correspond to cutoffs $\{\Lambda,\ \tilde{\Lambda}\}$ =$\{450,\ 500\}$ MeV, $\{600,\ 500\}$ MeV, $\{450,\ 700\}$ MeV, $\{600,\ 700\}$ MeV, respectively, whereas for NNLO they are $\{\Lambda,\ \tilde{\Lambda}\}$ =$\{450,\ 500\}$ MeV, $\{650,\ 500\}$ MeV, $\{450,\ 700\}$ MeV, $\{650,\ 700\}$ MeV.

Chapter 4

The electromagnetic form factors of the proton in the timelike region *

4.1 Introduction

The electromagnetic form factors (EMFFs) of the proton and the neutron play an important role in our understanding of the nucleon structure. Experimental and theoretical studies of these quantities in the spacelike region, i.e. in electron-proton scattering, started already more than half a century ago. Over the last decades there is also an increased interest in their properties in the timelike region, accessible in the reactions $\bar{p}p \to e^+e^-$ and $e^+e^- \to \bar{p}p$, as witnessed by various publications [174–183] and a recent extensive review article [184]. In particular, the observation of a strong energy dependence of the proton EMFFs close to the $\bar{p}p$ threshold, i.e. at momentum transfers $q^2 \simeq (2M_p)^2$, has attracted quite some attention. This behavior was first reported by the PS170 collaboration [185], and detected in a measurement of the $\bar{p}p \to e^+e^-$ reaction cross section at LEAR. In recent years the BaBar collaboration has measured the cross section for the time-reversed process $e^+e^- \to \bar{p}p$ [186, 187]. Their data are of similar precision as those from the PS170 collaboration and cover also energies very close to the $\bar{p}p$ threshold. The form factor deduced from those data substantiates the finding of the PS170 collaboration.

A strong dependence of the proton EMFFs on the momentum transfer simply reflects the fact that the underlying (measured) $e^+e^- \to \bar{p}p$ cross section shows a significant enhancement near the $\bar{p}p$ threshold. Such near-threshold enhancements were also reported in entirely different reactions involving the $\bar{p}p$ system, for example, in the $\psi(3686) \to \gamma\bar{p}p$ [113] and the $B^+ \to \bar{p}pK^+$ [111] decays, and in particular in the radiative decay $J/\psi \to \gamma\bar{p}p$ [110, 113]. For the latter case several explanations have been put forth, including scenarios that invoke $N\bar{N}$ bound states or so far unobserved meson resonances. However, it was also shown that a conventional but plausible interpretation of the data can be given simply in terms of the final-state interaction (FSI) between the produced proton and antiproton [114–117, 188]. Specifically, calculations of our group, utilizing the Jülich $N\bar{N}$

*This chapter has been published online, arXiv:1405.1628 [nucl-th], and is submitted for publication.

model [92–94] and performed within the Watson-Migdal approach [27,28], could reproduce the mass dependence of the $\bar{p}p$ spectrum close to the threshold by the S-wave $\bar{p}p$ FSI for various decays [116, 118, 122].

The success of those investigations suggests that the same effects, namely the FSI between proton and antiproton, could be also responsible for the near-threshold enhancement in the $e^+e^- \to \bar{p}p$ cross section and, accordingly, for the strong q^2 dependence of the proton EMFF in the timelike region near $q^2 \approx (2M_p)^2$. Indeed, a few years ago we have studied the energy dependence of the $e^+e^- \leftrightarrow \bar{p}p$ cross section close to threshold, within the Watson-Migdal approach [119]. We could show that the near-threshold enhancement in the $e^+e^- \to \bar{p}p$ cross section can be explained qualitatively by $\bar{p}p$ FSI effects in the ${}^3S_1$ partial wave as generated by the Jülich nucleon-antinucleon model [92]. Similar results were also reported by other authors based on somewhat different approaches and employing other $\bar{N}N$ interactions [126, 189–194].

The present study of the proton EMFF in the timelike region aims at an improvement of our earlier work [119] in various aspects: First and foremost the new calculation of the $e^+e^- \leftrightarrow \bar{p}p$ transition is based on a refined and formally exact treatment of the effects from the $\bar{N}N$ interaction in the initial or final state. Second, we take into account the coupling between the ${}^3S_1$ and ${}^3D_1$ partial waves. In the commonly adopted one-photon approximation these are the only two partial waves that can contribute. The inclusion of the ${}^3D_1$ state allows us to extend the energy range of our study. Furthermore, it enables us to obtain non-trivial results for angular distributions and compare those to available data, and we can make concrete predictions for (not yet measured) spin-dependent observables. Finally, in the meantime results of a new partial-wave analysis (PWA) of $\bar{p}p$ scattering data have been published [108]. Based on that work an $\bar{N}N$ potential has been constructed by us, see Chap. 3, in the framework of chiral effective field theory (EFT), that reproduces the amplitudes determined in the PWA very well up to laboratory energies of $T_{\rm lab} \approx 200 - 250$ MeV. This potential will be now employed for the final-state interaction, besides the phenomenological $\bar{N}N$ model of the Jülich group [92] used in our earlier work [119].

The paper is structured in the following way: In the subsequent section we summarize the formalism. Specifically, we provide details about how the $\bar{p}p$ FSI is included in our calculation. In Sect. 3 we compare our results with measured integrated and differential cross sections for the reactions $e^+e^- \to \bar{p}p$ and $\bar{p}p \to e^+e^-$ in the region near the $\bar{p}p$ threshold. Furthermore, we provide predictions for spin-dependent observables for which so far there is no experimental information. Finally, we present results for the EMFFs G_E and G_M, for their ratio as well as for the relative phase. The paper closes with a summary.

4.2 Formalism

We adopt the standard conventions so that the differential cross section for the reaction $e^+e^- \to \bar{p}p$ is given by [184]

$$\frac{d\sigma}{d\Omega} = \frac{\alpha^2\beta}{4s}\, C_p(s)\, \left[|G_M(s)|^2 \,(1+\cos^2\theta) + \frac{4M_p^2}{s}\, |G_E(s)|^2 \sin^2\theta \right] . \tag{4.1}$$

Here, $\alpha = 1/137.036$ is the fine-structure constant and $\beta = k_p/k_e$ a phase-space factor, where k_p and k_e are the center-of-mass three-momenta in the $\bar{p}p$ and e^+e^- systems, respectively, related to the total energy via $\sqrt{s} = 2\sqrt{M_p^2+k_p^2} = 2\sqrt{m_e^2+k_e^2}$. Further, $m_e\,(M_p)$ is the electron (proton) mass. The S-wave Sommerfeld-Gamow factor $C_p(s)$ is given by $C_p = y/(1-e^{-y})$ with $y = \pi\alpha M_p/k_p$. G_E and G_M are the electric and magnetic form factors, respectively. The cross section as written in Eq. (4.1) results from the one-photon exchange approximation and by setting the electron mass m_e to zero (in that case $\beta = 2k_p/\sqrt{s}$). We will restrict ourselves throughout this work to the one-photon exchange so that the total angular momentum is fixed to $J = 1$ and the e^+e^- and $\bar{N}N$ system can be only in the partial waves ${}^3S_1$ and ${}^3D_1$. We use the standard spectral notation ${}^{(2S+1)}L_J$, where S is the total spin and L the orbital angular momentum. Let us mention that there are indications that two-photon exchange contributions are important in the spacelike region and can account for the discrepancy between the form factor values extracted from polarization data and from Rosenbluth separation of cross section data [195–200]. Their importance in the timelike region is less clear, see for example Refs. [201, 202].

The integrated reaction cross section is readily found to be

$$\sigma_{e^+e^-\to\bar{p}p} = \frac{4\pi\alpha^2\beta}{3s}\, C_p(s)\, \left[|G_M(s)|^2 + \frac{2M_p^2}{s}\, |G_E(s)|^2 \right] . \tag{4.2}$$

Another quantity used in various analyses is the effective proton form factor $G_{\rm eff}$ which is defined by

$$|G_{\rm eff}(s)| = \sqrt{\frac{\sigma_{e^+e^-\to\bar{p}p}(s)}{\frac{4\pi\alpha^2\beta}{3s}\, C_p(s) \left[1+\frac{2M_p^2}{s}\right]}} . \tag{4.3}$$

In the helicity basis, the amplitudes for the reaction $e^+e^- \to \bar{p}p$ for one-photon exchange are given by [203, 204]

$$\begin{aligned}
\phi_1 = \langle ++|F|++\rangle &= -\frac{2\,m_e\,M_p\alpha}{s}\cos\theta\, G_E = \langle ++|F|--\rangle = \phi_2 \ , \\
\phi_3 = \langle +-|F|+-\rangle &= -\frac{\alpha}{2}\,(1+\cos\theta)\, G_M \ , \\
\phi_4 = \langle +-|F|-+\rangle &= -\frac{\alpha}{2}\,(1-\cos\theta)\, G_M \ ,
\end{aligned} \tag{4.4}$$

$$\phi_5 = \langle ++|F|+-\rangle = \frac{M_p\alpha}{\sqrt{s}}\sin\theta\, G_E = -\langle ++|F|-+\rangle = -\phi_7 \ ,$$

$$\phi_6 = \langle +-|F|++\rangle = -\frac{m_e\alpha}{\sqrt{s}}\sin\theta\, G_M = -\langle -+|F|++\rangle = -\phi_8 \ .$$

For convenience we include the electron mass explicitly here and in the formulae below and also in our numerical calculation. In terms of those amplitudes the differential cross section is given by

$$\frac{d\sigma}{d\Omega} = \frac{1}{2s}\,\beta\, C_p \sum_{i=1}^{8} |\phi_i|^2 \ , \tag{4.5}$$

which reduces to the result in Eq. (4.1) for $m_e \to 0$. Note that the amplitudes for the inverse reaction $\bar{p}p \to e^+e^-$ are given by the same expressions but with the obvious replacements $\phi_5 \to -\phi_6$ and $\phi_6 \to -\phi_5$.

In order to implement the FSI we perform a partial wave projection of the $e^+e^- \to \bar{p}p$ amplitudes and switch from the helicity basis to the more convenient LSJ representation. The corresponding formalism is documented in various publications in the literature. We follow here the procedure described in detail in the Appendices B and C of Ref. [205]. Then we end up with four amplitudes, corresponding to the coupling between the e^+e^- and the $\bar{p}p$ systems and the coupled ${}^3S_1 - {}^3D_1$ partial waves. We can write these in the form $F_{L\,L'}$, where $L'(L) = 0, 2$ characterizes the orbital angular momentum in the initial (final) state. The explicit expressions for the reaction $e^+e^- \to \bar{N}N$ are

$$\begin{aligned}
F^{\mu\nu}_{2\,2} &= -\frac{2\alpha}{9}\left[G_M - \frac{2M_p}{\sqrt{s}}G_E\right]\left[1 - \frac{2m_e}{\sqrt{s}}\right] \ , \\
F^{\mu\nu}_{0\,0} &= -\frac{4\alpha}{9}\left[G_M + \frac{M_p}{\sqrt{s}}G_E\right]\left[1 + \frac{m_e}{\sqrt{s}}\right] \ , \\
F^{\mu\nu}_{0\,2} &= -\frac{2\sqrt{2}\alpha}{9}\left[G_M + \frac{M_p}{\sqrt{s}}G_E\right]\left[1 - \frac{2m_e}{\sqrt{s}}\right] \ , \\
F^{\mu\nu}_{2\,0} &= -\frac{2\sqrt{2}\alpha}{9}\left[G_M - \frac{2M_p}{\sqrt{s}}G_E\right]\left[1 + \frac{m_e}{\sqrt{s}}\right] \ .
\end{aligned} \tag{4.6}$$

For reasons of clarity we include in Eq. (4.6) and in the next few lines superscripts for the channels ($\nu = e^+e^-$ and $\mu = \bar{p}p$), but we will omit them again later in order to simplify the notation. Time reversal invariance requires that $F^{\mu\nu}_{L\,L'}(p,p') = F^{\nu\mu}_{L'\,L}(p',p)$ so that for the reaction $\bar{p}p \to e^+e^-$ the amplitudes $F_{0\,2}$ and $F_{2\,0}$ are interchanged.

It is obvious from Eq. (4.6) that the amplitude $F^{\mu\nu}_{L\,L'}$ can be written as a product of factors, which is simply a consequence of the one-photon exchange which amounts to an s-channel pole diagram in the reactions $e^+e^- \leftrightarrow \bar{p}p$. The factors correspond to the $e^+e^-\gamma$ and $\bar{p}p\gamma$ vertices, respectively, and reflect whether the coupling occurs in an S or D wave. Thus, we can write the amplitude in the form ($L,\ L' = 0, 2$)

$$F^{\mu\nu}_{L\,L'} = -\frac{4\alpha}{9}\,\mathcal{V}^{\mu}_{L}\,\mathcal{V}^{\nu}_{L'}, \quad \text{with}$$

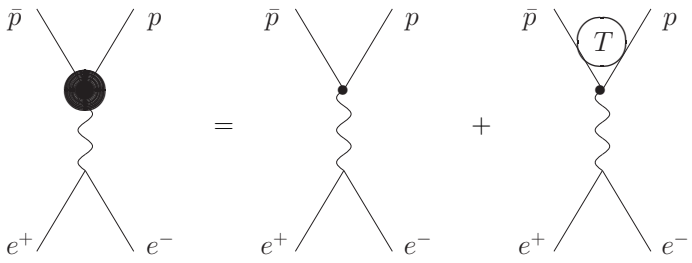

Figure 4.1: Graphic representation of our treatment of the reaction $e^+e^- \to \bar{p}p$. The small (large) filled circle symbolizes the bare (dressed) $\bar{N}N\gamma$ vertex while T stands for the $\bar{N}N$ scattering amplitude.

$$\mathcal{V}_0^\mu \;=\; \left(G_M + \frac{M_p}{\sqrt{s}}G_E\right),\; \mathcal{V}_2^\mu = \frac{1}{\sqrt{2}}\left(G_M - \frac{2M_p}{\sqrt{s}}G_E\right)\;, \tag{4.7}$$

and similar expressions for $\mathcal{V}_L^\nu$, the vertex functions of the e^+e^- pair. The FSI effects due to the $\bar{p}p$ interaction influence only the $\bar{p}p$ vertex and that means only $\mathcal{V}_L^\mu$ (simply denoted by $\mathcal{V}_L$ in the following), see Fig. 4.1. These effects can be calculated rigorously and within our formalism they amount to evaluating the equation

$$\mathcal{V}_{L'}(k;E_k) = \mathcal{V}_{L'}^0(k) + \sum_L \int_0^\infty \frac{dp\,p^2}{(2\pi)^3}\,\mathcal{V}_L^0(p)\frac{1}{2E_k - 2E_p + i0^+}T_{LL'}(p,k;E_k)\;, \tag{4.8}$$

where the first term on the right-hand side, the so-called Born term, represents the bare $\bar{N}N$ production vertex $\mathcal{V}_L^0$ and the integral provides the dressing of this vertex via $\bar{N}N$ rescattering. The quantity $T_{LL'}(p,p';E_k)$ is the $\bar{N}N$ scattering amplitude in the coupled ${}^3S_1 - {}^3D_1$ partial wave and is the solution of a corresponding Lippmann-Schwinger equation:

$$\begin{aligned} T_{L''L'}(p'',p';E_k) &= V_{L''L'}(p'',p') + \\ &\sum_L \int_0^\infty \frac{dp\,p^2}{(2\pi)^3}\,V_{L''L}(p'',p)\frac{1}{2E_k - 2E_p + i0^+}T_{LL'}(p,p';E_k)\;, \end{aligned} \tag{4.9}$$

see Chap. 3 . For the potential V in Eq. (4.9) we utilize the interaction derived within chiral EFT reported in Chap. 3 and one of the phenomenological $\bar{N}N$ models constructed by the Jülich group [92]. In the above equations $\sqrt{s} = 2\,E_k = 2\sqrt{M_p^2 + k^2}$, where k is the $\bar{p}p$ on-shell momentum.

The bare $\bar{N}N\gamma$ vertex functions, $\mathcal{V}_L^0$ (L=0, 2) in Eq. (4.8), can be written in terms of bare EMFFs, G_E^0 and G_M^0, in complete analogy to Eq. (4.7). On a microscopic level these quantities are given by the direct coupling of the photon to the $\bar{N}N$ system. But they can be also expressed in terms of the coupling of the photon to the hadrons through

intermediate vector mesons (ρ, ω, ϕ, etc.) which forms the basis of the vector meson dominance (VMD) model [180, 183, 206, 207]. There will be also contributions to $\mathcal{V}_L^0$ (or, equivalently, to G_E^0 and G_M^0) from intermediate mesonic states such as $\gamma \to \pi^+\pi^- \to \bar{p}p$, etc. Thus, in principle, $\mathcal{V}_0^0$ and $\mathcal{V}_2^0$ are complex and can depend on the total energy and on the (off-shell) momentum of the $\bar{N}N$ system.

In the present study we assume that the whole energy dependence of the dressed vertex functions $\mathcal{V}_L$ is generated by the FSI alone and that $\mathcal{V}_0^0$ and $\mathcal{V}_2^0$ themselves are energy-independent. In particular, we interpret the explicit dependence of $\mathcal{V}_L^0$ on $\sqrt{s}$ that is implied by Eq. (4.7) as a dependence on the momentum of the $\bar{N}N$ system. Accordingly, we use

$$\begin{aligned} \mathcal{V}_0^0(p) &= \left(G_M^0 + \frac{M_p}{2E_p}\, G_E^0\right) = \left(G_M^0 + \frac{M_p}{2\sqrt{M_p^2+p^2}}\, G_E^0\right) , \\ \mathcal{V}_2^0(p) &= \frac{1}{\sqrt{2}}\left(G_M^0 - \frac{M_p}{E_p}\, G_E^0\right) = \frac{1}{\sqrt{2}}\left(G_M^0 - \frac{M_p}{\sqrt{M_p^2+p^2}}\, G_E^0\right) , \end{aligned} \tag{4.10}$$

for the bare vertex functions, where p is the center-of-mass momentum in the $\bar{N}N$ system, and we assume that G_E^0 and G_M^0 are real and constant.

The replacement $\sqrt{s} \to 2E_p$ is anyhow required in order to guarantee the correct threshold behavior of the D-wave vertex function $\mathcal{V}_2^0(p)$ which has to behave like $\propto p^2$. Indeed, the partial-wave representation of the $e^+e^- \leftrightarrow \bar{p}p$ amplitudes in form of Eqs. (4.7) or (4.10) is rather instructive because it makes clear that the condition $G_E^0 = G_M^0$ and/or $G_E = G_M$ at the $\bar{p}p$ threshold is mandatory for implementing the proper threshold behavior of the D-wave amplitude. Assumptions like $|G_E| = 0$ imposed in the past in an analysis of the neutron form factor in the timelike region for energies fairly close to the threshold [209] constitute a drastic violation of this condition.

Our assumption that G_E^0 and G_M^0 are constant automatically implies that we have to set $G_E^0 = G_M^0$. G_E^0 (G_M^0) is taken to be real because any overall phase drops out in the evaluation of observables. Thus, there is only a *single* free parameter in our calculation. The bare vertex functions $\mathcal{V}_0^0$ and $\mathcal{V}_2^0$ are calculated from Eq. (4.10) and inserted into Eq. (4.8). Due to the FSI the resulting dressed vertex functions $\mathcal{V}_0$ and $\mathcal{V}_2$ are energy-dependent and also complex. Inverting Eq. (4.7) we can obtain G_E and G_M and then evaluate any $e^+e^- \leftrightarrow \bar{p}p$ observable based on the formulae provided at the beginning of this section. Note that also G_E and G_M are complex quantities and, in general, $G_E \neq G_M$ where the difference is likewise solely due to the FSI.

4.3 Results

For evaluating the FSI effects we employ amplitudes generated from an $\bar{N}N$ interaction that was recently derived by us within chiral EFT, see Chap. 3. In that reference, $\bar{N}N$ potentials up to next-to-next-to-leading order (NNLO) were constructed, based on a modified Weinberg power counting, in close analogy to pertinent studies of the nucleon-nucleon

interaction [106]. The low-energy constants associated with the arising contact interactions are fixed by a fit to phase shifts and inelasticities provided by a recently published phase-shift analysis of $\bar{p}p$ scattering data [108]. In the ${}^3S_1 - {}^3D_1$ partial wave that is needed for the study of the reaction $\bar{p}p \leftrightarrow e^+e^-$ good overall agreement with the antinucleon-nucleon phase shifts and inelasticities was obtained up to laboratory energies of around 200 MeV (see Chap. 3). For convenience the corresponding results are reproduced here, see Fig. 4.2. Accordingly, in the present study we restrict ourselves to excess energies $Q = \sqrt{s} - 2M_p$ of around 100 MeV in the $\bar{N}N$ system. In any case, it is primarily the threshold region where we expect that FSI effects are relevant and determine the energy dependence of the observables. At higher kinetic energies or, generally, over a larger energy region, the intrinsic energy- and momentum dependence of the $\bar{N}N$ production mechanism itself may become significant or even dominant and then our assumption that G_E^0 and G_M^0 are constant is no longer valid.

Besides the EFT interaction we consider again the Jülich $N\bar{N}$ model A(OBE) [92], which has already been used in our earlier study [119].

Results for the $e^+e^- \to \bar{p}p$ reaction cross section are displayed in Fig. 4.3 as a function of Q and compared with experiments [186, 187, 208, 209]. We are interested in the near-threshold region and, therefore, we compare to the BaBar data with a smaller bin size listed in Table VII of their papers [186, 187]. Since the old and new BaBar data are given for precisely the same bins we shifted the 2006 data [186] to slightly higher Q values in Fig. 4.3 for a better discrimination.

As said above, there is only a single parameter in our calculation, namely G_E^0, which, in essence, amounts to an overall normalization factor. It is fixed by a χ^2 fit to the $e^+e^- \to \bar{p}p$ cross section data up to $Q \approx 60$ MeV for each of the considered $\bar{N}N$ interactions. We want to emphasize again that the energy dependence of the cross section itself is not influenced by this parameter. It is given entirely by the FSI effects generated by the various potentials. In case of the EFT interactions (at NLO and NNLO) bands are shown. Those bands reflect the cutoff dependence of the corresponding results and can be viewed as an estimate for the theoretical uncertainty of the interactions, cf. the discussion in Chap. 3.

Obviously the energy dependence of the $e^+e^- \to \bar{p}p$ cross section is very well reproduced by all $\bar{N}N$ potentials considered for the FSI, over the whole energy range up to 100 MeV. This is reflected in the achieved χ^2/dof which amounts to $0.81 \cdots 1.01$ and $0.63 \cdots 0.71$ for the NLO and NNLO interactions, respectively, and to 0.64 for the Jülich model A(OBE). This is a strong support for the conjecture that the energy dependence exhibited by the cross section is dominated more or less completely by the one of the $\bar{N}N$ interaction. It is interesting to compare the present result with that of our earlier study [119], where only the ${}^3S_1$ partial wave was taken into account and which relied on the Migdal-Watson approximation with regard to the treatment of FSI effects. In that work only the rapid rise of the cross section close to the threshold could be reproduced and visible deviations started already at excess energies around 50 MeV. Now, with the coupling to the ${}^3D_1$ partial wave included and an accurate treatment of the FSI effects, there is quantitative agreement with the data (within the error bars) up to significantly higher energies.

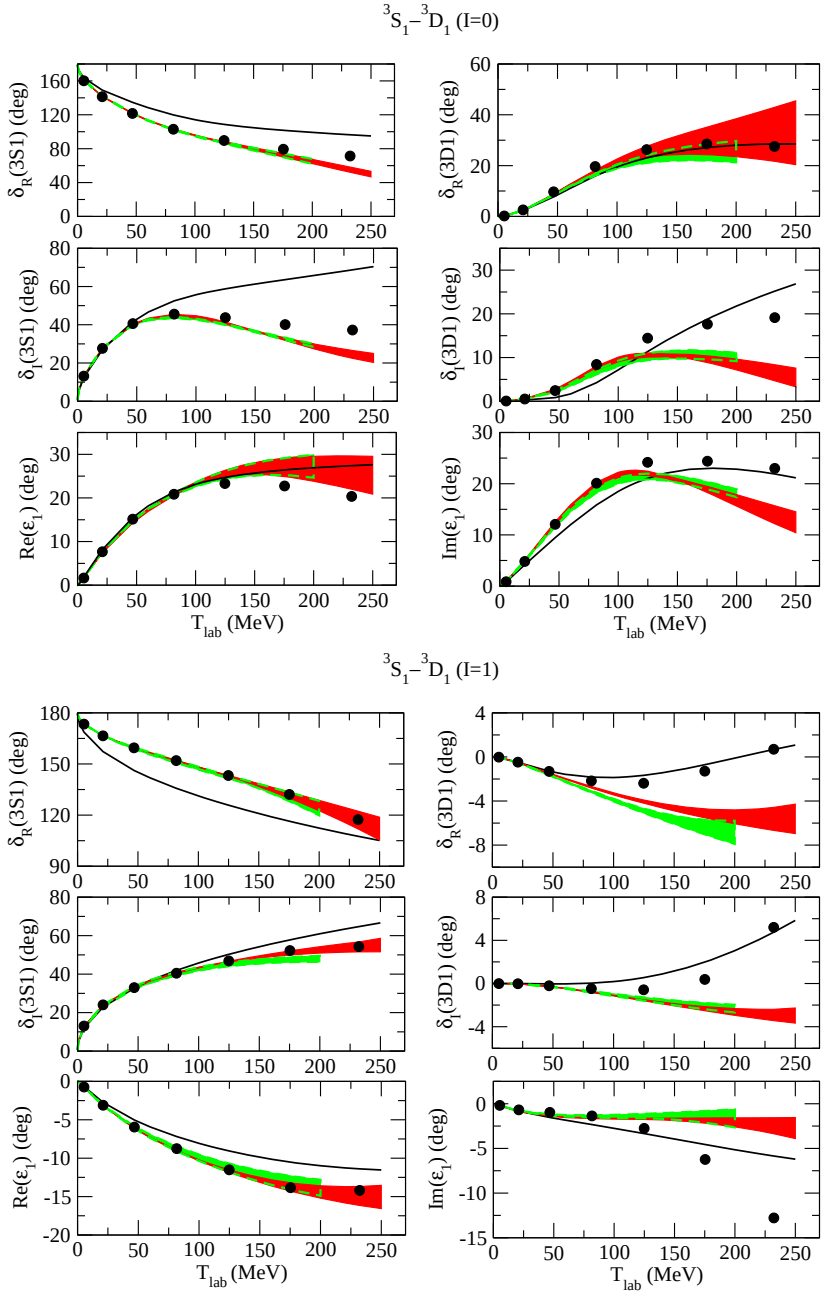

Figure 4.2: Real and imaginary parts of the phase shift in the $^3S_1$–$^3D_1$ partial wave in the isospin $I = 0$ and $I = 1$ channels. The red/dark band shows the chiral EFT results up to NNLO while the green/light band are results to NLO. The bands reflect the cutoff dependence of the results as discussed in Chap. 3. The solid line is the prediction of the Jülich $\bar{N}N$ model A(OBE) [92]. The circles represent the solution of the partial-wave analysis of Ref. [108].

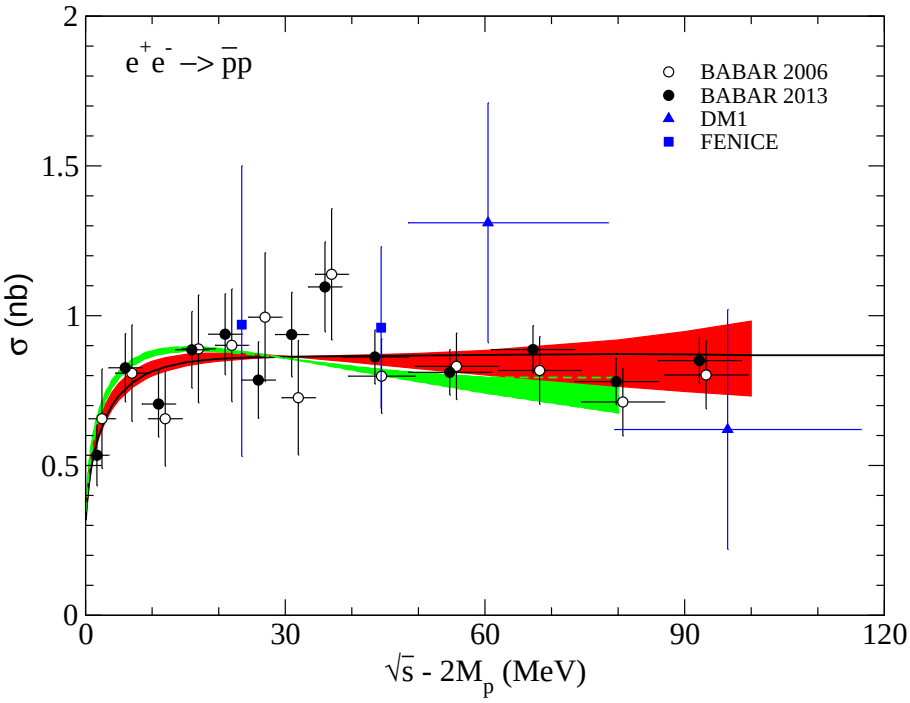

Figure 4.3: Cross section of the reaction $e^+e^- \to \bar{p}p$ as a function of the excess energy. The data are from the DM1 [208] (triangles), FENICE [209] (squares), and BaBar [186] (empty circles), [187] (filled circles) collaborations. The red/dark band shows results based on the $\bar{N}N$ amplitude of the chiral EFT interaction up to NNLO while the green/light band are those for NLO. The solid line is the result for the $\bar{N}N$ amplitude predicted by the Jülich model A(OBE) [92]. The BaBar 2006 data are shifted to slightly higher Q values, see text.

The results in Fig. 4.3 and those presented below are all obtained by using the $\bar{p}p$ amplitude in Eq. (4.8) which is the sum of the isospin $I = 0$ and $I = 1$ amplitudes, i.e. $T^{\bar{p}p} = (T^{I=1} + T^{I=0})/2$. However, we did perform exploratory calculations employing also $T^{I=1}$ and $T^{I=0}$ separately. The corresponding results turned out to be very similar to each other and also to the one based on the $\bar{p}p$ amplitude. Indeed, in all cases we obtain excellent agreement with the energy dependence exhibited by the data. Thus, we do not see any evidence for a possible dominance of the isoscalar amplitude as suggested in Ref. [193].

A comparison with data for the inverse reaction, $\bar{p}p \to e^+e^-$, that were taken by the PS170 Collaboration at LEAR is provided in Fig. 4.4. This cross section is related to the one for $e^+e^- \to \bar{p}p$ by detailed balance and time-reversal invariance, i.e. by

$$\sigma_{\bar{p}p\to e^+e^-} \simeq \frac{k_e^2}{k_p^2}\,\sigma_{e^+e^-\to\bar{p}p}\ . \tag{4.11}$$

There is a well-known systematical difference between the $e^+e^- \to \bar{p}p$ and $\bar{p}p \to e^+e^-$ cross section data [184], where the latter are smaller by a factor of about 1.47. But once we take

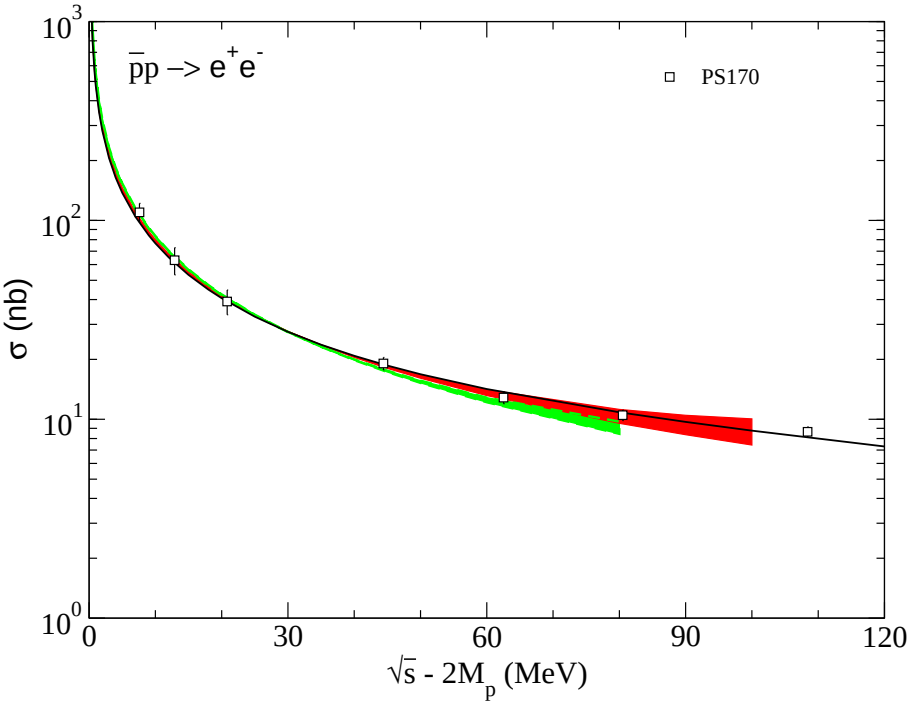

Figure 4.4: Cross section of the reaction $\bar{p}p \to e^+e^-$ as a function of the excess energy. The data are from the PS170 [185] collaborations. Same description of curves as in Fig. 4.3.

that into account by a proper renormalization of our results (using the same renormalization factor for all considered $\bar{N}N$ interactions) we reproduce the PS170 measurement rather nicely as can be seen in Fig. 4.4. Obviously, the energy dependence of the $\bar{p}p \to e^+e^-$ cross section revealed by the PS170 data [185] is perfectly consistent with the one of the $e^+e^- \to \bar{p}p$ data measured by the BaBar collaboration [186, 187].

Results for the effective proton form factor in the timelike region, defined in Eq. (4.3), are displayed in Fig. 4.5. Data for this quantity, which provides a quantitative indication for the deviation of the measured cross section from the point-like case [184] can be readily found in those publications where experiments for $e^+e^- \leftrightarrow \bar{p}p$ were reported [186, 187, 208, 209]. The effective form factor for the point-like case would be simply a straight line in Fig. 4.5, i.e. there would be no dependence on the excess energy. The experimental form factor, on the other hand, shows a significant rise for energies close to the threshold as already mentioned in the Introduction. Our results that include the $\bar{N}N$ FSI are very well in line with this behaviour. This is not surprising in view of the fact that we reproduce the $e^+e^- \leftrightarrow \bar{p}p$ cross sections that form the basis for determining the effective proton form factor, see Eq. (4.3).

There is also experimental information on angular distributions. For the reaction $e^+e^- \to \bar{p}p$ such distributions are provided for different intervals of the $\bar{p}p$ invariant mass [186, 187]. We consider here solely the lowest two, because only those concern the

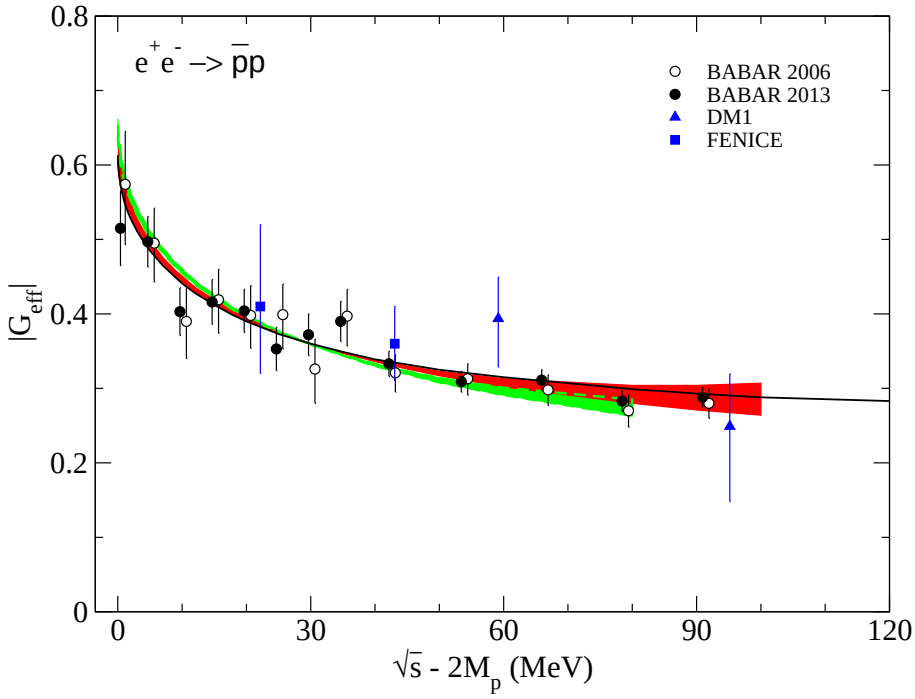

Figure 4.5: Effective proton form factor, defined in Eq. (4.3), as a function of the excess energy. The data are from the DM1 [208] (triangles), FENICE [209] (squares), and BaBar [186] (empty circles), [187] (filled squares) collaborations. Same description of curves as in Fig. 4.3. The BaBar 2006 data are shifted to slightly higher Q values, see text.

energy region for which our EFT $\bar{N}N$ potentials are designed. The corresponding intervals in terms of the excess energies are $0 \leq Q \leq 73$ MeV and $73 \leq Q \leq 148$ MeV. It is clear that data which sample over such a large energy range cannot reflect any more subtle variations of the angular distribution with energy. Thus, we perform our calculations for the average energies of those intervals, namely $Q = 36.5$ MeV and 110.5 MeV. The results are confronted with the BaBar data in Fig. 4.6. There is a remarkable agreement in case of EFT interactions. We want to emphasize that the angular distributions are genuine predictions. They are completely fixed by the properties of the employed $\bar{N}N$ FSI. Note that the overall normalization is arbitrary because only the number of events are given in Refs. [186, 187]. Again the 2006 data [186] are slightly shifted for a better discrimination.

In case of $\bar{p}p \to e^+e^-$ proper differential cross sections were measured, at laboratory momenta of 416, 505, 581, 681, and 888 MeV/c [185]. Also here we restrict ourselves to energies within the range where our EFT interactions are applicable which means we compare our results to the data at the first four momenta only. The corresponding excess energies are 43.5, 62.6, 80.9 and 107.5 MeV, respectively, and pertinent results are presented in Fig. 4.7. Again there is reasonable agreement of the results based on the EFT interactions with the trend exhibited by the experiment.

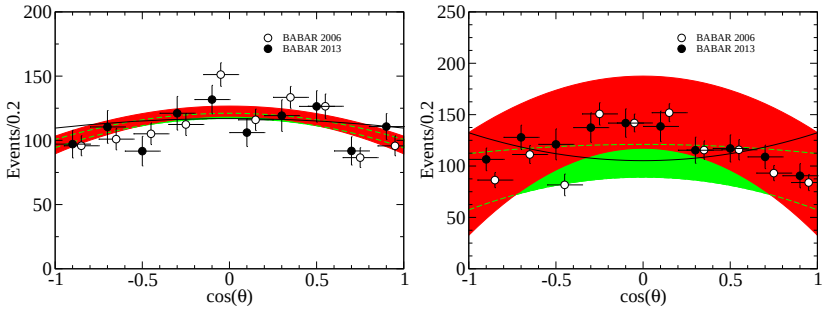

Figure 4.6: Differential cross section for $e^+e^- \to \bar{p}p$ at the excess energies $Q = 36.5$ MeV (left) and $Q = 110.5$ MeV (right). The data are an average over $0 \leq Q \leq 73$ MeV and over $73 \leq Q \leq 148$ MeV, respectively, and are taken from Refs. [186, 187]. Same description of curves as in Fig. 4.3. The BaBar 2006 data are slightly shifted, see text.

Note that in both cases the highest considered energy, $Q \approx 110$ MeV ($T_{\rm lab} \approx 220$ MeV), is already in a region where our NLO and NNLO interactions no longer reproduce the $\bar{p}p$ amplitudes of the PWA sufficiently well, see Fig. 4.2. Thus, those results may be questionable and they are also afflicted by large uncertainties as reflected by the bands. We show them only for illustrative purposes.

The prediction based on the phenomenological Jülich model disagrees with the trend shown by the BaBar data at the higher energy but is still in line with the PS170 measurement at practically the same excess energy ($Q \approx 107$ MeV). This $\bar{N}N$ potential produces a different D wave admixture in the $e^+e^- \leftrightarrow \bar{p}p$ amplitude as compared to the EFT interactions – which is not surprising in view of the differences in the corresponding $\bar{N}N$ phase shifts, cf. Fig. 4.2. Obviously, the differential cross sections are more sensitive to details of the $\bar{N}N$ interaction than the (energy dependence of the) integrated cross section where the results for all $\bar{N}N$ considered interactions more or less coincide. Thus, it would be indeed very valuable to have further data on differential cross sections with improved statistics.

Since our calculation agrees rather well with all measured $e^+e^- \leftrightarrow \bar{p}p$ observables in the near-threshold region it is instructive to consider now predictions for other quantities like spin observables and also for the EMFFs G_E and G_M themselves. Results for the latter are presented in Fig. 4.8 where we display the modulus and the argument of the ratio G_E/G_M as a function of the excess energy. The ratio $|G_E/G_M|$ drops to values slightly below 1 right above the $\bar{p}p$ threshold but quickly turns to values larger than 1 with increasing energy. At higher energies the EFT interaction fitted to the $\bar{N}N$ PWA and the Jülich meson-exchange model exhibit different trends for the ratio. Again this is simply due to differences in the pertinent $\bar{N}N$ amplitudes at these energies, as reflected in the phase shifts shown in Fig. 4.2. In that figure one can also see that the EFT interaction does not reproduce the ${}^3D_1$ phase shifts of the $\bar{N}N$ PWA so well anymore for energies above $T_{\rm lab} \approx 130$ MeV ($Q \approx 65$ MeV). Thus, since the D-waves are responsible for the deviation of $|G_E/G_M|$ from 1, one should refrain from associating the results based on our

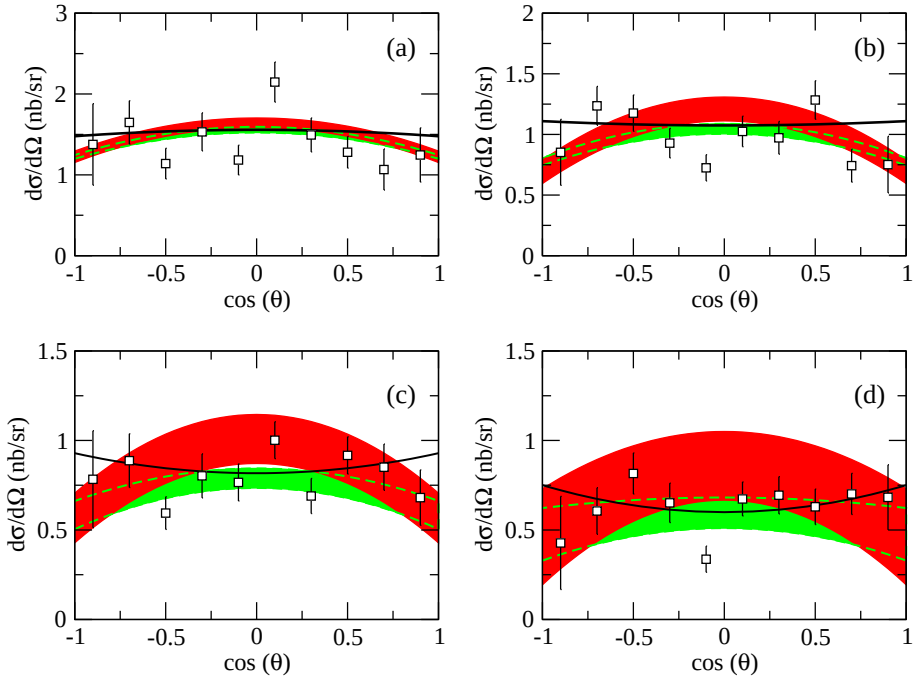

Figure 4.7: Differential cross section for $\bar{p}p \to e^+e^-$ at the excess energies $Q = 43.5$ (a), 62.6 (b), 80.9 (c), and 107.5 MeV (d), respectively. Data are taken from Ref. [185]. Same description of curves as in Fig. 4.3.

EFT interaction with those implied by the original $\bar{N}N$ amplitudes of the PWA at higher energies. In any case, there is also an increasing uncertainty due to the cutoff dependence as visible from the bands.

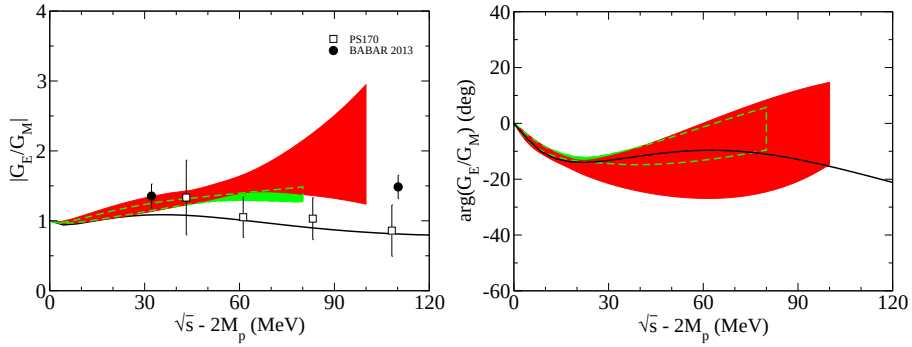

Figure 4.8: $|G_E/G_M|$ and arg(G_E/G_M) as a function of the excess energy. Data are taken from Refs. [185] and [187]. Same description of curves as in Fig. 4.3.

Predictions for the phase between G_E and G_M are shown in Fig. 4.8. It is negative over a larger energy range starting from the threshold. Also here the EFT interaction and the

Jülich model exhibit a different behavior for higher energies. Overall, the phase remains small with values between ±20 degrees.

Finally, let us present some results for spin-dependent observables for the reaction $\bar{p}p \to e^+e^-$, in particular, for the analyzing power A_y and the spin-correlation parameters A_{ij}. These observables can be written in terms of the $(e^+e^- \to \bar{p}p)$ helicity amplitudes given in Eq. (4.4) following the standard procedure outlined in Refs. [205, 210]:

$$\begin{aligned}
A_y &= -(\mathrm{Im}\,\phi_5^*(\phi_3-\phi_4) - \mathrm{Im}\,\phi_6^*(\phi_1+\phi_2))/D, \\
A_{xx} &= (\mathrm{Re}\,[\phi_1^*\phi_2 + \phi_3^*\phi_4] + |\phi_5|^2 - |\phi_6|^2)/D, \\
A_{yy} &= (\mathrm{Re}\,[\phi_1^*\phi_2 - \phi_3^*\phi_4] + |\phi_5|^2 + |\phi_6|^2)/D, \\
A_{zz} &= -(|\phi_1|^2 + |\phi_2|^2 - |\phi_3|^2 - |\phi_4|^2 + 2|\phi_5|^2 - 2|\phi_6|^2)/(2\,D), \\
A_{xz} &= -(\mathrm{Re}\,\phi_5^*(\phi_3-\phi_4) + \mathrm{Re}\,\phi_6^*(\phi_1+\phi_2))/D,
\end{aligned} \tag{4.12}$$

where $D = (\sum_{i=1}^{8} |\phi_i|^2)/2$. Corresponding expressions in terms of G_E and G_M are written as [201, 203, 211–213]

$$\begin{aligned}
A_y &= \frac{2M_p \sin 2\theta\ \mathrm{Im}\,(G_E^* G_M)/\sqrt{s}}{(1+\cos^2\theta)\,|G_M|^2 + 4M_p^2 \sin^2\theta\,|G_E|^2/s}, \\
A_{xx} &= \frac{\sin^2\theta(4M_p^2\,|G_E|^2 + |G_M|^2)/s}{(1+\cos^2\theta)\,|G_M|^2 + 4M_p^2 \sin^2\theta\,|G_E|^2/s}, \\
A_{yy} &= \frac{\sin^2\theta(4M_p^2\,|G_E|^2/s - |G_M|^2)}{(1+\cos^2\theta)\,|G_M|^2 + 4M_p^2 \sin^2\theta\,|G_E|^2/s}, \\
A_{zz} &= \frac{(1+\cos^2\theta)\,|G_M|^2 - 4M_p^2 \sin^2\theta\,|G_E|^2/s}{1+\cos^2\theta)\,|G_M|^2 + 4M_p^2 \sin^2\theta\,|G_E|^2/s}, \\
A_{xz} &= \frac{2M_p \sin 2\theta\ \mathrm{Re}\,(G_E^* G_M)/\sqrt{s}}{(1+\cos^2\theta)\,|G_M|^2 + 4M_p^2 \sin^2\theta\,|G_E|^2/s}
\end{aligned} \tag{4.13}$$

Our predictions for A_y and A_{ij} at the excess energy $Q = 45$ MeV are depicted in Figs. 4.9 and 4.10, respectively. These observables show clear symmetry properties in case of the one-photon exchange approximation considered here, as one can read off the formulae given in Ref. [203]. Specifically, A_y and A_{xz} are proportional to $\sin 2\theta$, and A_{xx} and A_{yy} are proportional to $\sin^2\theta$. The magnitudes of A_y and A_{xz} are given by the relative phase of G_E and G_M, namely by $\mathrm{Re}\,(G_E G_M^*)$ in case of the former and by $\mathrm{Im}\,(G_E G_M^*)$ for the latter [203]. Predictions for these quantities can be found in Fig. 4.11, again as a function of the excess energy.

Results for spin-dependent observables have been also published by other authors [178, 192, 211, 213, 214] based on various models, however, in general, for much higher energies.

An issue that arises in the context of any observed enhancement in the near-threshold $\bar{p}p$ production cross sections or in the corresponding $\bar{p}p$ invariant mass spectra is the question whether this is a signal for an $\bar{N}N$ bound state. Indeed sometimes it is argued that

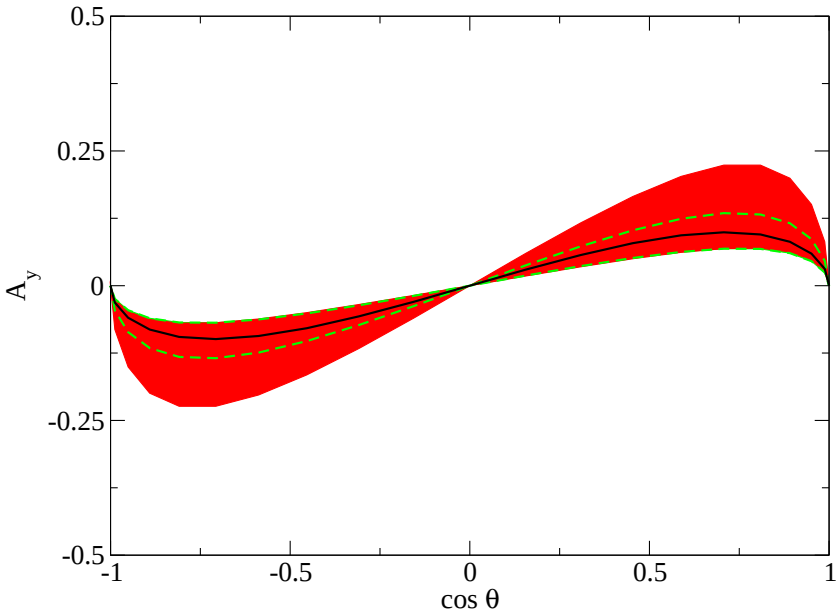

Figure 4.9: Analyzing power for $\bar{p}p \to e^+e^-$ at the excess energy $Q = 45$ MeV. Same description of curves as in Fig. 4.3.

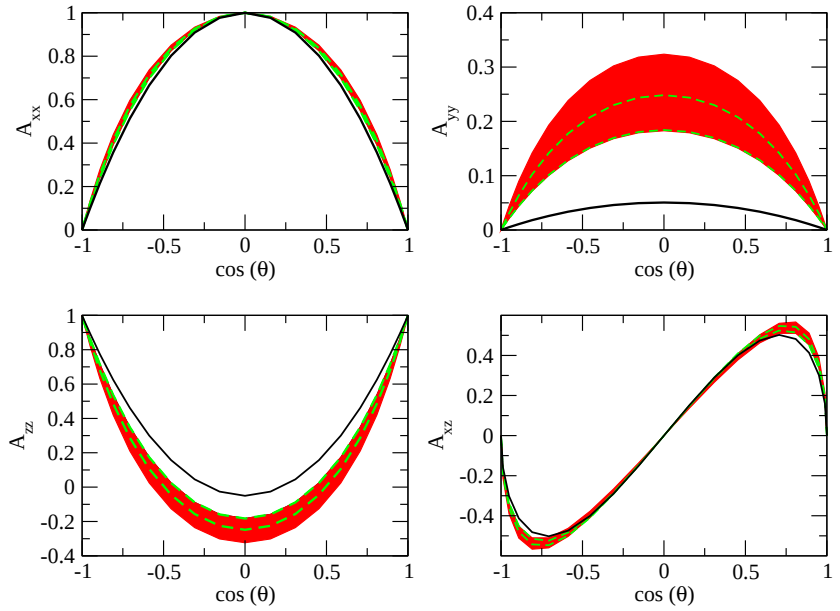

Figure 4.10: Spin correlation parameters for $\bar{p}p \to e^+e^-$ at the excess energy $Q = 45$ MeV. Same description of curves as in Fig. 4.3.

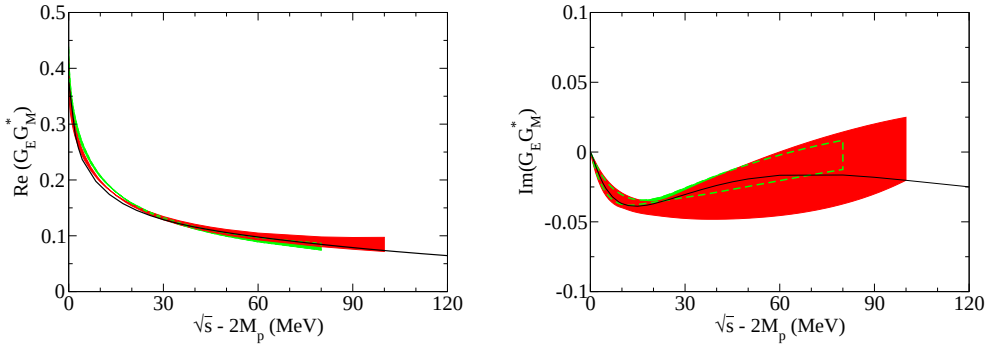

Figure 4.11: $\mathrm{Re}\,(G_E G_M^*)$ and $\mathrm{Im}\,(G_E G_M^*)$ as a function of the excess energy. Same description of curves as in Fig. 4.3.

explanations in terms of FSI effects or via an $\bar{N}N$ bound state would mutually exclude each other. This is clearly not the case as we know very well from studies of near-threshold pion production in the reaction $NN \to NN\pi$ [130]. In this case the NN forces in the ${}^1S_0$ and/or ${}^3S_1$ final NN state allow one to achieve a quantitative description of the enhancements seen in the measurements and the very same forces also produce the deuteron bound state in the ${}^3S_1$–${}^3D_1$ partial wave and a virtual state in the ${}^1S_0$. Of course, not every enhancement seen in the experiments is a signal for forces that are strong enough to produce a pole in the near-threshold region. For example, a pronounced near-threshold enhancement was also observed in the Λp invariant mass spectrum as measured in the reaction $pp \to p\Lambda K^+$, see for example [215]. However, evidently there is no near-threshold Λp bound state. Thus, one has to be cautious with conclusions concerning the existence of such bound states from production reactions.

Anyway, let us come back to the $\bar{N}N$ interaction investigated here. For the employed EFT potentials a search for poles near the threshold was performed and the results were reported in Chap. 3. No bound state was found for the ${}^3S_1$–${}^3D_1$ partial wave in the isospin $I = 1$ channel. There is a pole in the $I = 0$ channel, however, it corresponds to a "binding" energy of $Q_0 = +(5.6 \cdots 7.7) - \mathrm{i}\,(49.2 \cdots 60.5)$ MeV, depending on the cutoffs, at NLO and $Q_0 = +(4.8 \cdots 21.3) - \mathrm{i}\,(60.6 \cdots 74.9)$ MeV at NNLO. We used quotation marks above because the positive sign of the real part of Q_0 indicates that these poles are actually located above the $\bar{N}N$ threshold. They lie on the physical sheet and, therefore, do not correspond to resonances either. In Ref. [171] such poles are referred to as unstable bound states.

4.4 Conclusions

We analyzed the reactions $\bar{p}p \to e^+e^-$ and $e^+e^- \to \bar{p}p$ in the near-threshold region with specific emphasis on the role played by the interaction in the initial- or final $\bar{N}N$ state. The study is based on the one-photon approximation for the elementary reaction mechanism,

but takes into account rigorously the effects of the $\bar{p}p$ interaction. For the latter we utilized the $\bar{N}N$ potential reported in Chap. 3 and also one of the phenomenological $\bar{N}N$ meson-exchange models constructed by the Jülich group [92].

Our results confirm the conjecture drawn from previous studies [119,126,189–194] that the pronounced energy dependence of the $e^+e^- \leftrightarrow \bar{p}p$ cross section, seen in pertinent experiments, is indeed primarily due to the $\bar{p}p$ interaction. However, the evidence provided now is much more convincing. First the present calculation is technically superior to the earlier ones because it relies on an rigorous treatment of the FSI effects. Secondly, it utilizes $\bar{N}N$ amplitudes that have been determined from a PWA. And, finally, by including not only the $^3S_1$ but also the $^3D_1$ partial wave the energy dependence of the experimental cross sections can be described quantitatively and over a significantly larger energy region. In addition, even existing data on angular distributions are well reproduced.

Based on our results for the reactions $e^+e^- \leftrightarrow \bar{p}p$ we can produce reliable predictions for the proton electromagnetic form factors G_E and G_M in the timelike region, for q^2 near the $\bar{N}N$ threshold. The effective proton form factor usually considered in the literature exhibits a strong q^2-dependence for $q^2 \approx (2M_p)^2$ and this behavior is perfectly described by our calculation. The strong q^2-dependence is likewise a consequence of the interaction in the $\bar{p}p$ system. For the ratio $|G_E/G_M|$ we predict a non-trivial energy dependence. The ratio drops to values slightly below 1 right above the $\bar{N}N$ threshold but turns to values larger than 1 within a couple of MeV. The phase between the form factors, $\arg(G_E/G_M)$, is negative for energies close to the $\bar{N}N$ threshold with values in the order of -10 to -20 degrees.

The predictions for the differential cross sections, and also for $|G_E/G_M|$ and $\arg(G_E/G_M)$, based on the chiral EFT interaction and on the phenomenological Jülich $\bar{N}N$ potential, show different tendencies with increasing energy. The presently available data (for the differential cross section) are afflicted with sizable uncertainties and, thus, do not allow to discriminate between these differences. Moreover, the BaBar and the PS170 data themselves seem to be incompatible at higher excess energies as visible, for example, in the extracted ratio $|G_E/G_M|$ [187], see also Fig. 4.8. Therefore, it would be very interesting to perform new measurements of the reactions $e^+e^- \leftrightarrow \bar{p}p$ with improved statistics. As discussed in the review [184], such experiments could be accomplished at the VEPP-2000 accelerator in Novosibirsk [216] or the BEPC-II collider in Beijing (for $e^+e^- \to \bar{p}p$), but also by the $\bar{\text{P}}$ANDA set-up at the planned FAIR facility in Darmstadt [217] (for the inverse reaction $\bar{p}p \to e^+e^-$). Evidently, aside from pinning down the electromagnetic form factors in the time like region more accurately, such data would also provide further constraints on our knowledge of the elementary $\bar{N}N$ interaction where direct information in the near-threshold region is still rather scarce.

Conclusions and Outlook

Here we present a summary for what have been done in this thesis.

- for B_{l4} decays and the extraction of $|V_{ub}|$

  The Cabibbo–Kobayashi–Maskawa (CKM) matrix element $|V_{ub}|$ is not well-determined yet. It can be extracted from both inclusive or exclusive decays, like $B \to \pi(\rho) l \bar{\nu}_l$. However, in particular the exclusive determination from $B \to \rho l \bar{\nu}_l$ so far suffers from a large model dependence. In this thesis, we propose to extract $|V_{ub}|$ from the four-body semileptonic decay $B \to \pi\pi l \bar{\nu}_l$, where the form factors for the pion–pion system are treated in dispersion theory. This is a model-independent approach that takes into account the $\pi\pi$ rescattering effects, including the effect of the ρ meson. We demonstrate that both finite-width effects of the ρ meson as well as scalar $\pi\pi$ contributions can be considered completely in this way.

- for antinucleon-nucleon interactions below the laboratory energies around 250 MeV.

  Results of an exploratory study of the antinucleon-nucleon interaction within chiral effective field theory are reported. The antinucleon-nucleon potential is derived up to next-to-next-to-leading order, based on a modified Weinberg power counting, in close analogy to pertinent studies of the nucleon-nucleon interaction. The low-energy constants associated with the arising contact interactions are fixed by a fit to phase shifts and inelasticities provided by a recently published phase-shift analysis of antiproton-proton scattering data. The overall quality of the achieved description of the antinucleon-nucleon amplitudes is comparable to the one found in case of the nucleon-nucleon interaction at the same order. For most S-waves and several P-waves good agreement with the antinucleon-nucleon phase shifts and inelasticities is obtained up to laboratory energies of around 200 MeV.

- for the reactions $e^+e^- \leftrightarrow \bar{p}p$.

  The reactions $e^+e^- \to \bar{p}p$ and $\bar{p}p \to e^+e^-$ are analyzed in the near-threshold region. Specific emphasis is put on the role played by the interaction in the initial or final antinucleon-nucleon state which is taken into account rigorously. For that purpose the antinucleon-nucleon potentials presented in above, which is derived within chiral effective field theory and fitted to results of a new partial-wave analysis of $\bar{p}p$

scattering data published in 2012. Our results provide strong support for the conjecture that the pronounced energy dependence of the $e^+e^- \leftrightarrow \bar{p}p$ cross section, also seen in other pertinent experiments like the notable one $J/\psi \to \gamma\bar{p}p$ is primarily due to the $\bar{p}p$ interaction. Predictions for the proton electromagnetic form factors G_E and G_M in the timelike region, close to the antinculeon-nucleon threshold, and for spin-dependent observables are presented. The steep rise of the effective form factor for energies closed to the $\bar{p}p$ threshold is explained by solely in terms of $\bar{p}p$ interaction. The corresponding experimental information is quantitatively described by our calculation.

The above works can be further improved in some sense and also some other related topics can be studied. For B_{l4} decays, the above results are confined to the region for $\pi\pi$ invariant mass below 1 GeV, and in principle, one can take into the coupled-channel effects, i.e., $\pi\pi \to K\bar{K}$ reactions and then the $\pi\pi$ invariant mass can be extended to a higher region. Meantime these strategies developed for the topic of B_{l4} decays can be easily applied to D_{l4} decays, where we wish to provide a reliable description of form factors for the hadronic transitions since $|V_{cd}|$ has been very well measured. For the work on antinucleon-nucleon, as mentioned in Chap. 3, one can generalize the above analysis to the next-to-next-to-next-to-leading order, where Coulomb interaction as well as the mass difference between proton and neutron can be included. Only in that way, one can get a precise treatment of antinucleon-nucleon interaction and further, the experimental observables will be calculated. With such more advanced potential, the reactions $e^+e^- \leftrightarrow \bar{p}p$ can be updated. Besides, the enhancement phenomenon at $\bar{p}p$ threshold are also observed in other reactions, e.g., $J/\psi \to \gamma p\bar{p}$, $\psi' \to \gamma p\bar{p}$ and $J/\psi \to \omega p\bar{p}$, and the corresponding theoretical analyses in view of final state interaction can be done. Some ways to include the final state interaction has been discussed in Chap. 1.

Appendix A

Further details on B_{l4} decays

A.1 Tree-level amplitudes in heavy-meson chiral perturbation theory

Calculating the tree-level diagrams in Fig. 2.2 in heavy-meson chiral perturbation theory, one obtains the corresponding amplitudes [59] ($\mathcal{A}$–$\mathcal{D}$, in obvious correspondence to diagrams (A)–(D))

$$\begin{aligned}
\mathcal{A} &= \frac{if_B}{4f_\pi^2} p_B^\mu \,, \qquad \mathcal{B} = ip_-^\mu \mathcal{B}^{(1)} + ip_B^\mu \mathcal{B}^{(2)} \,, \\
\mathcal{B}^{(2)} &= -\frac{gf_B}{2f_\pi^2} \frac{v\cdot p_-}{v\cdot p_- + \Delta} = -\frac{v\cdot p_-}{m_B} \mathcal{B}^{(1)} \,, \\
\mathcal{C} &= ip_B^\mu \mathcal{C}^{(1)} + \epsilon^{\mu\alpha\beta\gamma} p_{B\alpha} p_{-\beta} p_{+\gamma} \mathcal{C}^{(2)} \,, \\
\mathcal{C}^{(1)} &= -\frac{g^2 f_B}{2f_\pi^2} \frac{p_+\cdot p_- - (v\cdot p_+)(v\cdot p_-)}{[v\cdot(p_+ + p_-)][v\cdot p_- + \Delta]} \,, \\
\mathcal{C}^{(2)} &= -\frac{g^2 f_B}{2f_\pi^2} \frac{1}{[v\cdot(p_+ + p_-) + \Delta]\,[v\cdot p_- + \Delta]} \,, \\
\mathcal{D} &= ip_B^\mu \mathcal{D}^{(1)} \,, \quad \mathcal{D}^{(1)} = -\frac{f_B}{4f_\pi^2} \frac{v\cdot(p_+ - p_-)}{v\cdot(p_+ + p_-)} \,.
\end{aligned} \tag{A.1}$$

Identifying the contributions to the individual decay form factors, we find for these as the leading-order (LO) results

$$\begin{aligned}
F^{\mathrm{LO}} &= R^{\mathrm{LO}} - G^{\mathrm{LO}}, \quad G^{\mathrm{LO}} = \frac{m_B}{2}\mathcal{B}^{(1)}, \quad H^{\mathrm{LO}} = -\frac{m_B^3}{2}\mathcal{C}^{(2)}, \\
R^{\mathrm{LO}} &= -\frac{m_B f_B}{4f_\pi^2} - m_B\Big(\mathcal{B}^{(2)} + \mathcal{C}^{(1)} + \mathcal{D}^{(1)}\Big) \,.
\end{aligned} \tag{A.2}$$

From these, it is then straightforward to identify the pole contributions given in Eq. (2.20), as well as the non-pole pieces of Eq. (2.23).

It is obvious that all diagrams (A)–(D) are formally of $\mathcal{O}(p^0)$ in terms of soft pion momenta. Note, however, that all pieces proportional to $p_B^\mu = P^\mu + L^\mu$ are effectively suppressed: the part $\propto L^\mu$ enters the form factor R, which is suppressed by the small lepton mass and neglected throughout the main text, while the part $\propto P^\mu$ leads to a chiral suppression by one order (and is at least partially an artifact of the heavy-meson approximation anyway). As a consequence, the only leading contributions are given by the amplitudes $\mathcal{B}^{(1)}$ and $\mathcal{C}^{(2)}$ in the above, and hence the B^* pole graphs. This was already pointed out in Ref. [65].

A.2 Dispersive representations for polynomial inhomogeneities

Consider a partial wave $f(s)$ given *at tree level* as a constant, $f^{\rm tree}(s) = A$. In this case, we can write down the dispersive representation including final-state interactions right away, *if* we assume a certain high-energy behavior of the amplitude: it is given as

$$f(s) = A\,\Omega(s)\,, \tag{A.3}$$

with the Omnès function $\Omega(s)$. Here, we assume (as in the main text) an Omnès function falling according to $1/s$, i.e. given by a phase shift approaching π asymptotically, and a partial wave that vanishes in the same way for large s. This assumption prevents us from multiplying $\Omega(s)$ with a polynomial of higher degree.

However, in the spirit of the solution discussed in the main text, it should also be possible to treat this constant as an inhomogeneity, and reconstruct the same solution from the corresponding formalism. Our solution is then of the form

$$f(s) = A + \Omega(s)\left\{a + a's + \frac{s^2}{\pi}\int_{4M_\pi^2}^\infty \frac{A\sin\delta(s')ds'}{|\Omega(s')|s'^2(s'-s)}\right\}, \tag{A.4}$$

where we have chosen the minimal number of subtractions (two) required to make the dispersion integral converge. Note that the subtraction constants a, a' are not *a priori* fixed from the tree-level input; we can set $a = 0$ by requiring the normalization of the amplitude at $s = 0$ to match the tree-level input. The integral in Eq. (A.4) can be performed explicitly, using a dispersive representation of the inverse of the Omnès function

$$\Omega^{-1}(s) = 1 - \dot\Omega(0)\,s - \frac{s^2}{\pi}\int_{4M_\pi^2}^\infty \frac{\sin\delta(s')ds'}{|\Omega(s')|s'^2(s'-s)}\,, \tag{A.5}$$

where $\dot\Omega(0) = d\Omega(s)/ds|_{s=0}$. As a result, we find

$$f(s) = \Omega(s)\Big\{A + \big[a' - A\,\dot\Omega(0)\big]s\Big\}\,. \tag{A.6}$$

Therefore, Eq. (A.3) is reproduced if we choose $a = 0$, $a' = A\,\dot{\Omega}(0)$. We essentially apply the same requirement on the high-energy behavior as in Eq. (A.3): terms that do not vanish for large s are only cancelled for this specific choice of a'.

More generally, if we match to a tree-level amplitude of the form $A\,s^n$, demanding the same *leading* behavior near $s = 0$ such that all subtraction terms $\propto s^{m\leq n}$ can be put to zero, the solution using this tree-level input as an inhomogeneity,

$$A\,s^n + \Omega(s)\left\{a' s^{n+1} + \frac{s^{n+2}}{\pi}\int_{4M_\pi^2}^{\infty} \frac{A\,s'^n \sin\delta(s')ds'}{|\Omega(s')|s'^{n+2}(s'-s)}\right\}, \tag{A.7}$$

agrees with the " canonical " solution $A\,s^n\,\Omega(s)$, with the " correct " high-energy behavior, only if $a' = A\,\dot{\Omega}(0)$.

A.3 Kinematical relations

To specify the angles in Sec. 2.2 more precisely, let $\vec{p}_+$ be three-momentum of π^+ in $\Sigma_{2\pi}$ and $\vec{p}_l$ the three-momentum of l in the system of Σ_{lv}. In Fig. 2.1, $\vec{v}$ denote a unit vector of direction of flight of dipion in Σ_B and $\vec{c}(\vec{d})$ a unit vector along the projection of $\vec{p}_+$ ($\vec{p}_l$) perpendicular to $\vec{v}$ ($-\vec{v}$),

$$\begin{aligned}\vec{c} &= \big(\vec{p}_+ - (\vec{v}\cdot\vec{p}_+)\vec{p}_+\big)/\big[(\vec{p}_+)^2 - (\vec{v}\cdot\vec{p}_+)^2\big]^{1/2}\\ \vec{d} &= \big(\vec{p}_l - (\vec{v}\cdot\vec{p}_l)\vec{p}_l\big)/\big[(\vec{p}_l)^2 - (\vec{v}\cdot\vec{p}_l)^2\big]^{1/2}.\end{aligned}$$

With these definitions, one has

$$\begin{aligned} s &= (p_+ + p_-)^2, \quad s_l = (p_l + p_\nu)^2 \qquad (A.8)\\ \cos\theta_\pi &= \vec{v}\cdot\vec{p}_+/|\vec{p}_+|, \quad \cos\theta_l = -\vec{v}\cdot\vec{p}_l/|\vec{p}_l|\\ \cos\phi &= \vec{c}\cdot\vec{d}, \quad \sin\phi = (\vec{c}\times\vec{v})\cdot\vec{d}. \qquad (A.9)\end{aligned}$$

The physical ranges of these are

$$\begin{aligned} 4M_\pi^2 &\leq s \leq (m_B - m_l)^2\\ m_l^2 &\leq s_l \leq (m_B - \sqrt{s})^2\\ 0 &\leq \theta_\pi,\,\theta_l \leq \pi, \quad 0 \leq \phi \leq 2\pi. \end{aligned}\tag{A.10}$$

Introducing the four-momenta

$$P = p_+ + p_-, \quad Q = p_+ - p_-, \quad L = p_l + p_\nu, \quad N = p_l - p_\nu, \tag{A.11}$$

the following Lorentz invariant scalar products can be computed:

$$P^2 = s, \quad Q^2 = 4M_\pi^2 - s, \quad L^2 = s_l, \quad N^2 = 2m_l^2 - s_l$$

$$
\begin{aligned}
PQ &= 0, \quad LN = m_l^2 \\
PL &= \frac{1}{2}(m_B^2 - s - s_l) \\
PN &= z_l PL + (1 - z_l) X \cos\theta_l \\
QL &= \sigma_\pi X \cos\theta_\pi \\
QN &= z_l QL + \sigma_\pi (1 - z_l)\big[PL \cos\theta_\pi \cos\theta_l - \sqrt{s s_l} \sin\theta_\pi \sin\theta_l \cos\phi\big] \\
< LNPQ > &\equiv \epsilon_{\mu\nu\rho\sigma} L^\mu N^\nu P^\rho Q^\sigma \\
&= -\sqrt{s s_l}\sigma_\pi (1 - z_l) X \sin\theta_\pi \sin\theta_l \sin\phi, \qquad \text{(A.12)}
\end{aligned}
$$

with

$$
\begin{aligned}
\sigma_\pi &= \sqrt{1 - \frac{4M_\pi^2}{s}} \\
z_l &= \frac{m_l^2}{s_l} \\
X &= \frac{1}{2}\lambda^{1/2}(m_B^2, s, s_l) \qquad \text{(A.13)}
\end{aligned}
$$

and the Källén triangle function

$$
\begin{aligned}
\lambda(a, b, c) &= [a - (\sqrt{b} + \sqrt{c})^2][a - (\sqrt{b} - \sqrt{c})^2] \\
&= a^2 + b^2 + c^2 - 2ab - 2ac - 2bc \qquad \text{(A.14)}
\end{aligned}
$$

The Mandelstam variables t and u can be defined through

$$
t = (p_B - p_+)^2, \qquad u = (p_B - p_-)^2 \qquad \text{(A.15)}
$$

and one has the relations

$$
\begin{aligned}
t + u &= \Sigma_0 - s \\
t - u &= -2\sigma_\pi X \cos\theta_\pi \qquad \text{(A.16)} \\
\Sigma_0 &= 2M_\pi^2 + m_B^2 + s_l \qquad \text{(A.17)}
\end{aligned}
$$

To obtain these equations, we first introduce Lorentz transformation formula, cf. section "Kinematics" in Ref. [35]. The energy E and three-momentum $\vec{p}$ of a particle with mass m form a four-vector $p = (E, \vec{p})$ whose square $p^2 = E^2 - |\vec{p}|^2 = m^2$. The velocity of the particle is $\vec{\beta} = \vec{p}/E$. The energy and momentum $(E^*, \vec{p}^*)$ viewed from a frame moving with velocity $\vec{\beta}_f$ are given by

$$
\begin{pmatrix} E^* \\ p_{||}^* \end{pmatrix} = \begin{pmatrix} \gamma_f & -\gamma_f\beta_f \\ -\gamma_f\beta_f & \gamma_f \end{pmatrix} \begin{pmatrix} E \\ p_{||} \end{pmatrix}, \qquad p_T^* = p_T, \qquad \text{(A.18)}
$$

where $\gamma_f = (1-\beta_f^2)^{-1/2}$ with β_f is the magnitude of $\vec{\beta}_f$ and $p_T(p_{||})$ are the components of $\vec{p}$ perpendicular (parallel) to $\vec{\beta}_f$. There is a velocity addition law related to the concept of rapidity for collinear motions,

$$\beta_{31} = \frac{\beta_{21}+\beta_{32}}{1+\beta_{21}\beta_{32}} \tag{A.19}$$

where β_{21} is the velocity of particle 2 relative to 1, the similar for others. Other 4-vectors transform in the same way. One can verify that the scalar product of two four-momenta $p_1 \cdot p_2 = E_1E_2 - \vec{p}_1 \cdot \vec{p}_2$ is invariant.

We first write out p_+, p_- in the dipion system $\Sigma_{2\pi}$, applying the Lorentz transformation, we then get the forms in rest B meson frame Σ_B, the same applied to the momenta of leptons p_l, p_ν. In dipion system $\Sigma_{2\pi}$, we have

$$\begin{aligned}
\Sigma_{2\pi}:\ p_+ &= \frac{\sqrt{s}}{2}(1\,,\ \ \sigma_\pi \sin\theta_\pi\,,\ \ 0\,,\quad \sigma_\pi \sin\theta_\pi) \\
\Sigma_{2\pi}:\ p_- &= \frac{\sqrt{s}}{2}(1\,,\ \ -\sigma_\pi \sin\theta_\pi\,,\ \ 0\,,\ \ -\sigma_\pi \sin\theta_\pi).
\end{aligned} \tag{A.20}$$

Boosting p_+ from dipion system $\Sigma_{2\pi}$ to Σ_B, one obtains

$$\begin{aligned}
\Sigma_B:\ p_+ &= \left(\frac{\sqrt{\vec{p}^{\,2}+s_\pi}}{2} + \frac{|\vec{p}|}{2}\sigma_\pi\cos\theta_\pi\,,\quad \frac{\sqrt{s}}{2}\sigma_\pi\sin\theta_\pi\,,\right. \\
&\qquad \left. 0\,,\quad \frac{|\vec{p}|}{2} + \frac{\sqrt{\vec{p}^{\,2}+s}}{2}\sigma_\pi\cos\theta_\pi\right),
\end{aligned} \tag{A.21}$$

similarly, boosting p_- from $\Sigma_{2\pi}$ to Σ_B one gets

$$\begin{aligned}
\Sigma_B:\ p_- &= \left(\frac{\sqrt{\vec{p}^{\,2}+s}}{2} - \frac{|\vec{p}|}{2}\sigma_\pi\cos\theta_\pi\,,\quad -\frac{\sqrt{s}}{2}\sigma_\pi\sin\theta_\pi\,,\right. \\
&\qquad \left. 0\,,\quad \frac{|\vec{p}|}{2} - \frac{\sqrt{\vec{p}^{\,2}+s}}{2}\sigma_\pi\cos\theta_\pi\right),
\end{aligned} \tag{A.22}$$

where $|\vec{p}|$ is the magnitude of three-momentum in the center-of-mass system (CMS) composed by two effective masses $\sqrt{s}$ and $\sqrt{s_l}$ for rest B meson, and reads

$$|\vec{p}| = \frac{X}{m_B}. \tag{A.23}$$

In the system of lepton pairs $\Sigma_{l\nu}$, we have

$$\begin{aligned}
\Sigma_{l\nu}:\ p_l &= \left(\frac{\sqrt{s_l}}{2}(1+z_l)\,,\quad \frac{\sqrt{s_l}}{2}(1-z_l)\sin\theta_l\cos\phi\,,\right. \\
&\qquad \left. -\frac{\sqrt{s_l}}{2}(1-z_l)\sin\theta_l\sin\phi\,,\quad -\frac{\sqrt{s_l}}{2}(1-z_l)\cos\theta_l\right)
\end{aligned}$$

$$\Sigma_{l\nu}:\ p_\nu = \left(\frac{\sqrt{s_l}}{2}(1-z_l)\,,\quad -\frac{\sqrt{s_l}}{2}(1-z_l)\sin\theta_l\cos\phi\,,\right.$$
$$\left.\frac{\sqrt{s_l}}{2}(1-z_l)\sin\theta_l\sin\phi\,,\quad \frac{\sqrt{s_l}}{2}(1-z_l)\cos\theta_l\right). \tag{A.24}$$

Applying Lorenz boost to Eq. (A.24), one gets

$$\Sigma_B:\ p_l = \left(\frac{\sqrt{|\vec{p}|^2+s_l}}{2}(1+z_l)+\frac{|\vec{p}|}{2}(1-z_l)\cos\theta_l\,,\quad \frac{\sqrt{s_l}}{2}(1-z_l)\sin\theta_l\cos\phi\,,\right.$$
$$\left.-\frac{\sqrt{s_l}}{2}(1-z_l)\sin\theta_l\sin\phi\,,\quad -\frac{|\vec{p}|}{2}(1+z_l)-\frac{\sqrt{|\vec{p}|^2+s_l}}{2}(1-z_l)\cos\theta_l\right)$$
$$\Sigma_B:\ p_\nu = \left(\frac{\sqrt{|\vec{p}|^2+s_l}}{2}(1-z_l)-\frac{|\vec{p}|}{2}(1-z_l)\cos\theta_l\,,\quad -\frac{\sqrt{s_l}}{2}(1-z_l)\sin\theta_l\cos\phi\,,\right.$$
$$\left.\frac{\sqrt{s_l}}{2}(1-z_l)\sin\theta_l\sin\phi\,,\quad -\frac{|\vec{p}|}{2}(1-z_l)+\frac{\sqrt{|\vec{p}|^2+s_l}}{2}(1-z_l)\cos\theta_l\right). \tag{A.25}$$

From Eqs. (A.21), (A.22) and (A.25), we then get the expressions for four-momenta P, Q, L and N in rest frame Σ_B,

$$\begin{aligned}
P &= \left(\sqrt{|\vec{p}|^2+s}\,,\ 0\,,\ 0\,,\ |\vec{p}|\right)\\
Q &= \left(|\vec{p}|\sigma_\pi\cos\theta_\pi\,,\ \sqrt{s}\sigma_\pi\sin\theta_\pi\,,\ 0\,,\ \sqrt{|\vec{p}|^2+s}\sigma_\pi\cos\theta_\pi\right)\\
L &= \left(\sqrt{|\vec{p}|^2+s_l}\,,\ 0\,,\ 0\,,\ -|\vec{p}|\right)\\
N &= \left(\sqrt{|\vec{p}|^2+s_l}z_l+|\vec{p}|(1-z_l)\cos\theta_l\,,\ \sqrt{s_l}(1-z_l)\sin\theta_l\cos\phi\,,\right.\\
&\qquad \left.-\sqrt{s_l}(1-z_l)\sin\theta_l\sin\phi\,,\ -|\vec{p}|z_l-\sqrt{|\vec{p}|^2+s_l}(1-z_l)\cos\theta_l\right)
\end{aligned} \tag{A.26}$$

Taking Eq. (A.26) at hand, the Lorentz scalar products written in Eq. (A.12) can be obtained easily. Then part of derivation for $d\Gamma_5$ is presented in Ref. [52]

A.4 Parametrization of $\pi\pi$ scattering phase shifts

In the Omnès representation Eq. (2.36), $\pi\pi$ scattering phase shifts are needed as input, which are known up to 1.42 GeV currently, see Appendix A in Ref. [80]. The parameters appearing in parametrization can be determined by two ways: unconstrained fits to data (UFD) and constrained fits (CFD). UFD is just a fitting with simple expressions. With it they check how well data satisfies dispersion relations. CFD is obtained from the UFD by imposing simultaneous fulfilment of dispersion relations. It turns out to be that CFD not only describes the data very precisely, also fulfils the requirement of analyticity, unitarity

and crossing symmetry. From this point of view, CFD is the more reliable one [218]. Below we review some selected results of Ref. [80], and Eqs. (A.27) to (A.35) are taken from Ref. [80].

- $S-$wave
  - for $s \leq s_M = (0.85\ \mathrm{GeV})^2$,

$$\begin{aligned} \cot\delta_0^0(s) &= \frac{\sqrt{s}}{2k}\frac{M_\pi^2}{s-\frac{1}{2}z_0^2}\left\{\frac{z_0^2}{M_\pi\sqrt{s}}+B_0+B_1w(s)+B_2w(s)^2+B_3w(s)^3\right\}, \\ w(s) &= \frac{\sqrt{s}-\sqrt{s_0-s}}{\sqrt{s}+\sqrt{s_0-s}}, \qquad k=\sqrt{s/4-M_\pi^2} \quad s_0=4M_K^2, \end{aligned} \tag{A.27}$$

    with the parameters

$$\begin{aligned} &B_0 = 7.14 \pm 0.23, \quad B_1 = -25.3 \pm 0.5, \quad B_2 = -33.2 \pm 1.2, \\ &B_3 = -26.2 \pm 2.3, \quad z_0 = M_\pi. \end{aligned} \tag{A.28}$$

  - At intermediate energies for $(0.85\ \mathrm{GeV})^2 \leq s \leq 4M_K^2$,

$$\begin{aligned} \delta_0^0(s) &= d_0\left(1-\frac{|k_2|}{k_M}\right)^2+\delta_M\frac{|k_2|}{k_M}\left(2-\frac{|k_2|}{k_M}\right) \\ &\quad +|k_2|(k_M-|k_2|)\left(8\delta'_M+c\frac{k_M-|k_2|}{M_K^3}\right) \end{aligned} \tag{A.29}$$

    and for $4M_K^2 \leq s \leq (1.42\ \mathrm{GeV})^2$,

$$\delta_0^0(s) = d_0 + B\frac{k_2^2}{M_K^2}+C\frac{k_2^4}{M_K^4}+D\,\theta(s-4M_\eta^2)\frac{k_3^2}{M_\eta^2}, \tag{A.30}$$

    with the parameters

$$\begin{aligned} &k_2=\sqrt{s/4-M_K^2}, \qquad k_3=\sqrt{s/4-M_\eta^2}, \\ &d_0 = (226.5 \pm 1.3)^\circ, \quad c = (-81 \pm 290)^\circ, \quad B = (93.3 \pm 2.3)^\circ, \\ &C = (48.7 \pm, 2.9)^\circ, \quad D = (-88.3 \pm 4.0)^\circ, \end{aligned} \tag{A.31}$$

    where $\delta_M = \delta(s_M)$, $\delta'_M = (d\delta(s)/ds)\,|_{s=s_M}$ are obtained from Eq. (A.27).

- $P-$wave
  - for $s \leq 4M_K^2$,

$$\begin{aligned} \cot\delta_1^1(s) &= \frac{\sqrt{s}}{2k^3}(M_\rho^2-s)\left\{\frac{2M_\pi^3}{M_\rho^2\sqrt{s}}+B_0+B_1w(s)\right\}, \\ w(s) &= \frac{\sqrt{s}-\sqrt{s_0-s}}{\sqrt{s}+\sqrt{s_0-s}}, \quad \sqrt{s_0}=1.05\ \mathrm{GeV}, \\ B_0 &= 1.043 \pm 0.011, \quad B_1 = 0.19 \pm 0.05. \end{aligned} \tag{A.32}$$

– At $4M_K^2 \leq s \leq (1.42\ \text{GeV})^2$,

$$\delta_1^1(s) = \lambda_0 + \lambda_1(\frac{\sqrt{s}}{2M_K} - 1) + \lambda_2(\frac{\sqrt{s}}{2M_K} - 1)^2, \tag{A.33}$$

with $\lambda_1 = 1.39 \pm 0.18,\ \lambda_2 = -1.7 \pm 0.49$ and λ_0 is fixed from $\delta_1(4M_K^2)$ obtained from Eq. (A.32) such that the phase shift is continuous.

- $D-$wave

$$\cot\delta_2^0 = \begin{cases} \frac{\sqrt{s}}{2k^5}(M_{f_2}^2 - s)M_\pi^2\left\{B_0 + B_1 w(s)\right\}, & s \leq 4M_K^2 \\ \frac{\sqrt{s}}{2k^5}(M_{f_2}^2 - s)M_\pi^2\left\{B_{0h} + B_{1h} w_h(s)\right\}, & 4M_K^2 \leq s \leq (1.42\ \text{GeV})^2 \end{cases} \tag{A.34}$$

and the parameters are given by

$$\begin{aligned} w(s) &= \frac{\sqrt{s} - \sqrt{s_0 - s}}{\sqrt{s} + \sqrt{s_0 - s}}, \quad \sqrt{s_0} = 1.05\ \text{GeV}, \\ w_h(s) &= \frac{\sqrt{s} - \sqrt{s_h - s}}{\sqrt{s} + \sqrt{s_h - s}}, \quad \sqrt{s_h} = 1.45\ \text{GeV}, \\ B_0 &= 12.40 \pm 0.12, \quad B_1 = 10.06 \pm 0.16, \quad B_{1h} = 43.2 \pm 1.8. \end{aligned} \tag{A.35}$$

Imposing continuity at the matching point fixes B_{0h} from the value of $\delta_2^0(4M_K^2)$, see the first equation in Eq. (A.34).

These phase shift parametrizations till $\sqrt{s} \leq 1.42$ GeV using the central values of the above parameters are plotted in Fig. A.1.

Note that both the parameters c in isospin-0 S-wave and B_{h2} in isospin-2 D-wave have large differences between UFD and CFD [80]. The reasons are: for the UFD set, their equations (called GKPY equation in Ref. [80]) are very badly described in the $f_0(980)$ region and the behavior at this region is controlled by c. That is why it changes a lot when the dispersion relations are imposed. For the parameter B_{h2} in the isospin-2 D-wave such a difference between UFD and CFD is due to the bad data quality, and once again it changes dramastically when dispersion relations are imposed into the fits.

At the high energy region beyond $(1.42\ \text{GeV})^2$, one conjectures a smooth function by taking care of the continuity and the asymptotic value Eq. (2.38), for e.g., [219],

$$\delta_{1H}^1(s) = \delta_{1M}^1(1.42^2) + \left(\pi - \delta_{1M}^1(1.42^2)\right)\frac{s - 1.42^2}{s} \tag{A.36}$$

with subscript "$M,\ H$" representing the parametrization for intermediate (cf. Eq. (A.33)) and high energy region ($s \geq 1.42\ \text{GeV})^2$). An alternative choice is

$$\delta_{1H}^1(s) = \delta_{1M}^1(1.42^2) + \left(\pi - \delta_{1M}^1(1.42^2)\right)\frac{2}{\pi}\arctan\left(\frac{s - 1.42^2}{\Lambda^2}\right) \tag{A.37}$$

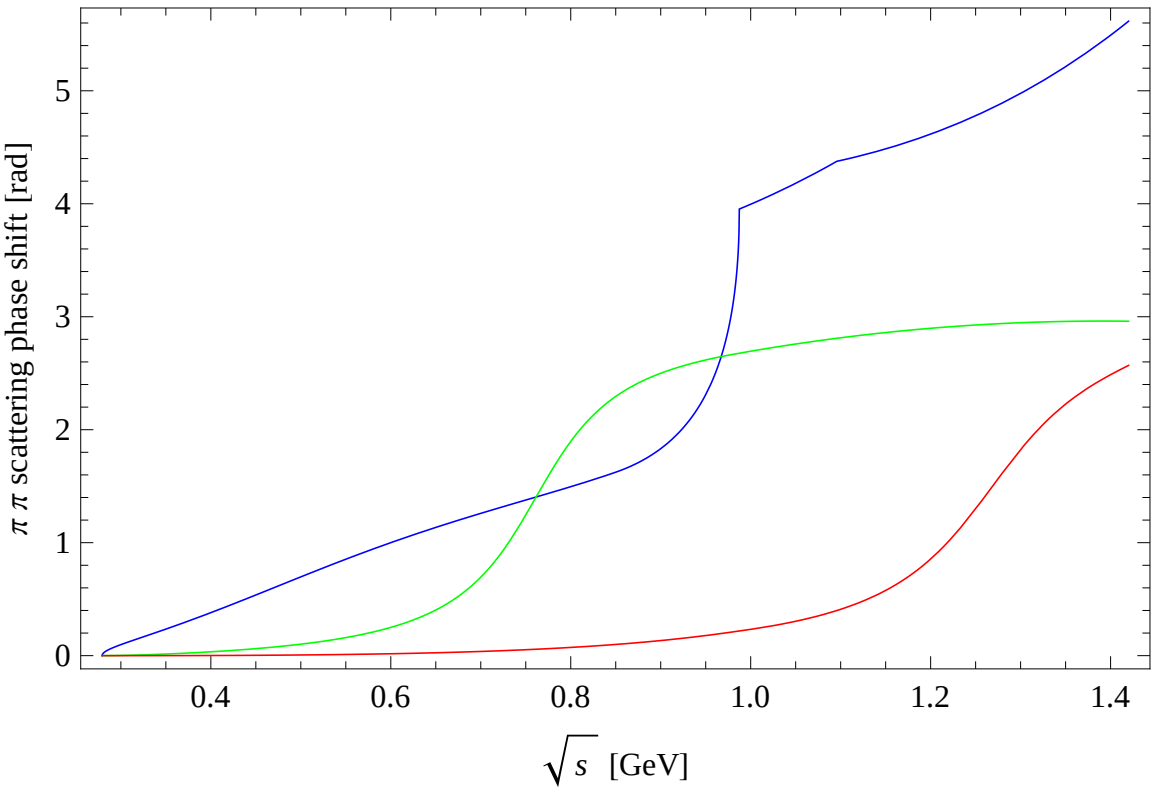

Figure A.1: $\pi\,\pi$ scattering phase shifts for isospin-0 S-, isospin-1 P- and isospin-0 D-waves up to 1.42 GeV, which are denoted by blue, green and red lines, respectively.

with a free parameter Λ. From the numerical calculations, we found different choices of Λ have tiny influence on the quantity in the low energy region.

It is important to find a reliable parametrization of $\pi\pi$ (and πK) scattering phase shifts in the low-energy QCD region. There have been lots of work on it. Another well-known form is the Schenk parametrization [220],

$$\tan\,\delta_l^I(k) = \sqrt{\frac{s-4M_\pi^2}{s}}k^{2l}\left(\frac{4M_\pi^2-s_l^I}{s-s_l^I}\right)\left\{A_l^I + B_l^I k^2 + C_l^I k^4 + D_l^I k^6\right\}, \qquad \text{(A.38)}$$

where s_L^I specifies the value of s at which the phase shifts go through $\pi/2$, the negative sign of s_0^2 indicates δ_0^2 remains below $\pi/2$. These parameters have been determined by analysis of Roy equations [79]. The update for combining it with theoretical inputs for scattering length from ChPT has been done in Ref. [84]. In Ref. [221], one could find the references for other works.

Appendix B

Further details on antinucleon-nucleon and nucleon-nucleon interactions

B.1 Solving Lippmann-Schwinger equation

The Lippmann-Schwinger equation for the T operator reads

$$T(z) = V(z) + V(z)G_0(z)T(z), \tag{B.1}$$

where z indicates the energy dependence of the operators. Defining $\langle p'|T(z)|p\rangle = T(p', p, z)$ and $\langle p'|V(z)|p\rangle = V(p', p, z)$ [1] one has the expression in the form of matrix elements for a given partial wave:

$$T(p', p, z) = V(p', p, z) + \int_0^\infty \frac{dk}{(2\pi)^3} \frac{k^2}{z - 2E_k + i0^+} V(p', k, z)T(k, p, z), \tag{B.2}$$

where the complete set $\int_{-\infty}^{\infty} \frac{d^3k}{(2\pi)^3} \, |k\rangle\langle\, k\,| \, = 1$ has been used and the angular part has been projected into partial waves. For simplifing notations, we omit the index of partial waves L, L', see Eq. (4.9). To solve Eq. (B.2), we will use the matrix inversion method proposed by Haftel and Tabakin [222]. In actual cases, only the half-off-shell quantities [2] are needed. matrix elements are needed. Choosing $z = 2E_p = 2\sqrt{p^2 + m_N^2}$ we rewrite Eq. (B.2) as

$$\begin{aligned} T(p', p, 2E_p) &= V(p', p, 2E_p) \\ &+ \mathcal{P} \int_0^\infty \frac{dk}{(2\pi)^3} \frac{k^2}{2E_p - 2E_k} V(p', k, 2E_p)T(k, p, 2E_p) \end{aligned}$$

[1] If not stated otherwise, $\vec{p}$ and $\vec{p}'$ are the three-momentum of the initial and final states, repectively, in the center-of-mass system (CMS); p and p' are the corresponding magnitudes.

[2] $z = E_i = E_f$ is called on-shell; $z = E_i \neq E_f$ or $z = E_f \neq E_i$ is called half-off-shell, and $z \neq E_i$ also $z \neq E_f$ is the full off-shell case, also abbreviated as off-shell, where E_i and E_f denote the energy of initial and final system, respectively.

$$- \quad i\pi \frac{pE_p}{2(2\pi)^3} V(p', p, 2E_p) T(p, p, 2E_p), \tag{B.3}$$

where the identity

$$\frac{1}{x - x' \pm i\epsilon} = \mathcal{P}\frac{1}{x - x'} \mp i\pi\delta(x - x') \tag{B.4}$$

has been used and $\mathcal{P}$ denotes the principal value. To further simplify the imaginary part, we have used

$$\delta\big(f(x)\big) = \sum_i \frac{\delta(x - x_i)}{|f'(x_i)|}, \tag{B.5}$$

where x_i denotes the roots of $f(x)$ and $f'(x)$ the derivative of $f(x)$. More apparently,

$$\begin{aligned} & \delta(2E_p - 2E_k) = \frac{1}{2}\delta(E_k - E_p) \\ = \quad & \frac{1}{2}\frac{E_p}{p}\left[\delta(k - p) + \delta(k + p)\right]. \end{aligned} \tag{B.6}$$

Since the integration starts at zero, the delta-function $\delta(k+p)$ does not play role. In order to implement a computer program that can conveniently calculate the principal value (singularity sits at $k = p$), there is a commonly used trick, i.e. recognizing that

$$\mathcal{P}\int_0^\infty \frac{dk}{(2\pi)^3} \frac{p^2\, 2E_p}{2(p^2 - k^2)} V(p', p, 2E_p) T(p, p, 2E_p) = 0. \tag{B.7}$$

Subtracting it from Eq. (B.3) and noting $1/(E_p - E_k) = -(E_p + E_k)/(k^2 - p^2)$, we will get

$$\begin{aligned} T(p', p, 2E_p) \quad = \quad & V(p', p, 2E_p) \\ & - \quad \mathcal{P}\int_0^\infty \frac{dk}{(2\pi)^3} \frac{1}{2(k^2 - p^2)} \Big\{ k^2(E_p + E_k) V(p', k, 2E_p) T(k, p, 2E_p) \\ & \qquad\qquad - p^2 2E_p V(p', p, 2E_p) T(p, p, 2E_p) \Big\} \\ & - \quad i\pi \frac{pE_p}{2(2\pi)^3} V(p', p, 2E_p) T(p, p, 2E_p). \end{aligned} \tag{B.8}$$

As a matter of fact, in Eq. (B.8), $\mathcal{P}$ is not needed anymore, since the function in the bracket (integrand) already does not involve any singularity. The integration will be performed by the finite summation,

$$\int_0^\infty F(k)dk = \sum_i s_i F(k_i), \tag{B.9}$$

where the Gaussian quadrature weights (s_i) and abscissae (k_i) [223] can be used. And for that purpose, one may need to map the interval $[0, \infty)$ to $[-1, 1]$. Let us look at it in more detail. Discretizing the off-shell p', p as N mesh points $k_j (1 \le j \le N)$, and defining k_{N+1}

as the on-shell momentum, $T(p', p, 2E_p)$ then becomes a matrix $T_{i,j} = T(k_i, k_j, 2E_p)$, with $i, j = 1, \ldots, N+1$. The half-off-shell elements have the form

$$T_{i,N+1} = V_{i,N+1} - \sum_{j=1}^{N+1} \omega_j V_{i,j} T_{j,N+1}, \tag{B.10}$$

with

$$\omega_j = \begin{cases} \frac{k_j^2 s_j (E_{k_{N+1}} + E_{k_j})}{2(2\pi)^3 (k_j^2 - k_{N+1}^2)}, & j \leq N \\ -\frac{1}{(2\pi)^3} k_{N+1}^2 E_{k_{N+1}} \sum_{m=1}^{N} \frac{s_m}{k_m^2 - k_{N+1}^2} + i\pi \frac{k_{N+1} E_{k_{N+1}}}{2(2\pi)^3}, & j = N+1 \end{cases}. \tag{B.11}$$

We can rewrite Eq. (B.10) as

$$\begin{aligned} V_{i,N+1} &= \sum_{j=1}^{N+1} \Omega_{i,j} T_{j,N+1} \\ \Omega_{i,j} &= \delta_{i,j} + \omega_j V_{i,j}, \end{aligned} \tag{B.12}$$

which is the component form of matrix equation $\Omega \cdot T = V$, where Ω is $N+1$ by $N+1$ square matrix while T, V are $N+1$ column vectors. $T(k_i, k_{N+1}, 2E_q)$ can thus be easily obtained by solving the $N+1$ linear equations. For coupled system, e.g. ${}^3S_1 - {}^3D_1$, the dimensions of matrices Ω, T, V will double, i.e., Ω matrix has dimensions $(2N+2) \times (2N+2)$, T and V becomes $(2N+2) \times 2$ matrices. As an exercise, one can use the separable potential presented in Ref. [224] to test the above procedure for solving Lippmann-Schwinger equation.

B.2 Partial-wave decomposition of potentials

For the baryon-baryon interaction including the current case of $\bar{N}N$, we usually work with partial waves, in which the phase shifts, bound states, etc., for each partial wave can be seen. To perform the partial wave decomposition, we closely follow Epelbaum's convention [145] to rewrite the potential for two body nucleon-nucleon scattering as

$$\begin{aligned} V(\vec{p}', \vec{p}) &= U_C + U_S \, \vec{\sigma}_1 \cdot \vec{\sigma}_2 + U_{LS} \left(-i\vec{S} \cdot (\vec{q} \times \vec{k}) \right) \\ &+ U_{\sigma L} \, \vec{\sigma}_1 \cdot (\vec{q} \times \vec{k}) \; \vec{\sigma}_2 \cdot (\vec{q} \times \vec{k}) + U_T \, \vec{\sigma}_1 \cdot \vec{q} \; \vec{\sigma}_2 \cdot \vec{q}. \end{aligned} \tag{B.13}$$

This means we take the convention $U_C = V_C + \boldsymbol{\tau}_1 \cdot \boldsymbol{\tau}_2 W_C$ etc., compared to Eq. (3.9). It is convenient to follow the steps proposed by Erkelenz et al. [225]:

- express the potentials in the helicity state representation $|\hat{p}\lambda_1\lambda_2\rangle$, with $\hat{p} = \vec{p}/p$, λ_1, λ_2 being the helicity quantum numbers corresponding to initial state particles 1 and 2.

- Using the transformation matrix $\langle \hat{p}\lambda_1\lambda_2|JM\lambda_1\lambda_2\rangle$ (given in Ref. [225]), one could express the potential in the $|JM\lambda_1\lambda_2\rangle$ representation.
- Exploiting the transformation matrix $\langle LSJM|JM\lambda_1\lambda_2\rangle$ (also given in Ref. [225]), one could finally switch to LSJ representation

The final results for singlet-triplet are:

$$\begin{aligned}
\langle J0J|V|J0J\rangle &= 2\pi\int_{-1}^{1} dx\big[U_C - 3U_S + p'^2p^2(x^2-1)U_{\sigma L} - q^2U_T\big]P_J(x),\\
\langle J1J|V|J1J\rangle &= 2\pi\int_{-1}^{1} dx\Big\{\big[U_C + U_S + 2p'pxU_{LS} - p'^2p^2(1+3x^2)U_{\sigma L} + 4k^2U_T\big]P_J(x)\\
&\quad +\big[-p'pU_{LS} + 2p'^2p^2xU_{\sigma L} - 2p'pU_T\big]\big(P_{J-1}(x) + P_{J+1}(x)\big)\Big\},
\end{aligned} \tag{B.14}$$

for coupled states it reads

$$\begin{aligned}
\langle J\pm1,1J|V|J\pm1,1J\rangle &= 2\pi\int_{-1}^{1} dx\Big\{p'p\big[-U_{LS} \pm \frac{2}{2J+1}(-p'pxU_{\sigma L} + U_T)\big]P_J(x)\\
&\quad +\big[U_C + U_S + p'pxU_{LS} + p'^2p^2(1-x^2)U_{\sigma L}\\
&\quad \pm\frac{1}{2J+1}\big(2p'^2p^2U_{\sigma L} - (p'^2+p^2)U_T\big)\big]P_{J\pm1}(x)\Big\},\\
\langle J\pm1,1J|V|J\mp1,1J\rangle &= 2\pi\frac{\sqrt{J(J+1)}}{2J+1}\int_{-1}^{1} dx\Big\{-4p'pU_TP_J(x)\\
&\quad +\Big[\mp\frac{2p'^2p^2}{2J+1}U_{\sigma L} + 2p'^2U_T\Big]P_{J\mp1}(x)\\
&\quad +\Big[\pm\frac{2p'^2p^2}{2J+1}U_{\sigma L} + 2p^2U_T\Big]P_{J\pm1}(x)\Big\}.
\end{aligned} \tag{B.15}$$

Here $P_J(x)$ are the standard Legendre polynomials. For $J=0$ the only two non-vanishing matrix elements are

$$\begin{aligned}
\langle 000|V|000\rangle &= 2\pi\int_{-1}^{1} dxU_C - 3U_S + p'^2p^2(x^2-1)U_{\sigma L} - q^2U_T,\\
\langle 110|V|110\rangle &= 2\pi\int_{-1}^{1} dx\Big\{xU_C + x\,U_S + p'p(x^2-1)U_{LS}\\
&\quad +p'^2p^2z(1-x^2)U_{\sigma L} - \big((p'^2+p^2)x - 2p'p\big)U_T\Big\}.
\end{aligned} \tag{B.16}$$

The above expression for the on-shell case agrees with Ref. [142] up to an overall factor.

Assuming isospin invariance, the states

$$pp, \quad nn, \quad \frac{1}{\sqrt{2}}(pn+np) \tag{B.17}$$

are degenerate isospin triplets. The combination $(pn-np)/\sqrt{2}$ is isospin singlet, similar to the spin case. Recalling that $U = V + \boldsymbol{\tau}_1 \cdot \boldsymbol{\tau}_2 W$, one has for the total isospin I ($I = 0$, 1),

$$U^I = V + (4I - 3)W, \tag{B.18}$$

because

$$\langle I, I_z^{'}|\boldsymbol{\tau}_1 \cdot \boldsymbol{\tau}_2|I, I_z\rangle = 2\left[I(I+1) - \frac{3}{2}\right] = \begin{cases} 1, & I = 1 \\ -3, & I = 0 \end{cases}. \tag{B.19}$$

B.3 Miscellany derivation details for the equations in Sec. 3.2.3

Miscellaneous mathematical derivation processes for the equations in Sec. 3.2.3 are provided here. The symbol ϵ below is defined as $\epsilon = 0^+$, i.e. a positive infinitesimal quantity.

Derivation of Eq (3.18):

$$\begin{aligned} q &= \epsilon - i\bar{\mu} \\ q^2 &= -\bar{\mu}^2 + \epsilon^2 - 2i\mu\epsilon \\ V_i(q) &= \frac{2}{\pi}\int_{2M_\pi}^{\infty} d\mu\, \mu \frac{\rho_i(\mu)}{\mu^2 - \bar{\mu}^2 + \epsilon^2 - 2i\mu\epsilon} \\ &= \frac{2}{\pi}\int_{2M_\pi}^{\infty} d\mu\, \mu \frac{\rho_i(\mu)}{\mu^2 - \bar{\mu}^2 - i\epsilon'} \\ &= \mathcal{P}\frac{2}{\pi}\int_{2M_\pi}^{\infty} d\mu\, \mu \frac{\rho_i(\mu)}{\mu^2 - \bar{\mu}^2} \\ &\quad + \frac{2}{\pi}\int_{2M_\pi}^{\infty} d\mu\, \mu i\pi\delta(\mu^2 - \bar{\mu}^2)\rho_i(\mu). \end{aligned} \tag{B.20}$$

Using

$$\delta(\mu^2 - \bar{\mu}^2) = \frac{1}{2\mu}\Big[\delta(\mu + \bar{\mu}) + \delta(\mu - \bar{\mu})\Big] \tag{B.21}$$

the integral over the δ-function can be easily done, and thus

$$\begin{aligned} &\mathrm{Im}V_i(q)\Big|_{q=0^+-i\bar{\mu}} = \rho_i(\bar{\mu}) \\ &\rho_i(\mu) = \mathrm{Im}\Big[V_i(0^+ - i\mu)\Big]. \end{aligned} \tag{B.22}$$

Derivation of Eq. (3.22):
We first have

$$\begin{aligned}
d^3l &= l^2\, dl\, d\cos\theta\, d\phi, \text{ (intgration over } d\phi \text{ gives } 2\pi),\\
\omega_-^2 &= q^2+l^2+4M_\pi^2-2ql\cos\theta\\
\omega_+^2 &= q^2+l^2+4M_\pi^2-2ql\cos\theta\\
\Sigma &\equiv q^2+l^2+4M_\pi^2\\
\int_{-1}^{1} d\cos\theta \frac{1}{\omega_-^2\omega_+^2} &= \int_{-1}^{1}\frac{1}{2\Sigma}\Big(\frac{1}{\Sigma-2ql\cos\theta}+\frac{1}{\Sigma+2ql\cos\theta}\Big)\\
&= \frac{1}{2ql}\frac{1}{2\Sigma}\int_{-1}^{1}\Big(\frac{1}{\Sigma-2\,q\,l\cos\theta}+\frac{1}{\Sigma+2ql\cos\theta}\Big)d(2ql\cos\theta)\\
&= \frac{1}{4\Sigma ql}\Big[\ln(\Sigma+2q\,l\cos\theta)\Big|_{\cos\theta=-1}^{\cos\theta=1}-\ln(2\,q\,l\cos\theta-\Sigma)\Big|_{\cos\theta=-1}^{\cos\theta=1}\Big]\\
&= \frac{1}{4\Sigma ql}\Big[\ln(\Sigma+2ql)-\ln(\Sigma-2ql)-\ln(2ql-\Sigma)+\ln(-2ql-\Sigma)\Big]\\
&= \frac{1}{4\Sigma ql}\cdot 2\Big[\ln(\Sigma+2ql)-\ln(\Sigma-2ql)\Big]. \qquad \text{(B.23)}
\end{aligned}$$

In the last equality, one needs to take care of $\ln(A)$ for $\mathrm{Re}\,(A)<0$ and $\mathrm{Im}\,(A)$ being an infinitesimal quantity, and the following relations [4, 226] can be used,

$$\begin{aligned}
\ln(A-i0^+) &= \ln(|A|)+\ln(e^{-i\pi})=\ln(|A|)-i\pi,\\
\ln(A+i0^+) &= \ln(|A|)+\ln(e^{+i\pi})=\ln(|A|)+i\pi. \qquad \text{(B.24)}
\end{aligned}$$

Replacing M_π^2 by $M_\pi^2-i0^+$ above (recall the standard Feynman propagator $1/(p^2-M_\pi^2+i0^+)$), one can determine the sign for $i0^+$, and further, the sign for $i\pi$. Here the terms $-i\pi$ and $+i\pi$ cancel with each other. Then Eq. (3.22) is proven.

Derivation of Eq. (3.23):
Let us keep in mind the identity

$$\frac{1}{x\pm i0^+}=\mathcal{P}\frac{1}{x}\mp i\pi\delta(x), \qquad \text{(B.25)}$$

then

$$\begin{aligned}
q &= \epsilon-i\mu, \quad \epsilon\equiv 0^+\\
l^2+q^2+4M_\pi^2 &= l^2-\mu^2-2i\mu\epsilon+\epsilon^2+4M_\pi^2
\end{aligned}$$

$$= \quad l^2 - \mu^2 + 4M_\pi^2 - i\epsilon', \quad \epsilon' \equiv 2\mu\epsilon, \tag{B.26}$$

where we keep $\mathcal{O}(\epsilon)$ and neglect $\mathcal{O}(\epsilon^2)$. Note that ϵ' is still a infinitesimal quantity, and thus only the sign plays a key role. The imaginary part involves a δ-function,

$$\begin{aligned}\delta(l^2 - \mu^2 + 4M_\pi^2) &= \frac{1}{2\sqrt{\mu^2 - 4M_\pi^2}}\Big[\delta(l + \sqrt{\mu^2 - 4M_\pi^2}) + \delta(l - \sqrt{\mu^2 - 4M_\pi^2})\Big] \\ &\sim \frac{1}{2\sqrt{\mu^2 - 4M_\pi^2}}\delta(l - \sqrt{\mu^2 - 4M_\pi^2}),\end{aligned} \tag{B.27}$$

where the first $\delta-$function does not play a role in integration due to

$$\int_0^{\tilde{\Lambda}} f(l)\,\delta(l + \sqrt{\mu^2 - 4M_\pi^2}) = 0. \tag{B.28}$$

Then

$$\begin{aligned}&\frac{l(l^2 - q^2)}{q(l^2 + q^2 + 4M_\pi^2)} \to \frac{\sqrt{\mu^2 - 4M_\pi^2}(2\mu^2 - 4M_\pi^2)}{-i\mu}\frac{1}{2\sqrt{\mu^2 - 4M_\pi^2}} \\ &\qquad l^2 - q^2 \to 2\mu^2 - 4M_\pi^2 \\ &\frac{3g_A^2}{128\pi^2 f_\pi^4}\cdot i\pi\cdot i\frac{1}{\mu}(\mu^2 - 2M_\pi^2)\Big[8c_1 M_\pi^2 + c_3(2\mu^2 - 4M_\pi^2)\Big] \\ = \quad &-\frac{3g_A^2}{64\pi f_\pi^4}(\mu^2 - 2M_\pi^2)\Big(2M_\pi^2(2c_1 - c_3) + c_3\mu^2\Big).\end{aligned} \tag{B.29}$$

Under the condition $l \to \sqrt{\mu^2 - 4M_\pi^2}$, $q \to \epsilon - i\mu$, the logarithm functions in Eq. (3.22) contributes $-i\pi$,

$$\begin{aligned}&\ln\frac{-2i\mu\epsilon + \epsilon^2 + 2\sqrt{\mu^2 - 4M_\pi^2}(\epsilon - i\mu)}{-2i\mu\epsilon + \epsilon^2 - 2\sqrt{\mu^2 - 4M_\pi^2}(\epsilon - i\mu)} \\ = \quad &\ln\frac{-2\mu\epsilon - i\epsilon^2 - i2\epsilon\sqrt{\mu^2 - 4M_\pi^2} + 2\mu\sqrt{\mu^2 - 4M_\pi^2}}{-2\mu\epsilon - i\epsilon^2 + 2i\epsilon\sqrt{\mu^2 - 4M_\pi^2} - 2\mu\sqrt{\mu^2 - 4M_\pi^2}} \\ = \quad &\ln(2\mu\sqrt{\mu^2 - 4M_\pi^2} - i\epsilon') - \ln(-2\mu\sqrt{\mu^2 - 4M_\pi^2} + i\epsilon') \\ = \quad &\ln(2\mu\sqrt{\mu^2 - 4M_\pi^2}) - \Big[\ln(2\mu\sqrt{\mu^2 - 4M_\pi^2}) + i\pi\Big] \\ = \quad &-i\pi.\end{aligned} \tag{B.30}$$

Derivations of Eqs. (3.25) **and** (3.26):
In Eqs. (3.12) and (3.14), the q^2 in polynomials can be replaced by $-\mu^2$ directly, while $L(q)$

and $A(q)$ (see Eqs. (3.13) and (3.15)) for $q = \epsilon - i\mu$ are the only sources for introducing imaginary parts. In the following, we will show how $\mathrm{Im}\, L(0^+ - i\mu)$ and $\mathrm{Im}\, A(0^+ - i\mu)$ are calculated. We recall the following relation for determining the multivalued square-root function,

$$\sqrt{-A - i0^+} = \sqrt{A e^{-i(\pi - 0^+)}} = \sqrt{A} e^{-\frac{i}{2}(\pi - 0^+)} = -i\sqrt{A}, \quad A > 0 \tag{B.31}$$

and similarly

$$\sqrt{-A + i0^+} = i\sqrt{A}, \quad A > 0. \tag{B.32}$$

Then

$$\begin{aligned}
L(q) &= \frac{\omega}{q} \ln \frac{\omega + q}{2M_\pi}, \quad \omega = \sqrt{q^2 + 4M_\pi^2} \\
&= \frac{\sqrt{(\epsilon - i\mu)^2 + 4M_\pi^2}}{\epsilon - i\mu} \ln \frac{\sqrt{(\epsilon - i\mu)^2 + 4M_\pi^2} + \epsilon - i\mu}{2M_\pi} \\
\sqrt{\epsilon - i\mu)^2 + 4M_\pi^2} &= \sqrt{-\mu^2 + 4M_\pi^2 + \epsilon^2 - 2i\mu\epsilon} = -i\sqrt{\mu^2 - 4M_\pi^2}, \quad \mu \geq 2M_\pi \\
L(q) &= \frac{-i\sqrt{\mu^2 - 4M_\pi^2}}{-i\mu} \ln \frac{-i\sqrt{\mu^2 - 4M_\pi^2} - i\mu}{2M_\pi} \\
&= \frac{\sqrt{\mu^2 - 4M_\pi^2}}{\mu} \ln(\rho e^{-i\frac{\pi}{2}}), \quad \rho \equiv \frac{\sqrt{\mu^2 - 4M_\pi^2} + \mu}{2M_\pi},
\end{aligned} \tag{B.33}$$

thus, it is easily seen

$$\mathrm{Im}\, L(\epsilon - i\mu) = -\frac{\pi}{2} \frac{\sqrt{\mu^2 - 4M_\pi^2}}{\mu}. \tag{B.34}$$

The derivation process for $\mathrm{Im}\, A(0^+ - i\mu)$ is as follows:

$$\begin{aligned}
A(q) &= \frac{1}{2q} \arctan \frac{q}{2M_\pi} \\
A(\epsilon - i\mu) &= \frac{1}{2(\epsilon - i\mu)} \arctan \frac{\epsilon - i\mu}{2M_\pi} \\
&= \frac{1}{-2i\mu} \arctan \frac{\epsilon - i\mu}{2M_\pi} \\
&= \frac{1}{-2i\mu} \cdot \frac{i}{2} \ln \frac{2M_\pi - \mu - i\epsilon}{2M_\pi + \mu + i\epsilon} \\
&= -\frac{1}{4\mu} \ln \frac{2M_\pi - \mu - i\epsilon}{2M_\pi + \mu + i\epsilon} \\
&= -\frac{1}{4\mu} \Big[\ln(2M_\pi - \mu - i\epsilon) - \ln(2M_\pi + \mu + i\epsilon) \Big]
\end{aligned}$$

$$
\begin{aligned}
&= -\frac{1}{4\mu}\Big[\Big(\ln(\mu-2M_\pi)-i\pi\Big)-\ln(2M_\pi+\mu)\Big] \\
&= -\frac{1}{4\mu}\Big(\ln\frac{\mu-2M_\pi}{\mu+2M_\pi}-i\pi\Big), \\
\mathrm{Im}A(\epsilon-i\mu) &= \frac{\pi}{4\mu}. \qquad \text{(B.35)}
\end{aligned}
$$

Derivation of Eq. (3.27):
we will take $\eta_T^{\tilde{\Lambda}(3)}$ (see Eq. (3.26)) and $\rho_T^{\tilde{\Lambda}(2)}$ (see Eq. (3.25)) as specific examples. Let us leave out the factor $-g_A^2/(128f_\pi^4)\cdot c_4$ for the sake of writing. The integration part is performed as follows,

$$
\begin{aligned}
I &= \frac{2}{\pi}\int_{2M_\pi}^{\infty} d\mu\mu\frac{(4M_\pi^2-\mu^2)/\mu}{\mu^2+q^2} \\
&= \frac{2}{\pi}\int_{2M_\pi}^{\infty} d\mu\frac{4M_\pi^2-\mu^2}{\mu^2+q^2} \\
&= -\frac{2}{\pi}\int_{2M_\pi}^{\infty} d\mu\frac{\mu^2+q^2-(q^2+4M_\pi^2)}{\mu^2+q^2} \\
&= \underbrace{-(\Lambda-2M_\pi)}_{\text{constant, will be absorbed by contact term}} + \int_{2M_\pi}^{\infty} d\mu\frac{q^2+4M_\pi^2}{\mu^2+q^2} \\
&= \frac{q^2+4M_\pi^2}{q}\arctan\frac{\mu}{q}\Big|_{\mu=2M_\pi}^{\mu=\tilde{\Lambda}} \\
&= \frac{q^2+4M_\pi^2}{q}\arctan\frac{q(\tilde{\Lambda}-2M_\pi)}{q^2+2\tilde{\Lambda}M_\pi}. \qquad \text{(B.36)}
\end{aligned}
$$

In the last equality, we have used the relation

$$
\arctan(x)-\arctan(y)=\arctan\frac{x-y}{1+xy}\,. \qquad \text{(B.37)}
$$

One then easily finds

$$
W_T^{\tilde{\Lambda}(3)}(q)=-\frac{g_A^2}{32\pi f_\pi^4}c_4(q^2+M_\pi^2)A(q) \qquad \text{(B.38)}
$$

with

$$
A(q)=\frac{1}{2q}\arctan\frac{q(\tilde{\Lambda}-2M_\pi)}{q^2+2\tilde{\Lambda}M_\pi}. \qquad \text{(B.39)}
$$

For the evaluation of potential $V_T^{\tilde{\Lambda}(2)}$, we confront with the integration

$$
I(q)=\int_{2M_\pi}^{\tilde{\Lambda}}\frac{\sqrt{\mu^2-4M_\pi^2}}{\mu^2+q^2}. \qquad \text{(B.40)}
$$

Setting $\mu = 2M_\pi \sec\theta$, we have

$$\begin{aligned}
\mu^2 - 4M_\pi^2 &= 4M_\pi^2 \tan^2\theta \\
q^2 + \mu^2 &= q^2 + 4M_\pi^2 \sec^2\theta \\
d\mu &= 2M_\pi \tan\theta \sec\theta d\theta \\
\sqrt{\mu^2 - 4M_\pi^2} &= 2M_\pi \tan\theta,
\end{aligned} \tag{B.41}$$

I is then simplified as

$$\begin{aligned}
I &= \int_{2M_\pi}^{\tilde{\Lambda}} \frac{2M_\pi \tan\theta}{q^2 + 4M_\pi^2 \sec^2\theta} \cdot 2M_\pi \tan\theta \sec\theta d\theta \\
&= \int_{2M_\pi}^{\tilde{\Lambda}} \frac{4M_\pi^2 \sin^2\theta/\cos^3\theta}{q^2 + 4M_\pi^2/\cos^2\theta} = \int_{2M_\pi}^{\tilde{\Lambda}} \frac{4M_\pi^2 \sin^2\theta/\cos\theta}{q^2\cos^2\theta + 4M_\pi^2} d\theta \\
&= 4M_\pi^2 \int_{2M_\pi}^{\tilde{\Lambda}} \frac{\sin^2\theta\cos\theta}{\cos^2\theta(q^2\cos^2\theta + 4M_\pi^2)} d\theta = 4M_\pi^2 \int_{2M_\pi}^{\tilde{\Lambda}} \frac{\sin^2\theta d(\sin\theta)}{\cos^2\theta(q^2\cos^2 + 4M_\pi^2)} \\
&\overset{\sin\theta = x}{=\!=\!=} 4M_\pi^2 \int_{2M_\pi}^{\tilde{\Lambda}} \frac{x^2 dx}{(1-x^2)\big(q^2(1-x^2) + 4M_\pi^2\big)} \\
&\overset{\omega = \sqrt{q^2+4M_\pi^2}}{=\!=\!=} 4M_\pi^2 \int_{2M_\pi}^{\tilde{\Lambda}} \frac{x^2 dx}{(1-x^2)(\omega^2/q^2 - x^2)} = \frac{4M_\pi^2}{\omega^2} \int_{2M_\pi}^{\tilde{\Lambda}} \frac{x^2 dx}{(1-x^2)(1 - q^2x^2/\omega^2)} \\
&= \int_{2M_\pi}^{\tilde{\Lambda}} \left(\frac{1}{1-x^2} - \frac{1}{1 - q^2x^2/\omega^2} \right) dx \\
&= \int_{2M_\pi}^{\tilde{\Lambda}} dx \left[\frac{1}{2}\frac{1}{1-x} + \frac{1}{2}\frac{1}{1+x} - \frac{1}{2(1 - qx/\omega)} - \frac{1}{2(1 + qx\omega)} \right] \\
&= \Bigg[\underbrace{\frac{1}{2}\ln\frac{x+1}{x-1}}_{\text{will be constant and thus absorbed by contact terms}} - \frac{1}{2}\frac{\omega}{q}\ln\frac{qx/\omega + 1}{qx/\omega - 1} \Bigg] \Bigg|_{x=0}^{x=\sqrt{\tilde{\Lambda}^2 - 4M_\pi^2}/\tilde{\Lambda}} \\
&= -\frac{\omega}{2q}\ln\frac{qx + \omega}{qx - \omega}\Bigg|_{x=0}^{x=\sqrt{\tilde{\Lambda}^2 - 4M_\pi^2}/\tilde{\Lambda}} \\
&= -\frac{\omega}{2q}\left[\ln\frac{q\bar{s} + \omega\tilde{\Lambda}}{q\bar{s} - \omega\tilde{\Lambda}} - \ln(-1) \right], \quad \bar{s} = \sqrt{\tilde{\Lambda}^2 - 4M_\pi^2} \\
&= -\frac{\omega}{2q}\ln\frac{\omega\tilde{\Lambda} + q\bar{s}}{\omega\tilde{\Lambda} - q\bar{s}} = -\frac{\omega}{2q}\ln\frac{(\omega\tilde{\Lambda} + q\bar{s})^2}{4M_\pi^2(\tilde{\Lambda}^2 + q^2)}.
\end{aligned} \tag{B.42}$$

The upper and lower limit for x are determined as

$$\begin{aligned} \sec\theta &\in \left[1,\ \tilde{\Lambda}/(2M_\pi)\right], \quad \cos\theta \in \left[2M_\pi/\tilde{\Lambda},\ 1\right] \\ x = \sin\theta &\in \left[0,\ \sqrt{1-(2M_\pi/\tilde{\Lambda})^2}\right] = \left[0,\ \sqrt{\tilde{\Lambda}^2-4M_\pi^2}/\tilde{\Lambda}\right]. \end{aligned} \tag{B.43}$$

Combining the overall factor $3g_A^4/(128\pi f_\pi^4)\cdot(2/\pi)$, one will get

$$V_T^{\tilde{\Lambda}(2)}(q) = -\frac{3g_A^4}{64\pi^2 f_\pi^4} L(q) \tag{B.44}$$

with

$$L(q) = \frac{\omega}{2q}\ln\frac{(\omega\tilde{\Lambda}+q\bar{s})^2}{4M_\pi^2(\tilde{\Lambda}^2+q^2)}, \quad \bar{s} = \sqrt{\tilde{\Lambda}^2-4M_\pi^2}. \tag{B.45}$$

B.4 Generalized Stapp parametrization for antinucleon-nucleon sector

One can parameterize $S-$matrix elements by phase shifts and mixing angles. The parametrization proposed by Stapp et al. [160] (also known as "bar phase shifts") is a widely spread-convention in NN elastic scattering. For $\bar{N}N$ interactions, the annihilation occurs, which results in inelasticities. The generalized form of the Stapp parametrization for $\bar{N}N$ scattering is elaborated below. We start from the definition

$$\begin{pmatrix} S_{LL} & S_{LL'} \\ S_{L'L} & S_{L'L'} \end{pmatrix} = \sqrt{[\eta]}\, e^{i[\delta]}\ e^{-2i\epsilon_J\sigma_1}\ \sqrt{[\eta]}\, e^{i[\delta]}, \tag{B.46}$$

where σ_1, σ_2, σ_3 are the conventional Pauli matrices

$$\sigma_1 = \begin{pmatrix} 0 & 1 \\ 1 & 0 \end{pmatrix}, \quad \sigma_2 = \begin{pmatrix} 0 & -i \\ i & 0 \end{pmatrix}, \quad \sigma_3 = \begin{pmatrix} 1 & 0 \\ 0 & -1 \end{pmatrix}, \tag{B.47}$$

and $[\delta]$ ($[\eta]$) can be understood as the eigenvalue for phase shift (inelasticity), and $e^{-2i\bar{\epsilon}^J\sigma^1}$ as the mixing term,

$$\begin{aligned} [\eta] &= \begin{pmatrix} \eta_L & \\ & \eta_{L'} \end{pmatrix}, \\ [\delta] &= \begin{pmatrix} \delta_L & \\ & \delta_{L'} \end{pmatrix} \qquad \Longrightarrow \qquad e^{i[\delta]} = \begin{pmatrix} e^{i\delta_L} & \\ & e^{i\delta_{L'}} \end{pmatrix}. \end{aligned} \tag{B.48}$$

To simplify the mixing term, the following relation is at hand,

$$e^{i\lambda\sigma_n} = \cos(\lambda)\, I_{2\times 2} + i\sigma_n \sin(\lambda), \tag{B.49}$$

where σ_n is the projection of $\vec{\sigma}$ onto unit vector $\vec{n}$ and $I_{2\times 2}$ is the two-dimensional identity matrix. We then have

$$\begin{aligned} e^{-2i\epsilon_J\sigma_1} &= e^{i(-2\epsilon_J)\sigma_1} = \cos(-2\epsilon_J)I_{2\times 2} + i\sigma_1 \sin(-2\epsilon_J) \\ &= \cos(2\epsilon_J)I_{2\times 2} - i\sin(2\epsilon_J)\sigma_1 \\ &= \begin{pmatrix} \cos 2\epsilon_J & \\ & \cos\epsilon_J \end{pmatrix} - i\sin 2\epsilon_J \begin{pmatrix} 0 & 1 \\ 1 & 0 \end{pmatrix} \\ &= \begin{pmatrix} \cos 2\epsilon_J & -i\sin 2\epsilon_J \\ -i\sin 2\epsilon_J & \cos 2\epsilon_J \end{pmatrix}. \end{aligned} \tag{B.50}$$

Combining

$$\sqrt{[\eta]}e^{i[\delta]} = \begin{pmatrix} \sqrt{\eta_L}e^{i\delta_L} & \\ & \sqrt{\eta_{L'}}e^{i\delta_{L'}} \end{pmatrix}. \tag{B.51}$$

and Eq. (B.50), one easily reads off

$$\begin{pmatrix} S_{LL} & S_{LL'} \\ S_{L'L} & S_{L'L'} \end{pmatrix} = \begin{pmatrix} \eta_L \cos 2\epsilon_J e^{2i\delta_L} & -i\sqrt{\eta_L\,\eta_{L'}}\sin 2\epsilon_J e^{i(\delta_L+\delta_{L'})} \\ -i\sqrt{\eta_L\,\eta_{L'}}\sin 2\epsilon_J e^{i(\delta_L+\delta_{L'})} & \eta_{L'}\cos 2\epsilon_J e^{2i\delta_{L'}} \end{pmatrix}. \tag{B.52}$$

From Eq. (B.52), one knows

$$\eta_L = \left|\frac{S_{LL}}{\cos 2\epsilon_J}\right|, \qquad \eta_{L'} = \left|\frac{S_{L'L'}}{\cos 2\epsilon_J}\right|. \tag{B.53}$$

Through

$$\begin{aligned} \mathrm{Im}\left(\frac{S_{LL}}{\cos 2\epsilon_J}\right) &= \eta_L \sin 2\delta_L, \\ \mathrm{Re}\left(\frac{S_{LL}}{\cos 2\epsilon^J}\right) &= \eta_L \cos 2\delta_L, \end{aligned}$$

we know the phase shift,

$$\delta_L = \frac{1}{2}\arctan\left(\frac{\mathrm{Im}\left(\frac{S_{LL}}{\cos 2\epsilon_J}\right)}{\mathrm{Re}\left(\frac{S_{LL}}{\cos 2\epsilon_J}\right)}\right), \tag{B.54}$$

and similarly,

$$\delta_{L'} = \frac{1}{2}\arctan\left(\frac{\mathrm{Im}\left(\frac{S_{L'L'}}{\cos 2\epsilon_J}\right)}{\mathrm{Re}\left(\frac{S_{L'L'}}{\cos 2\epsilon_J}\right)}\right). \tag{B.55}$$

The mixing parameter ϵ_J involves the off-diagonal elements and reads

$$\epsilon_J = \frac{1}{2}\arctan\left(\frac{i(S_{LL'} + S_{L'L})}{2\sqrt{S_{LL}\cdot S_{L'L'}}}\right). \tag{B.56}$$

For a concrete calculation, the mixing angle ϵ_J should be determined first.

For the recent partial wave analysis of $\bar{p}p$ scattering data [108], one can refer to Sec. VII of that reference. The convention there originates in Ref. [227] and also appears in Refs. [107, 108, 161]. Here we provide the formula for $S-$matrix elements reconstructed from their phase shifts and inelasticities listed in Tables VIII-X in Ref. [108]:

$$\begin{aligned} u &\equiv \omega_J + \epsilon_J, \quad v \equiv \omega_J - \epsilon_J, \\ S_{LL} &= e^{2i\delta_L}\left[\eta_L \cos u \cos v + \eta_{L'} \sin u \sin v + \frac{i}{2}(\eta_L - \eta_{L'})\sin(2\epsilon_J)\sin(2\omega_J)\right], \\ S_{LL'} &= e^{i(\delta_L+\delta_{L'})}\left[\frac{1}{2}(\eta_L - \eta_{L'})\cos(2\epsilon_J)\sin 2(\omega_J) + \frac{i}{2}(\eta_L + \eta_{L'})\sin(2\epsilon_J)\right], \\ S_{LL'} &= e^{2i\delta_{L'}}\left[\eta_L \sin u \sin v + \eta_{L'} \cos u \cos v + \frac{i}{2}(\eta_L - \eta_{L'})\sin(2\epsilon_J)\sin(2\omega_J)\right]. \end{aligned} \tag{B.57}$$

with $L = J - 1$ and $L' = J + 1$. In the case of vanishing inelasticity, this representation reinstates the form of the conventional Stapp parametrization (cf. Eq. (3.51) for $\eta_L = \eta_{L'} = 0$).

B.5 Unitarity constraints on antinucleon-nucleon annihilation

Let us first recall how the unitarity condition is imposed for S-matrix elements in the phenomenological meson-exchange potential models, see Ref. [228] for some details. One of the simplest way to include the annihilation dynamics is the optical model — adding a complex potential

$$V_{\rm ann} = V_R + iV_I \tag{B.58}$$

into the elastic part. $V_{\rm ann}$ is often constructed as state and energy independent [169], and the imaginary part V_I should be negative, only in such case we have the continuity equation

$$\mathrm{div}\,\vec{j} < 0. \tag{B.59}$$

This non-conserved flux means particles disappear from the system and never re-appear, i.e. $S^\dagger S < 1$ while $S^\dagger S > 1$ (go out the unitarity bound) happens for $V_I > 0$. Taking one-dimension case as an example, we present the derivation process for Eq. (B.59) below.

$$\begin{aligned} \hat{H}\psi &= E\psi, \\ \left(\frac{\hat{p}^2}{2m} + V\right)\psi &= E\psi, \\ -\frac{\hbar^2\nabla^2}{2m}\psi &= (E - V)\psi, \end{aligned}$$

$$
\begin{aligned}
-\nabla^2\psi &= 2m(E-V)\psi, \\
j &= \frac{\hbar}{2im}\psi^* \overleftrightarrow{\psi} = \frac{\hbar}{2im}\left(\psi^*\partial\psi - \psi\partial\psi^*\right), \\
\mathrm{div}\,\vec{j} &= \frac{1}{2im}\nabla\left(\psi^*\partial\psi - \psi\partial\psi^*\right) \\
&= \frac{1}{2im}\left[\nabla\psi^*\cdot\nabla\psi + \psi^*\nabla^2\psi - \nabla\psi\cdot\nabla\psi^* - \psi\nabla^2\psi^*\right] \\
&= \frac{1}{2im}(\psi^*\nabla^2\psi - \psi\nabla^2\psi^*) \\
&= \frac{1}{2im}(-2m)[\psi^*(E-V)\psi - \psi(E-V^*)\psi^*] \\
&= -i(\psi^*V\psi - \psi V^*\psi^*), \quad V - V^* = 2iV_I, \\
\mathrm{div}\,\vec{j} &= 2V_I|\psi|^2 < 0 \quad (V_I < 0).
\end{aligned}
\tag{B.60}
$$

The work of extension to three-dimensional case is trivial. Note that the derivation Eq. (B.60) is only valid for local potential, however, one can generalize it to the case of non-local potential. The Schrödinger equation with non-local potential in $\vec{r}-$space could generally be written as (see e.g. Ref. [229]):

$$
-\frac{\hbar^2}{2\mu}\nabla^2\psi(\vec{r}) + \int V(\vec{r},\vec{r}\,')\psi(\vec{r}\,')d\vec{r}\,' = E\psi(\vec{r}\,'),
\tag{B.61}
$$

with μ denoting the reduced mass of two interacting particles. Starting from Eq. (B.61) one gets

$$
\begin{aligned}
\mathrm{div}\,\vec{j} &= -i\left(\psi^*(\vec{r})\int V(\vec{r},\vec{r}\,')\psi(\vec{r}\,')d\vec{r}\,' - \psi(\vec{r})\int V^*(\vec{r},\vec{r}\,')\psi^*(\vec{r}\,')d\vec{r}\,'\right) \\
&= 2\mathrm{Im}\left[\psi^*(\vec{r})\int V(\vec{r},\vec{r}\,')\psi(\vec{r}\,')d\vec{r}\,'\right].
\end{aligned}
\tag{B.62}
$$

where the real part obviously drops out in the subtraction. Nevertheless, ending up with Eq. (B.62) we could not perform a further simplification and thus can not get a very clean constraint on the form of potential $V(\vec{r},\vec{r}\,')$.

In the Jülich models [92–94], the annihilation part is parametrized as a pure local potential with state and energy independence,

$$
V_{\mathrm{ann}}(\vec{r},\vec{r}\,') = (U_0 + iW_0)\exp\left(-\frac{(\vec{r}-\vec{r}\,')^2}{r_0^2}\right),
\tag{B.63}
$$

where U_0, W_0, r_0 are free parameters and have been determined by fitting to data as

$$
U_0 = -1260\,\mathrm{MeV}, \quad W_0 = -1575\,\mathrm{MeV}, \quad r_0 = 0.4\,\mathrm{fm}.
\tag{B.64}
$$

In the Kohno-Weise model [230], the annihilation potential is written as

$$V_{\rm ann}(r) = i\frac{W_0}{1+\exp\frac{r-R}{a}}\ , \quad r = |\vec{r}-\vec{r}\,'| \tag{B.65}$$

with $W_0 = -1.2$ GeV, $R = 0.55$ fm and $a = 0.2$ fm. Note that $W_0 < 0$ as explained above. Generally speaking, once the imaginary part of the potential is local and negative, the unitarity bound $S^\dagger S \leq 1$ will be satisfied.

A more elaborate approach is based on the coupled channel model, which is more sophisticated in microscopic view. We can explicit show the momentum dependence in Eq. (3.44) and write it as

$$\begin{aligned} V_{\rm ann}(\vec{p}\,',\vec{p}) &= \sum_X V_{\bar{N}N\to X}(\vec{p}\,',\vec{p}_X)G_X(E_{p_X})V_{X\to\bar{N}N}(\vec{p}_X,\vec{p}) \\ &= \sum_X \int \frac{d^3p_X}{(2\pi)^3} V_{\bar{N}N\to X}(\vec{p}\,',\vec{p}_X)\frac{1}{2E_k - 2E_{p_X} + i0^+}V_{X\to\bar{N}N}\left(\vec{p}_X,\vec{p}\right) \end{aligned} \tag{B.66}$$

where $E_k = \sqrt{k^2+m_N^2}$ is the on-shell energy and $E_{p_X} = \sqrt{p_X^2+m_N^2}$. Equation (B.66) means $\bar{N}N$ first annihilates into X intermediate states, and finally these X return into the initial $\bar{N}N$ states (re-annihilation), i.e. no particle loss, thus it preserves unitarity condition $S^\dagger S = 1$ (here S denotes the full S-matrix).

Starting from Eq. (B.66) the imaginary part of the annihilation potential is constrained to be

$$\mathrm{Im}\, V_{\rm ann} = -\pi \sum_X V_{\bar{N}N\to X} V_{X\to\bar{N}N}, \tag{B.67}$$

where the identity Eq. (B.25) has been used. By imposing the form of the imaginary part Im $V_{\rm ann}$, we obviously ensure the correct unitarity cut structure.

As we argued in Sec. 3.3.2, the annihilation does not introduce a new scale into the problem. The expansion for $V_{\bar{N}N\to x}$ can be done analogously to the $\bar{N}N$ scattering. For the ${}^1S_0$ partial wave, if we expand $V_{\bar{N}N\to x}$ to the leading order (LO), i.e.,

$$V_{\bar{N}N\to i} \sim a_i \text{ (constant)}, \tag{B.68}$$

we will get $V_{i\to\bar{N}N} \sim a_i$ due to $V_{\bar{N}N\to X}(\vec{p},\vec{p}\,') = V_{X\to\bar{N}N}(\vec{p}\,',\vec{p})$, thus

$$\mathrm{Im}\ V_{\rm ann}\left({}^1S_0\right) = -\pi\left(a_1^2+a_2^2+a_3^2+\cdots\right) \equiv -i\,\tilde{C}^a_{{}^1S_0}, \quad \tilde{C}^a_{{}^1S_0} > 0. \tag{B.69}$$

The expansion of the real part of the integral in Eq. (B.66) recovers the forms listed in Sec. 3.2.4. If we take the imaginary part of annihilation potential up to LO, we will have the following contact term,

$$V_{\rm ct}\left({}^1S_0\right) = \tilde{C}_{{}^1S_0} + C_{{}^1S_0}(p^2+p'^2) - i\,\tilde{C}^a_{{}^1S_0}\,,\ \tilde{C}^a_{{}^1S_0} > 0. \tag{B.70}$$

One can also expand the annihilation potential to next-to-leading order (NLO), which has the form

$$V_{\bar{N}N\to i} \sim a_i + b_i\,p^2, \tag{B.71}$$

then one gets $V_{i\to\bar{N}N} \sim a_i + b_i\, p'^2$, thus

$$\begin{aligned} \text{Im } V_{\text{ann}}\left({}^1S_0\right) &= -\pi\left((a_1+b_1p^2)(a_1+b_1p'^2)+(a_2+b_2p^2)(a_2+b_2p'^2)+\cdots\right), \\ &\equiv -\left(\tilde{C}^a_{{}^1S_0}+C^a_{{}^1S_0}p^2\right)\left(\tilde{C}^a_{{}^1S_0}+C^a_{{}^1S_0}p'^2\right). \end{aligned} \tag{B.72}$$

The contact term in this case reads

$$V_{\text{ct}}\left({}^1S_0\right) = \tilde{C}_{{}^1S_0} + C_{{}^1S_0}(p^2+p'^2) - i\left(\tilde{C}^a_{{}^1S_0}+C^a_{{}^1S_0}p^2\right)\left(\tilde{C}^a_{{}^1S_0}+C^a_{{}^1S_0}p'^2\right). \tag{B.73}$$

Similarly, for ${}^3S_1 - {}^3D_1$ partial wave, taking the LO imaginary part one has

$$\begin{aligned} V_{\text{ct}}\left({}^3S_1\right) &= \tilde{C}_{{}^3S_1} + C_{{}^3S_1}(p^2+p'^2) - i\,\tilde{C}^a_{{}^3S_1}, \\ V_{\text{ct}}({}^3S_1 - {}^3D_1) &= C_{\epsilon_1}p^2, \\ V_{\text{ct}}({}^3D_1 - {}^3S_1) &= C_{\epsilon_1}p'^2. \end{aligned} \tag{B.74}$$

while taking the imaginary part up to NLO

$$\begin{aligned} V_{\text{ct}}\left({}^3S_1\right) &= \tilde{C}_{{}^3S_1} + C_{{}^3S_1}(p^2+p'^2) - i\left(\tilde{C}^a_{{}^3S_1}+C^a_{{}^3S_1}p^2\right)\left(\tilde{C}^a_{{}^3S_1}+C^a_{{}^3S_1}p'^2\right), \\ V_{\text{ct}}({}^3S_1 - {}^3D_1) &= C_{\epsilon_1}p^2 - i\,C^a_{\epsilon_1}p^2\left(\tilde{C}^a_{{}^3S_1}+C^a_{{}^3S_1}p'^2\right), \\ V_{\text{ct}}({}^3D_1 - {}^3S_1) &= C_{\epsilon_1}p'^2 - i\,C^a_{\epsilon_1}p'^2\left(\tilde{C}^a_{{}^3S_1}+C^a_{{}^3S_1}p^2\right), \\ V_{\text{ct}}({}^3D_1) &= -i\,C^a_{\epsilon_1}p'^2\cdot C^a_{\epsilon_1}p^2. \end{aligned} \tag{B.75}$$

Equation (B.74) is, in fact, a special case of Eq. (B.75) by fixing $C^a_{{}^3S_1}=0$ and $C^a_{\epsilon_1}=0$. For P-waves, the contact terms are

$$V_{\text{ct}}(P) = C_\xi\, p\, p' - iC^a_\xi\, p\cdot C^a_\xi\, p', \tag{B.76}$$

where ξ denotes the partial waves ${}^1P_1$, ${}^3P_0$, ${}^3P_1$ or ${}^3P_2$.

In Sec. 3.3.2, Eqs. (B.73) and (B.75) are exploited. We have also examined the case where we use the contact terms listed in Eq. (B.74), and the results are shown in Fig. B.1. The corresponding LECs obtained by fitting to scattering data are listed in Table. B.1. As one expects, less parameters (here as a special case) will induce larger error bands (more precisely speaking, it is the cutoff dependence).

B.6 Partial-wave cross sections

Solving the Lippmann-Schwinger equation, one can get T-matrix elements, then the observables such as cross section, analysing power can be calculated and the corresponding formulas are organized in Appendix C. The total cross section σ_{tot} is calculated via optical theorem

$$\sigma_{\text{tot}} = \frac{4\pi}{k_i}\,\text{Im}\, f(0), \tag{B.77}$$

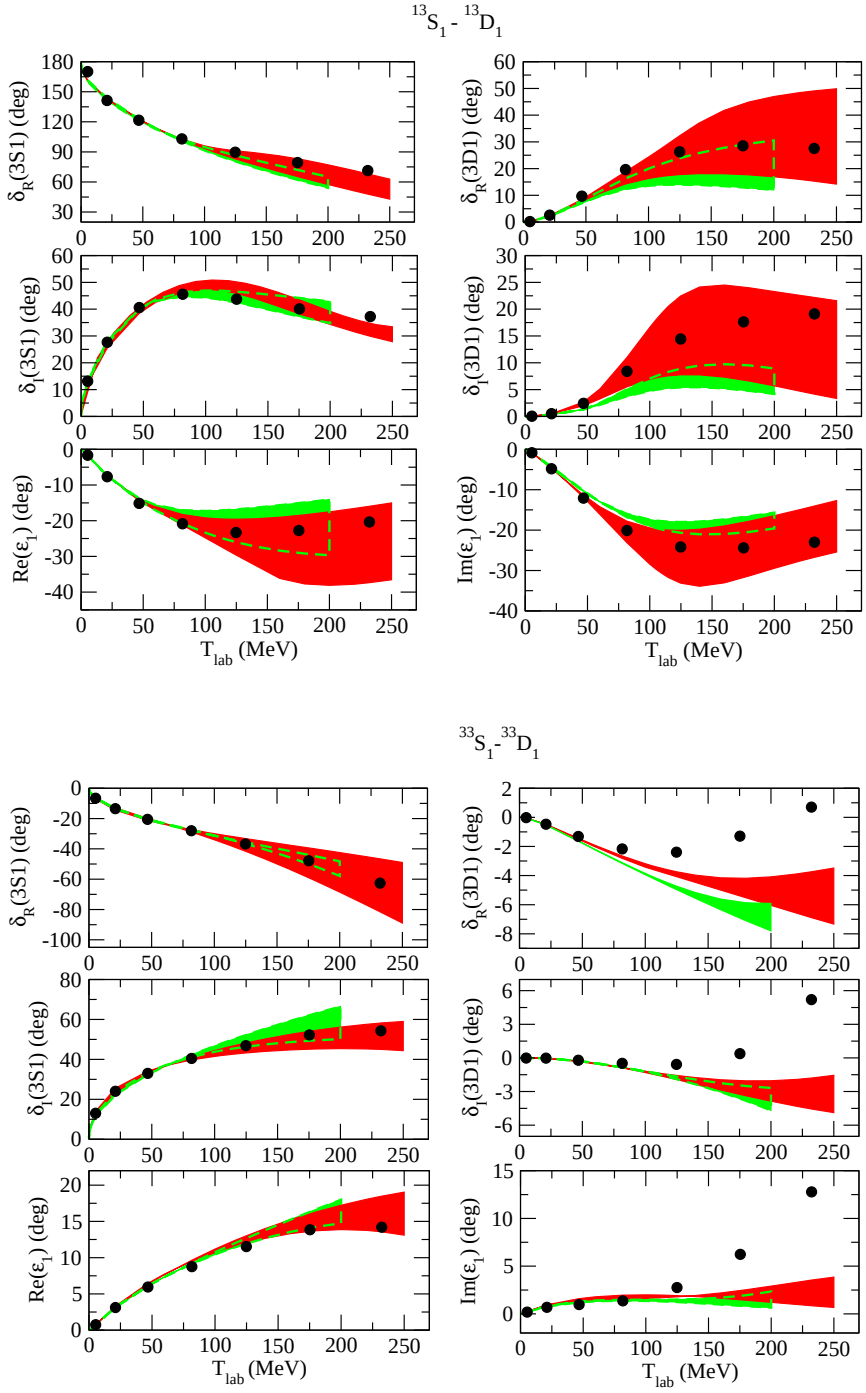

Figure B.1: Phase shifts and inelasticities of $^3S_1$–$^3D_1$, for notations see Fig. 4.2, but the contact terms is based on Eq. (B.74).

		NLO			
LEC		{450, 500}	{600, 500}	{450, 700}	{600, 700}
$I=0$	$\tilde{C}_{^3S_1}$	−0.123	−0.109	−0.122	−0.090
	$C_{^3S_1}$	−0.307	−0.557	−0.501	−0.792
	$\tilde{C}^a_{^3S_1}$	0.149	0.073	0.150	0.071
	C_{ϵ_1}	0.437	0.533	0.468	0.595
$I=1$	$\tilde{C}_{^3S_1}$	−0.076	−0.095	−0.079	−0.096
	$C_{^3S_1}$	0.665	0.309	0.709	0.314
	$\tilde{C}^a_{^3S_1}$	0.156	0.109	0.162	0.106
	C_{ϵ_1}	0.241	0.198	0.280	0.239
		NNLO			
LEC		{450, 500}	{650, 500}	{450, 700}	{650, 700}
$I=0$	$\tilde{C}_{^3S_1}$	−0.155	−0.182	−0.184	−0.330
	$C_{^3S_1}$	0.493	0.354	0.825	1.029
	$\tilde{C}^a_{^3S_1}$	0.156	0.090	0.162	0.172
	C_{ϵ_1}	0.160	0.233	0.043	0.061
$I=1$	$\tilde{C}_{^3S_1}$	−0.091	−0.125	−0.111	−0.275
	$C_{^3S_1}$	1.174	0.786	1.500	1.541
	$\tilde{C}^a_{^3S_1}$	0.169	0.100	0.181	0.276
	C_{ϵ_1}	0.326	0.286	0.413	0.450

Table B.1: LECs used in Fig. B.1, for notations see Table 3.1.

where k_i is the magnitude of the three-momentum of the initial state in the center-of-mass system (CMS), and $f(0)$ is the scattering amplitude at forward angle $\theta = 0$.

The partial-wave cross section for a transition $LSJ \to L'S'J$ is given by

$$\begin{aligned}\sigma^J_{L'S',LS} &= \pi\,(2J+1)\,\left|f^J_{L'S',LS}\right|^2, \quad \text{for } \bar{p}p \to \bar{p}p \\ \sigma^J_{L'S',LS} &= \pi\,(2J+1)\,\frac{k^2_{\bar{n}n}}{k^2_{\bar{p}p}}\left|f^J_{L'S',LS}\right|^2, \quad \text{for } \bar{p}p \to \bar{n}n,\end{aligned} \tag{B.78}$$

where $k_{\bar{p}p}$ ($k_{\bar{n}n}$) is the magnitude of three-momentum for $\bar{p}p$ ($\bar{n}n$) pairs in the CMS, and f is the corresponding scattering amplitude and related to S-matrix by Eq. (C.11).

The partial-wave cross sections for $\bar{p}p \to \bar{p}p$ and $\bar{p}p \to \bar{n}n$ in our calculations with chiral EFT are provided in Table B.2 and Table B.3, respectively. There one can also find

the corresponding numbers predicted by Jülich model D [94] and the recent partial-wave analysis [108]. Note in both tables the Coulomb interaction is not considered.

		$\bar{p}p \to \bar{p}p$			
	$p_{\rm lab}$ (MeV)	200	400	600	800
$^1S_0$	NLO	14.6	7.8	(4.0 $\cdots$ 4.1)	(2.2 $\cdots$ 2.5)
	NNLO	(14.5 $\cdots$ 14.6)	(7.8 $\cdots$ 7.9)	(3.9 $\cdots$ 4.0)	(1.7 $\cdots$ 2.4)
	model D	12.9	7.8	4.9	3.3
	PWA2012	15.7	7.9	4.1	2.1
$^3S_1$	NLO	(62.2 $\cdots$ 62.9)	(26.5 $\cdots$ 26.6)	(12.2 $\cdots$ 12.6)	(6.1 $\cdots$ 6.2)
	NNLO	(62.7 $\cdots$ 63.0)	26.5	(12.2 $\cdots$ 12.5)	(5.8 $\cdots$ 6.1)
	model D	68.2	22.8	9.8	6.3
	PWA2012	66.1	26.0	13.2	8.8
$^3P_0$	NLO	(3.7 $\cdots$ 4.1)	(4.4 $\cdots$ 5.0)	(6.1 $\cdots$ 7.4)	(3.5 $\cdots$ 5.5)
	NNLO	(3.5 $\cdots$ 3.7)	(4.3 $\cdots$ 5.0)	(6.2 $\cdots$ 7.0)	(3.4 $\cdots$ 4.9)
	model D	2.0	2.3	2.4	2.3
	PWA2012	4.9	5.4	5.0	3.5
$^1P_1$	NLO	(0.5 $\cdots$ 0.6)	(2.1 $\cdots$ 2.2)	(5.4 $\cdots$ 5.7)	(5.6 $\cdots$ 8.1)
	NNLO	(0.6 $\cdots$ 0.8)	(2.1 $\cdots$ 2.3)	(4.9 $\cdots$ 5.7)	(5.9 $\cdots$ 7.8)
	model D	4.1	7.5	7.2	6.0
	PWA2012	0.9	2.5	4.5	5.6
$^3P_1$	NLO	(2.0 $\cdots$ 2.1)	(7.1 $\cdots$ 7.4)	(5.8 $\cdots$ 7.0)	(4.0 $\cdots$ 9.6)
	NNLO	(1.9 $\cdots$ 2.1)	(6.7 $\cdots$ 7.2)	(6.2 $\cdots$ 8.0)	(4.0 $\cdots$ 5.4)
	model D	4.6	10.4	8.3	5.8
	PWA2012	1.8	4.9	4.0	3.5
$^3P_2$	NLO	(0.8 $\cdots$ 1.2)	(6.2 $\cdots$ 8.1)	(10.5 $\cdots$ 11.8)	(7.2 $\cdots$ 10.9)
	NNLO	(1.6 $\cdots$ 2.6)	(8.2 $\cdots$ 9.5)	(9.8 $\cdots$ 10.8)	(6.1 $\cdots$ 10.0)
	model D	4.9	14.7	14.3	11.5
	PWA2012	7.0	17.0	13.9	9.6

Table B.2: Partial-wave cross sections (in mb) for the elastic scattering $\bar{p}p \to \bar{p}p$ Results based on the NLO and NNLO potentials are given and compared with the predictions of the Jülich $\bar{N}N$ model D [94] and the recent partial wave analysis provided in Ref. [108].

		$\bar{p}p \to \bar{n}n$			
	$p_{\rm lab}$ (MeV)	200	400	600	800
$^1S_0$	NLO	$(0.5 \cdots 0.6)$	0.1		
	NNLO	$(0.5 \cdots 0.6)$	0.1		
	model D	0.8	0.1		
	PWA2012	0.7	0.1		
$^3S_1$	NLO	$(2.4 \cdots 2.6)$	$(0.9 \cdots 1.0)$	$(0.5 \cdots 0.6)$	0.5
	NNLO	2.6	0.9	$(0.5 \cdots 0.6)$	$(0.3 \cdots 0.4)$
	model D	4.9	1.4	0.4	0.1
	PWA2012	3.0	1.0	0.5	0.2
$^3P_0$	NLO	$(1.7 \cdots 1.9)$	$(0.9 \cdots 1.2)$	$(0.0 \cdots 0.2)$	$(0.0 \cdots 0.2)$
	NNLO	$(1.5 \cdots 1.7)$	$(0.9 \cdots 1.3)$	0.1	$(0.0 \cdots 0.5)$
	model D	2.5	0.6	0.1	
	PWA2012	1.5	0.8	0.1	
$^1P_1$	NLO	1.0	0.1	$(0.0 \cdots 0.1)$	$(0.1 \cdots 0.2)$
	NNLO	$(0.8 \cdots 1.0)$	0.1		
	model D	0.7	0.8	0.5	0.3
	PWA2012	0.8	0.1		
$^3P_1$	NLO	$(6.0 \cdots 6.1)$	$(4.6 \cdots 5.0)$	$(0.6 \cdots 1.2)$	$(0.3 \cdots 0.9)$
	NNLO	$(6.1 \cdots 6.3)$	$(4.4 \cdots 5.0)$	$(0.5 \cdots 1.6)$	$(0.3 \cdots 0.4)$
	model D	4.9	2.4	0.7	0.2
	PWA2012	4.9	2.9	0.2	0.1
$^3P_2$	NLO	$(0.1 \cdots 0.2)$	$(0.1 \cdots 0.5)$	$(0.0 \cdots 0.3)$	$(0.0 \cdots 0.1)$
	NNLO	$(0.2 \cdots 0.5)$	$(0.5 \cdots 0.7)$	$(0.0 \cdots 0.2)$	$(0.0 \cdots 0.1)$
	model D	0.6	0.6	0.2	0.1
	PWA2012	0.9	1.4	0.4	0.1

Table B.3: Partial-wave cross sections (in mb) for the charge-exchange process $\bar{p}p \to \bar{n}n$ Results based on the NLO and NNLO potentials are given and compared with the predictions of the Jülich $\bar{N}N$ model D [94] and the recent partial wave analysis provided in Ref. [108].

Appendix C

General formalism for two-body scattering of spin-1/2 particles

The process of two spin-1/2 particles scattering to two spin-1/2 ones in final states, e.g. nucleon-nucleon elastic scattering, hyperon-nucleon scattering, has been widely studied dated from several decades ago. In this section, we will briefly review the formalism for calculating physical observables. The on-shell 4×4 amplitude M acting on two spin-1/2 states can depend only on scalars built out of $\vec{\sigma}_1$, $\vec{\sigma}_2$ and $\hat{\boldsymbol{k}}_{\boldsymbol{i}}$, $\hat{\boldsymbol{k}}_{\boldsymbol{f}}$, where $\vec{\sigma}_{1,2}$ are spins of two particles and $\hat{\boldsymbol{k}}_{\boldsymbol{i}}$ ($\hat{\boldsymbol{k}}_{\boldsymbol{f}}$) the unit three-momentum in the center-of-mass system (CMS) of the initial (final) states. Introducing three unit vectors

$$\hat{\boldsymbol{P}} = \frac{\hat{\boldsymbol{k}}_{\boldsymbol{i}} + \hat{\boldsymbol{k}}_{\boldsymbol{f}}}{|\hat{\boldsymbol{k}}_{\boldsymbol{i}} + \hat{\boldsymbol{k}}_{\boldsymbol{f}}|}, \quad \hat{\boldsymbol{n}} = \frac{\hat{\boldsymbol{k}}_{\boldsymbol{i}} \times \hat{\boldsymbol{k}}_{\boldsymbol{f}}}{|\hat{\boldsymbol{k}}_{\boldsymbol{i}} \times \hat{\boldsymbol{k}}_{\boldsymbol{f}}|}, \quad \hat{\boldsymbol{K}} = \hat{\boldsymbol{n}} \times \hat{\boldsymbol{P}} \tag{C.1}$$

All the allowed scalar products (except for the trivial constant) are listed below [233]: In

$\underline{\vec{\sigma}_i \cdot \hat{\boldsymbol{K}}}$	$\vec{\sigma}_i \cdot \hat{\boldsymbol{n}}$	$\underline{\vec{\sigma}_i \cdot \hat{\boldsymbol{P}}}$	$i = 1,\ 2$
$\underline{(\vec{\sigma}_1 \times \vec{\sigma}_2) \cdot \hat{\boldsymbol{K}}}$	$(\vec{\sigma}_1 \times \vec{\sigma}_2) \cdot \hat{\boldsymbol{n}}$	$\underline{(\vec{\sigma}_1 \times \vec{\sigma}_2) \cdot \hat{\boldsymbol{P}}}$	
$(\vec{\sigma}_1 \cdot \hat{\boldsymbol{K}})(\vec{\sigma}_2 \cdot \hat{\boldsymbol{K}})$	$\underline{(\vec{\sigma}_1 \cdot \hat{\boldsymbol{K}})(\vec{\sigma}_2 \cdot \hat{\boldsymbol{n}})}$	$(\vec{\sigma}_1 \cdot \hat{\boldsymbol{K}})(\vec{\sigma}_2 \cdot \hat{\boldsymbol{P}})$	
$\underline{(\vec{\sigma}_1 \cdot \hat{\boldsymbol{n}})(\vec{\sigma}_2 \cdot \hat{\boldsymbol{K}})}$	$(\vec{\sigma}_1 \cdot \hat{\boldsymbol{n}})(\vec{\sigma}_2 \cdot \hat{\boldsymbol{n}})$	$\underline{(\vec{\sigma}_1 \cdot \hat{\boldsymbol{n}})(\vec{\sigma}_2 \cdot \hat{\boldsymbol{P}})}$	
$(\vec{\sigma}_1 \cdot \hat{\boldsymbol{P}})(\vec{\sigma}_2 \cdot \hat{\boldsymbol{K}})$	$\underline{(\vec{\sigma}_1 \cdot \hat{\boldsymbol{P}})(\vec{\sigma}_2 \cdot \hat{\boldsymbol{n}})}$	$(\vec{\sigma}_1 \cdot \hat{\boldsymbol{P}})(\vec{\sigma}_2 \cdot \hat{\boldsymbol{P}})$.	

principle, the product $\vec{\sigma}_1 \cdot \vec{\sigma}_2$ can occur, however, it is implicitly implied due to

$$\vec{\sigma}_1 \cdot \vec{\sigma}_2 = (\vec{\sigma}_1 \cdot \hat{\boldsymbol{K}})(\vec{\sigma}_2 \cdot \hat{\boldsymbol{K}}) + (\vec{\sigma}_1 \cdot \hat{\boldsymbol{n}})(\vec{\sigma}_2 \cdot \hat{\boldsymbol{n}}) + (\vec{\sigma}_1 \cdot \hat{\boldsymbol{P}})(\vec{\sigma}_2 \cdot \hat{\boldsymbol{P}}). \tag{C.2}$$

It is understandable that under a parity operation, one has

$$\begin{aligned} &\hat{\boldsymbol{K}} \to -\hat{\boldsymbol{K}}\ , \\ &\hat{\boldsymbol{P}} \to -\hat{\boldsymbol{P}}\ , \\ &\hat{\boldsymbol{n}} \to \hat{\boldsymbol{n}}\ , \end{aligned}$$

$$\vec{\sigma}_i \to \vec{\sigma}_i \ , \tag{C.3}$$

Then the underlined terms violate parity reversal invariance and are therefore forbidden. Therefore the general spin matrix M can be written as [205, 234]

$$\begin{aligned} M(\hat{\boldsymbol{k}}_{\boldsymbol{i}}, \hat{\boldsymbol{k}}_{\boldsymbol{f}}, \theta) &= \frac{1}{2}\Big\{(a+b)I_{4\times4} + (a-b)\vec{\sigma}_1\cdot\hat{\boldsymbol{n}}\vec{\sigma}_2\cdot\hat{\boldsymbol{n}} + (c+d)\vec{\sigma}_1\cdot\hat{\boldsymbol{K}}\vec{\sigma}_2\cdot\hat{\boldsymbol{K}} \\ &\quad +(c-d)\vec{\sigma}_1\cdot\hat{\boldsymbol{P}}\vec{\sigma}_2\cdot\hat{\boldsymbol{P}} + e(\vec{\sigma_1}+\vec{\sigma}_2)\cdot\hat{\boldsymbol{n}} + f(\vec{\sigma}_1-\vec{\sigma}_2)\cdot\hat{\boldsymbol{n}} \\ &\quad +g(\vec{\sigma}_1\cdot\hat{\boldsymbol{K}}\vec{\sigma}_2\cdot\hat{\boldsymbol{P}} + \vec{\sigma}_1\cdot\hat{\boldsymbol{P}}\vec{\sigma}_2\cdot\hat{\boldsymbol{K}}) + h\,\vec{\sigma}_1\times\vec{\sigma}_2\cdot\hat{\boldsymbol{n}}\Big\}, \end{aligned} \tag{C.4}$$

where $I_{4\times4}$ is the four-dimensional identity matrix. In fact, the scattering amplitude M has been decomposed into symmetric and anti-symmetric parts under the exchange of two particles, i.e. $\vec{\sigma}_1 \leftrightarrow \vec{\sigma}_2$. In Refs. [235, 236], the term $(\vec{\sigma}_1\cdot\hat{\boldsymbol{K}})(\vec{\sigma}_2\cdot\hat{\boldsymbol{P}}) - (\vec{\sigma}_1\cdot\hat{\boldsymbol{P}})(\vec{\sigma}_2\cdot\hat{\boldsymbol{K}})$ is used, which is just $(\vec{\sigma}_1\times\vec{\sigma}_2)\cdot\hat{\boldsymbol{n}}$ above. We give the proof as follows: noting that $\hat{\boldsymbol{n}} = \hat{\boldsymbol{K}}\times\hat{\boldsymbol{P}}$ and the relation $\vec{a}\times(\vec{b}\times\vec{c}) = \vec{b}(\vec{a}\cdot\vec{c}) - \vec{c}(\vec{a}\cdot\vec{b})$, one has

$$\begin{aligned} (\vec{\sigma}_1\times\vec{\sigma}_2)\cdot\hat{\boldsymbol{n}} &= \vec{\sigma}_1\cdot(\vec{\sigma}_2\times\hat{\boldsymbol{n}}) = \vec{\sigma}_1\cdot\Big(\vec{\sigma}_2\times(\hat{\boldsymbol{K}}\times\hat{\boldsymbol{P}})\Big) \\ &= \vec{\sigma}_1\cdot\Big(\hat{\boldsymbol{K}}(\vec{\sigma}_2\cdot\hat{\boldsymbol{P}}) - \hat{\boldsymbol{P}}(\vec{\sigma}_2\cdot\hat{\boldsymbol{K}})\Big) \\ &= (\vec{\sigma}_1\cdot\hat{\boldsymbol{K}})(\vec{\sigma}_2\cdot\hat{\boldsymbol{P}}) - (\vec{\sigma}_1\cdot\hat{\boldsymbol{P}})(\vec{\sigma}_2\cdot\hat{\boldsymbol{K}}). \end{aligned} \tag{C.5}$$

With the definition of M, the eight helicity-state matrix elements are defined as [234]

$$\begin{aligned} \phi_1 &= \langle++|M|++\rangle, & \phi_5 &= \langle++|M|+-\rangle, \\ \phi_2 &= \langle++|M|--\rangle, & \phi_6 &= \langle+-|M|++\rangle, \\ \phi_3 &= \langle+-|M|+-\rangle, & \phi_7 &= \langle++|M|-+\rangle, \\ \phi_4 &= \langle+-|M|-+\rangle, & \phi_8 &= \langle-+|M|++\rangle. \end{aligned} \tag{C.6}$$

Following the notations in Ref. [33], the helicity states can be expressed as

$$\begin{aligned} |\lambda_1\rangle &= \chi_{\lambda_1}, \qquad |\lambda_2\rangle = \chi_{-\lambda_2}, \\ |\lambda_1'\rangle &= \exp\Big(-\frac{i}{2}\sigma_y\theta\Big)\chi_{\lambda_1'}, \qquad |\lambda_2'\rangle = \exp\Big(-\tfrac{i}{2}\sigma_y\theta\Big)\chi_{-\lambda_2'}, \end{aligned} \tag{C.7}$$

where θ is the scattering angle, the superscript "prime" denotes final state, $|\lambda_i\rangle$ and $|\lambda_i'\rangle$ are the eigenstates of the helicity operators for the corresponding particles and χ's are the conventional Pauli spinors. Substituting Eqs. (C.4) and (C.7) into Eq. (C.6), one could obtain [234]

$$\begin{aligned} \phi_1 &= \frac{1}{2}(a\cos\theta + b - c + d + ie\sin\theta), \\ \phi_2 &= \frac{1}{2}(a\cos\theta - b + c + d + ie\sin\theta), \end{aligned}$$

$$\begin{aligned}
\phi_3 &= \frac{1}{2}(a\cos\theta + b + c + d - ie\sin\theta),\\
\phi_4 &= \frac{1}{2}(-a\cos\theta + b + c + d - ie\sin\theta),\\
\phi_5 &= \frac{1}{2}(-a\sin\theta + ie\cos\theta - if + g + h),\\
\phi_6 &= \frac{1}{2}(a\sin\theta - ie\cos\theta + if + g + h),\\
\phi_7 &= \frac{1}{2}(a\sin\theta - ie\cos\theta - if - g + h),\\
\phi_8 &= \frac{1}{2}(-a\sin\theta + ie\cos\theta + if - g + h).
\end{aligned} \tag{C.8}$$

Inversely, one can express $a, \cdots, h$ from ϕ's as

$$\begin{aligned}
a &= \frac{1}{2}\Big\{(\phi_1 + \phi_2 + \phi_3 - \phi_4)\cos\theta - (\phi_5 - \phi_6 - \phi_7 + \phi_8)\sin\theta\Big\},\\
b &= \frac{1}{2}\{\phi_1 - \phi_2 + \phi_3 + \phi_4\}\\
c &= \frac{1}{2}\{-\phi_1 + \phi_2 + \phi_3 + \phi_4\}\\
d &= \frac{1}{2}\{\phi_1 + \phi_2 - \phi_3 + \phi_4\},\\
e &= -\frac{i}{2}\Big\{(\phi_1 + \phi_2 + \phi_3 - \phi_4)\sin\theta + (\phi_5 - \phi_7 - \phi_6 + \phi_8)\cos\theta\Big\},\\
f &= \frac{i}{2}\{\phi_5 + \phi_7 - \phi_6 - \phi_8\},\\
g &= \frac{1}{2}\{\phi_5 - \phi_7 + \phi_6 - \phi_8\},\\
h &= \frac{1}{2}\{\phi_5 + \phi_7 + \phi_6 + \phi_8\}.
\end{aligned} \tag{C.9}$$

One could define the potentials $\langle JL'S'|V^J(q', q, z)|JLS\rangle$ as

$$\begin{aligned}
V_0^J &= \big\langle JJ0|V^J(k_i, k_f, z)|JJ0\big\rangle\\
V_1^J &= \big\langle JJ1|V^J(k_i, k_f, z)|JJ1\big\rangle\\
V_{ST}^J &= \langle JJ0|V^J(k_i, k_f, z)|JJ1\rangle\\
V_{TS}^J &= \langle JJ1|V^J(k_i, k_f, z)|JJ0\rangle\\
V_{++}^J &= \langle J(J+1)1|V^J(k_i, k_f, z)|\rangle J(J+1)1\rangle\\
V_{--}^J &= \langle J(J-1)1|V^J(k_i, k_f, z)|J(J-1)1\rangle
\end{aligned}$$

$$\begin{aligned} V^J_{+-} &= \langle J(J+1)1|V^J(k_i,k_f,z)|J(J-1)1\rangle \\ V^J_{-+} &= \langle J(J-1)1|V^J(k_i,k_f,z)|J(J+1)1\rangle, \end{aligned} \tag{C.10}$$

and similarly for the T-matrix elements. The S-matrix is defined as [1]

$$S^{\alpha\alpha'}_{LL'} = \delta^{\alpha\alpha'}\,\delta_{LL'} + 2i\sqrt{k_\alpha k_{\alpha'}} f^{\alpha\alpha'}_{LL'}\ , \tag{C.11}$$

and the scattering amplitude f in LSJ basis is related to T-matrix element by

$$f^{\alpha\alpha'}_{LL'} = -\frac{\pi}{(2\pi)^3}\sqrt{\frac{\rho_\alpha\rho_{\alpha'}}{k_\alpha k_{\alpha'}}} T^{\alpha\alpha'}_{LL'}, \tag{C.12}$$

where as the notations in Chap. 4, the superscript α' (α) denotes the initial (final) state and the subscript L' (L) denotes the obital angular momentum corresponding to α' (α). In Eq. (C.12), ρ is calculated from

$$\rho_{\alpha'} = k^2_{\alpha'}\frac{dk_{\alpha'}}{dE_{\alpha'}}, \quad \rho_\alpha = k^2_\alpha \frac{dk_\alpha}{dE_\alpha}, \tag{C.13}$$

where $E_{\alpha'}$ (E_α) is the total energy for the initial (final) state in CMS, e.g., for a reaction $1 + 2 \to 1' + 2'$,

$$E_\alpha = E_1(k_\alpha) + E_2(k_\alpha), \quad E_{\alpha'} = E_{1'}(k_{\alpha'}) + E_{2'}(k_{\alpha'}), \tag{C.14}$$

with the definition $E_i(k) = \sqrt{k^2 + m_i^2}$ ($i = 1, 2, 1', 2'$). Then one finds

$$\begin{aligned} \rho_\alpha &= k_\alpha \left(\frac{1}{E_1(k_\alpha)} + \frac{1}{E_2(k_\alpha)}\right)^{-1}, \\ \rho_{\alpha'} &= k_{\alpha'} \left(\frac{1}{E_{1'}(k_{\alpha'})} + \frac{1}{E_{2'}(k_{\alpha'})}\right)^{-1}. \end{aligned} \tag{C.15}$$

For the case of the antinucleon-nucleon interaction (a single channel), the relation between $f_{LL'}$ and $T_{LL'}$ is much simplified and is given by

$$f_{LL'} = -\frac{\pi}{(2\pi)^3}\frac{E_k}{2} T_{LL'}. \tag{C.16}$$

With the above quantites, ϕ's can be expressed by partial-wave amplitudes corresponding to total angular momentum J (a well-defined quantum number):

$$\begin{aligned} \phi_1 &= \sum_J (2J+1) f^J_1 d^J_{00}(\theta), & \phi_5 &= \sum_J (2J+1) f^J_5 d^J_{10}(\theta), \\ \phi_2 &= \sum_J (2J+1) f^J_2 d^J_{00}(\theta), & \phi_6 &= \sum_J (2J+1) f^J_6 d^J_{10}(\theta), \\ \phi_3 &= \sum_J (2J+1) f^J_3 d^J_{11}(\theta), & \phi_7 &= \sum_J (2J+1) f^J_7 d^J_{10}(\theta), \\ \phi_4 &= \sum_J (2J+1) f^J_4 d^J_{-11}(\theta), & \phi_8 &= \sum_J (2J+1) f^J_8 d^J_{10}(\theta), \end{aligned} \tag{C.17}$$

[1] We write k^α as k_α in order to avoid misunderstanding α as the power. Keeping the factor $1/(2\pi)^3$ in Eqs. (C.12) and (C.16) is the convention that we use in this thesis, which is consitent with Appendix B.1.

where $d^J_{mm'}(\theta)$ is the Wigner d-function, and

$$\begin{aligned} f_1^J &= \frac{1}{2}\Big(f_0^J + \mathcal{F}_{12}^J\Big), & f_5^J &= \frac{1}{2}\Big(-f_{ST}^J + \mathcal{F}_{57}^J\Big), \\ f_2^J &= \frac{1}{2}\Big(-f_0^J + \mathcal{F}_{12}^J\Big), & f_6^J &= \frac{1}{2}\Big(-f_{TS}^J + \mathcal{F}_{68}^J\Big), \\ f_3^J &= \frac{1}{2}\Big(f_1^J + \mathcal{F}_{34}^J\Big), & f_7^J &= \frac{1}{2}\Big(f_{ST}^J + \mathcal{F}_{57}^J\Big), \\ f_4^J &= \frac{1}{2}\Big(-f_1^J + \mathcal{F}_{34}^J\Big), & f_8^J &= \frac{1}{2}\Big(f_{TS}^J + \mathcal{F}_{68}^J\Big). \end{aligned} \tag{C.18}$$

The $f_{12}, f_{34}, \cdots$ are related to the LSJ basis by

$$\begin{aligned} \mathcal{F}_{12}^J &= \frac{1}{2J+1}\Big[(J+1)\ f_{++}^J + J\ f_{--}^J - \sqrt{J(J+1)}(f_{-+}^J + f_{+-}^J)\Big], \\ \mathcal{F}_{34}^J &= \frac{1}{2J+1}\Big[(J+1)\ f_{--}^J + J\ f_{++}^J + \sqrt{J(J+1)}(f_{-+}^J + f_{+-}^J)\Big], \\ \mathcal{F}_{57}^J &= \frac{1}{2J+1}\Big[\sqrt{J(J+1)}(f_{--}^J - f_{++}^J) + J\ f_{-+}^J - (J+1)\ f_{+-}^J\Big], \\ \mathcal{F}_{68}^J &= \frac{1}{2J+1}\Big[\sqrt{J(J+1)}(f_{--}^J - f_{++}^J) + J\ f_{+-}^J - (J+1)\ f_{-+}^J\Big]. \end{aligned} \tag{C.19}$$

Similarly, transforming the helicity basis to the LSJ basis one has

$$\begin{aligned} f_{++}^J &= \frac{1}{2J+1}\left[(J+1)\ V_{12}^J + J\ V_{34}^J - \sqrt{J(J+1)}\left(V_{57}^J + V_{68}^J\right)\right], \\ f_{--}^J &= \frac{1}{2J+1}\left[J\ V_{12}^J + (J+1)\ V_{34}^J + \sqrt{J(J+1)}\left(V_{57}^J + V_{68}^J\right)\right], \\ f_{+-}^J &= -\frac{\sqrt{J(J+1)}}{2J+1}\left[V_{12}^J - V_{34}^J + \frac{1}{\sqrt{J(J+1)}}\left((J+1)\ V_{57}^J - J\ V_{68}^J\right)\right], \\ f_{-+}^J &= -\frac{\sqrt{J(J+1)}}{2J+1}\left[V_{12}^J - V_{34}^J - \frac{1}{\sqrt{J(J+1)}}\left(J\ V_{57}^J - (J+1)\ V_{68}^J\right)\right]. \end{aligned} \tag{C.20}$$

In fact, the relation between helicty amplitudes and the amplitude in LSJ basis is relegated into a matrix equation

$$\boldsymbol{f}_{LSJ} = \boldsymbol{M}^{\boldsymbol{T}} \boldsymbol{f}_{\rm Hel} \boldsymbol{M}, \tag{C.21}$$

where $\boldsymbol{f}_{LSJ}$ and $\boldsymbol{f}_{\rm Hel}$ are given by

$$\boldsymbol{f}_{LSJ} = \begin{pmatrix} f_0^J & f_{ST}^J & 0 & 0 \\ f_{TS}^J & f_1^J & 0 & 0 \\ 0 & 0 & f_{--}^J & 0 \\ 0 & 0 & f_{+-}^J & f_{++}^J \end{pmatrix} \tag{C.22}$$

(C.23)

$$\boldsymbol{f}_{\rm Hel} = \begin{pmatrix} f_1^J & f_5^J & f_7^J & f_2^J \\ f_6^J & f_3^J & f_4^J & f_8^J \\ f_8^J & f_4^J & f_3^J & f_6^J \\ f_2^J & f_7^J & f_5^J & f_1^J \end{pmatrix}. \tag{C.24}$$

The transformation matrix $\boldsymbol{M}$ reads

$$\boldsymbol{M} = \begin{pmatrix} \frac{1}{\sqrt{2}} & 0 & A & -B \\ 0 & -\frac{1}{\sqrt{2}} & B & A \\ 0 & \frac{1}{\sqrt{2}} & B & A \\ -\frac{1}{\sqrt{2}} & 0 & A & -B \end{pmatrix}, \tag{C.25}$$

with

$$A = \frac{J}{2(2J+1)}\ , \quad B = \frac{J+1}{2(2J+1)}\ , \tag{C.26}$$

and $\boldsymbol{M}$ satisfies the orthogonality relation

$$\boldsymbol{M}\,\boldsymbol{M^T} = \boldsymbol{M^T}\,\boldsymbol{M} = I_{4\times 4}. \tag{C.27}$$

With the helicity amplitudes, the differential cross section can be written as

$$\frac{d\sigma}{d\Omega} = \frac{1}{2}\frac{k_f}{k_i}\Big(|\phi_1|^2 + |\phi_2|^2 + |\phi_3|^2 + |\phi_4|^2 + |\phi_5|^2 + |\phi_6|^2 + |\phi_7|^2 + |\phi_8|^2\Big), \tag{C.28}$$

in terms of $a, \cdots, h$, one obtains

$$\frac{d\sigma}{d\Omega} = \frac{1}{2}\frac{k_f}{k_i}\Big(|a|^2 + |b|^2 + |c|^2 + |d|^2 + |e|^2 + |f|^2 + |g|^2 + |h|^2\Big). \tag{C.29}$$

Integrating out angles, the integrated cross section can be obtained. With the density matrix ρ_i (initial state) and ρ_f (final state), the expectation value of any arbitrary spin observable can be calculated as [233]

$$\langle \hat{O} \rangle_f = \frac{{\rm Tr}\{\rho_f O\}}{{\rm Tr}\{\rho_f\}} = \frac{{\rm Tr}\{M\rho_i M^\dagger O\}}{{\rm Tr}\{M\rho_i M^\dagger\}} \tag{C.30}$$

For a process of two-body scattering between spin-1/2 particles, there are total 16 scattering amplitudes as functions of energy E and scattering angle θ. Parity invariance constraints that only eight of them are independent. This happens for the general hyperon-nucleon interaction, like $\Sigma p \to \Lambda n$, where the above formalism are applied, see also Ref. [237]. For the type of $A + B \to A + B$, e.g., $e^- N \to e^- N$, $\Lambda N \to \Lambda N$, time reversal invariance can be imposed, which requires $g = h = 0$, the simplifed formulas can be found in Ref. [238]. For scattering between purely identical particles, e.g. $pp \to pp$,

the Pauli principle furthermore requires f to vanish, i.e. only five amplitudes a, b, c, d, e survive, which is the case in Ref. [210]. It is useful to note that in Ref. [239], as a test of CPT invariance, all the observables are expressed in terms of the 16 amplitudes.

In the following, we discuss the spin-dependent observables for the reaction $\bar{p}p \to e^+e^-$ in the Holzenkamp et al's convention [205]. As mentioned in the text in Chap. 4, we transform the helicities Eq. (4.4) to LSJ basis where the $\bar{p}p$ interaction is taken into account. Then the amplitudes f_{++}, f_{+-}, f_{+-}, f_{-+} in LSJ basis can be obtained. Again inserting them into Eq. (C.17), one gets the helicity amplitudes with inclusion of the $\bar{p}p$ interaction. Using Eq. (C.9), one can get the quantities a, b, c, d, e, g (f and h vanish). The analyzing power A_y and spin-correlation parameters A_{ij} are expressed as

$$\begin{aligned}
A_y &= \frac{2[\mathrm{Re}\,(a\,e^*) - \mathrm{Im}\,(d\,g^*)]}{|a|^2+|b|^2+|c|^2+|d|^2+|e|^2+|g|^2}, \\
A_{xx} &= -\frac{2[\mathrm{Re}\,(a\,d^* + b\,c^*) - \mathrm{Im}\,(g\,e^*)]}{|a|^2+|b|^2+|c|^2+|d|^2+|e|^2+|g|^2}, \\
A_{yy} &= \frac{|a|^2-|b|^2-|c|^2+|d|^2+|e|^2+|g|^2}{|a|^2+|b|^2+|c|^2+|d|^2+|e|^2+|g|^2}, \\
A_{zz} &= \frac{2[\mathrm{Re}\,(a\,d^* - b\,c^*) - \mathrm{Im}\,(g\,e^*)]}{|a|^2+|b|^2+|c|^2+|d|^2+|e|^2+|g|^2}, \\
A_{xz} &= -\frac{2[\mathrm{Re}\,(a\,g^*) + \mathrm{Im}\,(d\,e^*)]}{|a|^2+|b|^2+|c|^2+|d|^2+|e|^2+|g|^2}.
\end{aligned} \tag{C.31}$$

Then the theoretical predictions for them are shown in Fig. C.1. A_y and A_{yy} are indentical with those in Figs. 4.9 and 4.10 in Chap. 4 and thus not shown here anymore. However, for A_{xx}, A_{zz} and A_{xz}, the curves in Fig.C.1 are different from those in Fig. 4.10, because the two kinds of results are based on different coordinate systems. For calculating the curves in Fig. 4.10, one chooses z axis along the direction of incoming antiproton, the y axis normal to the scattering plane, and the x axis to form a left-handed coordinate system [204, 212], while the result in Fig. C.1 is based on the coordinate system Eq. (C.1).

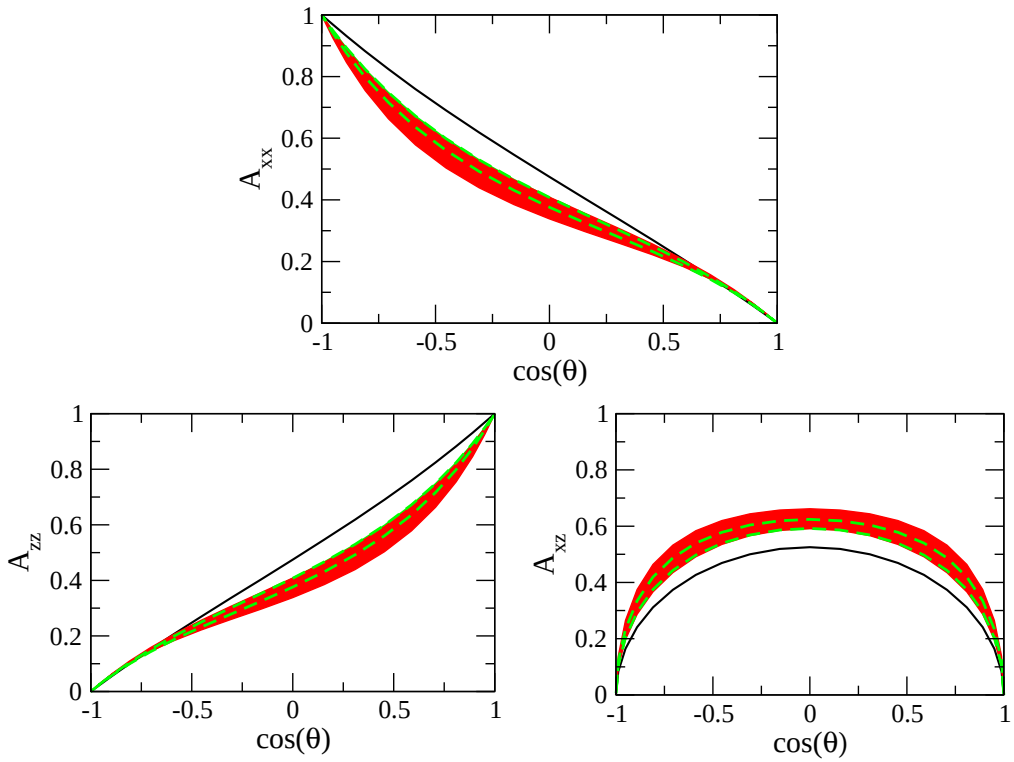

Figure C.1: Spin correlation parameters for $\bar{p}p \to e^+e^-$ at the excess energy $Q = 45$ MeV. Same description of curves as in Fig. 4.3.

Bibliography

[1] S. Weinberg, *Phenomenological Lagrangians*, Physica A **96**, 327 (1979).

[2] J. Gasser and H. Leutwyler, *Chiral Perturbation Theory to One Loop*, Annals Phys. **158**, 142 (1984).

[3] J. Gasser and H. Leutwyler, *Chiral Perturbation Theory: Expansions in the Mass of the Strange Quark*, Nucl. Phys. B **250**, 465 (1985).

[4] S. Scherer, *Introduction to chiral perturbation theory*, Adv. Nucl. Phys. **27**, 277 (2003) [hep-ph/0210398].

[5] C. Vafa and E. Witten, *Restrictions on Symmetry Breaking in Vector-Like Gauge Theories*, Nucl. Phys. B **234**, 173 (1984).

[6] M. Gell-Mann, R. J. Oakes and B. Renner, *Behavior of current divergences under SU(3) × SU(3)*, Phys. Rev. **175**, 2195 (1968).

[7] U.-G. Meißner, *Recent developments in chiral perturbation theory*, Rept. Prog. Phys. **56**, 903 (1993) [hep-ph/9302247].

[8] G. Ecker, *Chiral perturbation theory*, Prog. Part. Nucl. Phys. **35**, 1 (1995) [hep-ph/9501357].

[9] A. Pich, *Chiral perturbation theory*, Rept. Prog. Phys. **58**, 563 (1995) [hep-ph/9502366].

[10] V. Bernard and U.-G. Meißner, *Chiral perturbation theory*, Ann. Rev. Nucl. Part. Sci. **57**, 33 (2007) [hep-ph/0611231].

[11] M. B. Wise, *Chiral perturbation theory for hadrons containing a heavy quark*, Phys. Rev. D **45**, 2188 (1992).

[12] T. -M. Yan, H. -Y. Cheng, C. -Y. Cheung, G. -L. Lin, Y. C. Lin and H. -L. Yu, *Heavy quark symmetry and chiral dynamics*, Phys. Rev. D **46**, 1148 (1992) [Erratum-ibid. D **55**, 5851 (1997)].

[13] A. V. Manohar and M. B. Wise, *Heavy Quark Physics*, Cambridge University Press (2000).

[14] H. Georgi, *Heavy quark effective field theory*, HUTP-91-A039.

[15] J. Gasser, M.E. Sainio and A. Švarc, *Nucleons with Chiral Loops*, Nucl. Phys. B **307**, 779 (1988).

[16] S. Weinberg, *Pion scattering lengths*, Phys. Rev. Lett. **17**, 616 (1966);

Y. Tomozawa, *Axial vector coupling renormalization and the meson baryon scattering lengths*, Nuovo Cim. A **46**, 707 (1966)

[17] E. E. Jenkins and A. V. Manohar, *Baryon chiral perturbation theory using a heavy fermion Lagrangian*, Phys. Lett. B **255**, 558 (1991).

[18] V. Bernard, N. Kaiser, J. Kambor and U.-G. Meißner, *Chiral structure of the nucleon*, Nucl. Phys. B **388**, 315 (1992).

[19] N. Fettes, U.-G. Meißner, M. Mojzis and S. Steininger, *The Chiral effective pion nucleon Lagrangian of order* p^4, Annals Phys. **283**, 273 (2000) [Erratum-ibid. **288**, 249 (2001)]

[20] N. Fettes, U.-G. Meißner and S. Steininger, *Pion - nucleon scattering in chiral perturbation theory. 1. Isospin symmetric case*, Nucl. Phys. A **640**, 199 (1998) [hep-ph/9803266].

[21] N. Fettes, *Pion nucleon physics in chiral perturbation theory*, PhD thesis, JUL-3814 (2000).

[22] K. M. Watson, *Some general relations between the photoproduction and scattering of* π *mesons*, Phys. Rev. **95**, 228 (1954).

[23] R. Omnès, *On the Solution of certain singular integral equations of quantum field theory*, Nuovo Cim. **8**, 316 (1958).

[24] A. V. Anisovich and H. Leutwyler, *Dispersive analysis of the decay* $\eta \to 3\pi$ Phys. Lett. B **375**, 335 (1996) [hep-ph/9601237].

[25] P. Stoffer, *A Dispersive Treatment of* K_{l4} *decays*, Master thesis, Bern University (2010).

[26] V. Bernard, S. Descotes-Genon and M. Knecht, *Isospin breaking in the phases of the* K_{e4} *form factors*, Eur. Phys. J. C **73**, 2478 (2013) [arXiv:1305.3843 [hep-ph]].

[27] K. M. Watson, *The Effect of final state interactions on reaction cross-sections*, Phys. Rev. **88**, 1163 (1952)

[28] A. B. Migdal, *The theory of nuclear reactions with production of slow particles*, JETP **1**, 2 (1955).

[29] M. L. Goldberger and K. M. Watson, *Collision Theory*, John Willey and Sons (1967).

[30] A. Gasparyan, J. Haidenbauer, C. Hanhart and J. Speth, *How to extract the ΛN scattering length from production reactions*, Phys. Rev. C **69**, 034006 (2004) [hep-ph/0311116].

[31] A. Gasparyan, J. Haidenbauer and C. Hanhart, *Extraction of scattering lengths from final-state interactions*, Phys. Rev. C **72**, 034006 (2005) [nucl-th/0506067].

[32] A. Sibirtsev, J. Haidenbauer, H.-W. Hammer and S. Krewald, *Resonances and final state interactions in the reaction $pp \to pK^+\Lambda$*, Eur. Phys. J. A **27**, 269 (2006) [nucl-th/0512059].

[33] R. Machleidt, K. Holinde and C. Elster, *The Bonn Meson Exchange Model for the Nucleon Nucleon Interaction*, Phys. Rept. **149**, 1 (1987).

[34] N. Cabibbo, *Unitary Symmetry and Leptonic Decays*, Phys. Rev. Lett. **10**, 531 (1963);

M. Kobayashi and T. Maskawa, *CP Violation in the Renormalizable Theory of Weak Interaction*, Prog. Theor. Phys. **49**, 652 (1973).

[35] J. Beringer et al. [Particle Data Group], *Review of particle physics*, Phys. Rev. D **86**, 010001 (2012) and 2013 partial update for the 2014 edition. For a review of $|V_{ub}|$ extractions, see the section "Determination of V_{ub}."

[36] Heavy Flavor Averaging Group (HFAG), http://www.slac.stanford.edu/xorg/hfag.

[37] M. Bona et al. [UTfit Collaboration], http://www.utfit.org.

[38] J. Charles et al. [CKMfitter Group Collaboration], *CP violation and the CKM matrix: Assessing the impact of the asymmetric B factories* Eur. Phys. J. C **41**, 1 (2005) [hep-ph/0406184]; updated results and plots available at: http://ckmfitter.in2p3.fr;

J. Charles et al., *Predictions of selected flavour observables within the Standard Model*, Phys. Rev. D **84**, 033005 (2011) [arXiv:1106.4041 [hep-ph]].

[39] M. Bona et al. [UTfit Collaboration], *The Unitarity Triangle Fit in the Standard Model and Hadronic Parameters from Lattice QCD: A Reappraisal after the Measurements of Δm_s and $BR(B \to \tau\nu_t au)$*, JHEP **0610**, 081 (2006) [hep-ph/0606167].

[40] B. H. Behrens et al. [CLEO Collaboration], *Measurement of $B \to \rho l\nu$ decay and $|V_{ub}|$*, Phys. Rev. D **61**, 052001 (2000) [hep-ex/9905056].

[41] S. B. Athar et al. [CLEO Collaboration], *Study of the q^2 dependence of $B \to \pi l\nu$ and $B \to \rho(\omega) l\nu$ decay and extraction of $|V_{ub}|$* Phys. Rev. D **68**, 072003 (2003) [hep-ex/0304019].

[42] B. Aubert et al. [BABAR Collaboration], *Measurement of the CKM matrix element $|V_{ub}|$ with $B \to \rho e \nu$ decays*, Phys. Rev. Lett. **90**, 181801 (2003) [hep-ex/0301001].

[43] P. del Amo Sanchez et al. [BaBar Collaboration], *Study of $B \to \pi \ell \nu$ and $B \to \rho \ell \nu$ Decays and Determination of $|V_{ub}|$*, Phys. Rev. D **83**, 032007 (2011) [arXiv:1005.3288 [hep-ex]].

[44] P. Gambino and J. F. Kamenik, *Lepton energy moments in semileptonic charm decays*, Nucl. Phys. B **840**, 424 (2010) [arXiv:1004.0114 [hep-ph]].

[45] M. Antonelli et al., *Flavor Physics in the Quark Sector*, Phys. Rept. **494**, 197 (2010) [arXiv:0907.5386 [hep-ph]].

[46] U.-G. Meißner and W. Wang, $\mathbf{B_s \to K^{(*)} \ell \bar{\nu}}$*, Angular Analysis, S-wave Contributions and* $\mathbf{|V_{ub}|}$, JHEP **1401**, 107 (2014) [arXiv:1311.5420 [hep-ph]].

[47] On the theoretical side see e.g. W.-Y. Wang and Y.-L. Wu, *$B \to \rho l \nu$ decay and V_{ub}*, Phys. Lett. B **519**, 219 (2001) [hep-ph/0106208];

A. H. S. Gilani, Riazuddin and T. A. Al-Aithan, *Ward identities, $B \to \rho$ form-factors and $|V_{ub}|$* JHEP **0309**, 065 (2003) [hep-ph/0304183];

J. M. Flynn, Y. Nakagawa, J. Nieves and H. Toki, *$|V_{ub}|$ from Exclusive Semileptonic $B \to \rho$ Decays* Phys. Lett. B **675**, 326 (2009) [arXiv:0812.2795 [hep-ph]].

[48] S. Faller, T. Feldmann, A. Khodjamirian, T. Mannel and D. van Dyk, *Disentangling the Decay Observables in $B^- \to \pi^+ \pi^- l^- \bar{\nu}_l$*, Phys. Rev. D **89**, 014015 (2014) [arXiv:1310.6660 [hep-ph]].

[49] J. Bijnens, G. Colangelo and J. Gasser, *K_{l4} decays beyond one loop*, Nucl. Phys. B **427**, 427 (1994) [hep-ph/9403390].

[50] N. Cabibbo and A. Maksymowicz, *Angular Correlations in K_{e4} Decays and Determination of Low-Energy pi-pi Phase Shifts*, Phys. Rev. **137**, B438 (1965) [Erratum-ibid. **168**, 1926 (1968)];

A. Pais and S. B. Treiman, *Pion Phase-Shift Information from K_{l4} Decays*, Phys. Rev. **168**, 1858 (1968);

L. Rosselet et al., *Experimental Study of 30000 K_{e4} Decays* Phys. Rev. D **15**, 574 (1977).

[51] F. A. Berends, A. Donnachie and G. C. Oades, *A note on the K_{e4} and $K_{\mu 4}$ decay rates*, Phys. Lett. **26B**, 109 (1967);

Theoretical Study of K_{l4} Decay, Phys. Rev. **171**, 1457 (1968).

[52] P. Stoffer, *Isospin Breaking Effects in $K_{\ell 4}$ Decays*, arXiv:1312.2066 [hep-ph].

[53] N. M. Queen and G. Violini, *Dispersion Theory in High-Energy Physics*, Macmillan, London (1974).

[54] J. F. Donoghue, J. Gasser and H. Leutwyler, *The Decay Of A Light Higgs Boson*, Nucl. Phys. B **343**, 341 (1990).

[55] J. Gasser and U.-G. Meißner, *Chiral expansion of pion form-factors beyond one loop*, Nucl. Phys. B **357**, 90 (1991).

[56] see e.g., S. Eidelman and L. Lukaszuk, *Pion form-factor phase, $\pi\pi$ elasticity and new e^+e^- data* Phys. Lett. B **582**, 27 (2004) [hep-ph/0311366].

[57] see e.g., F. Karsch, M. Hess, E. Laermann and I. Wetzorke, *Constituent quarks, diquarks and the N–Δ mass splitting*, Nucl. Phys. Proc. Suppl. **73**, 213 (1999) [hep-lat/9809011].

[58] D. B. Lichtenberg, W. Namgung, J. G. Wills and E. Predazzi, *Light and Heavy Hadron Masses in a Relativistic Quark Potential Model With Diquark Clustering*, Z. Phys. C **19**, 19 (1983).

[59] C. L. Y. Lee, M. Lu and M. B. Wise, *B_{l4} and D_{l4} decay* Phys. Rev. D **46**, 5040 (1992).

[60] For a review of the applications of heavy meson chiral Lagrangian, see R. Casalbuoni, A. Deandrea, N. Di Bartolomeo, R. Gatto, F. Feruglio and G. Nardulli, *Phenomenology of heavy meson chiral Lagrangians*, Phys. Rept. **281**, 145 (1997) [hep-ph/9605342].

[61] See the section "Decay constants of charged pseudo-scalar mesons" in Ref. [35].

[62] H. Ohki, H. Matsufuru and T. Onogi, *Determination of $B^*B\pi$ coupling in unquenched QCD*, Phys. Rev. D **77**, 094509 (2008) [arXiv:0802.1563 [hep-lat]].

[63] B. Samways et al., *The $B^*B\pi$ coupling with relativistic heavy quarks*, arXiv:1311.2251 [hep-lat].

[64] S. Aoki et al., *Review of lattice results concerning low energy particle physics*, arXiv:1310.8555 [hep-lat].

[65] G. Burdman and J. F. Donoghue, *Union of chiral and heavy quark symmetries*, Phys. Lett. B **280**, 287 (1992).

[66] G. Colangelo, E. Passemar and P. Stoffer, *A Dispersive Treatment of $K_{\ell 4}$ Decays*, EPJ Web Conf. **37**, 05006 (2012) [arXiv:1209.0755 [hep-ph]].

[67] J. Kambor, C. Wiesendanger and D. Wyler, *Final state interactions and Khuri–Treiman equations in $\eta \to 3\pi$ decays*, Nucl. Phys. B **465**, 215 (1996) [arXiv:hep-ph/9509374].

[68] J. B. Bronzan, *Overlapping Resonances in Dispersion Theory*, Phys. Rev. **134**, B687 (1964);

J. B. Bronzan and C. Kacser, *Khuri-Treiman Representation and Perturbation Theory*, Phys. Rev. **132**, 2703 (1963);

C. Kacser, *Analytic Structure of Partial-Wave Amplitudes for Production and Decay Processes*, Phys. Rev. **132**, 2712 (1963).

[69] S. Lanz, $\eta \to 3\pi$ *and quark masses*, PoS **CD12**, 007 (2013) [arXiv:1301.7282 [hep-ph]].

[70] F. Niecknig, B. Kubis and S. P. Schneider, *Dispersive analysis of* $\omega \to 3\pi$ *and* $\phi \to 3\pi$ *decays*, Eur. Phys. J. C **72**, 2014 (2012) [arXiv:1203.2501 [hep-ph]].

[71] M. Büchler, G. Colangelo, J. Kambor and F. Orellana, *Dispersion relations and soft pion theorems for* $K \to \pi\pi$, Phys. Lett. B **521**, 22 (2001) [hep-ph/0102287].

[72] R. García-Martín and B. Moussallam, *MO analysis of the high statistics Belle results on* $\gamma\gamma \to \pi^+\pi^-, \pi^0\pi^0$ *with chiral constraints* Eur. Phys. J. C **70**, 155 (2010) [arXiv:1006.5373 [hep-ph]]

[73] M. Hoferichter, D. R. Phillips and C. Schat, *Roy-Steiner equations for* $\gamma\gamma \to \pi\pi$, Eur. Phys. J. C **71**, 1743 (2011) [arXiv:1106.4147 [hep-ph]].

[74] T. N. Truong, *Study of* $\gamma\pi \to \pi\pi$ *below 1-GeV using integral equation approach*, Phys. Rev. D **65**, 056004 (2002) [hep-ph/0105123].

[75] M. Hoferichter, B. Kubis and D. Sakkas, *Extracting the chiral anomaly from* $\gamma\pi \to \pi\pi$, Phys. Rev. D **86**, 116009 (2012) [arXiv:1210.6793 [hep-ph]].

[76] G. P. Lepage and S. J. Brodsky, *Exclusive Processes in Perturbative Quantum Chromodynamics*, Phys. Rev. D **22**, 2157 (1980).

[77] S. Descotes-Genon, *private communication*; following C. W. Bauer, S. Fleming, D. Pirjol, I. Z. Rothstein and I. W. Stewart, *Hard scattering factorization from effective field theory*, Phys. Rev. D **66**, 014017 (2002) [hep-ph/0202088];

C. W. Bauer, D. Pirjol and I. W. Stewart, *Power counting in the soft collinear effective theory*, Phys. Rev. D **66**, 054005 (2002) [hep-ph/0205289].

[78] G. Colangelo, J. Gasser and H. Leutwyler, *The* $\pi\pi$ *S wave scattering lengths*, Phys. Lett. B **488**, 261 (2000) [hep-ph/0007112];

G. Colangelo, *Theoretical progress on* $\pi\pi$ *scattering lengths and phases*, PoS **KAON**, 038 (2008) [arXiv:0710.3050 [hep-ph]];

G. Ecker, *Strong interactions of light flavors*, hep-ph/0011026.

[79] B. Ananthanarayan, G. Colangelo, J. Gasser and H. Leutwyler, *Roy equation analysis of pi pi scattering*, Phys. Rept. **353**, 207 (2001) [hep-ph/0005297].

[80] R. García-Martín, R. Kamiński, J. R. Peláez, J. Ruiz de Elvira and F. J. Ynduráin, *The Pion-pion scattering amplitude. IV: Improved analysis with once subtracted Roy-like equations up to 1100 MeV*, Phys. Rev. D **83**, 074004 (2011) [arXiv:1102.2183 [hep-ph]].

[81] B. Moussallam, $N(f)$ *dependence of the quark condensate from a chiral sum rule*, Eur. Phys. J. C **14**, 111 (2000) [hep-ph/9909292].

[82] B. Ananthanarayan, I. Caprini, G. Colangelo, J. Gasser and H. Leutwyler, *Scalar form-factors of light mesons*, Phys. Lett. B **602**, 218 (2004) [hep-ph/0409222].

[83] M. Hoferichter, C. Ditsche, B. Kubis and U.-G. Meißner, *Dispersive analysis of the scalar form factor of the nucleon*, JHEP **1206**, 063 (2012) [arXiv:1204.6251 [hep-ph]].

[84] G. Colangelo, J. Gasser and H. Leutwyler, $\pi\pi$ *scattering*, Nucl. Phys. B **603**, 125 (2001) [hep-ph/0103088].

[85] J. Bijnens, G. Colangelo and P. Talavera, *The Vector and scalar form-factors of the pion to two loops*, JHEP **9805**, 014 (1998) [hep-ph/9805389].

[86] C. Hanhart, *A New Parameterization for the Pion Vector Form Factor*, Phys. Lett. B **715**, 170 (2012) [arXiv:1203.6839 [hep-ph]].

[87] C. G. Callan and S. B. Treiman, *Equal Time Commutators and K Meson Decays*, Phys. Rev. Lett. **16**, 153 (1966);

V. de Alfaro, S. Fubini, G. Furlan and C. Rossetti, *Currents in Hadron Physics,* North-Holland Publishing Company, (1973).

[88] C. B. Dover and J. M. Richard, *Elastic, Charge Exchange, and Inelastic* $\bar{p}p$ *Cross-Sections in the Optical Model*, Phys. Rev. C **21**, 1466 (1980).

[89] C. B. Dover and J. M. Richard, *Spin Observables in Low-energy Nucleon Anti-nucleon Scattering*, Phys. Rev. C **25**, 1952 (1982).

[90] J. Côté, M. Lacombe, B. Loiseau, B. Moussallam and R. Vinh Mau, *On the Nucleon - anti-Nucleon Optical Potential*, Phys. Rev. Lett. **48**, 1319 (1982).

[91] P. H. Timmers, W. A. van der Sanden and J. J. de Swart, *An Anti-nucleon - Nucleon Potential*, Phys. Rev. D **29**, 1928 (1984); Erratum-ibid. D **30**, 1995 (1984).

[92] T. Hippchen, J. Haidenbauer, K. Holinde and V. Mull, *Meson - baryon dynamics in the nucleon - anti-nucleon system. 1. The Nucleon - anti-nucleon interaction*, Phys. Rev. C **44**, 1323 (1991).

[93] V. Mull, J. Haidenbauer, T. Hippchen and K. Holinde, *Meson - baryon dynamics in the nucleon - anti-nucleon system. 2. Annihilation into two mesons*, Phys. Rev. C **44**, 1337 (1991).

[94] V. Mull and K. Holinde, *Combined description of $\bar{N}N$ scattering and annihilation with a hadronic model*, Phys. Rev. C **51**, 2360 (1995) [nucl-th/9411014].

[95] D. R. Entem and F. Fernandez, *The $N\bar{N}$ interaction in a constituent quark model: Baryonium states and protonium level shifts*, Phys. Rev. C **73**, 045214 (2006).

[96] B. El-Bennich, M. Lacombe, B. Loiseau and S. Wycech, *Paris $N\bar{N}$ potential constrained by recent antiprotonic-atom data and antineutron-proton total cross sections* Phys. Rev. C **79**, 054001 (2009) [arXiv:0807.4454 [nucl-th]].

[97] C. Amsler and F. Myhrer, *Low-energy anti-proton physics*, Ann. Rev. Nucl. Part. Sci. **41**, 219 (1991).

[98] C. B. Dover, T. Gutsche, M. Maruyama and A. Faessler, *The Physics of nucleon - anti-nucleon annihilation*, Prog. Part. Nucl. Phys. **29**, 87 (1992).

[99] E. Klempt, F. Bradamante, A. Martin and J. -M. Richard, *Antinucleon nucleon interaction at low energy: Scattering and protonium*, Phys. Rept. **368**, 119 (2002).

[100] S. Weinberg, *Nuclear forces from chiral Lagrangians*, Phys. Lett. B **251**, 288 (1990).

[101] S. Weinberg, *Effective chiral Lagrangians for nucleon - pion interactions and nuclear forces*, Nucl. Phys. B **363**, 3 (1991).

[102] E. Epelbaum, H.-W. Hammer and U.-G. Meißner, *Modern Theory of Nuclear Forces*, Rev. Mod. Phys. **81**, 1773 (2009) [arXiv:0811.1338 [nucl-th]].

[103] R. Machleidt and D. R. Entem, *Chiral effective field theory and nuclear forces*, Phys. Rept. **503**, 1 (2011) [arXiv:1105.2919 [nucl-th]].

[104] E. Epelbaum, *Few-nucleon forces and systems in chiral effective field theory*, Prog. Part. Nucl. Phys. **57**, 654 (2006) [nucl-th/0509032].

[105] D. R. Entem, R. Machleidt, *Accurate charge dependent nucleon nucleon potential at fourth order of chiral perturbation theory*, Phys. Rev. C **68**, 041001 (2003) [nucl-th/0304018].

[106] E. Epelbaum, W. Glöckle, U.-G. Meißner, *The Two-nucleon system at next-to-next-to-next-to-leading order*, Nucl. Phys. A **747**, 362 (2005) [nucl-th/0405048].

[107] R. Timmermans, Th. A. Rijken and J. J. de Swart, *Anti-proton - proton partial wave analysis below 925-MeV/c*, Phys. Rev. C **50**, 48 (1994) [nucl-th/9403011].

[108] D. Zhou and R. G. E. Timmermans, *Energy-dependent partial-wave analysis of all antiproton-proton scattering data below 925 MeV/c*, Phys. Rev. C **86**, 044003 (2012) [arXiv:1210.7074 [hep-ph]].

[109] W. Erni et al. [Panda Collaboration], *Physics Performance Report for PANDA: Strong Interaction Studies with Antiprotons*, arXiv:0903.3905 [hep-ex].

[110] J. Z. Bai et al. [BES Collaboration], *Observation of a near threshold enhancement in the $p\bar{p}$ mass spectrum from radiative $J/\psi \to \gamma p\bar{p}$ decays*, Phys. Rev. Lett. **91**, 022001 (2003) [hep-ex/0303006].

[111] B. Aubert et al. [BaBar Collaboration], *Measurement of the $B^+ \to p\bar{p}K^+$ branching fraction and study of the decay dynamics*, Phys. Rev. D **72**, 051101 (2005) [hep-ex/0507012].

[112] B. Aubert et al. [BaBar Collaboration], *A Study of $e^+e^- \to p\bar{p}$ using initial state radiation with BABAR*, Phys. Rev. D **73**, 012005 (2006) [hep-ex/0512023].

[113] M. Ablikim et al. [BESIII Collaboration], *Spin-Parity Analysis of $p\bar{p}$ Mass Threshold Structure in J/ψ and ψ' Radiative Decays*, Phys. Rev. Lett. **108**, 112003 (2012) [arXiv:1112.0942 [hep-ex]].

[114] D. V. Bugg, *Reinterpreting several narrow 'resonances' as threshold cusps*, Phys. Lett. B **598**, 8 (2004) [hep-ph/0406293].

[115] B. S. Zou and H. C. Chiang, *One pion exchange final state interaction and the $p\bar{p}$ near threshold enhancement in $J/\psi \to \gamma p\bar{p}$ decays*, Phys. Rev. D **69**, 034004 (2004) [hep-ph/0309273].

[116] A. Sibirtsev, J. Haidenbauer, S. Krewald, U.-G. Meißner and A. W. Thomas, *Near threshold enhancement of the $p\bar{p}$ mass spectrum in J/ψ decay*, Phys. Rev. D **71**, 054010 (2005) [hep-ph/0411386].

[117] B. Loiseau and S. Wycech, *Antiproton-proton channels in J/ψ decays*, Phys. Rev. C **72**, 011001 (2005) [hep-ph/0501112].

[118] J. Haidenbauer, U.-G. Meißner and A. Sibirtsev, *Near threshold $p\bar{p}$ enhancement in B and J/ψ decay*, Phys. Rev. D **74**, 017501 (2006) [hep-ph/0605127].

[119] J. Haidenbauer, H.-W. Hammer, U.-G. Meißner and A. Sibirtsev, *On the strong energy dependence of the $e^+e^- \leftrightarrow p\bar{p}$ amplitude near threshold*, Phys. Lett. B **643**, 29 (2006) [hep-ph/0606064].

[120] D. R. Entem and F. Fernández, *Final State Interaction Effects In Near Threshold Enhancement Of The $p\bar{p}$ Mass Spectrum In B And J/ψ Decays*, Phys. Rev. D **75**, 014004 (2007).

[121] J.-P. Dedonder, B. Loiseau, B. El-Bennich, and S. Wycech, *On the structure of the $X(1835)$ baryonium*, Phys. Rev. C **80**, 045207 (2009) [arXiv:0904.2163 [nucl-th]].

[122] J. Haidenbauer and U.-G. Meißner, *The proton-antiproton mass threshold structure in $\psi(3686)$ radiative decay revisited*, Phys. Rev. D **86**, 077503 (2012) [arXiv:1208.3343 [hep-ph]].

[123] E. Epelbaum, W. Glöckle and U.-G. Meißner, *Improving the convergence of the chiral expansion for nuclear forces. 1. Peripheral phases*, Eur. Phys. J. A **19**, 125 (2004) [nucl-th/0304037].

[124] E. Epelbaum, W. Glöckle and U.-G. Meißner, *Improving the convergence of the chiral expansion for nuclear forces. 2. Low phases and the deuteron*, Eur. Phys. J. A **19**, 401 (2004) [nucl-th/0308010].

[125] E. Epelbaum, W. Glöckle and U.-G. Meißner, *Nuclear forces from chiral Lagrangians using the method of unitary transformation. 1. Formalism*, Nucl. Phys. A **637**, 107 (1998) [nucl-th/9801064].

[126] G. Y. Chen, H. R. Dong and J. P. Ma, *Near Threshold Enhancement of $p\bar{p}$ System and $p\bar{p}$ Elastic Scattering*, Phys. Lett. B **692**, 136 (2010) [arXiv:1004.5174 [hep-ph]].

[127] G. Y. Chen and J. P. Ma, *$N\bar{N}$ Scattering at NLO Order in An Effective Theory*, Phys. Rev. D **83**, 094029 (2011) [arXiv:1101.4071 [hep-ph]].

[128] D. B. Kaplan, M. J. Savage and M. B. Wise, *Two nucleon systems from effective field theory*, Nucl. Phys. B **534**, 329 (1998) [nucl-th/9802075].

[129] V. E. Tarasov, A. E. Kudryavtsev, A. I. Romanov and V. M. Weinberg, *$\bar{p}p$-annihilation processes in the tree approximation of $SU(3)$ chiral effective theory*, Phys. Atom. Nucl. **75**, 1536 (2012) [arXiv:1202.4086 [nucl-th]].

[130] C. Hanhart, *Meson production in nucleon-nucleon collisions close to the threshold*, Phys. Rept. **397**, 155 (2004) [hep-ph/0311341].

[131] R. Machleidt, *The High precision, charge dependent Bonn nucleon-nucleon potential (CD-Bonn)*, Phys. Rev. C **63**, 024001 (2001) [nucl-th/0006014].

[132] M. Lacombe, B. Loiseau, J. M. Richard, R. Vinh Mau, J. Cote, P. Pires and R. De Tourreil, *Parametrization of the Paris n n Potential*, Phys. Rev. C **21**, 861 (1980).

[133] V. G. J. Stoks, R. A. M. Klomp, C. P. F. Terheggen and J. J. de Swart, *Construction of high quality N N potential models*, Phys. Rev. C **49**, 2950 (1994) [nucl-th/9406039].

[134] R. B. Wiringa, V. G. J. Stoks and R. Schiavilla, *An Accurate nucleon-nucleon potential with charge independence breaking*, Phys. Rev. C **51**, 38 (1995) [nucl-th/9408016].

[135] R. Machleidt and I. Slaus, *The Nucleon-nucleon interaction: Topical review*, J. Phys. G **27**, R69 (2001) [nucl-th/0101056].

[136] M. Naghdi,*Nucleon-Nucleon Interaction: A typical/Concise Review*, nucl-th/0702078.

[137] U.-G. Meißner, *Modern theory of nuclear forces*, Nucl. Phys. A **751**, 149 (2005) [nucl-th/0409028].

[138] S. Weinberg, *Three body interactions among nucleons and pions*, Phys. Lett. B **295**, 114 (1992) [hep-ph/9209257].

[139] U. van Kolck, *Few nucleon forces from chiral Lagrangians*, Phys. Rev. C **49**, 2932 (1994).

[140] S. N. Yang and W. Glöckle, *Three-body Mesonic Retardation Effect*, Phys. Rev. C **33**, 1774 (1986).

[141] S. A. Coon and J. L. Friar, *Pionic retardation effects in two-pion-exchange three-Nucleon Forces* Phys. Rev. C **34**, 1060 (1986).

[142] N. Kaiser, R. Brockmann and W. Weise, *Peripheral nucleon-nucleon phase shifts and chiral symmetry*, Nucl. Phys. A **625**, 758 (1997) [nucl-th/9706045].

[143] N. Kaiser, *Chiral 2π exchange NN potentials: Two loop contributions*, Phys. Rev. C **64**, 057001 (2001) [nucl-th/0107064].

[144] N. Kaiser, *Chiral 2π exchange NN potentials: Relativistic $1/M^2$ corrections*, Phys. Rev. C **65**, 017001 (2002) [nucl-th/0109071].

[145] E. Epelbaum, *The nucleon-nucleon interaction in a chiral effective field theory*, Ph.D thesis, Bochum University (2000).

[146] J. J. de Swart, M. C. M. Rentmeester and R. G. E. Timmermans, *The Status of the pion - nucleon coupling constant*, PiN Newslett. **13**, 96 (1997) [nucl-th/9802084].

[147] D. V. Bugg, *The pion nucleon coupling constant*, Eur. Phys. J. C **33**, 505 (2004).

[148] V. Baru, C. Hanhart, M. Hoferichter, B. Kubis, A. Nogga and D. R. Phillips, *Precision calculation of threshold $\pi^- d$ scattering, πN scattering lengths, and the GMO sum rule*, Nucl. Phys. A **872**, 69 (2011) [arXiv:1107.5509 [nucl-th]].

[149] V. Bernard, N. Kaiser and U.-G. Meißner, *Chiral dynamics in nucleons and nuclei*, Int. J. Mod. Phys. E **4**, 193 (1995) [hep-ph/9501384].

[150] E. Epelbaum, W. Glöckle and U.-G. Meißner, *Nuclear forces from chiral Lagrangians using the method of unitary transformation. 2. The two nucleon system*, Nucl. Phys. A **671**, 295 (2000) [nucl-th/9910064].

[151] J. F. Donoghue and B. R. Holstein, *Improved treatment of loop diagrams in SU(3) baryon chiral perturbation theory*, Phys. Lett. B 436, 331 (1998).

[152] J. F. Donoghue, B. R. Holstein and B. Borasoy, *SU(3) baryon chiral perturbation theory and long distance regularization*, Phys. Rev. D **59**, 036002 (1999) [hep-ph/9804281].

[153] B. Borasoy, B. R. Holstein, R. Lewis and P. P. A. Ouimet, *Long distance regularization in chiral perturbation theory with decuplet fields*, Phys. Rev. D **66**, 094020 (2002) [hep-ph/0210092].

[154] V. Bernard, T. R. Hemmert and U.-G. Meißner, *Cutoff schemes in chiral perturbation theory and the quark mass expansion of the nucleon mass*, Nucl. Phys. A **732**, 149 (2004) [hep-ph/0307115].

[155] E. Marji, A. Canul, Q. MacPherson, R. Winzer, C. Zeoli, D. R. Entem and R. Machleidt, *Nonperturbative renormalization of the chiral nucleon-nucleon interaction up to next-to-next-to-leading order*, Phys. Rev. C **88**, 054002 (2013) [arXiv:1309.5114 [nucl-th]].

[156] E. Epelbaum, U.-G. Meißner, W. Glöckle and C. Elster, *Resonance saturation for four nucleon operators*, Phys. Rev. C **65**, 044001 (2002) [nucl-th/0106007].

[157] C. Ordonez, L. Ray and U. van Kolck, *Nucleon-nucleon potential from an effective chiral Lagrangian*, Phys. Rev. Lett. **72**, 1982 (1994).

The Two nucleon potential from chiral Lagrangians, Phys. Rev. C **53**, 2086 (1996) [hep-ph/9511380].

[158] P. Büttiker and U.-G. Meißner, *Pion nucleon scattering inside the Mandelstam triangle*, Nucl. Phys. A **668**, 97 (2000) [hep-ph/9908247].

[159] H. Krebs, A. Gasparyan and E. Epelbaum, *Chiral three-nucleon force at N^4LO I: Longest-range contributions*, Phys. Rev. C **85**, 054006 (2012) [arXiv:1203.0067 [nucl-th]].

[160] H. P. Stapp, T. J. Ypsilantis and N. Metropolis, *Phase shift analysis of 310-MeV proton proton scattering experiments*, Phys. Rev. **105**, 302 (1957).

[161] R. A. Arndt, L. D. Roper, R. A. Bryan, R. B. Clark, B. J. VerWest and P. Signell, *Nucleon-Nucleon Partial Wave Analysis to 1-GeV*, Phys. Rev. D **28**, 97 (1983).

[162] J. Bystricky, C. Lechanoine-Leluc and F. Lehar, *Nucleon-nucleon phase shift analysis*, J. Physique **48**, 199 (1987).

[163] S. Deser, M. L. Goldberger, K. Baumann and W. E. Thirring, *Energy level displacements in π mesonic atoms*, Phys. Rev. **96**, 774 (1954);

T. L. Trueman, *Energy level shifts in atomic states of strongly-interacting particles*, Nucl. Phys. **26**, 57 (1961).

[164] D. Gotta, *Precision spectroscopy of light exotic atoms*, Prog. Part. Nucl. Phys. **52** (2004) 133.

[165] M. Ziegler et al. [ASTERIX Collaboration], *Measurement of the Strong Interaction Shift and Broadening of the Ground State of the $p\bar{p}$ Atom*, Phys. Lett. B **206**, 151 (1988).

[166] M. Augsburger et al., *Measurement of the strong interaction parameters in anti-protonic hydrogen and probable evidence for an interference with inner bremsstrahlung*, Nucl. Phys. A **658**, 149 (1999).

[167] K. Heitlinger et al., *Precision measurement of anti-protonic hydrogen and deuterium x-rays*, Z. Phys. A **342**, 359 (1992).

[168] D. Gotta et al., *Balmer alpha transitions in anti-protonic hydrogen and deuterium*, Nucl. Phys. A **660**, 283 (1999).

[169] J. Carbonell, J.-M. Richard and S. Wycech, *On the relation between protonium level shifts and nucleon-antinucleon scattering amplitudes*, Z. Phys. A **343** (1992) 325.

[170] D. Gotta, private communication.

[171] A. M. Badalian, L. P. Kok, M. I. Polikarpov, Y. A. Simonov, *Resonances in Coupled Channels in Nuclear and Particle Physics*, Phys. Rep. **82**, 31 (1982).

[172] H. Polinder, J. Haidenbauer and U.-G. Meißner, *Hyperon-nucleon interactions: A Chiral effective field theory approach*, Nucl. Phys. A **779**, 244 (2006) [nucl-th/0605050].

[173] J. Haidenbauer, S. Petschauer, N. Kaiser, U.-G. Meißner, A. Nogga and W. Weise, *Hyperon-nucleon interaction at next-to-leading order in chiral effective field theory*, Nucl. Phys. A **915**, 24 (2013) [arXiv:1304.5339 [nucl-th]].

[174] M. A. Belushkin, H.-W. Hammer and U.-G. Meißner, *Dispersion analysis of the nucleon form-factors including meson continua*, Phys. Rev. C **75**, 035202 (2007).

[175] H.-W. Hammer, U.-G. Meißner and D. Drechsel, *Dispersion theoretical analysis of the nucleon electromagnetic form-factors: Inclusion of timelike data*, Phys. Lett. B **385**, 343 (1996) [hep-ph/9604294].

[176] H.-W. Hammer and U.-G. Meißner, *Updated dispersion theoretical analysis of the nucleon electromagnetic form-factors*, Eur. Phys. J. A **20**, 469 (2004) [hep-ph/0312081].

[177] R. Bijker and F. Iachello, *Re-analysis of the nucleon space- and time-like electromagnetic form-factors in a two-component model*, Phys. Rev. C **69**, 068201 (2004).

[178] A. Z. Dubnickova, S. Dubnicka and M. Erdelyi, *Predictions of polarization observables in $e^+e^- \to p\bar{p}$ by eight- and ten-resonance U&A models*, Prog. Part. Nucl. Phys. **61**, 162 (2008).

[179] J. P. B. C. de Melo, T. Frederico, E. Pace, S. Pisano and G. Salme, *Time- and Space-like Nucleon Electromagnetic Form Factors beyond Relativistic Constituent Quark Models*, Phys. Lett. B **671**, 153 (2009).

[180] Y. Yan, K. Khosonthongkee, C. Kobdaj and P. Suebka, *$e^-e^+ \to \bar{N}N$ at Threshold and Proton Form Factor*, J. Phys. G **37**, 075007 (2010).

[181] E. A. Kuraev, E. Tomasi-Gustafsson and A. Dbeyssi, *A Model for space and time-like proton (neutron) form factors*, Phys. Lett. B **712**, 240 (2012).

[182] Y. .A. Simonov, *Theory of time-like baryon form factors near thresholds*, Phys. Rev. D **85**, 125025 (2012).

[183] E. L. Lomon and S. Pacetti, *Time-like and space-like electromagnetic form factors of nucleons, a unified description*, Phys. Rev. D **85**, 113004 (2012) [Erratum-ibid. D **86**, 039901 (2012)].

[184] A. Denig and G. Salmè, *Nucleon Electromagnetic Form Factors in the Timelike Region*, Prog. Part. Nucl. Phys. **68**, 113 (2013).

[185] G. Bardin et al., *Determination of the electric and magnetic form-factors of the proton in the timelike region*, Nucl. Phys. B **411**, 3 (1994).

[186] B. Aubert et al., [BABAR Collaboration] *A Study of $e^+e^- \to p\bar{p}$ using initial state radiation with BABAR* Phys. Rev. D **73**, 012005 (2006).

[187] J. P. Lees et al., [BABAR Collaboration] *Study of $e^+e^- \to p\bar{p}$ via initial-state radiation at BABAR*, Phys. Rev. D **87**, 092005 (2013).

[188] B. Kerbikov, A. Stavinsky, and V. Fedotov, *Model independent view on the low mass proton anti-proton enhancement*, Phys. Rev. C **69**, 055205 (2004) [hep-ph/0402054].

[189] V. F. Dmitriev and A. I. Milstein, *Final state interaction effects in the $e^+e^- \to N\bar{N}$ process near threshold*, Phys. Lett. B **658**, 13 (2007).

[190] G. Y. Chen, H. R. Dong and J. P. Ma, *Rescattering Effect and Near Threshold Enhancement of $p\bar{p}$ System*, Phys. Rev. D **78**, 054022 (2008).

[191] O. D. Dalkarov, P. A. Khakhulin and A. Y. Voronin, *On the electromagnetic form factors of hadrons in the time-like region near threshold*, Nucl. Phys. A **833**, 104 (2010).

[192] A. E. Bondar, V. F. Dmitriev, A. I. Milstein and V. M. Strakhovenko, *Nucleon polarization in the process $e^+e^- \to N\bar{N}$ near threshold*, Phys. Lett. B **697**, 159 (2011).

[193] V. F. Dmitriev and A. I. Milstein, *Final state Coulomb interaction and asymmetry of pair production close to threshold in e^+e^- annihilation*, Phys. Lett. B **722**, 83 (2013).

[194] V. F. Dmitriev, A. I. Milstein and S. G. Salnikov, *Isoscalar amplitude dominance in e^+e^- annihilation to $N\bar{N}$ pair close to the threshold*, arXiv:1307.0936 [hep-ph].

[195] P. A. M. Guichon and M. Vanderhaeghen, *How to reconcile the Rosenbluth and the polarization transfer method in the measurement of the proton form factors*, Phys. Rev. Lett. **91**, 142303 (2003).

[196] P. G. Blunden, W. Melnitchouk and J. A. Tjon, *Two-photon exchange and elastic electron proton scattering*, Phys. Rev. Lett. **91**, 142304 (2003).

[197] Y. C. Chen, A. Afanasev, S. J. Brodsky, C. E. Carlson and M. Vanderhaeghen, *Partonic calculation of the two-photon exchange contribution to elastic electron proton scattering at large momentum transfer*, Phys. Rev. Lett. **93**, 122301 (2004).

[198] M. P. Rekalo and E. Tomasi-Gustafsson, *Model independent properties of two-photon exchange in elastic electron proton scattering*, Eur. Phys. J. A **22**, 331 (2004).

[199] M. A. Belushkin, H.-W. Hammer and U.-G. Meißner, *Model-independent extraction of two-photon effects in elastic electron-proton scattering*, Phys. Lett. B **658**, 138 (2008).

[200] J. Arrington, P. G. Blunden and W. Melnitchouk, *Review of two-photon exchange in electron scattering*, Prog. Part. Nucl. Phys. **66**, 782 (2011).

[201] G. I. Gakh and E. Tomasi-Gustafsson, *Polarization effects in the reaction $\bar{p}p \to e^+e^-$ in presence of two-photon exchange*, Nucl. Phys. A **761**, 120 (2005).

[202] G. I. Gakh and E. Tomasi-Gustafsson, *General analysis of polarization phenomena in $e^+e^- \to N\bar{N}$ for axial parametrization of two-photon exchange*, Nucl. Phys. A **771**, 169 (2006).

[203] N. H. Buttimore and E. Jennings, *Polarisation observables in lepton antilepton to proton antiproton reactions including lepton mass*, Eur. Phys. J. A **31**, 9 (2007) [hep-ph/0607227].

[204] N. H. Buttimore and E. Jennings, *Helicity amplitudes and crossing relations for antiproton proton reactions*, Eur. Phys. J. A **33**, 21 (2007) [hep-ph/0702248].

[205] B. Holzenkamp, K. Holinde and J. Speth, *A Meson Exchange Model for the Hyperon Nucleon Interaction*, Nucl. Phys. A **500**, 485 (1989).

[206] J. G. Körner and M. Kuroda, e^+e^- *Annihilation Into Baryon-anti-Baryon Pairs*, Phys. Rev. D **16**, 2165 (1977).

[207] R. A. Williams, S. Krewald and K. Linen, *Vector resonances and electromagnetic nucleon structure*, Phys. Rev. C **51**, 566 (1995).

[208] B. Delcourt et al., *Study of the Reaction* $e^+e^- \to p\bar{p}$ *in the Total Energy Range 1925 MeV – 2180 MeV*, Phys. Lett. B **86**, 395 (1979).

[209] A. Antonelli et al., *The first measurement of the neutron electromagnetic form-factors in the timelike region*, Nucl. Phys. B **517**, 3 (1998).

[210] J. Bystricky, F. Lehar, P. Winternitz, *Formalism of Nucleon-Nucleon Elastic Scattering Experiments*, J. Physique **39**, 1 (1978).

[211] S. M. Bilenky, C. Giunti and V. Wataghin, *The Process* $\bar{p}p \to e^-e^+$ *with polarized initial particles and proton form-factors in timelike region*, Z. Phys. C **59**, 475 (1993).

[212] E. Tomasi-Gustafsson, F. Lacroix, C. Duterte and G. I. Gakh, *Nucleon electromagnetic form-factors and polarization observables in space-like and time-like regions*, Eur. Phys. J. A **24**, 419 (2005) [nucl-th/0503001].

[213] G. I. Gakh, N. P. Merenkov and E. Tomasi-Gustafsson, *Analysis of polarization observables and radiative effects for the reaction* $\bar{p} + p \to e^+ + e^-$, Phys. Rev. C **83**, 045202 (2011).

[214] A. Dbeyssi, E. Tomasi-Gustafsson, G. I. Gakh and M. Konchatnyi, *Proton-antiproton annihilation into massive leptons and polarization*, Nucl. Phys. A **894**, 20 (2012).

[215] M. Röder *et al.* [COSY-TOF Collaboration], *Final-State Interactions in the Process* $\vec{p}p \to pK^+\Lambda$, Eur. Phys. J. A **49**, 157 (2013).

[216] E. P. Solodov [CMD3 Collaboration], *First results from the CMD3 Detector at the VEPP2000 Collider*, arXiv:1108.6174 [hep-ex].

[217] M. Sudol *et al.*, *Feasibility studies of the time-like proton electromagnetic form factor measurements with PANDA at FAIR*, Eur. Phys. J. A **44**, 373 (2010).

[218] J. R. Pelaez, private communication;

R. Kaminski, Private communication.

[219] J. De Trocóniz and F. J. Ynduráin, *Precision determination of the pion form-factor and calculation of the muon* $g-2$, Phys. Rev. D **65**, 093001 (2002) [hep-ph/0106025].

[220] A. Schenk, *Absorption and dispersion of pions at finite temperature*, Nucl. Phys. B **363**, 97 (1991).

[221] S. Lanz, *Determination of the quark mass ratio Q from $\eta \to 3\pi$*, PhD thesis, Bern University (2011).

[222] M. I. Haftel and F. Tabakin, *Nuclear Saturation And The Smoothness Of Nucleon-nucleon Potentials*, Nucl. Phys. A **158**, 1 (1970).

[223] see e.g., M. Abramowitz and I. A. Stegun, *Handbook of Mathematical Functions with Formulas, Graphs, and mathematical Tables*, New York:Dover Publications, 1972.

[224] H. Zankel, W. Plessas and J. Haidenbauer, *Sensitivity of N-d polarization observables on the off-shell behavior of the N-N interaction*, Phys. Rev. C **28**, 538 (1983).

[225] K. Erkelenz, R. Alzetta and K. Holinde, *Momentum space calculations and helicity formalism in nuclear physics*, Nucl. Phys. A 176, 413 (1976).

[226] R. K. Ellis and G. Zanderighi, *Scalar one-loop integrals for QCD*, JHEP **0802**, 002 (2008) [arXiv:0712.1851 [hep-ph]].

[227] R. Bryan, *Parametrization of the Elastic Sector of the Nucleon Nucleon Scattering, Matrix. I*, Phys. Rev. C **24**, 2659 (1981).

[228] J. Carbonell, *Nucleon-antinucleon interaction*, `http://rmf.fciencias.unam.mx/pdf/rmf-s/47/2/47_2_70.pdf`

[229] O. Kidun, N. Fominykh and J. Berakdar, *Scattering and bound-state problems with non-local potentials: application of the variable-phase approach*, `http://www.mpi-halle.mpg.de/mpi/publi/pdf/4035_02.pdf`

[230] M. Kohno and W. Weise, *Proton - Anti-proton Scattering and Annihilation Into Two Mesons*, Nucl. Phys. A **454**, 429 (1986).

[231] C. J. Joachain, *Quantum Collision Theory*, North Holland, Amsterdam (1975).

[232] R. G. Newton, *Scattering theory of waves and particles*, McGraw-Hill, 2nd Edition (1966), P.459 .

[233] W. Glöckle, The Quantum Mechanical Few-Body Problem (Springer Verlag, Berlin, Heiderberg, 1983).

[234] B. Holzenkamp, PhD thesis, Bonn University (1988) (In German).

[235] M. M. Nagels, T. A. Rijken and J. J. de Swart, *Baryon Baryon Scattering in a One Boson Exchange Potential Approach. 2. Hyperon-Nucleon Scattering*, Phys. Rev. D **15**, 2547 (1977), see Eqs. (2.28)-(2.30). There is typo in Eq. (2.30), $\vec{n} := \vec{q}_i \times \vec{q}_f = \vec{q} \times k$.

[236] P. M. M. Maessen, Th. A. Rijken and J. J. de Swart, *Soft Core Baryon Baryon One Boson Exchange Models. 2. Hyperon - Nucleon Potential*, Phys. Rev. C **40**, 2226 (1989), see Eqs. (11)-(13).

[237] J. Bystricky, F. Lehar and P. Winternitz, *On Tests Of Time Reversal Invariance In Nucleon Nucleon Scattering*, CRMA-1127.

[238] P. LaFrance and P. Winternitz, *Scattering formalism for nonidentical spinor particles*, J. Phys. (France) 41, 1391 (1980).

[239] P. LaFrance, F. Lehar, B. Loiseau and P. Winternitz, *Anti-nucleon - nucleon scattering formalism and possible tests of CPT invariance*, Helv. Phys. Acta **65**, 611 (1992).

Acknowledgement

I thank Prof. Dr. Ulf-G.Meißner, who made it possible for my coming to Jülich as a PhD student. I thank Prof. Dr. Bastian Kubis and Prof. Dr. Christoph Hanhart, with whom I collaborate on the contents of Chap. 2. Bastian had impressed me for his frequent pertinent answers to my questions. I also benefit much from Dr. Johann Haidenbauer for the low energy antiproton-proton physics, which leads to the contents of Chap. 3 and 4. Johann was always available when I needed help. He always responded my email quickly, and give me his comments for the drafts of this thesis in time. Here I should give him a special "thanks".

I also thank my master supervisor Prof. Dr. Hai-Bo Li, who arranged the talks for me when I visited Beijing. It provided the opportunity for presenting the results in this thesis. Mr. Guenter Sterzenbach is also acknowledged since he had fixed some computer problems.

At last, I should mention my family, who always help and support me, and make the life promising and happy. I thank their understandings on a (somewhat) unusual research life.

Curriculum Vitae

Personal Data

Xian-Wei Kang
Düsseldorfer Str 1
52428 Jülich

Tel.: 0049 (0)157 7576878
E-Mail: x.kang@fz-juelich.de

Geb. am 02. 10. 1987 in Yuzhou county, Henan province, China
married, Chinese

Degrees and Research

09/2011–08/2014	PhD student in University of Bonn, the thesis work is performed in Forschungszentrum Jülich.
09/2008–07/2011	Master, Department of Physics, Henan Normal University, Xinxiang, China & Institute of High Energy Physics (IHEP), Chinese Academy of Sciences (CAS), Beijing, China
09/2004–07/2008	B.S. Physics, Department of Physics, Henan Normal University, Xinxiang, China.

Education

09/2001–07/2004	No.1 High School, Yuzhou County, Henan Province, China
09/1998–07/2001	No.2 Middle School, Liangbei Town, Yuzhou County, Henan Province, China
09/1992–07/1998	Primary School, Ji'a Village, Liangbei Town, Yuzhou County, Henan Province, China

Publication List

[1] J. Haidenbauer, X.-W. Kang and U.-G. Meißner, "The electromagnetic form factors of the proton in the timelike region," arXiv:1405.1628 [nucl-th].

[2] X.-W. Kang, B. Kubis, C. Hanhart and U.-G. Meißner, "B_{l4} decays and the extraction of $|V_{ub}|$," Phys. Rev. D **89**, 053015 (2014) [arXiv:1312.1193 [hep-ph]].

[3] X.-W. Kang, J. Haidenbauer and U.-G. Meißner, "Antinucleon-nucleon interaction in chiral effective field theory," JHEP **1402**, 113 (2014) [arXiv:1311.1658 [hep-ph]].

Talks

14.01.2014	"$N\bar{N}$ scattering up to NNLO in Chiral EFT", Peking University, Beijing, China.
10.01.2014	"$N\bar{N}$ interaction: phenomenologcal models and the recent EFT results", Institute of Modern Physics, Lanzhou, China.
09.01.2014	"$N\bar{N}$ interactions and the $p\bar{p}$ threshold enhancement", Lanzhou University, Lanzhou, China.
21.06.2013	"Nucleon Anti-Nucleon Interactions and Its Implication on $X(1835)$", Technische Universität München (TUM), Munich, Germany.
08.11.2012	"$\|V_{ub}\|$" from the four-body semileptonic B decay, Institute of High Energy Physics, Beijing, China.
08.11.2012	"B_{l4} decay and $\|V_{ub}\|$'s extraction", Peking University, Beijing, China.
28.08.2012	"Nucleon Anti-Nucleon Interactions", Workshop on Open Threshold Phenomena, IHEP, Beijing, China.

Note: The publications and talks listed above correspond to the works performed during my PhD study.

Bonn, 10. May 2014